6-10-2019 10:00 AM

Field-Scale Implementation of Sulfidated Nano Zerovalent Iron for In-Situ Remediation

Ariel Nunez Garcia
The University of Western Ontario

Supervisor
O'Carroll, Denis M.
University of New South Wales (UNSW) Co-Supervisor
Herrera, Jose
The University of Western Ontario

Graduate Program in Civil and Environmental Engineering
A thesis submitted in partial fulfillment of the requirements for the degree in Doctor of Philosophy

Abstract

As far back as the mid-1990s, biogenic sulfidation has been observed during the implementation of iron-based materials for groundwater remediation. This phenomenon has largely been a consequence of natural biogeochemical processes and the prospects of utilizing engineered sulfidated zerovalent iron (ZVI) particles – nano- and/or micro- sized – were not extensively explored. More recently sulfidation of zerovalent iron (ZVI) particles has received considerable attention, highlighting the benefits that engineered/abiotic sulfidation can offer to nZVI, but to date, no field demonstration of the technology has been conducted. The first part of this thesis aims to report the unique challenges and unanswered questions that remain in relation to the emplacement of S-nZVI. nZVI was synthesized on-site using sodium borohydride ($NaBH_4$) and stabilized with carboxymethylcellulose (CMC). Sulfidation was performed in an aqueous-solid fashion with sodium dithionite ($Na_2S_2O_4$) as the sulfidating agent. The slurry was gravity fed into a non-native sandy material by a designated injection well. Multiple monitoring wells were installed upstream and downstream of the injection well to monitor particle breakthrough and changes in the aquifer system. In terms of performance, the study suggests the on-site synthesized S-nZVI is mobile in the subsurface. Transport of S-nZVI to the monitoring wells, both downgradient and upgradient, resulted in a significant shift in aqueous phase concentrations of chlorinated volatile organic compounds (cVOCs). Compound specific isotope analysis (CSIA), changes in concentrations of intermediate degradation products, and the increase of ethene concentrations confirmed cVOC dechlorination.

The field demonstration was followed by a bench – scale study on the aging characteristics and reactivity of S-nZVI. Particles were aged in dithionite immediately after synthesis (i.e., without washing). Aged S-nZVI remained reactive towards trichloroethene (TCE) after a 21-day aging period. Results from the aging study suggest particles synthesized on-site under these conditions could remain operational after extended storage.

As knowledge of this growing area increases, this work presents foundational material on field-application of S-nZVI. Results from this field demonstration show sulfidation is a suitable amendment for the development of more efficient nZVI-based treatments for in-situ remediation.

Keywords

nZVI, Nano Zerovalent Iron, ISCR, In-Situ Chemical Reduction, groundwater, chlorinated solvents, dithionite, sulfidation, remediation

Co-Authorship Statement

This thesis was written in accordance with the guidelines and regulations for an integrated-article format stipulated by the School of Graduate and Postdoctoral Studies at The University of Western Ontario. This work was conducted under the supervision of Dr. Denis O'Carroll and Dr. Jose Herrera. The candidate conducted all field work, coordinated and performed laboratory work with several collaborators, and led the data analysis. The candidate wrote the thesis and was the lead author on all the chapters.

Contributions

Chapter 2: Literature Review

Ariel Nunez Garcia:	primary author/writer, developed outline, reviewed references
Denis O'Carroll:	reviewed/revised chapter
Jose Herrera:	reviewed/revised chapter

Chapter 3: Fate and Transport of Sulfidated Nano Zerovalent Iron (S-nZVI): A Field Study

Ariel Nunez Garcia:	primary author/writer, performed field work, collected field samples, conducted laboratory analysis, interpreted and analyzed data
Hardiljeet K. Boparai:	assisted in field samples analysis, interpreted and analyzed data, reviewed/revised chapter
Ahmed I. A. Chowdhury:	assisted in field work, analyzed samples and aided in data analysis
Cjestmir de Boer:	designed monitoring network, constructed wells, assisted in field work and laboratory analysis and reviewed/revised chapter
Chris M.D. Kocur:	designed monitoring network, constructed wells, assisted in field work, aided in data analysis
Leanne M. Austrins:	coordinated regulatory approvals and field activities
Audrey Sidebottom:	coordinated regulatory approvals

Richard L. Johnson:	assisted in field work and performed CRP analysis
Jose Herrera:	assisted in field work and data interpretation, provided formative discussion, reviewed/revised chapter
Denis M. O'Carroll:	initiated work, planning and regulatory approval, grantee of funding, assisted in field work and data interpretation, reviewed/revised chapter

Chapter 4: Sulfidated Nano Zerovalent Iron (S-nZVI) for In-Situ Treatment of Chlorinated Solvents: A Field Study

Ariel Nunez Garcia:	primary author/writer, performed field work, collected field samples, conducted laboratory analysis, interpreted and analyzed data
Hardiljeet K. Boparai:	established aqueous phase chlorinated solvent extraction methods, assisted in field samples analysis, interpreted and analyzed data, reviewed/revised chapter
Ahmed I. A. Chowdhury:	assisted in field work, aided in data analysis
Cjestmir de Boer:	assisted in field work
Chris M.D. Kocur:	assisted in field work, aided in data analysis and reviewed/revised chapter
Elodie Passeport:	performed CSIA analysis and aided in data interpretation
Leanne Austrins:	coordinated regulatory approvals and field activities
Audrey Sidebottom:	coordinated regulatory approvals
Jose Herrera:	assisted in field work and data interpretation, provided formative discussion, reviewed/revised chapter
Denis M. O'Carroll:	initiated work, planning and regulatory approval, grantee of funding, assisted in field work and data interpretation, reviewed/revised chapter

Chapter 5: Aging of Nano Zerovalent Iron Under Sulfidic Conditions: Characterization and Reactivity

Ariel Nunez Garcia:	primary author/writer, designed and supervised experiments, interpreted and analyzed data
Daniel Appleton:	design/performed experiments, aided in data interpretation, and reviewed/revised chapter
Keming Chen:	design/performed experiments, aided in data interpretation, and reviewed/revised chapter
Matthew Lee:	contributed ideas for data analysis, provided formative discussion, reviewed/revised chapter
Denis M. O'Carroll:	initiated work, grantee of funding, designed experiments, assisted in data interpretation, reviewed/revised chapter

Acknowledgments

I would like to thank Dr. Denis O'Carroll and Dr. Jose Herrera for their mentorship during my time at Western. To Dr. O'Carroll, for giving me the opportunity to work in many interesting projects. His insights, as well as enthusiasm and positive attitude, were paramount to helping me push through in hard times. This work would not have been possible without his guidance. To Dr. Herrera, for all the discussions and for asking the hard questions. His comments, insights and critical thought helped me to develop a more vigorous approach to research. I am also grateful for his guidance and support throughout my doctoral studies.

I would also like to thank Dr. Chris Kocur, Dr. Cjestmir de Boer, Dr. Ahmed Chowdhury and Dr. Hardiljeet Boparai. They all worked incredible hard and spent a considerable amount of time during various stages of the project. Special thanks to Hardiljeet, I really enjoyed discussing field data and research with her. Hardiljeet also taught me everything I know about sample analysis and has been a mentor during my studies.

This project would not have been successful without the assistance of multiple summer students. The staff at CH2M were of great help in coordinating field activities and providing support on – site. Thanks to Leanne Austrins, Chris Peace, Jennifer Hayman and Brian Wilson. To the staff at the Department of Civil and Environmental Engineering, both administrative and technical, for all their support throughout the years.

RESTORE was not only a research group, but also like a family to me. It has been an honour to be part of this group. I am grateful to the RESTORE directors, Dr. Clare Robinson and Dr. Jason Gerhard for their mentorship. I would like to acknowledge all the advice and fruitful discussion - about research and life in general – received from Daoping Guo, Sabina Rakhimbekova, Laura Vogel, Tarek Rashwan, and Marco Zanoni.

I am grateful to my collaborators at the University of New South Wales (UNSW); to Daniel Appleton, Keming Chen, and Dr. Matthew Lee.

My special thanks to my family for supporting me since the moment I left, and to my wife for giving an ear to my typical "grad student speeches" (I love you).

Lastly, to the Lord, for His unending love: "And whatever you do, in word or deed, do everything in the name of the Lord Jesus, giving thanks to God the Father through Him." Colossians 3:17 (ESV)

Table of Contents

List of Tables

List of Figures

Chapter 1

1 Introduction

1.1 Background on Site Contamination

Large-scale generation of hazardous waste has been historically tied to economic development in the industrialized world. In the United States, rapid economic growth initiated during the industrial revolution accelerated in the first half of the 20th century after two world wars, and so did the production of industrial and municipal waste. The onset of World War I halted the import of chemical exports from European countries, resulting in the proliferation of the synthetic organic chemical industry in the United States.[1] In the 1920's alone, production of synthetic organic chemicals increased to more than 287 million kg (633 million pounds) in 1929, from a reported 9.5 million kg (21 million pounds) in 1921. Such rapid expansion is intrinsically linked to the diverse application of chlorinated solvents, which at the time were the preferred agent used by small dry-cleaning shops.[1] The need for chlorinated solvents, and other chlorinated compounds, was only exacerbated during the Second World War, with legislation granting priority usage to military purposes.[1] The high demand continued during the post-war era, and with shifting focus from armaments to the production of consumer goods, the generation of both solid and hazardous waste was not met in an environmentally protective manner.[2] Legislature was enacted after the recognition of the serious threat that these types of waste pose to ecological systems and public health. Starting with the Solid Waste Disposal Act (SWDA) of 1965, and then its subsequent amendment in 1976, Resource Conservation and Recovery Act (RCRA), measures were taken to regulate solid and hazardous waste. While SWDA provided funding to improve solid waste disposal practices and RCRA expanded the provisions for the management of hazardous waste, these were primarily prevention-oriented programs.[2] In order to address the problem of abandoned or inactive contaminated sites, in 1980 the United States Congress passed the Comprehensive Environmental Response, Compensation and Liability Act (CERCLA), commonly known as 'Superfund.' CERCLA authorized the enforcement of a "cost recovery mechanism" by identifying responsible parties (owners, operators, generators, etc.) and levying a tax to recover cleanup costs. The Superfund Program spends hundreds of millions of dollars every year on remediation projects,

despite being just one of many cleanup programs in the United States (e.g., Brownfields Programs, RCRA-Corrective Action program, etc.).[3] To date, remediation of hazardous waste sites has become one of the most costly endeavors in U.S. environmental policy history.[2, 3]

In Canada, the creation of a five-year National Contaminated Sites Remediation Program (NCSRP) in 1989, was the first major step by the Government of Canada to address the environmental legacy of contaminated sites.[4] Further action was taken in 1995 by forming the Contaminated Sites Management Working Group (CSMWG), a group entrusted with developing a strategy to manage legacy sites. In 2005, the Federal Contaminated Sites Action Plan (FCSAP) was launched with the goal to reduce environmental and human health risk from contaminated sites under federal jurisdiction. The FCSAP was allocated a budget of $4.54 billion over 15-years and is the most recent program established by the Government of Canada. With the program coming to an end in 2020, more initiatives are sure to follow, considering the more than five thousand active sites remaining, according to the Federal Contaminated Sites Inventory (FCSI).[5] This number does not include sites contaminated by private individuals or firms and should be seen as an underestimation of the potential active sites in the country. This is an issue that not only concerns North America. In Europe, the situation is more complex due to variability in the legislative frameworks between countries and different definitions and/or standards of what constitute a "contaminated site." According to a recent survey, however, there is a staggering 2.5 million potentially contaminated sites, out of which 342,000 have already been identified.[6] In Australia, it has been estimated that more than 160,000 sites are contaminated with an array of chemicals, comprising as many as 75,000 different contaminants.[7]

Accumulation of practical experience and sharing of knowledge and information has aided in the advancement of more comprehensive data collection, site inventories and remediation technologies. Whilst this is the case for developed countries, in developing countries and/or emerging economies where other issues such as poor health or poverty understandably takes precedence, awareness that site contamination is even a valid and prominent environmental issue is lacking.[8] Action is already being taken by a number of countries that are in the process of establishing national inventories (e.g., Brazil, Chile and Mexico). There have been studies and surveys conducted to quantify the number of contaminated sites worldwide but estimates to date are likely low due to gaps in data and lack of participation by many countries. With increasing

industrialization and urbanization around the world an increase in the number of contaminated sites is expected. However, by learning from the mistakes of more developed and industrialized countries, involvement of developing countries could be accelerated. This could occur by technology transfer or an already established management framework for site remediation.[8]

Historically, industrialization has been followed by site contamination. This is a global issue, identified first in developed countries but now being recognized worldwide. Though significant advances in remediation technologies, site characterization, nature of contaminants as well as environmental policies have occurred since the 1970s, the remediation of contaminated sites still present major challenges. There is no "good for all" solution and development of new and more cost-effective remediation technologies is an area of active research.

1.2 Research Focus

The use of nanomaterials for environmental applications has attracted a lot of attention over the last 25 years. The most applied nanomaterial for the remediation of water and soil is nano zerovalent iron (nZVI).[9] nZVI is capable of treating many environmental pollutants, including chlorinated solvents, polychlorinated biphenyls (PCBs), chlorinated pesticides, nitro aromatic compounds and metals, among others.[10] Other applications include stabilization of biosolids, discoloration of dyes, antifouling agent and treatment of nuclear waste.[11] nZVI offers advantages over its micro-scale counter-part, allowing for direct injections into the subsurface as a slurry, avoiding trenching methods such as permeable reactive barriers (PRBs).[12, 13] This has sprouted a great deal of research on understanding its properties and developing surface amendments to increase its practicability,[9] yet some key technical challenges remain. Its low subsurface mobility and poor selectivity due to side reactions with non-targeted compounds has halted more widespread acceptance of nZVI as a viable and competitive remediation technology.[14, 15]

The overarching goal of this research is to address some of these limitations by using a new method for improving the performance of nZVI. This method is now known to researchers as sulfidation, and consists of treating nZVI with reduced sulfur compounds, such as sodium dithionite ($Na_2S_2O_4$). Sulfidation with sodium dithionite has shown to improve particles' selectivity, longevity and reactivity,[15, 16] addressing some of the challenges outlined above.

1.3 Research Objectives

This research work seeks to further the fundamental understanding of sulfidation by sodium dithionite and evaluate its field performance. The specific objectives include:

- Demonstrate the field applicability of sulfidated nZVI (S-nZVI) by conducting an on-site synthesis and injection at an active contaminated site with the aim to:
    1. Track the subsurface mobility of S-nZVI and concurrent changes in in-situ geochemical conditions.
    2. Characterize the field-synthesized particles pre – and post – injection to evaluate the longevity and fate of S-nZVI in the subsurface.
    3. Evaluate the short – and long – term in-situ degradation of chlorinated volatile organic compounds (cVOCs) by S-nZVI.
- Evaluate the aging characteristics of S-nZVI and its effect on the reactivity of model pollutants, namely, trichloroethene (TCE) and chloroform (CF).

1.4 Thesis Outline

This thesis is written in "Integrated Article Format." A brief description of each chapter is presented below:

Chapter 1 provides historical and legislative background on site contamination and outlines the focus and objectives of the thesis.

Chapter 2 reviews the various synthesis methods, stabilizer options, surface modification procedures, and field applicability of nZVI. As the central theme of this review, emphasis will be placed on the sulfidation technique and its recent advancements.

Chapter 3 titled "Fate and Transport of Sulfidated Nano Zerovalent Iron (S-nZVI): A Field Study" discusses the characterization of the nanoparticles and their transport in the subsurface.

Chapter 4 titled "Sulfidated Nano Zerovalent Iron (S-nZVI) for In-Situ Treatment of Chlorinated Solvents: A Field Study" presents the short – and long – term effects of the S-nZVI injection on cVOCs concentrations.

Chapter 5 titled "Aging of Nano Zerovalent Iron Under Sulfidic Conditions: Characterization and Reactivity" examines the physicochemical changes of S-nZVI aged in dithionite, and corresponding effects on reactivity. Raw data for this chapter was previously published in the undergraduate thesis of Daniel Appleton[17] and in the Masters of Engineering thesis of Keming Chen.[18] Permission to use the data set was obtained from primary authors.

Chapter 6 summarizes the major conclusions of the thesis, discusses practical and environmental implications of the study and identify future research needs.

Appendices provide supporting information that was not included in the chapters.

1.5 References

1. Doherty, R. E., A History of the Production and Use of Carbon Tetrachloride, Tetrachloroethylene, Trichloroethylene and 1,1,1-Trichloroethane in the United States: Part 1—Historical Background; Carbon Tetrachloride and Tetrachloroethylene. *Environmental Forensics* **2000,** *1*, (2), 69-81.

2. Soesilo, J. A.; Wilson, S. R., *Site Remediation Planning and Management*. Lewis Publishers: Boca Raton, FL, 1997; p 409.

3. Karn, B.; Kuiken, T.; Otto, M., Nanotechnology and in Situ Remediation: A Review of the Benefits and Potential Risks. *Environ Health Persp* **2009,** *117*, (12), 1823-1831.

4. Government of Canada. About federal contaminted sites. www.canada.ca/en/environment-climate-change/services/federal-contaminated-sites.html (January 6, 2019).

5. Treasury Board of Canada Secretariat. Federal Contaminated Sites Inventory. http://www.tbs-sct.gc.ca/fcsi-rscf/home-accueil-eng.aspx (January 6, 2019).

6. European Environment Agency (EEA). *Progress in management of contaminted sites*; Denmark, 2014; p 51.

7. Plant, R.; Wimot, K.; Ege, C. *Contaminted Soil Wastes in Australia*; Institute for Sustainable Futures: Sydney, 2014; p 69.

8. Brandon, E., *Global Approaches to Site Contamination Law*. Springer Netherlands: 2012.

9. Stefaniuk, M.; Oleszczuk, P.; Ok, Y. S., Review on nano zerovalent iron (nZVI): From synthesis to environmental applications. *Chem Eng J* **2016,** *287*, 618-632.

10. O'Carroll, D.; Sleep, B.; Krol, M.; Boparai, H.; Kocur, C., Nanoscale zero valent iron and bimetallic particles for contaminated site remediation. *Adv Water Resour* **2013,** *51*, 104-122.

11. Zou, Y.; Wang, X.; Khan, A.; Wang, P.; Liu, Y.; Alsaedi, A.; Hayat, T.; Wang, X., Environmental Remediation and Application of Nanoscale Zero-Valent Iron and Its Composites for the Removal of Heavy Metal Ions: A Review. *Environ Sci Technol* **2016,** *50*, (14), 7290-7304.

12. Li, X.-q.; Elliott, D. W.; Zhang, W.-x., Zero-Valent Iron Nanoparticles for Abatement of Environmental Pollutants: Materials and Engineering Aspects. *Critical Reviews in Solid State and Materials Sciences* **2006,** *31*, (4), 111-122.

13. Mukherjee, R.; Kumar, R.; Sinha, A.; Lama, Y.; Saha, A. K., A review on synthesis, characterization, and applications of nano zero valent iron (nZVI) for environmental remediation. *Crit Rev Env Sci Tec* **2016,** *46*, (5), 443-466.

14. Fan, D.; O'Carroll, D. M.; Elliott, D. W.; Xiong, Z.; Tratnyek, P. G.; Johnson, R. L.; Nunez Garcia, A., Selectivity of Nano Zerovalent Iron in In Situ Chemical Reduction: Challenges and Improvements. *Remediation Journal* **2016**.

15. Fan, D.; O'Brien Johnson, G.; Tratnyek, P. G.; Johnson, R. L., Sulfidation of Nano Zerovalent Iron (nZVI) for Improved Selectivity During In-Situ Chemical Reduction (ISCR). *Environ Sci Technol* **2016,** *50*, (17), 9558-9565.

16. Nunez Garcia, A.; Boparai, H. K.; O'Carroll, D. M., Enhanced Dechlorination of 1,2-Dichloroethane by Coupled Nano Iron-Dithionite Treatment. *Environ Sci Technol* **2016,** *50*, (10), 5243-5251.

17. Appleton, D. Investigating the effect of aging on modified nanoscale zero-valent iron (nZVI) when employed for the remediation of organohalides. University of Birmingham, Birmingham, United Kingdom, 2018.

18. Chen, K. Aging Study of Sulfidated nZVI in Anoxic Aqueous Solution: Effect on Reactivity and Fe(0) Content. The University of New South Wales, New South Wales, Australia, 2017.

Chapter 2

2 Advances in Nano Zerovalent Iron (nZVI) for Environmental Remediation

2.1 Introduction

Chlorinated methanes, ethanes and ethenes are frequently the target of remediation efforts because of their widespread contamination. This is a result of their extensive industrial applications and recalcitrant nature under typical environmental conditions.[1] After their release to the subsurface these chlorinated solvents can be found as dense non-aqueous phase liquids (DNAPLs), an immiscible liquid denser than water. As the DNAPL migrate, redistribute and age in the subsurface it can partition into the vapor, aqueous and/or sorbed phase. Such partitioning will largely depend on the physical and chemical properties of the compounds (e.g., solubility, vapor pressure and Henry's Law constants) as well as aquifer properties. Estimation of the contaminant mass in each of these four phases listed above is therefore a key factor in the design, implementation and evaluation of any remediation technology.[2] For sites where DNAPL is present, reaching compliance with regulatory standards is rare, and it is now recognized that setting maximum contaminant levels (MCLs) as a remedial action objective (RAOs) is not practical. This makes remediation of such sites difficult, with even aggressive treatment leaving residual contamination.[3, 4] Other alternatives, such as decreases in concentration and mass removal, have become more widely accepted as metrics for successful remediation even if site closure is not immediately achieved.

Table 2.1 summarizes a variety of technologies used in the groundwater and soil remediation industry. In the 1970s and 1980s the most common technology employed was pump – and – treat, mostly due to their availability and ease of application. But by the early 1990s it was well established that pump – and – treat systems were not capable of remediating DNAPL source zones within reasonable time frames (e.g., years).[5] The long term management cost of pump – and – treat systems forced the industry to shift focus to more aggressive techniques such as *In Situ* Chemical Oxidation (ISCO), *In Situ* Thermal Treatments (ISTT) and *In Situ* Chemical Reduction (ISCR),

among others. Nowadays there is no agreed upon technology with universal application and integrated strategies are often needed at many contaminated sites.[2]

Table 2.1 Treatment Technologies for sites contaminated with Chlorinated Solvents (Reprinted with permission from McCarty [6] Copyright 2010 Springer).

Conventional Pump-and-Treat	**Flushing**
Ex situ Air Stripping	Cosolvent Flushing
Ex situ Activated Carbon Adsorption	Surfactant Flushing
Ex situ Catalytic Oxidation	
Air Injection	***In Situ* Thermal Technologies**
Vapor Extraction	Hot Fluid Injection-Air, Water, Steam
Bioventing	Electrical Resistive Heating
Air Sparging	Thermal Conductive Heating
Biodegradation	***In Situ* Chemical Processes**
Aerobic Cometabolism	Oxidative Chemical Processes
Anaerobic Reductive Dehalogenation	Reductive Chemical Processes

2.2 *In Situ* Chemical Reduction (ISCR)

The term *In Situ C*hemical Processes, divided into oxidative (ISCO) and reductive (ISCR) reactions, typically refers to abiotic pathways (i.e., no direct role of microorganism). Both technologies rely on either the oxidation of the chlorinated solvent to carbon dioxide or the reduction of the organic carbon to a lower oxidation state (e.g., ethene) while releasing the covalently bonded chlorine as chloride. The application of ISCO technologies are generally well established and possible oxidants are hydrogen peroxide, sodium or potassium permanganate ($NaMnO_4$/$KMnO_4$), sodium persulfate (NaS_2O_8) and ozone.[2, 7, 8] In the case of ISCR several chemical reductants can be applied, the most common proceeding from reduced metal species (zerovalent iron (ZVI or Fe^0), ferrous iron (Fe^{2+})) and reduced sulfur species (HS^-, $S_2O_4^{2-}$, FeS). Broadly speaking, ISCR technologies can be classified in two major categories:[9]

1. Intrinsic reductants formed under natural environmental conditions or those generated through *in situ* stimulation of what would otherwise occur by natural biogeochemical processes. These include, but are not limited to, minerals deriving their reducing properties from Fe^{2+} and/or S^{2-} (magnetite, green rust or mackinawite).

2. Engineered chemical reductants. These would include zerovalent metals, the most common being zerovalent iron.

The specific ISCR treatment also varies depending on the mode of application. Based on this, they can be further classified between those used for more active and direct destruction of source zones and those designed for more passive treatment of the dissolved phase, for instance, plume containment. These classification schemes are illustrated in Figure 2.1.

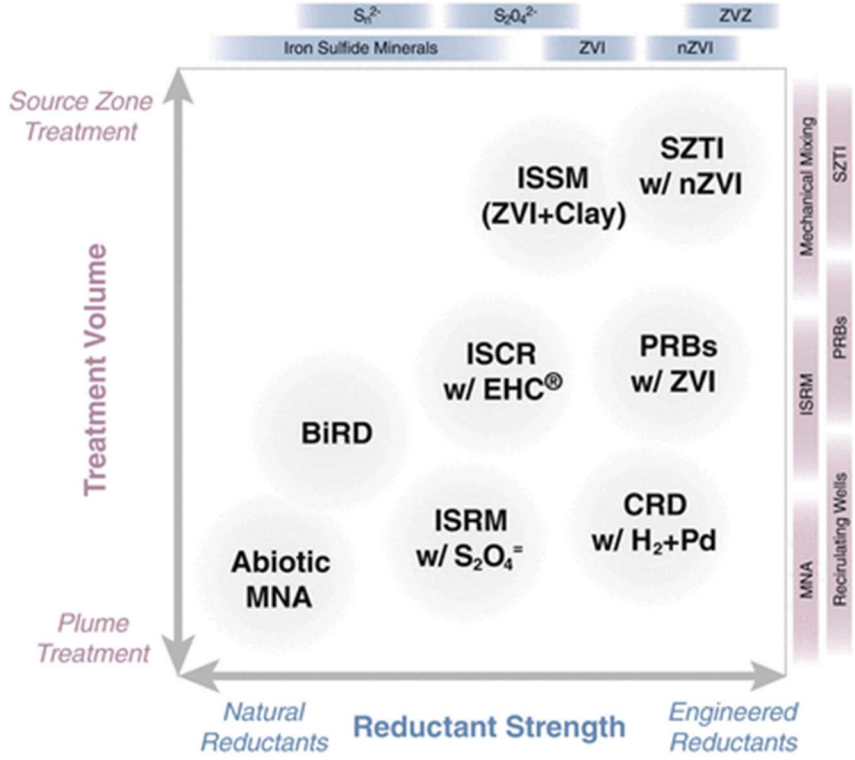

Figure 2.1 ISCR technologies currently in practice. Acronyms are defined as follow: Monitored Natural Attenuation (MNA), In Situ Redox Manipulation (ISRM), Biogeochemical Reductive Dechlorination (BiRD), Permeable Reactive Barrier (PRB), Catalytic Reductive Dechlorination (CRD), In Situ Soil Mixing (ISSM) and Source Zone Targeted Injection (SZTI) (Reprinted with permission from Tratnyek et al. [9] Copyright 2014 Springer New York).

2.3 Nano Zerovalent Iron (nZVI)

2.3.1 Background

As shown in Figure 2.1 the most aggressive ISCR treatments (clustered on the upper – right side) are those that involve a zerovalent metal such as iron. Environmental application of zerovalent metals for removal of chlorinated organic compounds was first reported in the patent literature as early as 1972.[10] But it was only until the late 1980s that iron powder was considered as an alternative for removal of chlorinated compounds (1,1,2,2-tetrachloroethane (1,1,2,2-TCA) and trichloroethylene (TCE)) from wastewater.[11, 12] Subsequent work studied the potential of zerovalent iron for *in situ* remediation of groundwater contaminated with chlorinated solvents.[13, 14] Since then a myriad of research articles have dedicated their efforts to engineering more efficient forms of ZVI by manipulating the size, dispersibility, and surface chemistry of the particles. This also launched field trials, pilot-scale, and full-scale demonstrations of various forms of ZVI for remediation applications, both *ex situ* and *in situ*. In fact, the use of zerovalent iron for the treatment of reducible contaminants has become an established technology. It is mostly applied in the form of micro – ZVI (mZVI) as permeable reactive barriers (PRBs).[15] To date, utilization of ZVI-based technologies (including both micro- and nano- size iron) have predominantly been directed towards dissolved phase plumes but source zone targeted injection (SZTI) is gaining attraction.[9] Nonetheless, it is recognized that ZVI treatments are more appropriate for source containment rather than direct source zone remediation.[4]

In terms of full – scale implementation, nano-ZVI (nZVI) is more prevalent in the United States, representing a minor portion of the remediation market.[16] In Europe it has been met with skepticism mainly due to non-technical issues.[17] Difficulty in getting approval from regulatory agencies stems from a reluctance to accept innovative remediation solutions and a fear of public backlash. Hence field demonstrations are essential not only to advance scientific understanding but also promote the technology to practitioners and regulators. The following sections will discuss different synthesis approaches for the preparation of nZVI, stabilizing agents, and field deployment of the technology.

2.3.2 Synthesis Approaches

Synthesis conditions can influence the crystallinity, morphology, size, and ultimately, the reactivity of nZVI. It is therefore essential to prepare the particles in a controlled and reproducible manner to obtain tunable structures capable of meeting the demands at hand.[18] To achieve this several synthesis methods have been developed over the years and are summarized in recent critical reviews.[18-20] In general, there are two basic approaches taken while synthesizing nZVI: a top – down or a bottom – up approach. The top – down approach entails the diminution and processing of bulk iron materials.[19] An example includes precision milling processes.[21] This method is environmentally benign and considered more cost effective than aqueous phase reduction of iron salts (described below). Unfortunately, there is limited control over the particle size distribution and morphology, resulting in nanoparticles with irregular shape and strong tendency for aggregation. In the bottom – up approach reducing agents are applied to reduce iron oxides or Fe^{2+} (in the form of iron salts) to form nZVI. Multiple methods are included in this approach (e.g., carbothermal reduction,[22, 23] ultrasound assisted synthesis,[24] electrochemical methods,[25, 26] green synthesis[27] and chemical reduction[28]). The latter remains the most frequently used synthesis protocol for nZVI production in laboratory settings due to its simplicity and chemical homogeneity.[19] It consists of the reduction of ferrous or ferric salts by sodium borohydride to precipitate nZVI (Eq. 2.1 and Eq. 2.2).[29, 30] Though borohydride is the most commonly used reductant, its high price (estimated as more than $200 US per kg nZVI in 2013) and the potential hazard of generating hydrogen gas has made scalability an issue for field applications.[31] For these reasons other reductants, such as sodium dithionite ($Na_2S_2O_4$) (see Section 2.4.2.2), have also been proposed as the sole reducing agent (Eq. 2.3).[32-34]

$$4Fe^{3+} + 3BH_4^- + 9H_2O \rightarrow 4Fe^0 + 3H_2BO_3^- + 12H^+ + 6H_2 \quad (2.1)$$

$$2Fe^{2+} + BH_4^- + 3H_2O \rightarrow 2Fe^0 + H_2BO_3^- + 4H^+ + 2H_2 \quad (2.2)$$

$$Fe^{2+} + S_2O_4^{2-} + 4OH^- \rightarrow Fe^0 + 2SO_3^{2-} + 2H_2O \quad (2.3)$$

The bottom – up synthesis process has been generally described in the following steps: 1) super saturation of the solution; 2) nucleation of the nZVI cluster; 3) growth of nZVI nuclei; and 4) agglomeration of nZVI.[35] Nuclei formation has been found to be the most important step in

determining nZVI characteristics. It is therefore important to carefully control synthesis conditions, mainly reductant delivery rate, reductant and reagent concentration, and reaction time. These variables can be easily altered, making the chemical reduction by borohydride a very versatile method. Alterations to nZVI particles are typically performed during the synthesis process to improve the decontamination capability of the nanoparticles. For example, an increase in the dehalogenation rate can be achieved by simply doping nZVI with a second metal through a water – based approach.[36] Palladium is commonly used as the preferred noble metal (Eq. 2.4) but environmental concerns over its introduction into the subsurface and the short lifespan of the highly reactive bimetallic particles have limited its field implementation.[31, 37] Ultimately, the desired properties of the end product and its intended application will dictate the synthesis method, protocol and conditions.

$$Pd^{2+} + Fe^{0} \rightarrow Pd^{0} + Fe^{2+} \quad (2.4)$$

2.3.3 Surface Coatings

One of the major challenges to *in situ* implementation of nZVI is its low colloidal stability due to strong magnetic forces between particles.[38, 39] Formation of larger aggregates limits mobility in porous media and decreases particle surface area. To prevent aggregation and further agglomeration several surface coatings or stabilizers have been studied. These stabilizers include carboxymethyl cellulose (CMC),[40] guar gum,[41] starch,[38] SDBS surfactants and triblock copolymer (PMAA-PMMA-PSS),[42] hydrophilic carbon and poly(acrylic acid) (PAA),[43] among others. Anionic polyelectrolytes are preferred because they provide both electro-static and steric interparticle repulsion.[44, 45] Therefore, the high molecular weight and high densities of charged functional groups make polymers like CMC ideal.[31] The stabilizing agent can be applied by introducing the polymer into the synthesis mixture before the reducing agent is added (pre – synthesis stabilization) or by physical absorption to existing nZVI particles (post – synthesis stabilization).[31, 37] This distinction is important as the mode of application will affect the stability and reactivity.[40, 46]

Dispersion of the particles in an oil-water emulsion was proposed as a way to increase the hydrophobicity of nZVI and enhance partitioning to the NAPL – water interface.[47, 48] Encapsulation of the nZVI in an oil emulsion allows for the destruction of contaminants within the

NAPL phase and shields particles from reacting with non-targeted groundwater constituents. Other frequent methods used to modify the surface include trapping nZVI in a matrix (calcium alginate and chitosan) and deposition on a carrier or support (granular activated carbon).[19] Figure 2.2 shows an illustration of these methods. A more recent surface modification method consists of developing an iron sulfide layer by incorporating lower-valent forms of sulfur during the synthesis process.[16, 49, 50] This method will be discussed in detail in Section 2.4.

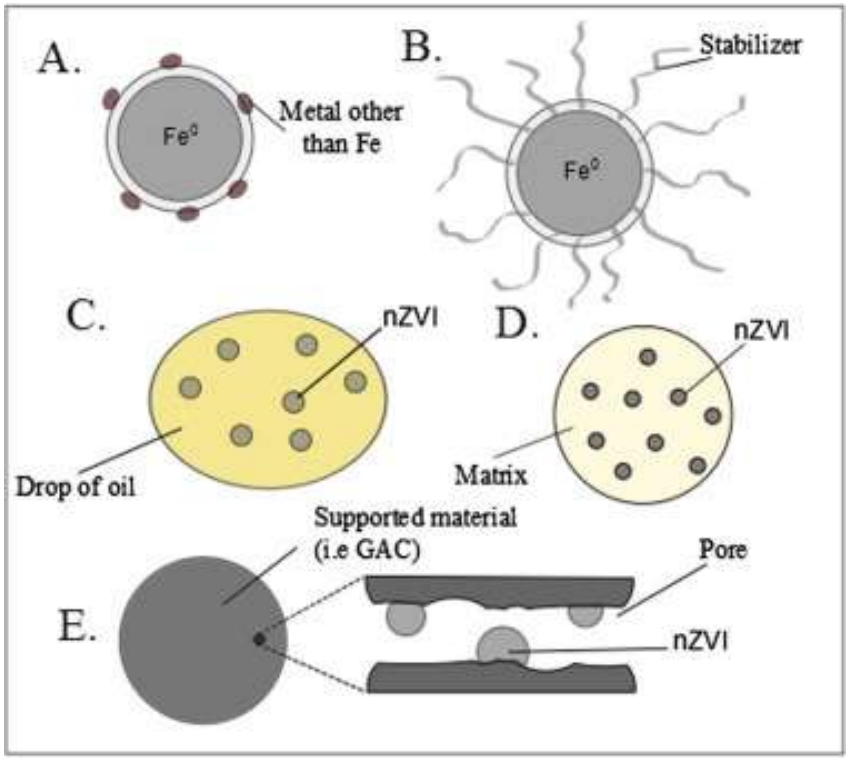

Figure 2.2 Common modification methods for nZVI. A) Doping with a secondary metal; B) Coating with a polyelectrolyte; C) emulsification (emulsified nZVI or EZVI); D) encapsulation in a matrix, and E) deposition on a support (Reprinted with permission from Stefaniuk et al. [19] Copyright 2016 Elsevier).

2.3.4 Field Deployment

Multiple field studies have been conducted to bridge the gap between laboratory and real aquifer systems (Table 2.2). The highly heterogenous nature of subsurface environments, size of treatment zone, nature of contaminants, differences in nanoparticle preparation and delivery methods of nZVI make comparison between these studies difficult.[31] However, a noticeable commonality between all studies is the almost exclusive application to aquifers contaminated with chlorinated ethanes, ethenes and methanes (henceforth referred to as chlorinated volatile organic compounds or cVOCs). In general, even though significant degradation is typically reported near the injection well, reactivity in surrounding wells (downstream or upstream) is less predictable. This can be a result of several converging factors including limited mobility of nanoparticles, short reactive life span and inadequate site characterization. Interferences related to fluid displacement or dilution also complicates accurate assessment of field performance. These issues are intrinsic to any technology that relies on the direct injection of a reactive fluid for *in situ* remediation. Therefore, installation of a well-defined monitoring network is crucial to effectively evaluate the success of nZVI delivery. This might require implementation of more closely spaced monitoring wells. In addition, the used of conventional wells can lead to improper assessment of the true vertical distribution of contaminants due to the possibility of dilution with uncontaminated water, resulting in contaminant mixing.[51] These biases and false positives could lead to unreliable conclusions. For example, the composite samples obtained from “long” screened single interval wells would underestimate maximum concentrations in the aquifer and overestimate the true efficiency of the *in situ* treatment employed. This is confounded by proximity to a DNAPL pool where concentration gradients with depth can be high. Given the complexity of the vertical distribution of contaminants, use of multilevel sampling devices is recommended. Several configurations have been developed to date, yet application of such devices for nZVI field studies has been limited to nested wells.[52]

Table 2.2 Peer-reviewed field studies on nZVI.

Particles	Aquifer Material	Delivery method	References
Bimetallic nZVI (Pd/Fe)	Sand	Gravity	53
Nanoscale Emulsified ZVI (EZVI)	Fine/medium sand	Pressure	48
Stabilized bimetallic nZVI	Sand	Gravity	54
Commercial and on-site [a] synthesized bimetallic nZVI (Pd/Fe)	Sand	Gravity	52
[b] Stabilized bimetallic nZVI (Pd/Fe)	Sand, gravel and clay	Gravity and Pressure	55
[b] Stabilized bimetallic nZVI (Pd/Fe)	Silt and clay with coarse-grained sediments	Push-Pull test	56
[b] Stabilized nZVI	Sand, silt and clay	Gravity	57
[b] Stabilized nZVI	Sand, silt and clay	Gravity	58
[a] nZVI Supported on activated carbon	Sand, silt and gravel	Injection/extraction	59
[c] LECS	Sandy loam	Pressure	60
[d] Nanofer 25S	Alluvial	Not specified	61

[a] Stabilized using an unnamed nonionic surfactant
[b] Stabilized using Carboxymethyl Cellulose (CMC)
[c] Long-Lasting Emulsified Colloidal Substrate (LECS); composed of nZVI, lactate, vegetable oil and surfactants
[d] nZVI coated with Poly Acrylic Acid (PAA)

Limited mobility in porous media has been an obstacle to more widespread implementation of nZVI at the field scale.[9, 37] This is in spite of the advances made in the development of surface coatings for improve stability (Section 2.3.3). Initially, field studies on nZVI focused on the destruction of contaminants; only briefly addressing mobility and delivery. While contaminant removal is the end goal of *in situ* remediation treatments, ensuring adequate distribution of nZVI within the treatment zone is essential. Hence, in order to find the optimal formulation capable of achieving good distribution of nanoparticles, it is instructive to review the different types of nZVI that have been used in the field. Elliott and Zhang [53] conducted the first field study with nZVI. They injected a total of 1340 L of a bimetallic nZVI suspension (Pd-nZVI) over a 2-day period. The peak total iron concentrations found in a piezometer 1.5 m from the injection well was 10 – 20 mg L^{-1}. At most, this represents ~2.7% of the lowest iron concentration injected on day 2 (0.75 g L^{-1}). Despite the limited mobility and the relatively low nZVI concentration employed, TCE concentrations declined throughout the site, only to be followed by varying degrees of concentration rebound. Subsequent field studies tested different types of nZVI, including emulsified and stabilized nanoparticles. Henn and Waddill [54] used a polymer coated nZVI doped with palladium at a site contaminated with various cVOCs. The type of polymer was proprietary and not disclosed. In this study a recirculation program within the source zone was established to increase mass transfer from sorbed and nonaqueous phases with the dissolve phase. The iron was well distributed over the treatment area, resulting in between 65 and 99 % decrease in aqueous – phase cVOC concentrations. Based on changes to the dissolved oxygen (DO) and oxidation – reduction potential (ORP), nZVI was reported to reach as far as 6 m (~20 ft) downgradient from the recirculation array. Wei et al. [52] reported travelled distances of up to 3 m (~10 ft) for a stabilized bimetallic nZVI suspension based on increases in suspended solids (SS) and total solid (TS) concentrations. Similarly, He et al. [55] observed CMC stabilized nZVI 3 m downgradient of the injection well (based on total iron) when injected at a pressure <5 psi, but only at a small fraction of the injected iron (~2%). In contrast, at 1.5 m this value was 84%. When injected by gravity, the normalized peak concentration was 15 and ~3% at 1.5 m and 3 m from the injection well, respectively. Busch et al. [59] reported a breakthrough of 12% of the colloid – supported nZVI introduced utilizing a recirculation system with two wells separated by 5.3 m. These particles were also stabilized with CMC, which has become the most common polymer employed in nZVI field studies (Table 2.2). nZVI stabilized with PAA (Nanofer 25S) has also been used and authors

reported a peak total iron concentration of 31% (C C_0^{-1}, where C_0 is the mean injected concentration of 8 g L^{-1}) at a distance of approximately 5 m.[61] Common to most of these studies, nZVI transport was inferred from changes in the subsurface geochemistry (e.g., ORP, DO) and aesthetic properties of the groundwater (e.g., color). But the use of these indirect parameters have been called into question since they do not directly confirm the presence of nZVI.[37, 62] This has led to the utilization of more sophisticated techniques, such as chromatographic [57] and spectrophotometric methods.[62] For example, Kocur et al. [57] used acid digestion to confirm the presence of Fe^0 1 m from the injection well, and it was found at 17.8% of the total iron measured. There were also no major morphological changes between the injected and recovered nanoparticles as revealed by Transmission Electron Microscopy (TEM) analysis. It is interesting to note that while initial studies used bare (or un-stabilized nZVI), inclusion of some form of stabilizer is now a standard practice during field injection. This can also be attributed to the recognition that certain polymers, such as CMC, can serve as precursory substrates for enhanced biotic dechlorination.[63]

Several factors are considered to influence nZVI transport, including particle aggregation and settling,[64, 65] composition and heterogeneity of porous media,[66-68] natural reductant demand of aquifers (NRD),[62] among others. The significance of NRD processes (e.g., reactions with water, dissolved oxygen, natural organic matter, mineral surfaces, or any other redox-active materials) on the performance of ISCR technologies is not well developed or established among researchers and practitioners (as compared to natural oxidant demand, NOD, for ISCO technologies).[9, 62] Johnson et al. [62] concluded that oxidation of the nZVI front caused by NRD processes has a significant impact on nZVI delivery. In the same way, nZVI corrosion by water, one of the major NRD processes, generates hydrogen gas,[37] which could clog the pore space [57] and limit nZVI transport. Minimizing the effect of these processes can potentially improve nZVI transport and delivery to contaminated zones.

2.4 Sulfidated Nano Zerovalent Iron (S-nZVI)

2.4.1 Background

The benefits of treating ZVI with sulfur compounds have been known to researchers for several years. Lipczynska-Kochany et al. [69] found that various sulfur compounds (including sodium sulfate – Na_2SO_4, sodium sulfide – Na_2S, ferrous sulfide – FeS, pyrite – FeS_2, and an organosulfonic acid) significantly accelerated the reactivity of metallic iron for carbon tetrachloride (CCl_4) dechlorination. Faster rates have also been reported for trichloroethelyne (TCE) after treatment of iron metal with dissolved sulfide.[70, 71] Despite early evidence that showed rate enhancement of (n)ZVI particles after induced precipitation of iron sulfides, the potential of utilizing engineered sulfidation was not extensively explored until recently. Kim et al. [72] reported a method for synthesizing zerovalent iron nanoparticles coated with iron sulfides (Fe/FeS). It consists of a modified approach to the borohydride reduction method, whereby dithionite is added to borohydride and the resulting solution is added dropwise to the iron precursor. These nanoparticles showed increased reactivity for TCE at the optimal dithionite/iron ratio. Subsequent studies have highlighted the benefits that controlled sulfidation can offer to in-situ applications.[49, 50] Sulfidation achieved with sodium dithionite, at a Fe/S ratio of 2, was able to preserve iron in its zerovalent state in an aqueous solution for more than one year, exceeding previously reported lifespans for these nanoparticles.[73] A more recent study proposed that sulfidation of nZVI with sodium sulfide or sodium dithionite could result in improved selectivity, reducing reaction with water and increasing nanoparticles' longevity.[74] The authors also noted that the degree to which the sulfur compounds were able to preserve zerovalent iron is highly dependent on the Fe/S ratio. It has also been suggested that the FeS coating formed on the surface of nZVI decreases magnetic attractions between the particles which could lead to a lower degree of aggregation.[75] Less nZVI particle aggregation and higher stability in solution has led to greater mobility in porous media.[64] The easy production and benefits offered by sulfidation led to an increased number of publications over the last five years (Figure 2.3). The key aspects to this technology will be summarized in the following sections, with an emphasis on the most recent articles.

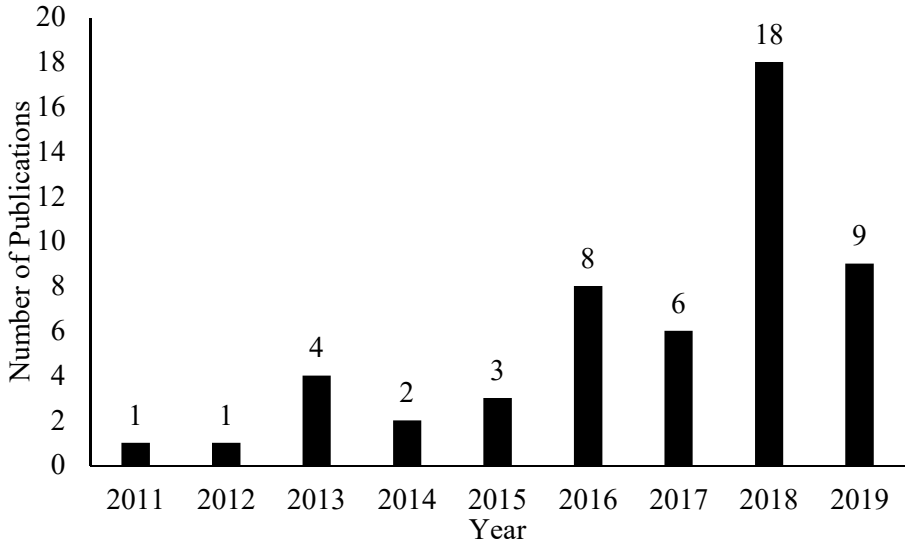

Figure 2.3 Cumulative number of peer-reviewed publications per year since 2011. Key words: sulfidation, Iron – Dithionite, S-nZVI, sulfide-modified nZVI, sulfur – modified nZVI, Fe/FeS, sulfide – coated iron nanoparticles, sulfidated nZVI or mZVI.

2.4.2 Synthesis Methods

Sulfidation is generally defined as the chemical modification of iron – based materials by lower - valent sulfur species. It can be achieved by a variety of sulfur compounds, the most common being dithionite ($S_2O_4^{2-}$) and sulfide (S^{2-}). A description of these compounds will be discussed in detail in Section 2.4.2.2. The sulfidation methods can be classified in two general categories: 1) aqueous-aqueous, and 2) aqueous-solid.[49] Elsewhere, the same processes have been categorized as one-step synthesis (aqueous-aqueous) and two-step synthesis methods (aqueous-solid) (Figure 2.4).[50] More recently the use of elemental sulfur (S^0) has also been proposed for synthesis under dry conditions in a method denoted as solid – solid (not shown in Figure 2.4).[49]

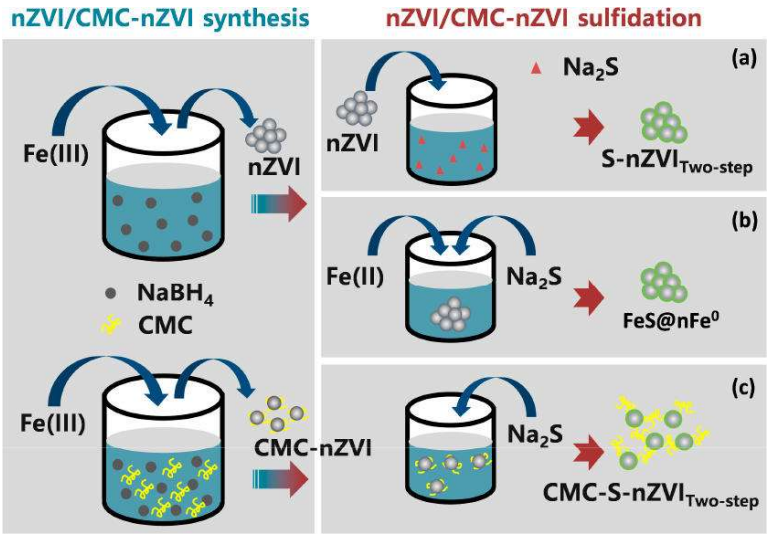

Figure 2.4 Sulfidation methods for nZVI: a) Aqueous – solid, b) Aqueous – aqueous, and c) Aqueous – solid with a stabilizing agent (Reprinted with permission from Li et al. [50] Copyright 2017 American Chemical Society).

In the aqueous-aqueous approach the sulfidating agent is mixed with borohydride before reduction of the iron salt, hence forming Fe^0 and FeS in parallel. The structure of S-nZVI was identified as a mixed core of Fe^0 and S^0, surrounded by a shell of iron oxides and flake-like particles, regarded as iron sulfides (FeS_x).[75] In the aqueous-solid approach, nZVI is first synthesized and then treated with the sulfidating agent, resulting in iron sulfides being present predominantly at the surface.[76] These two methods described above encompasses the initial and most commonly used approaches for the synthesis of S-nZVI. In addition, recent publications have employed innovative synthesis techniques to enhance material properties. These include seeded nucleation, deposition of a support, and partial reduction or resuspension of the iron salt. This section will discuss these various procedures. Details on the characterization will be discussed in Section 2.4.3.

As is the case with nZVI, fixing S-nZVI on a support can lead to greater stability in suspension and more control over the aggregate size. Supported – nZVI have been prepared with numerous materials, including silica, activated carbon, biochar, zeolites, bentonite and kaolinite, among others.[19] In contrast, studies on supported – S-nZVI to date have primarily tested biochar, albeit from different sources and under various conditions. Biochar (BC) is a porous and carbon – rich adsorbent material made from a variety of biomass residues (e.g., tea residue, straw, husk, sludge, etc.).[77] In recent years it had been used to aid in the dispersion and stabilization of engineered

nanoparticles. Biochar – supported S-nZVI (S-nZVI/BC) was prepared for the removal of Cr(VI),[78] methyl orange,[79] and nitrobenzene.[80] The supported S-nZVI/BC particles were found to be well dispersed on the BC surface as well as its channels. Xu et al. [81] prepared biochar – supported S-nZVI with a pre-treatment of phosphoric acid (H_3PO_4) to functionalize the biochar with phosphorus groups (pBC). Compared to S-nZVI/BC, this pre-treatment led to smaller well dispersed particles, labeled pBC-S-nZVI. Phosphorus groups have a strong affinity for Fe^{2+} and can improve the precipitation/adsorption of Fe^{2+} on the biochar surface. Rate enhancements were observed for the removal of the antibiotic florfenicol (FF) which was attributed to the greater dispersion of the pBC-S-nZVI. Another biochar based S-nZVI was synthesized by Pang et al. [82] for the reductive removal of U(VI) (uranium). *Dictyophora indusiate* (DI) – derived biochar was selected because of its high specific surface area, ample functional groups, and facile synthesis method. DI-S-nZVI was prepared by first mixing ferrous sulfate (Fe_2SO_4), dithionite ($S_2O_4^{2-}$) and *Dictyophora indusiate* biochar before reduction by borohydride. Enhanced removal of U(VI), as compared to S-nZVI and nZVI, was attributed to adsorptive and reductive processes derived from the abundant functional groups and FeS_x shell of DI-S-nZVI. In another study Su et al. [83] synthesized a nanorion – hybrid material utilizing a typical heterogeneous nucleation method called 'seeded nucleation.' To prepare S-nZVI, a mixture of sodium dithionite and sodium borohydride was seeded with different amounts of nano-SiO_2 and then titrated into a $FeCl_3$ solution. Nano-SiO_2 enhanced the final Fe^0 content, increased magnetization and showed high cadmium removal capacity.

Besides deposition on a support, simpler modifications to S-nZVI synthesis techniques have been developed. Duan et al. [84] partially reduced the iron salt at 1/3, 1/2 and 2/3 Fe^{2+} to Fe^0 and then added Na_2S dropwise to precipitate the remaining 2/3, 1/2 and 1/3 of Fe^{2+}. The authors stated that this method would minimize reactivity loss of the Fe^0 core during the preparation of S-nZVI. For example, in the aqueous-solid approach precipitation of FeS upon addition of the sulfidating agent depends on the corrosion of Fe^0 to generate Fe^{2+}, leading to a loss of the initial iron core. The new modified S-nZVI, labeled FeS@Fe^0, was used for the immobilization of U(VI). They reported a higher reduction rate compared to ZVI or FeS particles. Another approach that could minimize corrosion of Fe^0 during S-nZVI synthesis consists of the precipitation of FeS utilizing a secondary source of Fe^{2+}. Du et al. [85] adopted a similar method by re-suspending freshly prepared Fe^0 in a $FeSO_4$ solution, followed by addition of Na_2S. In this case, Cr (VI) uptake by these particles was

found to be superior to nZVI alone. In these two studies the rate of reaction was not compared to S-nZVI synthesized with the typical aqueous – aqueous or aqueous – solid methods. Hence, it is not yet clear if these methods would yield rate enhancements relative to other types of S-nZVI.

Other studies have altered the synthesis procedure, not necessarily to develop a new method, but with the aim of studying the influence of various groundwater constituents on reactivity. For example, Bhattacharjee and Ghoshal [86] synthesized S-nZVI in the presence of two macromolecules, humic acid (HA) and rhamnolipid (RL). nZVI was synthesized by ball milling and the sulfidation process conducted in two ways. First, nZVI was first sulfidated with sodium sulfide (Na_2S) and then contacted with RL or HA (categorized as pre-sulfidation), and second, nZVI was first contacted with RL or HA and then sulfidated (categorized as post-sulfidation). A decrease in reactivity towards TCE was observed for both methods due to inhibited deposition of sulfide on the nZVI surface and blocking of reactive sites. In the aforementioned studies the only type of iron tested was nZVI prepared with the borohydride reduction method. However, abiotic sulfidation of iron has not been limited solely to sulfidation of nZVI prepared using borohydride. Sulfidation of micro – scale ZVI (mZVI) and iron oxides represent a more recent development in this field and will be discussed next.

2.4.2.1 Sulfidation of mZVI (S-mZVI) and iron oxides

Although most of the initial focus was on nZVI, sulfidation of micro-ZVI (mZVI)[87-95] has also been attracting attention due to its ease of implementation. Gu et al. [88] developed a process to synthesize microscale sulfidated ZVI by mechanochemically mixing iron powders with elemental sulfur using ball milling. A major advantage of ball milling is that it can be conducted under dry conditions; circumventing limitations intrinsic to the aqueous phase processes (e.g., the generation of large quantities of liquid waste). The final product, labeled as S-mZVI^{bm}, exhibited reduced aggregation and homogenous distribution of Fe and S, as well as less H_2 formation when compared to unsulfidated mZVI. S-mZVI^{bm} was used for TCE dechlorination and products were consistent with a β-elimination pathway. The ball milling process has been employed for the removal of different kinds of dyes[92] and treatment of chromate (Cr(VI)).[93] Other authors have used wet methods to prepare S-mZVI. Xu et al. [87] first mixed 1 g of ZVI with a deoxygenated solution of acetic acid (HAc) and sodium acetate (NaAc) (0.2 M, pH 6) for 30 min. 1 M of Na_2S was then

injected and left to pre-equilibrate for 12 hours. S-mZVI prepared with this method showed enhanced removal of azo dye (Orange I). Subsequent studies adopted this method to evaluate the removal efficiency of S-mZVI on antimonite (Sb(III)),[89] chromate (Cr(VI)),[90, 93, 95] a combined solution of both Sb(III) and Cr(VI),[91] and an azo dye called acid red 79 (AR73).[94] Zhang et al. [94] and Jia et al. [95] both modified this technique by adding either a chelating agent or a second transition metal. Zhang et al. [94] coupled S-mZVI with EDTA (ethylenediamine tetraacetic acid). They reported enhanced removal of AR 79 due to the Fe(II)-EDTA complex formed. The use of a chelating agent like EDTA can inhibit the oxidation of Fe(II) and decrease the redox potential of the solution. Jia et al. [95] doped S-mZVI with copper by adding the particles into an aqueous solution of $CuSO_4$. Addition of Cu to S-mZVI was found to increase the sequestration capacity of Cr (VI). These last two approaches have only been applied to mZVI and not S-nZVI.

More recently sulfidation of iron oxides has attracted some interest,[96-99] but this will likely change due to the low-cost of iron oxides relative to (n)ZVI. In fact, iron oxides that are currently deemed to have low reactivity could be considered, upon sulfidation, as possible alternatives to more expensive options. In the study of Guo et al. [98] α-Fe_2O_3 was doped with S (α-Fe_2O_3/S) by a hybrid hydrothermal – calcination treatment using ferrous sulfate (Fe_2SO_4) and sodium thiosulfate ($Na_2S_2O_3$). The S – doped α-Fe_2O_3 was prepared to serve as a heterogenous Fenton catalyst and tested for the degradation of acid orange 7 (AO7), a typical azo – dye. Even though pristine α-Fe_2O_3 is less reactive than γ-Fe_2O_3, γ-FeOOH or α-FeOOH, when doped with sulfur it showed excellent heterogenous photo – Fenton reactivity under UV or visible light irradiation in the presence of H_2O_2. Subsequent work also studied sulfur – modified iron oxides for advanced oxidation processes (AOPs). Du et al. [96] prepared a type of mesoporous iron oxide modified with sulfur (MS-Fe) via a precipitation – calcination process. Oxalate ($C_2H_2O_4 \cdot 2H_2O$) was used to precipitate a mixed solution of Fe_2SO_4 and $Na_2S_2O_3$, followed by a calcination process at 300 °C for 1 hour (4 °C min^{-1}). The MS-Fe composite showed high catalytic activity for the activation of H_2O_2 to degrade bisphenol A (BPA). In a separate study, Du et al. [97] prepared a sulfur – doped iron oxide composite (S/Fe) via alkali hydro precipitation of Fe_2SO_4 and $Na_2S_2O_3$, followed by air calcination. The new S/Fe material served as an excellent peroxydisulfate (PDS) activator for the degradation of Rhodamine B (RhB). In the studies presented above sulfate and hydroxyl radicals were the main reactive species. Thus far, sulfur modified iron oxides have played an indirect role in the degradation of contaminants, serving as activators in oxidative processes. This is in sharp

contrast to typical applications of S-nZVI or S-mZVI where the sulfidated particles are the main reductant and directly responsible for the destruction of contaminants. Hence further research into the reductive capability of sulfidated iron oxides is necessary.

2.4.2.2 Sulfur Compounds

Elemental sulfur (S^0) is an inexpensive and relative stable solid. Under ambient conditions it is usually found in the form of an eight-membered ring (S_8) crystals.[100] More than 60 million tons are produced annually, mostly generated as a by-product of the hydrodesulfurization process in petroleum refining. Elemental sulfur is mostly utilized for the production of chemicals such as sulfuric acid and phosphates as well as synthetic rubber. The abundance of this element makes it an attractive option in environmental applications. Sierra-Alvarez et al. [101] used S^0 to support denitrification in a process called Sulfur-Limestone Autotrophic Denitrification (SLAD). In this process limestone is used as a buffering agent (in this study it was applied at a S^0:limestone ratio of 1:1 v/v). Results indicates S^0 can be used as an effective electron donor under anoxic conditions to support denitrification, with rates increasing concurrently with sulfur concentrations. Seidel et al. [102] compared commercially available sulfur powder ('technical sulfur') and microbially produced sulfur ('biological sulfur') for the efficiency on bioleaching of heavy metals from contaminated sediments. Biological sulfur is a by-product of the microbial treatment of sulfide-containing water (e.g., from sewage sludge treatment). Biological sulfur was found to be superior than technical sulfur for leaching of heavy metals which was attributed to its hydrophilic properties. This further emphasizes the wide range of possible sources for sulfur and its availability. To date elemental sulfur has only been utilized in the dry synthesis of sulfidated micro – scale ZVI[88, 92, 93] (solid – solid approach) and has received less attention compared to the next two options.

Dissolved sulfide (S^{2-}) exist in environmental systems mainly as hydrogen sulfide (H_2S) and bisulfide (HS^-), with minor S^{2-}.[103] In aqueous solutions, its speciation is highly pH-dependent. At acidic pH H_2S is the dominant species, followed by HS^- at neutral pH, and S^{2-} in more alkaline solutions.[104] For sulfidation of (n)ZVI, sulfide solutions are typically prepared with sodium sulfide (Na_2S), which is prone to release H_2S. Though not considered a good electron donor, H_2S behaves as such in the presence of Fe^{2+} species.[103] However, only the protonated H_2S is volatile and

considered a major health and safety hazard. Hydrogen sulfide is a toxic gas, water-soluble, and colorless; well-known for its distinct rotten egg odor. Exposure to H_2S between 2 and 15 min at concentrations above 100 to 150 ppm may cause olfactory fatigue, inhibiting the ability to smell the gas.[105] Nonetheless, sulfide remains one of the most frequently used sulfur species during sulfidation.

Dithionite ($S_2O_4^{2-}$) is a strong reductant (Eh = -1.12), widely used in the remediation industry in the *In Situ* Redox Manipulation (ISRM) technology. During ISRM, direct injection of sodium dithionite into the subsurface can result in the reduction of existing Fe(III)-(hydr)oxides to generate Fe(II)-bearing minerals as well as sustaining favorable conditions to prevent premature oxidation of Fe^{2+} (Eq. 2.5).[106, 107] Ferrous iron (Fe^{2+}) is known to be the main electron donor for TCE dechlorination on mineral surfaces.[108]

$$S_2O_4^{2-} + 2Fe^{3+} + 2H_2O \rightarrow 2SO_3^{2-} + 2Fe^{2+} + 4H^+ \quad (2.5)$$

Although dithionite is expected to be rapidly consumed in aqueous solutions, its decomposition products may also play a role in the direct treatment of contaminants. Self-decomposition of dithionite in aqueous solution yields sulfite (SO_3^{2-}), thiosulfate ($S_2O_3^{2-}$) and hydrogen ions (H^+), decreasing the pH from an initial ~6.2 to 3 – 4 (Eq. 2.6).[73, 107, 109] At basic pH values, dithionite ion dissociates into two sulfur dioxide radicals ($SO_2^{\cdot-}$) responsible for its high reactivity (Eq. 2.7).[107] In the same way, at basic pH, dithionite dissociation products (SO_3^{2-} and $S_2O_3^{2-}$) can serve as reductants upon oxidation to sulfate (SO_4^{2-}) (Eq. 2.8 and 2.9). For these reasons buffer agents are always included during field applications.[107]

$$2S_2O_4^{2-} + H_2O \rightarrow 2SO_3^{2-} + S_2O_3^{2-} + 2H^+ \quad (2.6)$$

$$4SO_2^{\cdot-} \leftrightarrow 2S_2O_4^{2-} \quad (2.7)$$

$$S_2O_3^{2-} + 5H_2O \leftrightarrow 2SO_4^{2-} + 8e^- + 10H^+ \quad (2.8)$$

$$2SO_3^{2-} + 2H_2O \rightarrow 2SO_4^{2-} + 4e^- + 4H^+ \quad (2.9)$$

A combined treatment of dithiontie and nZVI yielded increases in dechlorination rates towards 1,2-Dichloroethane (1,2-DCA), a well-known recalcitrant compound.[73] It was proposed that

dithionite could also serve as a scavenger for electron accepting compounds (e.g., O_2 or H_2O), maintaining reducing conditions favorable for nZVI. This concept is analogous to that proposed by Fan et al. [110] In this case, nZVI is proposed as the scavenger, used not for the direct reduction of target contaminants but rather for sustaining a reducing environment to favor microbial sulfate reduction.

As discussed in Section 2.3.2, sodium dithionite was proposed as the reducing agent for the synthesis of nZVI (henceforth denoted as $nZVI_D$). Ma et al. [34] studied the structure, composition and reactivity of $nZVI_D$ and concluded these are mainly composed of magnetite or ferrous sulfite, with an irregular spherical shape and edges made of thin platelets. X-ray photoelectron spectroscopy (XPS) suggest the predominance of iron species dominated by higher oxidation states but with a distinguishable peak characteristic of Fe^0 at ~707 eV. However, it was recognized that FeS_2 also exhibits similar binding energies that could interfere with that of Fe^0. $nZVI_D$ were also found to be less reactive than nZVI, as it was unable to completely dechlorinate TCE in 120 hours.[34] In contrast Sun et al. [33] reported $nZVI_D$ and nZVI as having similar reaction rates for TCE and it was concluded these particles are very thin platelet-like crystals consistent with the chemical formula Fe(II)-$HSO_3 \cdot H_2O$.

Thiosulfate has also been considered an alternative to both dithionite and sulfide. It is a weaker reductant than dithionite and readily decomposes to release elemental sulfur and sulfide (Eq. 2.10 – Eq. 2.13).[71, 111] Considering these advantages it was surprising to find that only one study used thiosulfate as the preferred reagent for preparation of S-nZVI,[112] while another study used it in combination with dithionite and sulfide for S-mZVI.[113] Limited use of thiosulfate could be partly explained by the similarities between the reactivity of S-nZVI synthesized with these three reagents.[112] This observation by Han and Yan [112] could have led other researchers to select the more widely employed sulfide or dithionite.

$$2S_2O_3^{2-} + H^+ \rightarrow HSO_3^- + SO_3^{2-} + 2S^0 \quad (2.10)$$

$$S_2O_3^{2-} + 4H_2 \rightarrow 2HS^- + 3H_2O \quad (2.11)$$

$$S^0 + H_2 \rightarrow H_2S \quad (2.12)$$

$$H_2S \leftrightarrow S^{2-} + 2H^+ \quad (2.13)$$

2.4.3 Characterization of S-nZVI

nZVI particles synthesized by the borohydride reduction method have long been recognized to possess a core – shell structure.[30, 114] The metallic iron precipitated by the reduction of the iron salt spontaneously oxidizes to form a diverse layer of iron oxides. The characteristics of this layer, its thickness, chemical composition, and physical structure depend on the synthesis process, storage conditions, and particle size. Since the surface mediates most aspects of nZVI chemistry,[31] proper manipulation of the surface can lead to improvements in reactivity and stability. In fact, one of the most interesting aspects of contaminant destruction with nZVI is the complementary nature of the core and outer layer. Proposed reaction mechanisms reflect properties from both iron oxides and metallic iron.[31] For this reason, the synthesis of multicomponent nZVI particles has been widely studied leading to the development of the sulfidation step. At the most basic level, the sulfidation step seeks to prepare multicomponent particles capable of utilizing the chemical properties of both iron sulfides and metallic iron.[72] Therefore, while the precipitation and coverage of the nZVI surface by iron sulfides is key, care must be taken to properly preserve enough metallic iron for reaction with pollutants. This section focusses on the characteristics of the core-shell structure of S-nZVI, the formation of the iron sulfide layer, and its interaction with the iron core.

The mechanism of FeS formation and precipitation during aqueous-solid sulfidation is more well-known than its aqueous-aqueous counterpart due to its analogy to sulfur-induced corrosion.[49] In the case of sulfide (S^{2-}), HS^- replaces adsorbed OH^- to then form a thin layer of FeS on the surface of Fe^0 (Eq. 2.14 – Eq. 2.16):[49]

$$Fe - OH^-_{Ads} + HS^- \leftrightarrow Fe + HS^-_{Ads} + OH^- \tag{2.14}$$

$$Fe - HS^-_{Ads} \leftrightarrow Fe - HS^+_{Ads} + 2e^- \tag{2.15}$$

$$Fe - HS^+_{Ads} \rightarrow Fe(II) - S_{1-x} + xHS^- + (1-x)H^+ \tag{2.16}$$

The mechanism would differ, however, depending on the source of sulfur. The complex chemistry of dithionite might lead to additional interactions with its sulfur decomposition products. This difference is important as the Fe^0 content remaining after sulfidation has been linked to the source of sulfur employed. It was shown that when dithionite was used instead of sulfide more Fe^0 is

converted to FeS.[16, 74] Despite the advantages offered by sulfide in this respect, its highly hygroscopic nature would pose storage and handling difficulties.[112] This makes dithionite a more practical option during field applications.

Regardless of the reagent (i.e., dithionite, sulfide or thiosulfate) the first FeS phase formed is typically amorphous or nanocrystalline mackinawite.[73, 75, 110, 115] Further transformation of the initial FeS, as well as the characteristics of the core-shell structure of S-nZVI as a whole, are dependent on the synthesis method, S/Fe ratio and sulfidation duration.[49, 50] For example, the morphology of S-nZVI differs depending on the method of sulfidation (aqueous-aqueous vs aqueous-solid). During aqueous-aqueous sulfidation, sulfur is distributed uniformly within the iron particle.[72, 75] Particles would exhibit the typical chain-like nZVI structure but with flake-like and platy structures, attributed to FeS, and a mixed core of Fe^0 and S^0.[75, 112] The outer layer contains not only FeS, but also iron oxides (FeO).[116-118] In the case of aqueous-solid sulfidation, particles possess similar morphology to traditional nZVI but with an outer shell covered by FeS precipitates.[73, 76, 97, 119] These FeS precipitates appear to be present as a laminar phase nonuniformly distributed on the surface of nZVI.[110]

Bhattacharjee and Ghoshal [120] studied the differences between the particles produced by the aqueous – aqueous (named S-nZVI$_{co}$) and aqueous – solid (named S-nZVI$_{post}$) methods using Na_2S. TEM images revealed key differences in the morphology and structures between the two of particles (Figure 2.5). Four distinct morphologies were identified: 1) needle and plate-like structures (Type I), 2) spherical particles (Type II), 3) small irregular particles (Type III), and 4) well-define (smooth) spheres (Type IV). A wider range of particles were observed with the aqueous-aqueous method. Type I – III morphologies exist in the latter, affecting the roughness of the spherical particles. The authors proposed FeS would be present not only on the nZVI surface, but also within the particles. Likewise, Su et al. [117] reported sulfur to be distributed within the whole particle using the aqueous – aqueous method; but no information on the oxidation state was provided. They proposed that various sulfur species from dithionite disproportionation (e.g., S^{2-}, SO_3^{2-}) could be incorporated into the nanoparticle as well as into the iron hydroxide flakes. This contrasts with earlier investigations of the aqueous-aqueous approach where only S^0 was reported within the particles and FeS found merely on the surface (as stated above). The difference in FeS distribution could be due to the different sulfidating agents (Na_2S vs $Na_2S_2O_4$).[120] Type IV (smooth

spheres) particles were more abundant with S-nZVI$_{post}$, followed by Type I (needle, plate-like). Unlike S-nZVI$_{co}$, the distribution of FeS did not deviate from earlier studies, with FeS structures located largely on the surface. These results demonstrate the importance of the synthesis method and sulfidating agent on the morphology and structure of the particles.

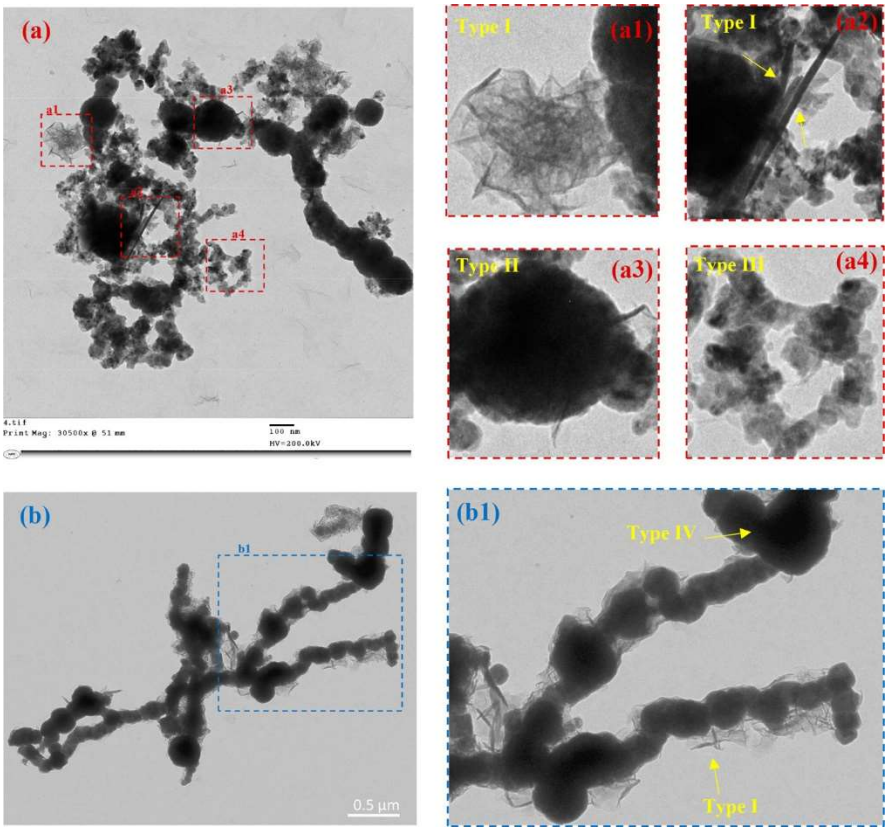

Figure 2.5 Differences in the morphologies between S-nZVI nanoparticles synthesized using a) aqueous – aqueous and b) aqueous – solid sulfidation (Reprinted with permission from Bhattacharjee and Ghoshal [120] Copyright 2018 American Chemical Society).

The structure described above is relatively consistent across the various synthesis procedures discussed in Section 2.4.2, including seeded nucleation and deposition on a support. Seeded nucleation with nano-SiO_2 accelerated iron reduction by ~19%, yielding a nanohybrid material with an Fe^0 core and a highly sulfidized layer.[83] Biochar – supported S-nZVI exhibited a clear core-shell structure, with spherical nanoparticles covered by a flake-like shell deposited on the support,[78-82] and in some cases, separate acicular phases were noted.[81] In a separate study by Bhattacharjee and Ghoshal [86], there were no differences reported in the morphology or primary

size of particles synthesized in the presence of humic acid (HA) or rhamnolipid (RL). The main differences were found to be in the aggregate sizes where particles showed significantly smaller aggregates, attributed to the electrostatic stabilization by RL and HA.

Differences in the characteristics of S-nZVI and S-mZVI arise not necessarily due to the sulfidation step, but primarily to the intrinsic differences between the nano – and micro – size ZVI. For example, typical mZVI particles used in these sulfidation studies has been characterized as roughly spherical and irregular[87, 89, 91] unlike the spherical nanoparticles described above. A common feature in the S-mZVI studies is the increase in surface roughness after sulfidation (also observed in S-nZVI studies), which is believed to contribute to its higher reactivity. Finally, a key factor to consider is the sources of iron employed. Studies on micro – scale ZVI typically employed commercial iron powder (e.g., from Alfa Aesar), whereas studies on nano – scale ZVI are predominantly synthesized by the borohydride reduction method. The different synthesis methods and storage conditions between commercial iron powder and borohydride reduced nZVI would invariably lead to differences between the structure and morphology of the particles.

2.4.4 Contaminant Transformation by S-(n)ZVI

Contaminant removal by S-(n)ZVI can occur through a series of complex processes, ranging from sorption, coprecipitation, and redox reactions. The relevant processes are contaminant specific, and in some cases, concomitant (e.g., reduction and coprecipitation can take place simultaneously). The removal capacity of S-(n)ZVI for several pollutants of concern have been evaluated and are summarized in Table 2.3, where they are first separated based on pollutant studied, and then on the different types of particles employed. As chlorinated volatile organic compounds (cVOCs) are the main contaminants of interest to this work, a more in-depth discussion on their reactivity with S-(n)ZVI to is presented below; including proposed mechanisms and influence of different geochemical conditions.

Table 2.3 Compilation of studies on abiotic Sulfidation. Unless otherwise specified all studies utilized nano-scale ZVI.

Model Pollutant	Synthesis Approach	References / Sources of Sulfur			
		Dithionite	Sulfur	Sulfide	Others
Antimonite (Sb (III))	Aqueous-solid			89[§]	
Arsenite (As (III))	Aqueous-aqueous	116			
Benzoic Acid (BA)	Aqueous-aqueous	121[a]			
Cadmium (II)	Aqueous-aqueous	118, 83, 75			
Carbon Tetrachloride (CT)	Aqueous-aqueous	122			
Chromium (Cr (VI))	Aqueous-aqueous	123, 115			
	Aqueous-solid	78		85, 95[b§], 90[§], 91[c§], 93[§]	
	Solid-solid/aqueous-solid		93[§]		
Diclofenac (DCF)	Aqueous-aqueous	117, 124			
Dichloroethane (1,2-DCA)	Aqueous-solid	73			
Dyes	Aqueous-solid	79[f]		94[d§], 87[§]	
	Solid-solid		92[§]		
Escherichia coli (E. Coli) [‡]	Aqueous-aqueous	125			
Florfenicol (FF)	Aqueous-solid	81[f]			
	Aqueous-aqueous	126			
Hexabromocyclododecane	Aqueous-aqueous	127			
Heavy Metals [†]	Aqueous-aqueous				Sulfate:128
Nitrobenzene (NB)	Aqueous-aqueous	80[f]			
Perfluoroalkyl acids	Aqueous-solid			129	
Pertechnetate	Aqueous-solid			110	
p-nitrophenol (PNP)	Aqueous-solid			119[e]	
rhodamine B	Aqueous-solid				Thioacetamide:130
Sulfamethazine	Aqueous-aqueous	131[a]			
Tetrabromobisphenol A	Aqueous-aqueous	132			
Trichloroethylene (TCE)	Aqueous-aqueous	133, 134[a], 135, 136, 72		76	
	Aqueous-solid	74		137, 86, 74	
	Aqueous-aqueous/-solid	112		120, 112	Thiosulfate:112
	Solid-solid		88[§]		
Uranium (U(VI))	Aqueous-solid	82[f]		84	

[§]Micro-scale ZVI
[†]Heavy Metal from mine tailings, including: Cu^{2+}, Zn^{2+}, Mn^{2+}, Ni^{2+}, Pb^{2+}, Ag^{+} & As^{5+}
[‡]Studied the toxicity of S-nZVI towards E. Coli
[a] S-nZVI used for persulfate activation
[b] S-mZVI doped with copper
[c] Simultaneous sequestration of Cr (VI) and Sb (III)
[d] S-mZVI coupled with EDTA
[e] Commercial nZVI (Nanofer 25 from NANOIRON Company, Czech Republic, EU)
[f] Modified with biochar

2.4.4.1 Reaction Mechanisms with Chlorinated Volatile Organic Compounds (cVOCs)

Trichloroethylene (TCE) is by far the most well-studied compound in this category. The initial interest in treating nZVI with sulfur compounds during synthesis arouse from the remarkable rate enhancements of TCE dechlorination observed by Kim et al. [72] at the optimal dithionite concentration. The surface area normalized rate constant was reported as 1.83×10^{-2} L m^{-2} h^{-1} for S-nZVI (dithionite concentration of 2 g L^{-1}) compared to 1.43×10^{-3} L m^{-2} h^{-1} for unamended nZVI and 7.34×10^{-3} L m^{-2} h^{-1} for RNIP (commercial reactive nanoscale iron particles). It was hypothesized that FeS on the nZVI surface can facilitate the conduction of electrons from the iron core to the adsorbed TCE due to the presence of delocalized electrons in the FeS layers, making them better metallic conductors than iron oxides. Henceforth, several researchers have dedicated their efforts to characterizing the products, pathways and mechanisms of TCE abiotic dechlorination by S-nZVI. Rajajayavel and Ghoshal [76] reported S-nZVI yielded lower hydrogen evolution rates than nZVI (6.95 μmol L^{-1} h^{-1} vs 2.75 μmol L^{-1} h^{-1}) while at the same time attaining higher degradation rates for TCE. The authors proposed the FeS layer enhanced local binding of TCE as a result of its higher hydrophobic nature relative to iron oxides, which would then lead to more electrons being conducted to TCE as compared to water.

Han and Yan [112] proposed an alternative hypothesis whereby sulfur poisons hydrogen recombination reactions resulting in a surface rich in adsorbed hydrogen atoms. This would slow down H_2 evolution and in turn favor reduction of chlorinated ethenes involving atomic hydrogen. According to this hypothesis surface-bound sulfur is not directly involved in the reaction, but rather has an indirect role in modifying the surface such that key reactive species are available for TCE reduction. Fan et al. [49] noted this mechanism is inconsistent with data on the effect of pH in the dechlorination rates of TCE. Furthermore, the basis for this hypothesis relied on the different reaction mechanism for carbon tetrachloride (CT) and TCE. CT dechlorination would occur through direct electron transfer from iron corrosion[138, 139] while TCE dechlorination can take place through both electron transfer and reduction by atomic hydrogen.[14, 140] After observing nearly identical dechlorination rates for CT using unamended nZVI and S-nZVI, Han and Yan [112] concluded that electron transfer through accelerated iron corrosion could not be the main cause behind the rate enhancement of S-nZVI. However, a recent study compared the efficiency of S-

nZVI, nZVI and FeS on the degradation of CT, and found S-nZVI to be the most reactive amongst all the options tested.[122] All reductants were tested at 0.5 g L^{-1} and CT at 3 mg L^{-1} for 2 hours. S-nZVI achieved more than 90% degradation, nZVI approximately 50% and no apparent decrease with FeS (no rate constants were provided). Results from this research are consistent with the previous mechanism on the catalytic effect of the FeS layer.[76]

He et al. [137] further evaluated the role of the FeS layer by comparing the reactivity of bimetallic nZVI (metals: Pd, Ni, Cu, and Ag), S-nZVI, and nZVI under 'excess' TCE conditions (TCE: 2.28 mM, particles: 0.25 g L^{-1}). Though both treatments (i.e., sulfidation and doping with a second transition metal) resulted in accelerated electron transfer from Fe^0, key differences were identified between their respective degradation mechanisms. For bimetallic nZVI (designated as Fe-Me) there was a positive correlation between the hydrogen evolution rate (HER) and the TCE dechlorination rates. This suggest the dechlorination of TCE by Fe – Me is controlled by the same factors as that of HER. After doping the nZVI with a noble or transition metal, Fe – Me bimetallic systems behave as a galvanic couple. This increases the electron transfer from Fe^0 to the metal surface *via* a galvanic effect and enhances the reduction of protons ($H^+ + e^- \rightarrow Me - H_{ads}$). Since HER in Fe – Me systems is a result of adsorbed atomic hydrogen ($\cdot H_{ads}$) combination and desorption as hydrogen gas (e.g., $Me - H_{ads} + Me - H_{ads} \rightarrow 2Me + H_2$), this indicates TCE dechlorination is also mediated by $\cdot H_{ads}$ on the metal surface. This is also consistent with the product analysis from Fe – Me (primarily 1,1-DCE and *cis*-DCE) which suggest hydrogenolysis as the major dechlorination pathway. In contrast, S-nZVI resulted in reduced HER while increasing TCE dechlorination suggesting the mechanism is not mediated by $\cdot H_{ads}$. To explain the coexisting/counterintuitive pattern between HER and TCE dechlorination, the authors proposed a two folded/parallel mechanism: 1) FeS_x facilitate the conduction of electrons to TCE, while 2) iron oxides mediate the conduction of electrons for HER. Figure 2.6 illustrates the proposed mechanism for Fe – Me and S-nZVI systems.

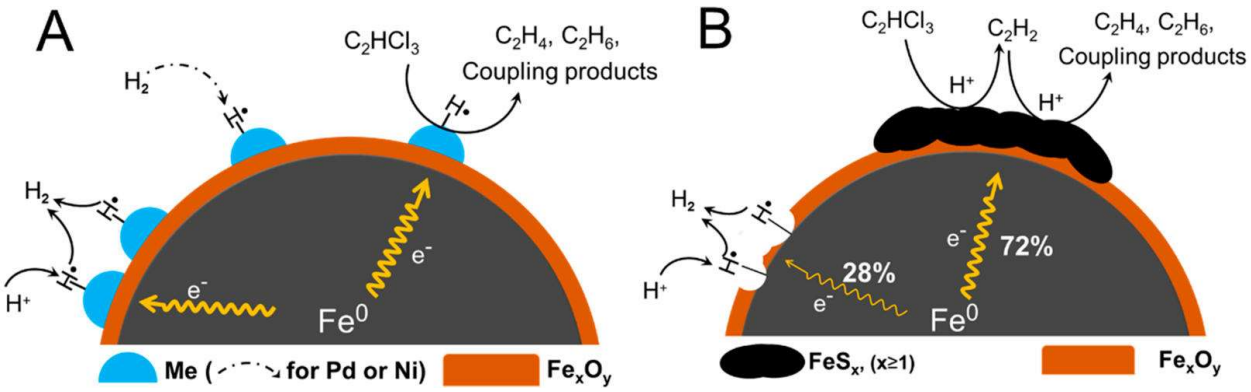

Figure 2.6 TCE dechlorination and hydrogen evolution reaction (HER) on A) Bimetallic nZVI (Fe – Me), and B) S-nZVI (Reprinted with permission from He et al. [137] Copyright 2018 American Chemical Society).

This model is corroborated by the product distribution. Acetylene constituted 70% of the daughter products for S-nZVI, and only 20% for nZVI, indicating β-elimination as a dominant pathway for both particles while at the same time pointing to differences between the mechanisms. Acetylene has also been previously detected as a product for S-mZVI[88] and S-nZVI.[76, 86, 112, 120] The previous studies also reported ethene and ethane as products, suggesting hydrogenolysis and hydrogenation also take place to some extent.

The observation that sulfidation can hinder the reaction of nZVI with water is a point of great interest and have been the subject of extended research. Some have argued the limited hydrogen production by S-nZVI is the greatest benefit of this treatment, allowing for more electrons to be directed to contaminant degradation instead of water.[16, 49, 74] This can result in increased longevity of the S-nZVI in aqueous solution, making it more persistent for abiotic dechlorination over longer periods of time. This would facilitate the treatment of more recalcitrant compounds, for instance, 1,2-dichloroethane (1,2-DCA).[73] On the other hand, even though sulfidation could not completely prevent side reactions with dissolved oxygen (DO), the FeS layer still appears to alleviate surface passivation caused by DO oxidation.[135] The effect of other common groundwater constituents on the reactivity of TCE will be discussed in Section 2.4.4.2.

The mechanism illustrated in Figure 2.6 would apply to iron nanoparticles treated with either a transition metal or sulfur, but not both. Kim et al. [133] studied the effect of metal amendments on the reactivity of S-nZVI. With the aim of investigating the interactions over a range of reduction

potentials, the metals selected were Pd, Cu, Ni, Co, and Mn. The mixed systems were prepared by reacting 2 g L^{-1} S-nZVI with 1 mM solution containing the respective metal for 10 min (categorized as 'fresh) and 15 hours (categorized as 'aged'). k_{obs} values from TCE dechlorination shows Pd, Ni, and Co enhances the reaction rate while Cu and Mn inhibits it. The different effects between these metals appeared to be related to the type of metal interaction with Fe^0, for example, reduction to their zerovalent states (Pd, Cu), a combination of reduction and complexation (Ni, Co) or sorption (Mn). Furthermore, the influence of aging on the reactivity provided substantial insights into the mechanism of TCE dechlorination. After 15 hours aging period the relative order of the rate constants between the metal amendments remained unchanged (Cu < Mn < Co < Ni), with the exception of Pd where k_{obs} decreased from $27.96 \pm 1.28 \times 10^{-2}$ min^{-1} to $6.39 \pm 0.42 \times 10$ min^{-1}. The decrease in reactivity was attributed to metal poisoning by sulfide, as reported in other studies.[73, 141-143] Though the metal amendments were mostly associated with the iron oxide on the surface of Fe^0, some appeared to be associated with the FeS, which could have grown and diversified during aging. Since Pd is a more active hydrogenation catalyst, it is therefore more susceptible to poisoning due to the prominent role of atomic hydrogen in fresh Pd – amended iron systems.[144] This points to an important consideration when evaluating bimetallic S-nZVI treatments; the possibility of multiple pathways with aging of the nanoparticles. Kim et al. [133] concluded that 1) fresh bimetallic S-nZVI reactivity will be dominated by metal catalyzed reactive hydrogen species; 2) gradual poisoning during aging will lead to a shift in the dominant pathway to one dominated by electron transfer, as revealed by electrochemical analysis. These processes might vary with the type of metal dopant used and should be taken as a generalization. Though the He et al. [137] model might be appropriate to describe basic systems of S-nZVI with TCE, these studies show that a specific mechanistic interpretation is not necessarily applicable across a range of solution compositions or even other modification approaches to nZVI. Nevertheless, a better understanding of these processes could aid in predicting the dechlorination efficiency of S-nZVI as well as inform design calculations and mass estimation of the amount of iron required to meet a specific target goal. Finally, it is important to acknowledge that elucidating the mechanism of reactivity for chlorinated ethanes and ethenes on nZVI has proven to be a challenging endeavor, sometimes with apparently irreconcilable models being proposed by researchers. Such difficulty is aggravated when nanoparticles are exposed/suspended in aqueous solutions of complex geochemistry, like

those of groundwater systems. It is therefore essential to evaluate the reactivity of S-nZVI under these conditions to better predict performance during in situ remediation.

2.4.4.2 Effect of Water Chemistry

Kim et al. [136] evaluated the reactivity of S-nZVI under conditions meant to represent groundwater systems. Experiments were conducted with TCE in synthetic water matrices containing humic acid (representing natural organic matter (NOM)), and monovalent (Na^{2+}) and divalent (Ca^{2+}, Mg^{2+}) cations. Varying the ionic strength with the monovalent cation (from 0.1 mM to 10 mM with NaCl) had negligible impact on the rate of reaction. Divalent cations, on the other hand, significantly enhanced TCE reduction rates, with solutions of Mg^{2+} being more reactive. Electrochemical studies have shown that nZVI solutions containing Ca^{2+} and Mg^{2+} showed higher corrosion currents than in DI water.[145] Therefore, higher reaction rates are expected under these conditions. The presence humic acid (HA) decreased the rate of TCE removal, possibly due to adsorption on the iron surface and blocking of reactive sites. When coupled with Ca^{2+} and Mg^{2+} the inhibitory effect of HA seemed to be offset. This was attributed to changes in the adsorption behavior of HA due to complexation with divalent cations in solution. Kim et al. [136] also conducted experiments with real groundwater from rural areas of Korea by spiking them with TCE five times at 3 hour intervals. Results indicated that the extent of S-nZVI inhibition due to groundwater constituents was less than generally observed with unsulfidated iron. Bhattacharjee and Ghoshal [86] also investigated the role of humic acid on the reactivity of S-nZVI using TCE. In this study, rhamnolipid (RL) was included as a second representative macromolecule and sulfidation done under two different scenarios labeled pre – and post – sulfidation (detailed in Section 2.4.2). Both macromolecules decreased S-nZVI reactivity to TCE, although to a different extent. For the case of pre – sulfidated nZVI with RL, only a loading of 150 mg TOC per g nZVI was needed to decrease k_{obs} from 0.055 h^{-1} to 0.015 h^{-1} whereas much higher concentrations of HA were necessary (500 to 986 mg TOC per g nZVI) to cause similar decreases. It was also observed that adsorption of RL was greater than HA, possibly explaining the difference in the degradation rates. The lower degradation rates were attributed to blocking of reactive surface sites by the macromolecules, inhibiting the reduction of TCE. In the post – sulfidation experiments, for both RL and HA, decreases in reactivity was attributed to lower deposition of sulfide on the nZVI surface. In the case of HA, uptake of aqueous sulfide was also identified as a contributing factor. Though the pre

– sulfidation method is typically used in laboratory settings, the post – sulfidation approach serves as a good model for predicting the efficiency of biogenic sulfidation after emplacement. For example, the overall effect of *in-situ* sulfidation (possible under conditions favoring sulfate reducing bacteria (SRB)) on the performance of (n)ZVI might diminish as a result of the interaction of iron with dissolve organic matter (DOC). Taken together, these studies demonstrate that typical groundwater constituents can both serve an inhibitory and/or promoting role on the performance of S-nZVI.

The influence of pH on the reactivity of zerovalent iron has been extensively investigated. Many studies have reported a decrease in reaction rate with increasing pH for both mZVI[14, 146-149] and nZVI.[1, 150, 151] This trend is generally attributed to the passivation of the iron surface by precipitation of iron oxyhydroxides at high pH, blocking reactive sites and limiting Fe^0 corrosion (Eq. 2.17 – Eq. 2.21).

$$Fe^0 + 2H_2O \rightarrow Fe^{2+} + H_2 + 2OH^- \quad (2.17)$$

$$2Fe^0 + O_2 + 2H_2O \rightarrow 2Fe^{2+} + 4OH^- \quad (2.18)$$

$$4Fe^{2+} + 4H^+ + O_2 \rightarrow 4Fe^{3+} + 2H_2O \quad (2.19)$$

$$Fe^{3+} + 3OH^- \rightarrow Fe(OH)_3 \quad (2.20)$$

$$Fe(OH)_3 + 3H^+ \rightarrow FeOOH + H_2O \quad (2.21)$$

It has also been proposed that other factors, such as the composition of the oxides formed and lower density of crevices could also influence the decrease in rate.[146] However, in the case of S-nZVI reactivity increased with increasing pH,[76, 135, 136, 146] showing an opposite trend to that observed for unamended (n)ZVI. This could be due to differences in the pH dependencies of Fe^0 and FeS mediated reductive dechlorination.[146] Increases in pH significantly increases the reactivity of FeS particles.[70, 152] To explain this trend, Butler and Hayes [152] proposed a pH-dependent acid-base equilibrium model based on the FeS surface species. It was assumed that under the experimental conditions, the FeS surface consists of hydroxide and bisulfide functional groups. These functional groups would undergo deprotonation at high pH, yielding more deprotonated surface functional groups (e.g., $\equiv FeOH_2^+ \leftrightarrow \equiv FeOH + H^+$ or $\equiv FeSH \leftrightarrow \equiv FeS^- + H^+$, where ≡

represents the bulk material). These surface species are better reducing agents due to the higher electron density on deprotonated ligands, which would increase the driving force for electron donation. This model has also been used to explain the higher reactivity observed at high pH for other iron species. Magnetite (Fe_3O_4) showed an increase in reaction rate constants with increasing pH (6 to 10) for the reduction of carbon tetrachloride (CCl_4).[153] Jeong et al. [154] studied the impact of pH on the reactivity of different Fe minerals to reduce *cis*-dichloroethylene (*cis*-DCE). For the Fe species formed, the dechlorination rate increased with pH, with the iron oxyhydroxides (green rust and γ-FeOOH) being more reactive than Fe_3O_4 or FeS.

2.5 Conclusions

Zerovalent iron is entering its third decade since its introduction as a remediation technology. From initial studies using micro-scale ZVI in the form of iron powders to more complex formulations with nano-scale ZVI, substantial progress has been made in expanding its application. Whilst ZVI-based treatments are commonly applied by practitioners for plume containment in the form of permeable reactive barriers (PRBs), deployment of nZVI is often met with skepticism. Due to its cost of production (driven mostly by borohydride) and intrinsic limitations (e.g., poor selectivity and rapid aggregation), nZVI is considered to offer a less competitive advantage over other options in the ISCR family (for instance, mZVI). This helps explain the apparent disconnect between the plethora of research articles based on bench-scale investigations and the state of the practice at the field-scale. To address these challenges multiple synthesis methods have been developed to produce more reactive and colloidally stable nanoparticles. These include most notably preparation of nanoparticles in the presence of anionic polyelectrolytes (e.g., CMC, guar gum, starch, ect.) which serve as surface coatings and provide electro-steric stabilization. Nonetheless, research on improving the selectivity of nZVI and increasing its reactive life-span are mostly lacking in comparison.

In the last eight years controlled abiotic sulfidation has emerged as a promising method capable of increasing the selectivity of nZVI. Concurrently, there has been shift in efforts amongst researchers from the study of bimetallic formulations with noble metals such as palladium (e.g., Pd-nZVI) to the treatment of nZVI with sulfur compounds of various oxidation states (e.g., S^0, $S_2O_4^{2-}$, S^{2-}). Sulfur – modified nZVI exhibits enhanced reactivity with common groundwater pollutants (e.g.,

trichloroethylene, carbon tetrachloride, 1,2-dichloroethane), less hydrogen formation in aqueous suspensions, increased longevity, and lower aggregation. Sulfidation has grown to include other iron – based materials such as S-mZVI and iron oxides. It has also expanded to incorporate other modifiers during synthesis, including biochar supported S-nZVI, copper doped S-nZVI or S-mZVI coupled with a chelator. The wide range of formulations achievable with S-nZVI (and for that matter, with ZVI particles in general) is demonstrative of the flexibility of this technology. Despite the increasing interest on this method; the fate, transport and reactivity of S-nZVI in the subsurface is largely unknown. To date, no peer-reviewed study has documented the performance of S-nZVI at the field-scale. There is also a need to better understand the transformations of S-nZVI during aging as in-situ applications sometimes requires on-site storage of the nanoparticles before injection.

2.6 References

1. Song, H.; Carraway, E. R., Reduction of chlorinated ethanes by nanosized zero-valent iron: Kinetics, pathways, and effects of reaction conditions. *Environ Sci Technol* **2005,** *39*, (16), 6237-6245.

2. Kueper, B. H.; Stroo, H. F.; Vogel, C. M.; Ward, C. H., Source Zone Remediation: The State of the Practice. In *Chlorinated Solvent Source Zone Remediation*, Kueper, B. H.; Stroo, H. F.; Vogel, C. M.; Ward, C. H., Eds. Springer New York: New York, NY, 2014; pp 1-27.

3. Soga, K.; Page, J. W. E.; Illangasekare, T. H., A review of NAPL source zone remediation efficiency and the mass flux approach. *Journal of hazardous materials* **2004,** *110*, (1-3), 13-27.

4. Stroo, H. F.; Leeson, A.; Marqusee, J. A.; Johnson, P. C.; Ward, C. H.; Kavanaugh, M. C.; Sale, T. C.; Newell, C. J.; Pennell, K. D.; Lebron, C. A.; Unger, M., Chlorinated Ethene Source Remediation: Lessons Learned. *Environ Sci Technol* **2012,** *46*, (12), 6438-6447.

5. Pankow, J. F.; Cherry, J. A., *Dense Chlorinated Solvents and Other DNAPLs in Groundwater: History, Behavior, and Remedation.* . Waterloo Press: Ontario, 1996.

6. McCarty, P. L., Groundwater Contamination by Chlorinated Solvents: History, Remediation Technologies and Strategies. In *In Situ Remediation of Chlorinated Solvent Plumes*, Stroo, H.; Ward, C., Eds. 2010; pp 1-28.

7. Chowdhury, A. I. A.; Gerhard, J. I.; Reynolds, D.; Sleep, B. E.; O'Carroll, D. M., Electrokinetic-enhanced permanganate delivery and remediation of contaminated low permeability porous media. *Water research* **2017,** *113*, 215-222.

8. Baciocchi, R.; D'Aprile, L.; Innocenti, I.; Massetti, F.; Verginelli, J., Development of technical guidelines for the application of in-situ chemical oxidation to groundwater remediation. *J Clean Prod* **2014,** *77*, 47-55.

9. Tratnyek, P. G.; Johnson, R. L.; Lowry, G. V.; Brown, R. A., IN SITU Chemical Reduction For Source Remediation. In *Chlorinated Solvent Source Zone Remediation*, Kueper, H. B.; Stroo, F. H.; Vogel, M. C.; Ward, H. C., Eds. Springer New York: New York, NY, 2014; pp 307-351.

10. Sweeny, K. H.; Fischer, J. R. Reductive degradation of halogenated pesticides. 1972.

11. Senzaki, T.; Kumagai, Y., Removal of chlorinated organic compounds from waterwater by reduction process: treatment of 1,1,2,2-tetrachloroethane with iron powder. *Kogyo Yosui* **1988,** *357*, 2 - 7.

12. Senzaki, T.; Kumagai, Y., Removal of chlorinated organic compounds from waterwater by reduction process: treatment of trichloroethylene with iron powder. *Kogyo Yosui* **1989,** *369*, 19 - 25.

13. Gillham, R. W.; Ohannesin, S. F., Enhanced Degradation of Halogenated Aliphatics by Zero-Valent Iron. *Ground Water* **1994,** *32*, (6), 958-967.

14. Matheson, L. J.; Tratnyek, P. G., Reductive Dehalogenation of Chlorinated Methanes by Iron Metal. *Environ Sci Technol* **1994,** *28*, (12), 2045-2053.

15. Tratnyek, P. G., Permeable reactive barrier of iron and other zero-valent metals. In *Chemical Degradation Methods for Wastes and Pollutants: Environmental and Industrial Applications*, Tarr, M. A., Ed. 2003; pp 371-421.

16. Fan, D.; O'Carroll, D. M.; Elliott, D. W.; Xiong, Z.; Tratnyek, P. G.; Johnson, R. L.; Nunez Garcia, A., Selectivity of Nano Zerovalent Iron in In Situ Chemical Reduction: Challenges and Improvements. *Remediation Journal* **2016**.

17. Mueller, N. C.; Braun, J.; Bruns, J.; Cernik, M.; Rissing, P.; Rickerby, D.; Nowack, B., Application of nanoscale zero valent iron (NZVI) for groundwater remediation in Europe. *Environ Sci Pollut R* **2012,** *19*, (2), 550-558.

18. Li, L.; Hu, J.; Shi, X.; Fan, M.; Luo, J.; Wei, X., Nanoscale zero-valent metals: a review of synthesis, characterization, and applications to environmental remediation. *Environ Sci Pollut R* **2016**, 1-21.

19. Stefaniuk, M.; Oleszczuk, P.; Ok, Y. S., Review on nano zerovalent iron (nZVI): From synthesis to environmental applications. *Chem Eng J* **2016,** *287*, 618-632.

20. Fang, Y.; Wen, J.; Zeng, G.; Shen, M.; Cao, W.; Gong, J.; Zhang, Y., From nZVI to SNCs: development of a better material for pollutant removal in water. *Environ Sci Pollut R* **2018**.

21. Li, S. L.; Yan, W. L.; Zhang, W. X., Solvent-free production of nanoscale zero-valent iron (nZVI) with precision milling. *Green Chem* **2009,** *11*, (10), 1618-1626.

22. Hoch, L. B.; Mack, E. J.; Hydutsky, B. W.; Hershman, J. M.; Skluzacek, I. M.; Mallouk, T. E., Carbothermal synthesis of carbon-supported nanoscale zero-valent iron particles for the remediation of hexavalent chromium. *Environ Sci Technol* **2008,** *42*, (7), 2600-2605.

23. Bystrzejewski, M., Synthesis of carbon-encapsulated iron nanoparticles via solid state reduction of iron oxide nanoparticles. *J Solid State Chem* **2011,** *184*, (6), 1492-1498.

24. Tao, N. R.; Sui, M. L.; Lu, J.; Lu, K., Surface nanocrystallization of iron induced by ultrasonic shot peening. *Nanostruct Mater* **1999,** *11*, (4), 433-440.

25. Chen, S. S.; Hsu, H. D.; Li, C. W., A new method to produce nanoscale iron for nitrate removal. *J Nanopart Res* **2004,** *6*, (6), 639-647.

26. Yoo, B. Y.; Hernandez, S. C.; Koo, B.; Rheem, Y.; Myung, N. V., Electrochemically fabricated zero-valent iron, iron-nickel, and iron-palladium nanowires for environmental remediation applications. *Water Science and Technology* **2007,** *55*, (1-2), 149-156.

27. Hoag, G. E.; Collins, J. B.; Holcomb, J. L.; Hoag, J. R.; Nadagouda, M. N.; Varma, R. S., Degradation of bromothymol blue by 'greener' nano-scale zero-valent iron synthesized using tea polyphenols. *J Mater Chem* **2009,** *19*, (45), 8671-8677.

28. Lien, H. L.; Elliott, D. W.; Sun, Y. P.; Zhang, W. X., Recent progress in zero-valent iron nanoparticles for groundwater remediation. *Journal of Environmental Engineering and Management* **2006,** *16*, (6), 10.

29. Zhang, W.-x.; Elliott, D. W., Applications of iron nanoparticles for groundwater remediation. *Remediation Journal* **2006,** *16*, (2), 7-21.

30. Sun, Y. P.; Li, X. Q.; Cao, J.; Zhang, W. X.; Wang, H. P., Characterization of zero-valent iron nanoparticles. *Adv. Colloid Interface Sci.* **2006,** *120*, (1-3), 47-56.

31. Yan, W.; Lien, H.-L.; Koel, B. E.; Zhang, W.-x., Iron nanoparticles for environmental clean-up: recent developments and future outlook. *Environmental Science: Processes & Impacts* **2013,** *15*, (1), 63.

32. Feitz, A. J.; Guan, J.; Waite, T. D. Process for Producing a Nanoscale Zero-Valent Metal. 2004.

33. Sun, Q.; Feitz, A. J.; Guan, J.; Waite, T. D., Comparison of the reactivity of nanosized zero-valent iron (nZVI) particles produced by borohydride and dithionite reduction of iron salts. *Nano* **2008,** *3*, (5), 341-349.

34. Ma, X.; He, D.; Jones, A. M.; Collins, R. N.; Waite, T. D., Reductive reactivity of borohydride- and dithionite-synthesized iron-based nanoparticles: A comparative study. *Journal of hazardous materials* **2016,** *303*, 101-110.

35. Hwang, Y.-H.; Kim, D.-G.; Shin, H.-S., Effects of synthesis conditions on the characteristics and reactivity of nano scale zero valent iron. *Applied Catalysis B: Environmental* **2011,** *105*, (1), 144-150.

36. Wang, C. B.; Zhang, W. X., Synthesizing nanoscale iron particles for rapid and complete dechlorination of TCE and PCBs. *Environ Sci Technol* **1997,** *31*, (7), 2154-2156.

37. O'Carroll, D.; Sleep, B.; Krol, M.; Boparai, H.; Kocur, C., Nanoscale zero valent iron and bimetallic particles for contaminated site remediation. *Adv Water Resour* **2013,** *51*, 104-122.

38. He, F.; Zhao, D. Y., Preparation and characterization of a new class of starch-stabilized bimetallic nanoparticles for degradation of chlorinated hydrocarbons in water. *Environ Sci Technol* **2005,** *39*, (9), 3314-3320.

39. Phenrat, T.; Saleh, N.; Sirk, K.; Tilton, R. D.; Lowry, G. V., Aggregation and sedimentation of aqueous nanoscale zerovalent iron dispersions. *Environ Sci Technol* **2007,** *41*, (1), 284-290.

40. He, F.; Zhao, D. Y., Manipulating the size and dispersibility of zerovalent iron nanoparticles by use of carboxymethyl cellulose stabilizers. *Environ Sci Technol* **2007,** *41*, (17), 6216-6221.

41. Tiraferri, A.; Chen, K. L.; Sethi, R.; Elimelech, M., Reduced aggregation and sedimentation of zero-valent iron nanoparticles in the presence of guar gum. *J Colloid Interf Sci* **2008,** *324*, (1-2), 71-79.

42. Saleh, N.; Sirk, K.; Liu, Y. Q.; Phenrat, T.; Dufour, B.; Matyjaszewski, K.; Tilton, R. D.; Lowry, G. V., Surface modifications enhance nanoiron transport and NAPL targeting in saturated porous media. *Environ Eng Sci* **2007,** *24*, (1), 45-57.

43. Schrick, B.; Hydutsky, B. W.; Blough, J. L.; Mallouk, T. E., Delivery vehicles for zerovalent metal nanoparticles in soil and groundwater. *Chem Mater* **2004,** *16*, (11), 2187-2193.

44. Busch, J.; Meißner, T.; Potthoff, A.; Oswald, S. E., Transport of carbon colloid supported nanoscale zero-valent iron in saturated porous media. *Journal of contaminant hydrology* **2014,** *164*, 25-34.

45. Phenrat, T.; Saleh, N.; Sirk, K.; Kim, H. J.; Tilton, R. D.; Lowry, G. V., Stabilization of aqueous nanoscale zerovalent iron dispersions by anionic polyelectrolytes: adsorbed anionic polyelectrolyte layer properties and their effect on aggregation and sedimentation. *J Nanopart Res* **2008,** *10*, (5), 795-814.

46. Phenrat, T.; Liu, Y. Q.; Tilton, R. D.; Lowry, G. V., Adsorbed Polyelectrolyte Coatings Decrease Fe-0 Nanoparticle Reactivity with TCE in Water: Conceptual Model and Mechanisms. *Environ Sci Technol* **2009,** *43*, (5), 1507-1514.

47. Berge, N. D.; Ramsburg, C. A., Oil-in-Water Emulsions for Encapsulated Delivery of Reactive Iron Particles. *Environ Sci Technol* **2009,** *43*, (13), 5060-5066.

48. Quinn, J.; Geiger, C.; Clausen, C.; Brooks, K.; Coon, C.; O'Hara, S.; Krug, T.; Major, D.; Yoon, W. S.; Gavaskar, A.; Holdsworth, T., Field demonstration of DNAPL dehalogenation using emulsified zero-valent iron. *Environ Sci Technol* **2005,** *39*, (5), 1309-1318.

49. Fan, D.; Lan, Y.; Tratnyek, P. G.; Johnson, R. L.; Filip, J.; O'Carroll, D. M.; Nunez Garcia, A.; Agrawal, A., Sulfidation of Iron-Based Materials: A Review of Processes and Implications for Water Treatment and Remediation. *Environ Sci Technol* **2017,** *51*, (22), 13070-13085.

50. Li, J.; Zhang, X.; Sun, Y.; Liang, L.; Pan, B.; Zhang, W.; Guan, X., Advances in Sulfidation of Zerovalent Iron for Water Decontamination. *Environ Sci Technol* **2017,** *51*, (23), 13533–13544.

51. Einarson, M. D., Multilevel ground-water monitoring. In *Practical Handbook of Environmental Site Characterization and Ground-Water Monitoring*, Nielsen, D. M., Ed. CRC Press: Boca Raton, FL, 2006; pp 808-848.

52. Wei, Y.-T.; Wu, S.-C.; Chou, C.-M.; Che, C.-H.; Tsai, S.-M.; Lien, H.-L., Influence of nanoscale zero-valent iron on geochemical properties of groundwater and vinyl chloride degradation: A field case study. *Water research* **2010,** *44*, (1), 131-140.

53. Elliott, D. W.; Zhang, W.-x., Field Assessment of Nanoscale Bimetallic Particles for Groundwater Treatment. *Environ Sci Technol* **2001,** *35*, (24), 4922-4926.

54. Henn, K. W.; Waddill, D. W., Utilization of nanoscale zero-valent iron for source remediation—A case study. *Remediation Journal* **2006,** *16*, (2), 57-77.

55. He, F.; Zhao, D.; Paul, C., Field assessment of carboxymethyl cellulose stabilized iron nanoparticles for in situ destruction of chlorinated solvents in source zones. *Water research* **2010,** *44*, (7), 2360-70.

56. Bennett, P.; He, F.; Zhao, D. Y.; Aiken, B.; Feldman, L., In situ testing of metallic iron nanoparticle mobility and reactivity in a shallow granular aquifer. *Journal of contaminant hydrology* **2010,** *116*, (1-4), 35-46.

57. Kocur, C. M.; Chowdhury, A. I.; Sakulchaicharoen, N.; Boparai, H. K.; Weber, K. P.; Sharma, P.; Krol, M. M.; Austrins, L.; Peace, C.; Sleep, B. E.; O'Carroll, D. M., Characterization of nZVI Mobility in a Field Scale Test. *Environ Sci Technol* **2014,** *48*, (5), 2862-2869.

58. Chowdhury, A. I. A.; Krol, M. M.; Kocur, C. M.; Boparai, H. K.; Weber, K. P.; Sleep, B. E.; O'Carroll, D. M., nZVI injection into variably saturated soils: Field and modeling study. *Journal of contaminant hydrology* **2015,** *183*, 16-28.

59. Busch, J.; Meißner, T.; Potthoff, A.; Bleyl, S.; Georgi, A.; Mackenzie, K.; Trabitzsch, R.; Werban, U.; Oswald, S. E., A field investigation on transport of carbon-supported nanoscale zero-valent iron (nZVI) in groundwater. *Journal of contaminant hydrology* **2015,** *181*, 59-68.

60. Sheu, Y. T.; Lien, P. J.; Chen, K. F.; Ou, J. H.; Kao, C. M., Application of NZVI-contained emulsified substrate to bioremediate PCE-contaminated groundwater – A pilot-scale study. *Chem Eng J* **2016,** *304*, 714-727.

61. Ahn, J.-Y.; Kim, C.; Kim, H.-S.; Hwang, K.-Y.; Hwang, I., Effects of oxidants on in situ treatment of a DNAPL source by nanoscale zero-valent iron: A field study. *Water research* **2016,** *107*, 57-65.

62. Johnson, R. L.; Nurmi, J. T.; Johnson, G. S. O.; Fan, D. M.; Johnson, R. L. O.; Shi, Z. Q.; Salter-Blanc, A. J.; Tratnyek, P. G.; Lowry, G. V., Field-Scale Transport and Transformation of Carboxymethylcellulose-Stabilized Nano Zero-Valent Iron. *Environ Sci Technol* **2013,** *47*, (3), 1573-1580.

63. Kocur, C. M. D.; Lomheim, L.; Molenda, O.; Weber, K. P.; Austrins, L. M.; Sleep, B. E.; Boparai, H. K.; Edwards, E. A.; O'Carroll, D. M., Long-Term Field Study of Microbial Community and Dechlorinating Activity Following Carboxymethyl Cellulose-Stabilized Nanoscale Zero-Valent Iron Injection. *Environ Sci Technol* **2016,** *50*, (14), 7658-7670.

64. Kocur, C. M.; O'Carroll, D. M.; Sleep, B. E., Impact of nZVI stability on mobility in porous media. *Journal of contaminant hydrology* **2013,** *145*, 17-25.

65. Phenrat, T.; Kim, H. J.; Fagerlund, F.; Illangasekare, T.; Tilton, R. D.; Lowry, G. V., Particle Size Distribution, Concentration, and Magnetic Attraction Affect Transport of Polymer-Modified Fe-0 Nanoparticles in Sand Columns. *Environ Sci Technol* **2009,** *43*, (13), 5079-5085.

66. Phenrat, T.; Cihan, A.; Kim, H. J.; Mital, M.; Illangasekare, T.; Lowry, G. V., Transport and Deposition of Polymer-Modified Fe-0 Nanoparticles in 2-D Heterogeneous Porous Media: Effects of Particle Concentration, Fe-0 Content, and Coatings. *Environ Sci Technol* **2010,** *44*, (23), 9086-9093.

67. Kim, H. J.; Phenrat, T.; Tilton, R. D.; Lowry, G. V., Effect of kaolinite, silica fines and pH on transport of polymer-modified zero valent iron nano-particles in heterogeneous porous media. *J Colloid Interf Sci* **2012,** *370*, 1-10.

68. Saleh, N.; Kim, H. J.; Phenrat, T.; Matyjaszewski, K.; Tilton, R. D.; Lowry, G. V., Ionic strength and composition affect the mobility of surface-modified Fe-0 nanoparticles in water-saturated sand columns. *Environ Sci Technol* **2008,** *42*, (9), 3349-3355.

69. Lipczynska-Kochany, E.; Harms, S.; Milburn, R.; Sprah, G.; Nadarajah, N., Degradation of Carbon-Tetrachloride in the Presence of Iron and Sulfur-Containing-Compounds. *Chemosphere* **1994,** *29*, (7), 1477-1489.

70. Butler, E. C.; Hayes, K. F., Factors influencing rates and products in the transformation of trichloroethylene by iron sulfide and iron metal. *Environ Sci Technol* **2001,** *35*, (19), 3884-3891.

71. Hassan, S. M., Reduction of halogenated hydrocarbons in aqueous media: I. Involvement of sulfur in iron catalysis. *Chemosphere* **2000,** *40*, (12), 1357-1363.

72. Kim, E. J.; Kim, J. H.; Azad, A. M.; Chang, Y. S., Facile Synthesis and Characterization of Fe/FeS Nanoparticles for Environmental Applications. *ACS Appl. Mater. Inter.* **2011,** *3*, (5), 1457-1462.

73. Nunez Garcia, A.; Boparai, H. K.; O'Carroll, D. M., Enhanced Dechlorination of 1,2-Dichloroethane by Coupled Nano Iron-Dithionite Treatment. *Environ Sci Technol* **2016,** *50*, (10), 5243-5251.

74. Fan, D.; O'Brien Johnson, G.; Tratnyek, P. G.; Johnson, R. L., Sulfidation of Nano Zerovalent Iron (nZVI) for Improved Selectivity During In-Situ Chemical Reduction (ISCR). *Environ Sci Technol* **2016,** *50*, (17), 9558-9565.

75. Su, Y.; Adeleye, A. S.; Keller, A. A.; Huang, Y.; Dai, C.; Zhou, X.; Zhang, Y., Magnetic sulfide-modified nanoscale zerovalent iron (S-nZVI) for dissolved metal ion removal. *Water research* **2015,** *74*, 47-57.

76. Rajajayavel, S. R. C.; Ghoshal, S., Enhanced reductive dechlorination of trichloroethylene by sulfidated nanoscale zerovalent iron. *Water research* **2015,** *78*, 144-153.

77. Wang, L.; Wang, Y.; Ma, F.; Tankpa, V.; Bai, S.; Guo, X.; Wang, X., Mechanisms and reutilization of modified biochar used for removal of heavy metals from wastewater: A review. *Science of The Total Environment* **2019**.

78. Gao, J.; Yang, L.; Liu, Y.; Shao, F.; Liao, Q.; Shang, J., Scavenging of Cr(VI) from aqueous solutions by sulfide-modified nanoscale zero-valent iron supported by biochar. *Journal of the Taiwan Institute of Chemical Engineers* **2018**.

79. Yang, L. Z.; Gao, J.; Liu, Y. Y.; Zhang, Z. J.; Zou, M. T.; Liao, Q. J. H.; Shang, J. G., Removal of Methyl Orange from Water Using Sulfur-Modified nZVI Supported on Biochar Composite. *Water Air Soil Poll* **2018,** *229*, (11).

80. Zhang, D.; Li, Y.; Tong, S.; Jiang, X.; Wang, L.; Sun, X.; Li, J.; Liu, X.; Shen, J., Biochar supported sulfide-modified nanoscale zero-valent iron for the reduction of nitrobenzene. *RSC Advances* **2018,** *8*, (39), 22161-22168.

81. Xu, J.; Cao, Z.; Wang, Y.; Zhang, Y.; Gao, X.; Ahmed, M. B.; Zhang, J.; Yang, Y.; Zhou, J. L.; Lowry, G. V., Distributing sulfidized nanoscale zerovalent iron onto phosphorus-functionalized biochar for enhanced removal of antibiotic florfenicol. *Chem Eng J* **2019,** *359*, 713-722.

82. Pang, H.; Diao, Z.; Wang, X.; Ma, Y.; Yu, S.; Zhu, H.; Chen, Z.; Hu, B.; Chen, J.; Wang, X., Adsorptive and reductive removal of U(VI) by Dictyophora indusiate-derived biochar supported sulfide NZVI from wastewater. *Chem Eng J* **2019,** *366*, 368-377.

83. Su, Y.; Adeleye, A. S.; Huang, Y.; Zhou, X.; Keller, A. A.; Zhang, Y., Direct Synthesis of Novel and Reactive Sulfide-modified Nano Iron through Nanoparticle Seeding for Improved Cadmium-Contaminated Water Treatment. *Scientific Reports* **2016,** *6*, 24358.

84. Duan, J.; Ji, H.; Liu, W.; Zhao, X.; Han, B.; Tian, S.; Zhao, D., Enhanced immobilization of U(VI) using a new type of FeS-modified Fe0 core-shell particles. *Chem Eng J* **2019,** *359*, 1617-1628.

85. Du, J. K.; Bao, J. G.; Lu, C. H.; Werner, D., Reductive sequestration of chromate by hierarchical FeS@Fe-0 particles. *Water research* **2016,** *102*, 73-81.

86. Bhattacharjee, S.; Ghoshal, S., Sulfidation of nanoscale zerovalent iron in the presence of two organic macromolecules and its effects on trichloroethene degradation. *Environmental Science: Nano* **2018**.

87. Xu, C. H.; Zhang, B. L.; Wang, Y. H.; Shao, Q. Q.; Zhou, W. Z.; Fan, D. M.; Bandstra, J. Z.; Shi, Z. Q.; Tratnyek, P. G., Effects of Sulfidation, Magnetization, and Oxygenation on Azo Dye Reduction by Zerovalent Iron. *Environ Sci Technol* **2016,** *50*, (21), 11879-11887.

88. Gu, Y.; Wang, B.; He, F.; Bradley, M. J.; Tratnyek, P. G., Mechanochemically Sulfidated Microscale Zero Valent Iron: Pathways, Kinetics, Mechanism, and Efficiency of Trichloroethylene Dechlorination. *Environ Sci Technol* **2017,** *51*, (21), 12653-12662.

89. Huang, S.; Xu, C.; Shao, Q.; Wang, Y.; Zhang, B.; Gao, B.; Zhou, W.; Tratnyek, P. G., Sulfide-modified zerovalent iron for enhanced antimonite sequestration: Characterization, performance, and reaction mechanisms. *Chem Eng J* **2018,** *338*, 539-547.

90. Shao, Q.; Xu, C.; Wang, Y.; Huang, S.; Zhang, B.; Huang, L.; Fan, D.; Tratnyek, P. G., Dynamic interactions between sulfidated zerovalent iron and dissolved oxygen: Mechanistic insights for enhanced chromate removal. *Water research* **2018,** *135*, 322-330.

91. Wang, Y.; Shao, Q.; Huang, S.; Zhang, B.; Xu, C., High performance and simultaneous sequestration of Cr(VI) and Sb(III) by sulfidated zerovalent iron. *J Clean Prod* **2018,** *191*, 436-444.

92. Wang, S.; Song, Y.; Sun, Y., Enhanced dyes removal by sulfidated zerovalent iron: Kinetics and influencing factors. *Environmental Technology & Innovation* **2018,** *11*, 339-347.

93. Li, J.; Zhang, X.; Liu, M.; Pan, B.; Zhang, W.; Shi, Z.; Guan, X., Enhanced Reactivity and Electron Selectivity of Sulfidated Zerovalent Iron toward Chromate under Aerobic Conditions. *Environ Sci Technol* **2018,** *52*, (5), 2988-2997.

94. Zhang, L.; Shao, Q.; Xu, C., Enhanced azo dye removal from wastewater by coupling sulfidated zero-valent iron with a chelator. *J Clean Prod* **2019,** *213*, 753-761.

95. Jia, T.; Zhang, B.; Huang, L.; Wang, S.; Xu, C., Enhanced sequestration of Cr(VI) by copper doped sulfidated zerovalent iron (SZVI-Cu): Characterization, performance, and mechanisms. *Chem Eng J* **2019,** *366*, 200-207.

96. Du, J. K.; Bao, J. G.; Fu, X. Y.; Lu, C. H.; Kim, S. H., Mesoporous sulfur-modified iron oxide as an effective Fenton-like catalyst for degradation of bisphenol A. *Appl Catal B-Environ* **2016,** *184*, 132-141.

97. Du, J.; Bao, J.; Fu, X.; Lu, C.; Kim, S. H., Facile preparation of S/Fe composites as an effective peroxydisulfate activator for RhB degradation. *Separation and Purification Technology* **2016,** *163*, 145-152.

98. Guo, L.; Chen, F.; Fan, X.; Cai, W.; Zhang, J., S-doped α-Fe2O3 as a highly active heterogeneous Fenton-like catalyst towards the degradation of acid orange 7 and phenol. *Applied Catalysis B: Environmental* **2010,** *96*, (1), 162-168.

99. Kumar, N.; Lezama Pacheco, J.; Noel, V.; Dublet, G.; Brown, G. E., Sulfidation mechanisms of Fe(iii)-(oxyhydr)oxide nanoparticles: a spectroscopic study. *Environmental Science: Nano* **2018**.

100. Chung, W. J.; Griebel, J. J.; Kim, E. T.; Yoon, H.; Simmonds, A. G.; Ji, H. J.; Dirlam, P. T.; Glass, R. S.; Wie, J. J.; Nguyen, N. A.; Guralnick, B. W.; Park, J.; Somogyi, Á.; Theato, P.; Mackay, M. E.; Sung, Y.-E.; Char, K.; Pyun, J., The use of elemental sulfur as an alternative feedstock for polymeric materials. *Nature Chemistry* **2013,** *5*, 518.

101. Sierra-Alvarez, R.; Beristain-Cardoso, R.; Salazar, M.; Gómez, J.; Razo-Flores, E.; Field, J. A., Chemolithotrophic denitrification with elemental sulfur for groundwater treatment. *Water research* **2007,** *41*, (6), 1253-1262.

102. Seidel, H.; Wennrich, R.; Hoffmann, P.; Löser, C., Effect of different types of elemental sulfur on bioleaching of heavy metals from contaminated sediments. *Chemosphere* **2006,** *62*, (9), 1444-1453.

103. Rickard, D.; Luther, G. W., Chemistry of iron sulfides. *Chem Rev* **2007,** *107*, (2), 514-562.

104. Loka Bharathi, P. A., Sulfur Cycle. In *Encyclopedia of Ecology*, Jørgensen, S. E.; Fath, B. D., Eds. Academic Press: Oxford, 2008; pp 3424-3431.

105. Rahnama-Moghadam, S.; Hillis, L. D.; Lange, R. A., Chapter 3 - Environmental Toxins and the Heart. In *Heart and Toxins*, Ramachandran, M., Ed. Academic Press: Boston, 2015; pp 75-132.

106. Ludwig, R. D.; Su, C. M.; Lee, T. R.; Wilkin, R. T.; Acree, S. D.; Ross, R. R.; Keeley, A., In situ chemical reduction of Cr(VI) in groundwater using a combination of ferrous sulfate and sodium dithionite: A field investigation. *Environ Sci Technol* **2007,** *41*, (15), 5299-5305.

107. Amonette, J. E.; Szecsody, J. E.; Schaef, H. T.; Gorby, Y. A.; Fruchter, J. S.; Templeton, J. C., Abiotic Reduction of Aquifer Materials by Dithionite: A Promising In-Situ Remediation Technology. In *In-Situ Remediation: Scientific Basis for Current and Future Technologies*, Gee, G. W.; Wing, N. R., Eds. Battelle Press: Columbus, OH, 1994; pp 851-881.

108. Szecsody, J. E.; Fruchter, J. S.; Williams, M. D.; Vermeul, V. R.; Sklarew, D., In situ chemical reduction of aquifer sediments: Enhancement of reactive iron phases and TCE dechlorination. *Environ Sci Technol* **2004,** *38*, (17), 4656-4663.

109. Nzengung, V. A.; Castillo, R. M.; Gates, W. P.; Mills, G. L., Abiotic transformation of perchloroethylene in homogeneous dithionite solution and in suspensions of dithionite-treated clay minerals. *Environ Sci Technol* **2001,** *35*, (11), 2244-2251.

110. Fan, D. M.; Anitori, R. P.; Tebo, B. M.; Tratnyek, P. G.; Pacheco, J. S. L.; Kukkadapu, R. K.; Engelhard, M. H.; Bowden, M. E.; Kovarik, L.; Arey, B. W., Reductive Sequestration of Pertechnetate ((TcO4-)-Tc-99) by Nano Zerovalent Iron (nZVI) Transformed by Abiotic Sulfide. *Environ Sci Technol* **2013,** *47*, (10), 5302-5310.

111. Miranda-Trevino, J. C.; Pappoe, M.; Hawboldt, K.; Bottaro, C., The Importance of Thiosalts Speciation: Review of Analytical Methods, Kinetics, and Treatment. *Crit Rev Env Sci Tec* **2013,** *43*, (19), 2013-2070.

112. Han, Y.; Yan, W., Reductive Dechlorination of Trichloroethene by Zero-valent Iron Nanoparticles: Reactivity Enhancement through Sulfidation Treatment. *Environ Sci Technol* **2016,** *50*, (23), 12992-13001.

113. Qin, H.; Guan, X.; Bandstra, J. Z.; Johnson, R. L.; Tratnyek, P. G., Modeling the Kinetics of Hydrogen Formation by Zerovalent Iron: Effects of Sulfidation on Micro- and Nano-Scale Particles. *Environ Sci Technol* **2018,** *52*, (23), 13887-13896.

114. Nurmi, J. T.; Tratnyek, P. G.; Sarathy, V.; Baer, D. R.; Amonette, J. E.; Pecher, K.; Wang, C. M.; Linehan, J. C.; Matson, D. W.; Penn, R. L.; Driessen, M. D., Characterization and properties of metallic iron nanoparticles: Spectroscopy, electrochemistry, and kinetics. *Environ Sci Technol* **2005,** *39*, (5), 1221-1230.

115. Gong, Y.; Gai, L.; Tang, J.; Fu, J.; Wang, Q.; Zeng, E. Y., Reduction of Cr(VI) in simulated groundwater by FeS-coated iron magnetic nanoparticles. *Science of The Total Environment* **2017,** *595*, 743-751.

116. Wu, D.; Peng, S.; Yan, K.; Shao, B.; Feng, Y.; Zhang, Y., Enhanced As(III) sequestration using sulfide-modified nanoscale zerovalent iron with a characteristic core-shell structure: Sulfidation and As distribution. *ACS Sustainable Chemistry & Engineering* **2018,** *6*, 3039-3048.

117. Su, Y.; Jassby, D.; Song, S.; Zhou, X.; Zhao, H.; Filip, J.; Petala, E.; Zhang, Y., Enhanced Oxidative and Adsorptive Removal of Diclofenac in Heterogeneous Fenton-like Reaction with Sulfide Modified Nanoscale Zerovalent Iron. *Environ Sci Technol* **2018,** *52*, (11), 6466-6475.

118. Lv, D.; Zhou, X.; Zhou, J.; Liu, Y.; Li, Y.; Yang, K.; Lou, Z.; Baig, S. A.; Wu, D.; Xu, X., Design and characterization of sulfide-modified nanoscale zerovalent iron for cadmium(II) removal from aqueous solutions. *Applied Surface Science* **2018,** *442*, 114-123.

119. Tang, J.; Tang, L.; Feng, H.; Zeng, G.; Dong, H.; Zhang, C.; Huang, B.; Deng, Y.; Wang, J.; Zhou, Y., pH-dependent degradation of p-nitrophenol by sulfidated nanoscale zerovalent iron under aerobic or anoxic conditions. *Journal of hazardous materials* **2016,** *320*, 581-590.

120. Bhattacharjee, S.; Ghoshal, S., Optimal design of sulfidated nanoscale zerovalent iron for enhanced trichloroethene degradation. *Environ Sci Technol* **2018**.

121. Rayaroth, M. P.; Lee, C. S.; Aravind, U. K.; Aravindakumar, C. T.; Chang, Y. S., Oxidative degradation of benzoic acid using Fe-0 - and sulfidized Fe-0-activated persulfate: A comparative study. *Chem Eng J* **2017,** *315*, 426-436.

122. Jin, X.; Chen, H.; Yang, Q.; Hu, Y. A.; Yang, Z. L., Dechlorination of Carbon Tetrachloride by Sulfide-Modified Nanoscale Zerovalent Iron. *Environ Eng Sci* **2018,** *35*, (6), 560-567.

123. Lv, D.; Zhou, J.; Cao, Z.; Xu, J.; Liu, Y.; Li, Y.; Yang, K.; Lou, Z.; Lou, L.; Xu, X., Mechanism and influence factors of chromium(VI) removal by sulfide-modified nanoscale zerovalent iron. *Chemosphere* **2019,** *224*, 306-315.

124. Song, S.; Su, Y.; Adeleye, A. S.; Zhang, Y.; Zhou, X., Optimal design and characterization of sulfide-modified nanoscale zerovalent iron for diclofenac removal. *Applied Catalysis B: Environmental* **2017,** *201*, 211-220.

125. Cheng, Y.; Dong, H.; Lu, Y.; Hou, K.; Wang, Y.; Ning, Q.; Li, L.; Wang, B.; Zhang, L.; Zeng, G., Toxicity of sulfide-modified nanoscale zero-valent iron to Escherichia coli in aqueous solutions. *Chemosphere* **2019,** *220*, 523-530.

126. Cao, Z.; Liu, X.; Xu, J.; Zhang, J.; Yang, Y.; Zhou, J. L.; Xu, X. H.; Lowry, G. V., Removal of Antibiotic Florfenicol by Sulfide-Modified Nanoscale Zero-Valent Iron. *Environ Sci Technol* **2017,** *51*, (19), 11269-11277.

127. Li, D.; Zhu, X. F.; Zhong, Y.; Huang, W. L.; Peng, P., Abiotic transformation of hexabromocyclododecane by sulfidated nanoscale zerovalent iron: Kinetics, mechanism and influencing factors. *Water research* **2017,** *121*, 140-149.

128. Cumbal, L. H.; Debut, A.; Delgado, D. A.; Jurado, C. B.; Stael, C., Synthesis of Multicomponent Nanoparticles for Immobilization of Heavy Metals in Aqueous Phase. *NanoWorld J* **2015,** *1*, (4), 103-109.

129. Zhang, Y.; Zhi, Y.; Liu, J.; Ghoshal, S., Sorption of Perfluoroalkyl Acids to Fresh and Aged Nanoscale Zerovalent Iron Particles. *Environ Sci Technol* **2018,** *52*, (11), 6300-6308.

130. Zhang, Q.; Guo, W.; Yue, X.; Liu, Z.; Li, X., Degradation of rhodamine B using FeS-coated zero-valent iron nanoparticles in the presence of dissolved oxygen. *Environ Prog Sustain* **2016,** *35*, (6), 1673-1678.

131. Dong, H.; Wang, B.; Li, L.; Wang, Y.; Ning, Q.; Tian, R.; Li, R.; Chen, J.; Xie, Q., Activation of persulfate and hydrogen peroxide by using sulfide-modified nanoscale zero-valent iron

for oxidative degradation of sulfamethazine: A comparative study. *Separation and Purification Technology* **2019,** *218*, 113-119.

132. Li, D.; Mao, Z.; Zhong, Y.; Huang, W.; Wu, Y.; Peng, P. a., Reductive transformation of tetrabromobisphenol A by sulfidated nano zerovalent iron. *Water research* **2016,** *103*, 1-9.

133. Kim, E.-J.; Kim, J.-H.; Chang, Y.-S.; Turcio-Ortega, D.; Tratnyek, P. G., Effects of Metal Ions on the Reactivity and Corrosion Electrochemistry of Fe/FeS Nanoparticles. *Environ Sci Technol* **2014,** *48*, (7), 4002-4011.

134. Dong, H.; Hou, K.; Qiao, W.; Cheng, Y.; Zhang, L.; Wang, B.; Li, L.; Wang, Y.; Ning, Q.; Zeng, G., Insights into enhanced removal of TCE utilizing sulfide-modified nanoscale zero-valent iron activated persulfate. *Chem Eng J* **2019,** *359*, 1046-1055.

135. Dong, H.; Zhang, C.; Deng, J.; Jiang, Z.; Zhang, L.; Cheng, Y.; Hou, K.; Tang, L.; Zeng, G., Factors influencing degradation of trichloroethylene by sulfide-modified nanoscale zero-valent iron in aqueous solution. *Water research* **2018,** *135*, 1-10.

136. Kim, E.-J.; Murugesan, K.; Kim, J.-H.; Tratnyek, P. G.; Chang, Y.-S., Remediation of Trichloroethylene by FeS-Coated Iron Nanoparticles in Simulated and Real Groundwater: Effects of Water Chemistry. *Ind Eng Chem Res* **2013,** *52*, (27), 9343-9350.

137. He, F.; Li, Z.; Shi, S.; Xu, W.; Sheng, H.; Gu, Y.; Jiang, Y.; Xi, B., Dechlorination of Excess Trichloroethene by Bimetallic and Sulfidated Nanoscale Zero-Valent Iron. *Environ Sci Technol* **2018,** *52*, (15), 8627–8637.

138. Li, T.; Farrell, J., Reductive dechlorination of trichloroethene and carbon tetrachloride using iron and palladized-iron cathodes. *Environ Sci Technol* **2000,** *34*, (1), 173-179.

139. Li, T.; Farrell, J., Electrochemical Investigation of the Rate-Limiting Mechanisms for Trichloroethylene and Carbon Tetrachloride Reduction at Iron Surfaces. *Environ Sci Technol* **2001,** *35*, (17), 3560-3565.

140. Farrell, J.; Melitas, N.; Kason, M.; Li, T., Electrochemical and Column Investigation of Iron-Mediated Reductive Dechlorination of Trichloroethylene and Perchloroethylene. *Environ Sci Technol* **2000,** *34*, (12), 2549-2556.

141. Lim, T. T.; Zhu, B. W., Effects of anions on the kinetics and reactivity of nanoscale Pd/Fe in trichlorobenzene dechlorination. *Chemosphere* **2008,** *73*, (9), 1471-1477.

142. Agarwal, S.; Al-Abed, S. R.; Dionysiou, D. D., A feasibility study on Pd/Mg application in historically contaminated sediments and PCB spiked substrates. *Journal of hazardous materials* **2009,** *172*, (2-3), 1156-1162.

143. Lin, C. J.; Liou, Y. H.; Lo, S. L., Supported Pd/Sn bimetallic nanoparticles for reductive dechlorination of aqueous trichloroethylene. *Chemosphere* **2009,** *74*, (2), 314-319.

144. Xie, Y.; Cwiertny, D. M., Chlorinated Solvent Transformation by Palladized Zerovalent Iron: Mechanistic Insights from Reductant Loading Studies and Solvent Kinetic Isotope Effects. *Environ Sci Technol* **2013,** *47*, (14), 7940-7948.

145. Turcio-Ortega, D.; Fan, D. M.; Tratnyek, P. G.; Kim, E. J.; Chang, Y. S., Reactivity of Fe/FeS Nanoparticles: Electrolyte Composition Effects on Corrosion Electrochemistry. *Environ Sci Technol* **2012,** *46*, (22), 12484-12492.

146. Tamara, M. L.; Butler, E. C., Effects of iron purity and groundwater characteristics on rates and products in the degradation of carbon tetrachloride by iron metal. *Environ Sci Technol* **2004,** *38*, (6), 1866-1876.

147. Chen, J.-L.; Al-Abed, S. R.; Ryan, J. A.; Li, Z., Effects of pH on dechlorination of trichloroethylene by zero-valent iron. *Journal of hazardous materials* **2001,** *83*, (3), 243-254.

148. Deng, B. L.; Burris, D. R.; Campbell, T. J., Reduction of vinyl chloride in metallic iron-water systems. *Environ Sci Technol* **1999,** *33*, (15), 2651-2656.

149. Alowitz, M. J.; Scherer, M. M., Kinetics of nitrate, nitrite, and Cr(VI) reduction by iron metal. *Environ Sci Technol* **2002,** *36*, (3), 299-306.

150. Song, H.; Carraway, E. R., Reduction of chlorinated methanes by nano-sized zero-valent iron. Kinetics, pathways, and effect of reaction conditions. *Environ Eng Sci* **2006,** *23*, (2), 272-284.

151. Liu, Y. Q.; Lowry, G. V., Effect of particle age (Fe-o content) and solution pH on NZVI reactivity: H-2 evolution and TCE dechlorination. *Environ Sci Technol* **2006,** *40*, (19), 6085-6090.

152. Butler, E. C.; Hayes, K. F., Effects of Solution Composition and pH on the Reductive Dechlorination of Hexachloroethane by Iron Sulfide. *Environ Sci Technol* **1998,** *32*, (9), 1276-1284.

153. Danielsen, K. M.; Hayes, K. F., pH Dependence of Carbon Tetrachloride Reductive Dechlorination by Magnetite. *Environ Sci Technol* **2004,** *38*, (18), 4745-4752.

154. Jeong, H. Y.; Anantharaman, K.; Hyun, S. P.; Son, M.; Hayes, K. F., pH impact on reductive dechlorination of cis-dichloroethylene by Fe precipitates: An X-ray absorption spectroscopy study. *Water research* **2013,** *47*, (17), 6639-6649.

Chapter 3

3 Fate and Transport of Sulfidated Nano Zerovalent Iron (S-nZVI): A Field Study

3.1 Introduction

Nano zerovalent iron (nZVI) is the most commonly applied nanomaterial for water and soil remediation[1] with several field studies and an increasing number of field-scale applications across Europe and North America.[2-4] Successful remediation projects using nZVI based technologies rely on the delivery of the nanoparticles to the targeted area and the establishment of a treatment zone. Despite advances in the design of nZVI, key technical challenges remain, limiting its more widespread acceptance as a viable and competitive remediation technology.[5, 6] These challenges mainly include poor selectivity and low subsurface mobility. Though the development of stabilizers[7-14] has led to its increased mobility,[15] limited research has been conducted to improve the selectivity of nZVI and to decrease its reaction with natural reductant demand (NRD) processes in the subsurface. Most notably, these include hydrogen evolution reactions (HER) with water (Eq. 3.1):

$$Fe^0 + 2H_2O \rightarrow Fe^{2+} + 2OH^- + H_2 \quad (3.1)$$

Decreases in hydrogen evolution rates have been observed after treating nZVI with lower valent forms of sulfur compounds (i.e., sulfidation), indicating that the reaction with water is inhibited to some extent.[5, 6, 16, 17] This has led to improvements in the longevity[16] and selectivity[6] of nZVI particles. For example, during a sulfidated nZVI (S-nZVI) treatability study, 63% of the iron was still in the zerovalent state after 400 days.[16] Sulfidation of nZVI has increased the removal efficiency of target pollutants (e.g., trichloroethelyne (TCE),[17-21] 1,2-dichloroethane (1,2-DCA),[16] tetrabromobisphenol,[22] 4-nitrophenol,[23] diclofenac,[24] and metal ions,[25-27]). Sulfidation methods can be classified as aqueous-aqueous or aqueous-solid, depending on when the sulfur compound is introduced to the synthesis solution.[21, 28] These methods have been reported to yield particles with varying physico-chemical and structural properties but almost similar reactivity in

dechlorinating TCE.[21] It has also been reported that sulfidation decreases magnetic attractions between the particles which decreases aggregation and sedimentation.[24, 26] Among the various sulfidation precursors tested so far,[28] sodium dithionite ($Na_2S_2O_4$) has been widely used in remediation applications (e.g., In Situ Redox Manipulation (ISRM)).[29]

Despite the increasing number of laboratory-based S-nZVI studies, no study has yet investigated field-scale S-nZVI transport. A number of studies have reported success related to the injectability and mobility of traditional polymer-coated nZVI at the field scale,[30-33] however, there is a need to assess the field applicability of emerging reactive formulations, such as S-nZVI. This study presents a field-scale demonstration showing the subsurface mobility of carboxymethyl cellulose (CMC) stabilized and $Na_2S_2O_4$ doped S-nZVI suspension. The specific objectives of this study were to: 1) scale up and develop an on-site field-scale S-nZVI synthesis method, 2) investigate changes to in-situ geochemistry following S-nZVI injection, 3) quantify in-situ S-nZVI transport, and 4) characterize field-synthesized S-nZVI suspension before injection and in the multi-level monitoring wells after injection. This study builds upon our previous understanding of nZVI field studies[30, 31, 34] by investigating the horizontal as well as vertical distribution of the injected solution, providing the first highly spatially-resolved characterization of S-nZVI suspension during subsurface transport.

3.2 Materials and Methods

3.2.1 Site Description

Field work was conducted in Sarnia, Ontario at a site adjacent to a demolished chlorinated solvents production facility. A description of the site can be found elsewhere.[31] In short, the study area is composed of a porous, non-native sandy material emplaced along a utility corridor within the native clay. Eight multi-level monitoring wells and one injection well (NIW) were installed. Each multi-level monitoring well consisted of seven color-coded intervals 0.305 m apart, with each having a screen length of 0.127 m (Figure 3.1). The screens were installed within a range of 2.9 to 4.9 meters below ground surface (bgs). During drilling, well logs were obtained for transects corresponding to the wells NA3, NIW, NA1, and NB2. NA4 could not be logged due to its very loose sand, but this well is known to be sandy backfill due to its proximity to a sump that was

emplaced in 2010. Figure 3.1 shows a plan and a cross-sectional view of well locations including a legend denoting the color codes for multiple well levels. This configuration was selected to maximize capturing of horizontal as well as vertical extent of S-nZVI breakthrough, downgradient of the injection well.

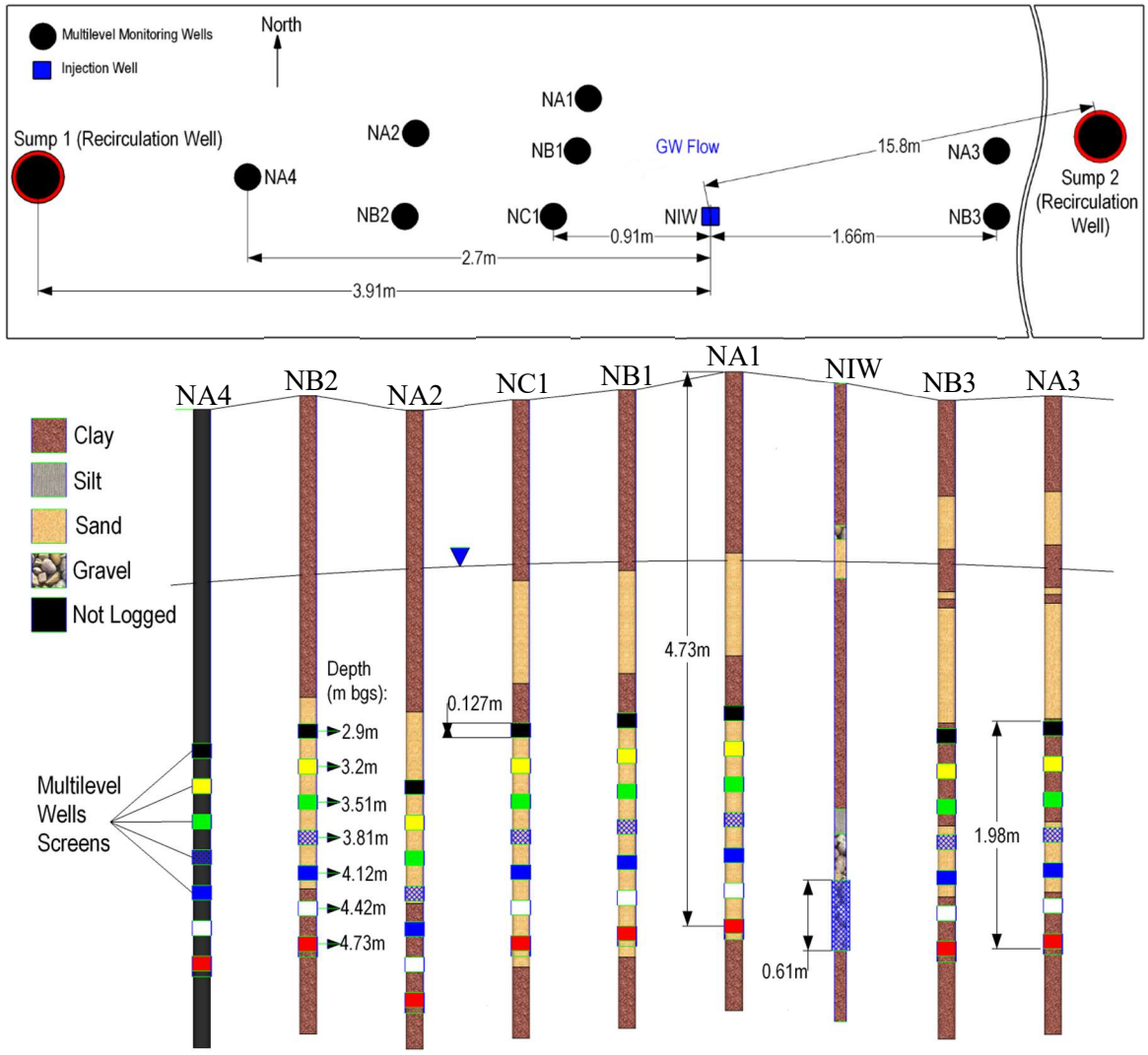

Figure 3.1 Plan and cross-sectional view of the study area. The injection well is denoted as NIW.

3.2.2 S-nZVI Synthesis and Injection

620 L of S-nZVI, stabilized with 0.8% w/v CMC, were synthesized on site in 4 distinct batches (155 L each). The mass and volume of each reagent used for the synthesis is reported in Appendix A (Table A.1). All reagents were dissolved in deoxygenated, deionized water. nZVI suspension was prepared by reducing ferrous sulfate (A&K Petrochem Ind. Ltd., Vaughn, ON) with sodium borohydride (GFS Chemicals Inc., Columbus, OH) in a process modified and optimized for field applications.[30-32, 35] Anoxic conditions were maintained by continuously purging the solutions and the headspace with high purity nitrogen gas (Praxair Canada Inc., Sarnia, ON). The freshly synthesized nZVI suspension was then treated with sodium dithionite (Alfa Aesar, Ward Hill, MA) to yield final dithionite and nZVI concentrations of 22 mM and 18 mM (1 g L^{-1}), respectively.

Large scale on-site synthesis of S-nZVI with dithionite can present unique health and safety (H&S) challenges and considerations. Though dithionite decomposition products can generate hydrogen sulfide (H_2S)[36] it has never been reported during the ISRM application in the field. However, during a preliminary S-nZVI synthesis trial for the current study, H_2S (6-7 ppm) was detected near the vicinity of the synthesis barrel after adding dithionite, although not near the breathing zone. Generation and off-gassing of H_2S might have come from the reaction of dithionite/decomposition products with the excess hydrogen gas (H_2) formed from the borohydride hydrolysis and/or during the nZVI synthesis process. Borohydride is typically added in stoichiometric excess (four times the amount needed) for rapid and uniform growth of nZVI particles.[37] To ensure sufficient time for the nucleation of nZVI particles and to allow the dissipation of H_2 gas to minimize the H_2S formation during the on-site synthesis, the nZVI suspension was continuously mixed for about an hour before adding dithionite. The final S-nZVI suspension was mixed for at least one hour before injecting into the subsurface. Because of the potential of H_2S generation in large quantities during the aqueous-aqueous sulfidation (as a result of direct reaction with borohydride) process, the aqueous-solid method is recommended as the preferred sulfidation approach for the on-site synthesis of S-nZVI when using dithionite.

S-nZVI suspension was injected by gravity over 16 hours, maintaining a constant head in the injection well. Injection rates ranged between 0.85-1 L min^{-1}. The hydraulic gradient was

controlled for 32 hours by using two recirculation wells (3.91 m downstream and 15.8 m upstream of injection well, Figure 3.1) to increase the advective flux throughout the study area.

3.2.3 Sample Collection and Analytical Methodology

With the exception of NB1 and NB2, for which all the intervals were monitored, groundwater monitoring targeted depths between 4.12 and 4.42 m bgs. This corresponded to the blue and white intervals at the majority of the wells (Figure 3.1). Locations of greater depth were not sampled (e.g., the red interval at 4.73 m bgs) due to the proximity of the source zone. To allow for the simultaneous sampling of all selected wells and intervals, a multiple-port set up was constructed. Quality assurance / quality control field protocols were followed including notes recording observations in the field, using dedicated and decontaminated sampling equipment, and minimizing the aeration during sample collection. All samples were collected in duplicate or triplicate in pre-cleaned laboratory supplied bottles with suitable preservatives. All bottles were clearly labeled with a designated sample identifier number, analytical parameters, and date and time of sampling. The samples were immediately stored in insulated coolers with ice packs to maintain low temperatures and shipped to the laboratory as soon as possible, noting the recommended maximum holding times.

Geochemical parameters, including oxidation-reduction potential (ORP) and pH, were measured using a water quality analyzer (YSI 556 MPS, Yellow Spring, OH). Colloidal stability of nZVI suspension was determined for the samples collected before and after addition of dithionite, using a UV-Vis spectrophotometer (Helios Alpha, Thermo-Fischer, Waltham, MA). Measurements were taken at 508 nm for 88 hours at 10 min intervals. It should be noted that batch samples were vacuum sealed immediately after collection, to minimize oxidation during transportation to the laboratory and storage before analysis (6-24 hours). The UV-Vis absorption spectra were also obtained for nZVI and S-nZVI suspensions from synthesis batches and for selected MW samples in the wavelength range of 200-900 nm. Zeta (ζ) potential and effective hydrodynamic diameter (quantified by Dynamic Light Scattering (DLS)) for the samples from synthesis batches and selected monitoring wells were determined using a Zeta Plus particle analyzer (BIC, Brookhaven, Holtsville, NY) and Zeta Plus software. To determine the particle size and morphology of the nanoparticles, transmission electron microscopy (TEM) analysis was conducted in both bright

(Philips CM10 TEM, Philips Electronics, Eindhoven, Netherlands) as well as dark (FEI Titan 80-300 TEM, FEI Technologies Inc., Oregon, USA) field modes along with selected area electron diffraction (SAED). Samples were prepared by diluting the nanoparticle suspensions with deoxygenated water and then a drop of the diluted sample was dried on a 400 mesh Formvar/Carbon copper grid (Tedpella Inc., Redding, CA) in the anaerobic glove box. Elemental composition of these samples was determined by energy dispersive x-ray spectroscopy (EDS) using the INCA detector (Oxford Instruments, Abingdon, UK) attached to the FEI Titan TEM. Samples for total iron, sulfur and boron were digested and diluted with hydrochloric acid (HCl) or nitric acid (HNO_3) and then analyzed using inductively coupled plasma-optical emission spectroscopy (ICP-OES, Varian Vista-Pro Axial, Agilent, Santa Clara, CA). Analysis for sulfate was performed using a high-performance liquid chromatograph (HPLC) equipped with a conductivity detector (Model 432, Waters, Milford, MA), a 4.6 × 50 cm IC-Pak Anion column (#Wat007355) and 12% acetonitrile in water eluent.

3.3 Results and Discussion

3.3.1 Horizontal Mobility

The S-nZVI suspension was quite mobile with significant transport to NA4-Blue and NA3-White, 2.7 m downgradient and 1.66 m upgradient from the injection well, respectively, at the first sampling time of 4.75 hours (Figure A.1). With time, increased total iron concentrations were also quantified in two other downgradient monitoring wells at a distance of 0.86 m (NB1-White) and 0.9 m (NC1-White) from the injection well. The highest total iron concentration was detected in NB1-White at 18 hours after the start of injection, reaching 8.8% of the total injected iron concentration (Figures 3.2a, A.1, & A.2a).

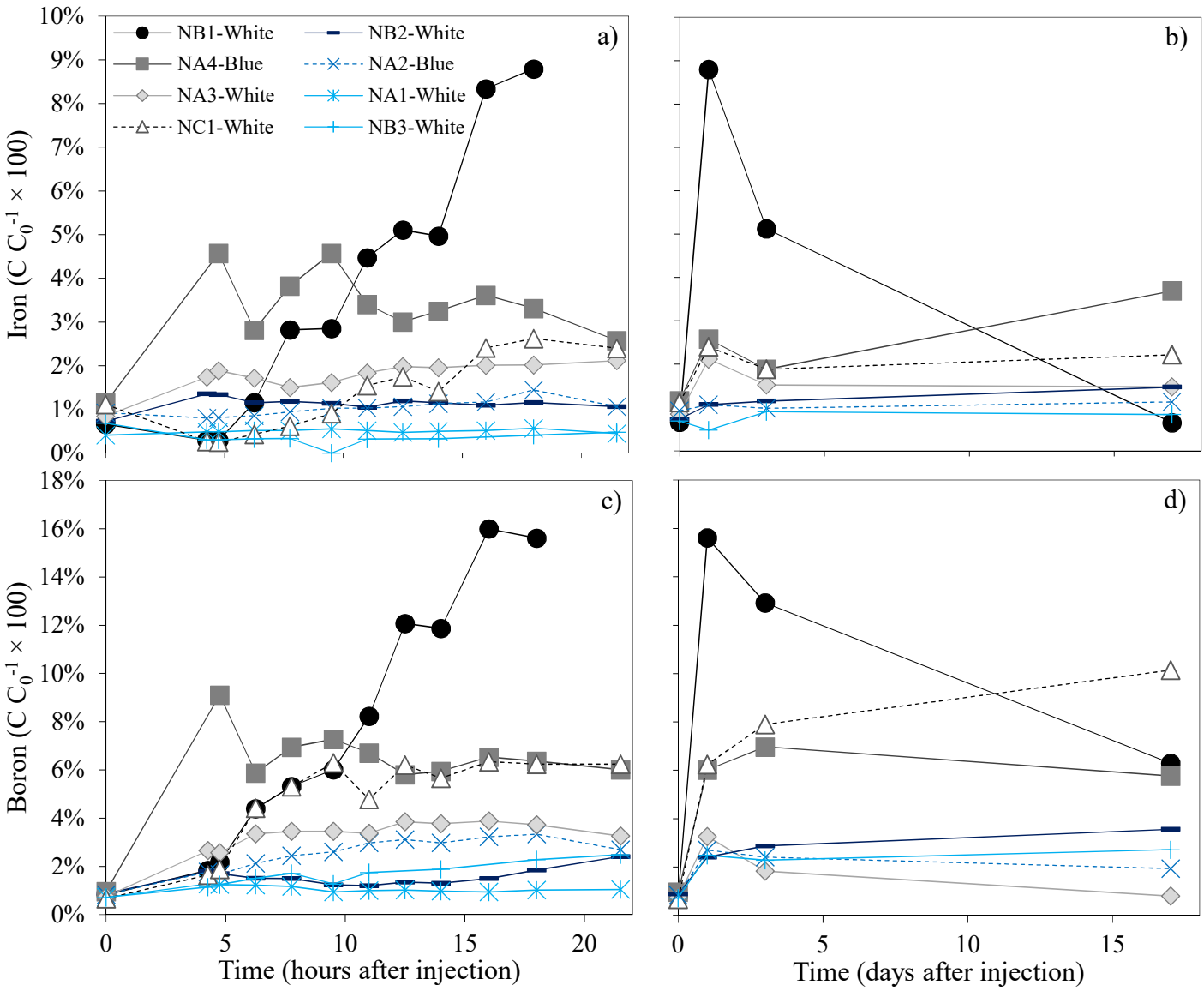

Figure 3.2 Percent of iron and boron with respect to the initial suspension (C_{0_Fe} = 14.9 mmol L^{-1} & C_{0_B} = 37.7 mmol L^{-1}) a & c) during and b & d) after injection. Initial time refers to background samples collected 28.5 hours prior.

In these four wells, sulfate, total sulfur and total boron concentrations often followed a similar trend as total iron (Figure A.2a-d). Notable 'upgradient' migration of the S-nZVI suspension to NA3-White might be due to the localized gradient caused by the injection well. Higher iron concentrations at NB1-White, NA4-Blue, NA3-White and NC1-White are also clearly illustrated in Figure 3.3 where all the sampled wells are compared for their Fe to B molar ratio (Fe/B) based on the Fe/B ratio (~0.39) of injected S-nZVI suspension. Boron and iron would undergo dispersion,

diffusion and dilution but only iron particles are presumed to be removed from the aqueous phase due to filtration. Boron is stable in aqueous environments and can be found as the boric acid (H_3BO_3) and the borate anion (e.g., $[BO_3]^{3-}$) (pKa = 9.25) species.[38] Uncharged boric acid is the dominant species found in most of the natural water systems and its surface adsorption is deemed unlikely due to the direct competition with water for available surface sites.[39, 40] It has been shown that boron is conserved during groundwater transport and can be considered as a conservative tracer under many conditions.[38, 40] However, it must be acknowledged that sodium borate can be precipitated on the outer layer of the nZVI particle during its synthesis with borohydride.[41] It is possible that some boron might have retained in this manner and the boron concentrations reported herein are an underestimation. For this reason, boron is rather operationally defined as a conservative tracer in this study. Therefore, deviation from the calculated Fe/B ratio, represented by a straight line in Figure 3.3, corresponds to the extent of retention of iron particles during transport to each well. Figure 3.3 shows that approximately 50% of the iron particles were retained during subsurface transport. Mobility results from this study are an improvement when compared to the previous traditional nZVI injections in the sandy media. For example, nZVI was detected only 1 m downstream of another injection well[31] in a previous trial at the current site. Another study conducted in an engineered aquifer reported only 4% of the total injected iron at a well 1 m downstream.[35] One reason for improved mobility could be the reduced interparticle magnetic attractive forces which would lead to sedimentation (discussed in Section 3.4.5).

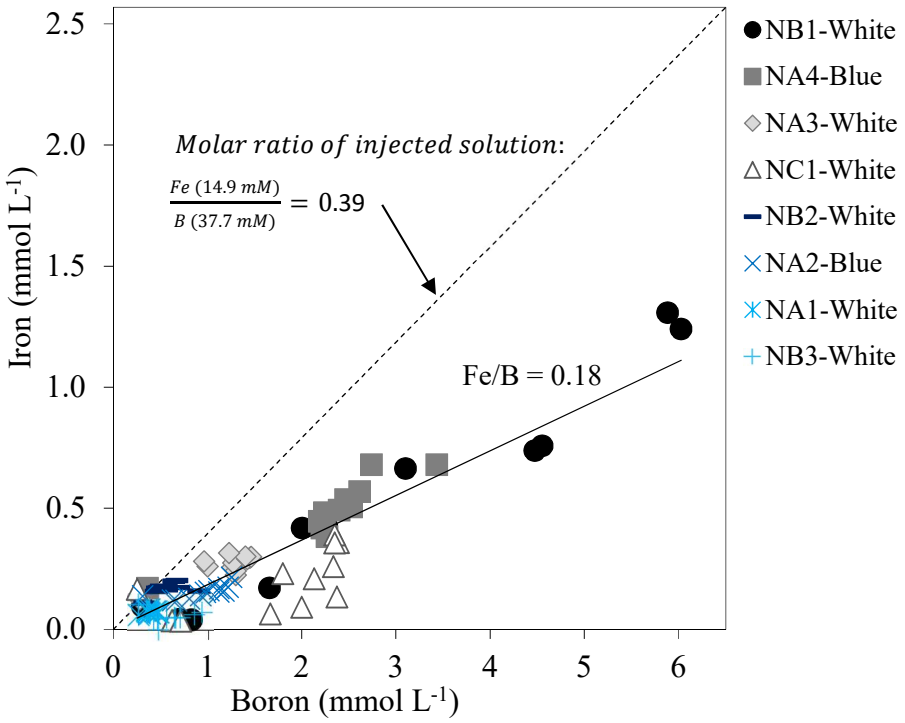

Figure 3.3 Iron and boron concentrations up to 22 hours. Dashed and solid lines represent the molar ratio of initial suspension and metal concentrations in groundwater, respectively.

Normalizing iron breakthrough to boron (obtained by calculating the area under the C C_0^{-1} vs time curve) enables quantification of the extent of S-nZVI particle retention. 53.4% and 55.9% particle breakthrough was observed at NA4-Blue and NA3-White, the wells further upstream and downstream (Figure A.3). Good particle mobility was also observed at the other monitoring locations. For example, normalized breakthrough of 46.9% and 30.1% was quantified at NB1-White and NC1-White, respectively. Using a similar normalization approach, He et al. [30] reported 37.4% iron breakthrough in a well 1.5 m away from the injection point. Kocur et al. [31] reported a peak breakthrough of 75% when normalized to a tracer, before decreasing to 50% for most of the injection period in a well 1 m downstream of the injection well. Busch et al. [42] injected activated carbon supported CMC-nZVI into a sandy aquifer and estimated 12.5% travelled (0.74 mg/L) to the extraction well but did not report tracer breakthrough data, making comparison difficult. This analysis should be used cautiously when both iron and boron are found in low concentrations. For example, NB2-White would seem to yield the highest transport, with 73.6% breakthrough based on the normalized Fe/B areas (Figure A.3), even though concentrations of iron did not exceed

1.4% (0.2 mmol L^{-1}) of the injected solution (Figure 3.2 & A.2). NA2-Blue, NA1-White and NB3-White were not considered in this discussion due to similarly low concentrations of iron and boron (Figure 3.2 & A.2).

S-nZVI transport was also quantified at 3 and 17 days after injection. Temporal changes in iron concentration were sometimes non-monotonic. Following the cessation of injection, iron concentrations decreased for NA3-White, NA4-Blue and NC1-White on day 3 (Figure 3.2). Similarly, the iron concentrations also decreased for NB2-Green, NB2-Blue, and all the intervals of NB1 (Table A.2). However, on day 17, concentrations remained relatively constant for NA3-White, NC1-White and NB2-Blue; increased for NA4-Blue, NB2-Green and NB2-Clear; and decreased for all the intervals of NB1 from Black to White (Figure 3.2, Table A.2). Increases in concentration from day 3 to day 17 at NA4-Blue may be due to the preferential transport of iron from the injection well, which still had retained high concentration of S-nZVI suspension, under a natural gradient. There is also evidence suggesting that preferential flow paths connect the injection well to NA4-Blue. S-nZVI particles were first observed at NA4-Blue, 4.75 hours after the start of the injection (Figure 3.2 & A.1). Given that NA4-Blue is the furthest monitoring well (Figure 3.1), it is suspected that site heterogeneities, including preferential flow paths, allowed the S-nZVI suspension to initially bypass NC1-White and NB2-White. 2D laboratory studies[43] as well as field injections[31, 32] have reported that polymer modified nZVI suspensions preferentially travel through the more conductive hydraulic pathways. The sharp decrease on day 17 at NB1, which is closest to the injection well, is likely affected by similar processes as well as particle deposition on the porous media.[31] It is important to note that the relatively high iron concentrations on day 3 represent a significant improvement in the stability of the particles when compared to previous field trials. For example, Kocur et al. [31] reported a decrease in the normalized iron concentration from an average of 50% during the injection period to 7.8% 16 hours after the injection was stopped.

3.3.2 Vertical Migration and Visual Observations

Concentrations of both iron and boron increased with depth in the NB1 well, with the highest recorded in the direct pathway of the injected suspension (i.e., 4.4 – 4.5 m bgs) (Figures 3.4a-b). The color of the NB1-White groundwater sample was found to be dark black (image not shown), further supporting the highest concentrations of iron at this location. The presence of S-nZVI suspension was also clearly visible in the upper levels of NB-1 (Figure A.4b), indicating that particles travelled vertically (~1.7 m), up to the Black interval which is 2.9 m bgs. For NB2, located 1.78 m from the injection well, the highest concentrations were measured at the Blue interval (i.e., 4.1 – 4.2 m bgs) at 21.25 hours, also visually indicated by the dark black color of the NB2-Blue groundwater sample. The metal concentrations were lower in the Clear interval (just above the Blue interval) as compared to the NB2-Green, with no significant change in the iron concentrations at the Yellow and Black intervals (Figure 3.4c). A similar trend was observed visually where NB2-Green has a darker black color than NB2-Clear (Figure A.4b). This could be due to the subsurface heterogeneity and preferential flow paths. In contrast, significant increase in boron concentrations were quantified at the Yellow and Black intervals of the NB2 well. The presence of boron at the upper most intervals suggests that iron particles were retained during vertical transport of the injected solution to these sampling points. Though iron concentrations were not measured for all the levels for NA4, the dark black color of groundwater samples indicates that the S-nZVI suspension had travelled vertically upwards even to the uppermost level of this well (Figure A.4b). Similarly, the upward migration of S-nZVI has been visually noticed for NC1 and NA3 up to Green and Clear intervals respectively. Other studies have also reported vertical migration of ZVI/nZVI.[44, 45]

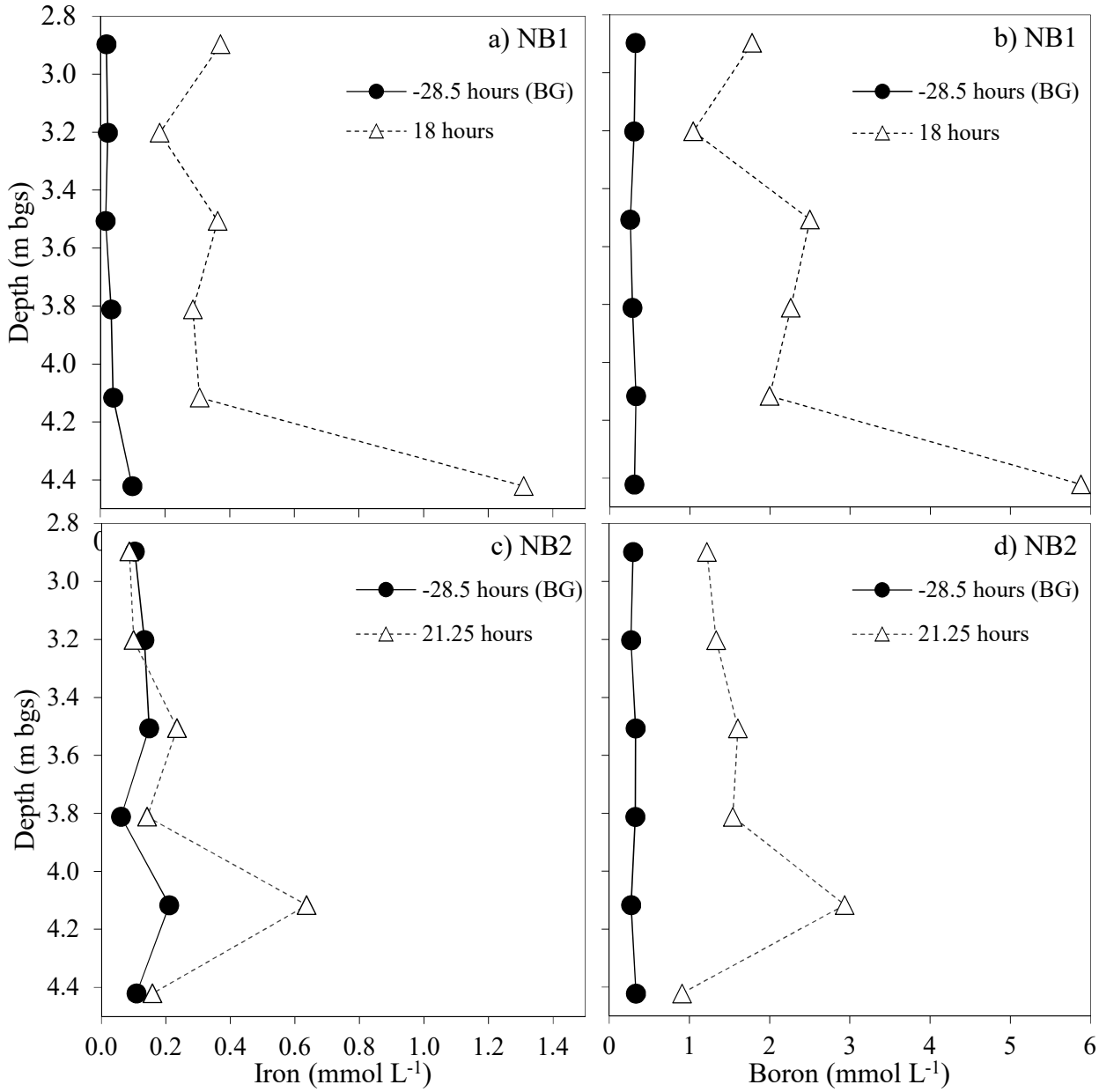

Figure 3.4 a & c) Iron and b & d) boron concentrations versus depth for the NB1 and NB2 well. Each data point denotes a depth interval from top to bottom: 1) Black (2.9 m), 2) Yellow (3.2 m), 3) Green (3.51 m), 4) Clear (3.81 m) 5) Blue (4.12 m) and 6) White (4.42 m).

Particles also remained in suspension at the Blue and Clear levels of NB1 at day 3 and day 17 (Figure A.4c). Presence of injected suspension is also clearly visible in NA4-Blue, NC1-White, NB1-White, NB3-White, and NB3-Blue on day 17 (Figure A.4d). In fact, suspended particles remained near the vicinity of the injection well for months following the injection period, as observed from a sample collected at 196 days (Figure A.4e), with 13.8% of the injected iron remaining.

3.3.3 Changes in Groundwater pH and ORP

In this study the pH did not change significantly at any of the monitoring wells and remained near neutral (7.0 ± 1.0) throughout the injection period (Figure A.5). Though pH is expected to increase due to the corrosion of iron by water,[4] other nZVI field studies have reported less than anticipated increases.[31, 46, 47] This suggests that dilution of the injected suspension and the buffering capacity of the subsurface media would also moderate the effect of nZVI on the groundwater pH. For S-nZVI, formation of an FeS coating limits corrosion by water[17] and could be partly responsible for the nearly constant pH measurements.

ORP was measured for discrete samples using a conventional platinum (Pt) electrode. During S-nZVI injection, a sharp drop in ORP was observed for NA4-Blue, NA3-White, and NB2-White at t = 4h (Figure A.6) which aligned with the arrival of S-nZVI suspension at these locations (Figure A.1). There was also a gradual decrease in the ORP for NB1-White and NC1-White. The lowest ORP (-175 mV) was recorded for NA4-Blue, six hours after injection. This was followed by NA3-White at -155 mV. Due to time constraints in the field, it was not possible to allow for enough equilibration time for all ORP measurements. Therefore, for some cases including NB1-White, measurements were recorded within 5-10 minutes and actual ORP values might be much lower than reported here. Decrease in ORP was concurrent with the iron and sulfate breakthrough, as shown in Figure A.7 for NB1-White. These results indicate a significant influence of the S-nZVI injection on the aquifer geochemistry. However, the decrease in the ORP was not as noticeable as reported in the previous field studies.[31, 35, 47] Changes in ORP are a function of the redox couples contributing to the measured mixed potentials (E_{mix}) in the system,[48] and not merely of the nZVI concentration. For nZVI suspensions, the major redox couples are H_2/H^+ and dissolved Fe^{2+}/Fe^{3+} species.[48, 49] To a lesser degree, other half reactions contributing to the E_{mix} are reduced S and B.[48]

Past research has reported lower H_2 evolution for S-nZVI during its corrosion by water and after acidification.[6, 17, 50] Inhibition of hydrogen evolution reactions (HER) has been attributed to surface coverage of Fe^0 by FeS, possibly by limiting access to water reactive sites.[51, 52] In current study, this could also partly be due to the consumption of H_2, if any generated, by excessive sulfur compounds in the system. Dithionite undergoes rapid self-decomposition to yield thiosulfate, sulfite and bisulfite ions which can react with H_2. Thus, the relatively mild decrease in ORP in the current study might be due to the lower generation of H_2 in the S-nZVI treatment as compared to the pristine nZVI. The Fe^{2+} speciation and concentrations would also be different for the S-nZVI treatment compared to pristine nZVI.[16, 17] Moreover, nZVI adsorption on the electrode and the type of electrode also play a significant role in the ORP measurements.[35, 49]

3.3.4 Characterization

3.3.4.1 TEM-EDS

Detailed particle characterization can be used to help elucidate operative transport processes as well as evaluate changes to nZVI particles due to sulfidation and subsurface transport.

TEM-EDS analysis of nZVI (before sulfidation) suspension from synthesis batch shows that particles were primarily small discrete spheres and mainly composed of iron (Figure A.8). However, larger irregular structures representing iron (oxy)(hydr)oxides were also present. Though the synthesis vessels were constantly purged with nitrogen, some level of oxidation is to be expected during the field synthesis. The SAED pattern for nZVI consists of diffused rings indicating its amorphous structure.

TEM micrographs of S-nZVI from the synthesis batches suggest that particles with two different morphologies were present following the sulfidation process (Figures A.9-A.10). Most of the particles were small discrete spheres which resembled the nZVI particles from the unsulfidated nZVI suspension (Figure A.8a). These particles, with an average size of 90 ± 13 nm (n = 82), were also found to be similar in size to those previously reported for the field-synthesized nZVI.[31] Han and Yan [21] also reported that the appearance of spherical particles in S-nZVI, formed during treatment of nZVI with thiosulfate, was akin to that of the unmodified nZVI. The presence of oxygen, observed in the EDS scans of the smaller particles, indicates that peripheral oxidation by

water might have resulted in the formation of an iron oxide coating (Figures A.9-A.10). There was low, or in some cases, no sulfur (S) present in these nZVI-like particles indicating either the presence of a small amount of FeS_X or their complete absence. This suggests that a major portion of S-nZVI suspension was still comprised of nZVI-like particles, which would mainly be Fe^0. Nunez Garcia et al. [16] found most of the iron to be still preserved in the zerovalent state after nZVI sulfidation. Han and Yan [21] also detected the presence of Fe^0 in their S-nZVI particles after thiosulfate treatment. The SAED pattern (Figure A.10) for nZVI-like particle in the S-nZVI shows that the rings are sharper and more distinct than that for the original nZVI (Figure A.8). Also some spots can be clearly seen in the S-nZVI sample. This suggests that the amorphous nZVI particles have started turning crystalline in S-nZVI. The second type of particles was larger flake-like structures (Figures A.9-A.10), composed mainly of iron and sulfur, with an average particle size of 505.2 ± 81.4 nm (n = 11). These were comparatively fewer in number (Figure A.9b). These particles were neither observed in the unsulfidated nZVI suspension (Figure A.8) from the current study nor in the samples from the previous nZVI field trial conducted at this site.[31] The morphology of these particles suggests that FeS_X distribution on some of the nZVI particles did not occur uniformly to form the typical core-shell structure.[25] Rather these particles were either overgrown into FeS_X flakes and/or the Fe^0 core was abundantly covered by the flaky FeS_X shell.[25, 26, 53-55] There is also a possibility that the few iron (oxy)(hydr)oxide particles present in the unsulfidated nZVI suspension would have transformed to FeS_X after dithionite addition.

Particles recovered from NB1-White and NB1-Clear (~0.86 m from NIW) were similar in morphology to those found in the injected S-nZVI suspension (Figures 3.5 a-c), possessing both spherical and flake – like structures. In a previous nZVI trial at the same site, Kocur et al. [31] also did not notice any significant morphological changes between the injected particles and those recovered from the monitoring well. Figure 3.5 shows that the nZVI-like particles, present as small discrete spheres (≥100 nm size), had either low or no sulfur content as depicted in the EDS spectra S1, S2 and S4. The EDS spectra of larger flake-like particles, showing significant S peaks along with Fe, indicate the presence of FeS_X phase (Figure 3.5 & A.11). These distinct FeS_X particles were also easily found in the NB1-Blue, NB2-Green and NB2-Clear (the latter two ~ 1.78 m from NIW) (Figures A.11-A.12). However, the small nZVI-like particles were not easily detectable in these monitoring well samples. The lower iron concentrations in these samples might have made it difficult to locate these particles during TEM analysis. These particles could also have

oxidized/sulfidized or retained as nZVI but aggregated into larger clusters. For example, a TEM image of NB1-Blue shows the presence of small spherical nZVI-like particles which are clustered together and covered by a thick sheet of possibly FeS_X (Figure A.11a-1). TEM-EDS data indicates that particles in the monitoring well samples, collected at 18 and 72 hours after injection, are similar to those collected from the original S-nZVI synthesis batches. SAED pattern for the NB1-Clear (Figure A11b Inset) shows well-defined spots in visible rings indicating polycrystalline nature of the particles.

It was interesting to see that the samples collected from NIW, at 196 days after the injection, were still black in color indicating the stability of the injected suspension (Figure A.4e). Over time, exposure to oxygenated water from upstream would result in the oxidation of iron sulfides. However, the ORP data shows that reduced conditions were still prevalent at this site (Figure A.6). The presence of Fe^{3+}, Cl^- and SO_4^{2-} would also favor the sulfide oxidation.[56, 57] In Figure A.13, TEM images show the presence of nano-spheres, plate-like particles, and larger flake-like structures presumably representing iron oxides, oxyhydroxides and sulfides. An et al. [58] reported the formation of lepidocrocite (γ-FeOOH) and magnetite (Fe_3O_4) from oxidative dissolution of amorphous FeS. Formation of akaganéite (FeO(OH,Cl)) was observed during the oxidation of iron sulfides from chloride-rich sulfidic sediments.[56] The presence of Cl peaks in the EDS spectra of NIW suggests the formation of FeO(OH,Cl) and sulfur peaks indicate the presence of sulfides (Figure 3.5 – EDS spectra S6 & S7). During oxidation, FeO(OH,Cl) might have coated the surface of FeS_X to form FeS_X-FeO(OH,Cl), thus suppressing further oxidation of FeS_X.[59] Moreover, the black color of suspension also suggests the presence of iron sulfides and/or Fe^{II} oxides (FeO, Fe_3O_4). Fe^{III} oxy(hydr)(oxides), if present, might be a minor species.

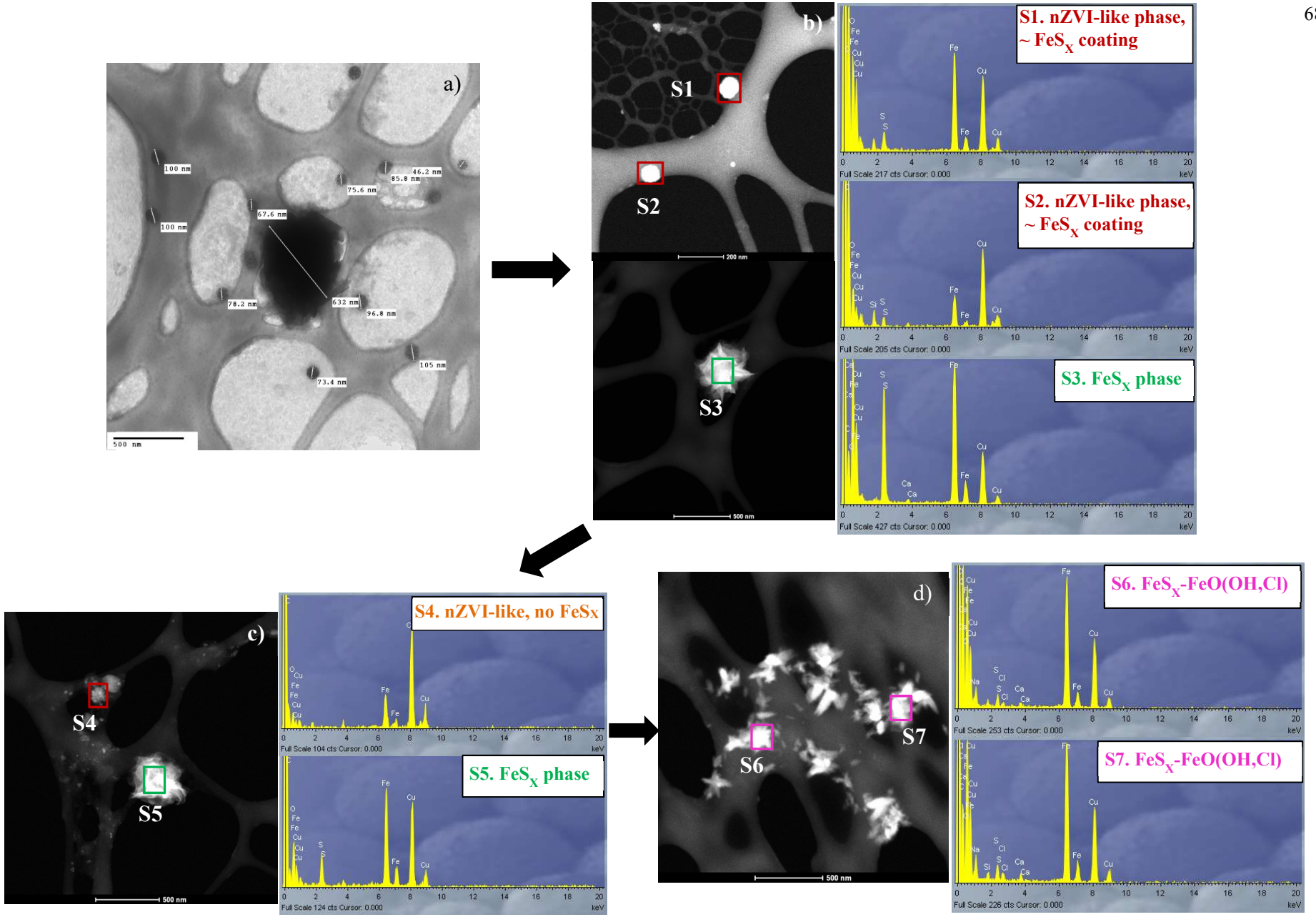

Figure 3.5 TEM and EDS of a) Synthesis batch, b) NB1-White at t = 18 h, c) NB1-Clear at t = 72 h, and d) NIW at t = 196 d after injection.

3.3.4.2 UV – Vis Spectra

Figure A.14a shows the absorbance spectra for nZVI, S-nZVI and NB1. Spectra for all the samples, collected from other monitoring wells during active injection, did not deviate from the one for NB1 well (Figure A.14b). Therefore, NB1 was chosen as a representative sample for comparison with nZVI and S-nZVI. The absorbance of nZVI gave small peaks between 300 and 372 nm, followed by a uniform decline up to 900 nm. In contrast, the S-nZVI spectrum sharply declined between 290 to 310 nm and then gradually decayed from 310 to 900 nm. The spectrum obtained from NB1 resembles that of S-nZVI, though with a lower intensity. It is also interesting to note that the NB2-Blue spectrum is of higher intensity and resembles the S-nZVI spectrum quite well. NB2-Blue was one of the samples with the darkest black color (Figure A.4b) and its concentration increased from a background value of 210 µM to 637 µM at the end of the injection (Table A.2).

To further compare these particles to the injected S-nZVI, another groundwater sample from NB1 was intentionally oxidized in the laboratory (labeled '$NB1_{ox}$') by exposing it to air. The $NB1_{ox}$ spectrum differs from the S-nZVI and unoxidized NB1, showing a more gradual decrease up to 550 nm, and very little absorbance afterwards. This data supports results from TEM micrographs suggesting the recovered samples from monitoring wells were similar to the injected S-nZVI suspension, experiencing minimal oxidation along the traveled distance from the injection well.

3.3.4.3 Particle Size Distribution (PSD)

TEM provides information about the inner electron-dense metal core and excludes the outer CMC layer. Thus, DLS was used to quantify the hydrodynamic diameter which includes both the metal particle as well as its outer CMC layer yielding the overall size of the particle. The hydrodynamic diameter of unsulfidated nZVI was 355.8 ± 1.8 nm with a monomodal particle size distribution (PSD) (Figure A.15a). However, the PSD changed to bimodal after addition of dithionite indicating the presence of two types of particles (Figure A.15b). These results are in alignment with the findings from the TEM analysis. For the multimodal PSD, the calculated hydrodynamic diameter does not give accurate particle size information. Thus, the DLS data for the samples with bimodal distributions is discussed in terms of size range rather than the median or mean diameter. The size of smaller particles for S-nZVI ranged from 357.4 to 438.7 nm which is close to the

hydrodynamic diameter of unsulfidated nZVI particles. The size of larger particles ranged from 881 to 1038 nm. Similarly, the MW samples also showed a bimodal distribution supporting the presence of smaller nZVI-like particles along with the larger FeS_X structures, as shown in TEM analysis (Figure A.15c-d). Some differences in the DLS sizes of smaller particles, for MW samples from the S-nZVI, could be due to the variability associated with the field sampling. However, the size of larger particles for MW samples was significantly greater than that of S-nZVI particles. This could be due to the formation of some larger clusters as seen in the TEM micrographs for MW samples.

3.3.4.4 Zeta (ζ) Potential

Zeta (ζ) potential values for the unsulfidated nZVI in the synthesis batches (-51.8 ± 0.98 mV, Figure A.16) were consistent with those in the literature,[15, 60, 61] whereas an increase was observed after adding dithionite. ζ-potential for the S-nZVI from synthesis batches was -44.89 ± 2.39 mV, close to the values reported for S-nZVI in past research.[17, 26, 62] This increase in ζ-potential can be attributed to the transformation of some Fe^0 to FeS_X. Another influencing factor could be the presence of dithionite and its decomposition products in the S-nZVI suspension, affecting its ionic strength. The average ζ-potential for multiple monitoring well samples collected during injection was -20.37 ± 1.27 mV (Figure A.16), which is less than half of the measured ζ-potential for the injected S-nZVI suspension. This differs from the study of Kocur et al. [31] where the particles recovered from monitoring well had similar ζ-potential (-48.3 ± 2.3 mV) to that of the synthesis batches (-49.2 ± 1.5 mV). The smaller ζ-potential observed for monitoring well samples in the current study could be due to the increased transformation of Fe^0 to iron sulfides during subsurface transport (Figure 3.5).

3.3.5 Colloidal Stability

Particle stability is a prerequisite for optimal nZVI delivery to the contaminated source zones as the settling of nZVI particles in the synthesis vessel, before injection, would limit the mass delivered to the subsurface.[15] In the current study, 50.5% of the unsulfidated nZVI, synthesized on site, aggregated and settled after 72 hours (Figure A.17). This is consistent with the sedimentation curves from a similar study where only 50% of the nZVI remained in the suspension at 24-32 hours

after on-site synthesis.[31] In contrast, only 7.7% sedimentation was observed for the on-site synthesized, dithionite-treated nZVI (i.e., S-nZVI) after 72 hours (Figure A.17). This data suggests that the injected S-nZVI particles would stay suspended for longer periods in the groundwater, increasing their mobility and delivery to the contaminated areas. Recent studies have suggested that sulfidation of nZVI can effectively inhibit its aggregation and sedimentation.[24, 26, 63, 64] The rate of aggregation depends on a range of factors including particle concentration, Fe^0 content, particle size distribution, and also the thickness of adsorbed polymer in the case of stabilized nZVI.[43] The rate of aggregation increases with increasing particle concentration and saturation magnetization.[65] In typical field applications, the nZVI particle concentration is quite important as the delivery of sufficient Fe^0 content for remediation purposes is essential, thus, leading to the application of relatively high nZVI concentrations (1 – 10 g/L).[3] These concentrations can lead to pore clogging, limiting the mobility of nZVI particles.[65-67] However, the influence of the magnetic properties of nZVI cannot be neglected. Within the core-shell structure of nZVI, the content of Fe^0 dictates the magnitude of inter-particle magnetic attractions.[43, 65, 67] It has been proposed that decreasing the Fe^0 content (oxidation to less magnetic particles) decreases nZVI agglomeration and favors its transport, resulting in enhanced mobility.[43] The greater stability of S-nZVI has been attributed to the lower magnetic attractions between iron sulfides (FeS_X).[26, 63] For example, Gong et al. [64] reported a decrease in the saturation magnetization from 165.6 emu/g for nZVI to 78.0 emu/g for S-nZVI. Thus, the decreased aggregation and sedimentation of S-nZVI in this study can be attributed to the decrease in Fe^0 content and the formation of iron sulfides, resulting in lower inter-particle magnetic attractions.

3.4 Conclusions

CMC-stabilized S-nZVI was successfully synthesized on-site by the borohydride reduction method and aqueous-solid sulfidation with sodium dithionite. To minimize health and safety concerns associated with side reactions between chemical precursors, it is recommended to work near the stoichiometry amount necessary for borohydride and to optimize the concentration of dithionite (by S/Fe ratio) for the intended application. For field-scale synthesis of relatively large quantities of S-nZVI, it is suggested to perform an aqueous-solid sulfidation over an aqueous-aqueous approach in order to reduce the possible generation of H_2S. In the present study, the suspension was mixed for 1 to 2 hours to allow time for the dissipation of any H_2S generated. TEM

images of S-nZVI synthesis batches revealed the presence of both discrete spherical nZVI particles as well as larger flake-like structures, associated with iron sulfides. S-nZVI was found to possess better colloidal stability than nZVI which could possibly contribute to its better transport in the subsurface. Approximately 620 L of S-nZVI was fed under gravity into a sandy aquifer by an injection well. S-nZVI suspension was mobile in the subsurface, achieving good horizontal and vertical distribution throughout the study area, with detection in multiple monitoring wells both downstream and upstream of the injection well. Travel distances ranged from 0.9 m to at least 2.7 m, which was the location of the farthest monitoring well. TEM-EDS analysis confirmed the presence of both nZVI-like as well as FeSx flaky structures in the MW samples, similar to those identified in the S-nZVI synthesis batches. This is further supported by the DLS analysis which showed a bimodal particle size distribution for the MW samples, similar to S-nZVI. In-situ geochemistry, especially changes to parameters such as ORP and pH, were not as noted as in previous studies. Results reported herein demonstrate S-nZVI is highly mobile at the field scale and stable under subsurface conditions.

3.5 References

1. Stefaniuk, M.; Oleszczuk, P.; Ok, Y. S., Review on nano zerovalent iron (nZVI): From synthesis to environmental applications. *Chem Eng J* **2016,** *287*, 618-632.

2. Karn, B.; Kuiken, T.; Otto, M., Nanotechnology and in Situ Remediation: A Review of the Benefits and Potential Risks. *Environ Health Persp* **2009,** *117*, (12), 1823-1831.

3. Mueller, N. C.; Braun, J.; Bruns, J.; Cernik, M.; Rissing, P.; Rickerby, D.; Nowack, B., Application of nanoscale zero valent iron (NZVI) for groundwater remediation in Europe. *Environ Sci Pollut R* **2012,** *19*, (2), 550-558.

4. O'Carroll, D.; Sleep, B.; Krol, M.; Boparai, H.; Kocur, C., Nanoscale zero valent iron and bimetallic particles for contaminated site remediation. *Adv Water Resour* **2013,** *51*, 104-122.

5. Fan, D.; O'Carroll, D. M.; Elliott, D. W.; Xiong, Z.; Tratnyek, P. G.; Johnson, R. L.; Nunez Garcia, A., Selectivity of Nano Zerovalent Iron in In Situ Chemical Reduction: Challenges and Improvements. *Remediation Journal* **2016**.

6. Fan, D.; O'Brien Johnson, G.; Tratnyek, P. G.; Johnson, R. L., Sulfidation of Nano Zerovalent Iron (nZVI) for Improved Selectivity During In-Situ Chemical Reduction (ISCR). *Environ Sci Technol* **2016,** *50*, (17), 9558-9565.

7. He, F.; Zhao, D. Y., Manipulating the size and dispersibility of zerovalent iron nanoparticles by use of carboxymethyl cellulose stabilizers. *Environ Sci Technol* **2007,** *41*, (17), 6216-6221.

8. He, F.; Zhao, D. Y.; Liu, J. C.; Roberts, C. B., Stabilization of Fe-Pd nanoparticles with sodium carboxymethyl cellulose for enhanced transport and dechlorination of trichloroethylene in soil and groundwater. *Ind Eng Chem Res* **2007,** *46*, (1), 29-34.

9. He, F.; Zhao, D. Y., Preparation and characterization of a new class of starch-stabilized bimetallic nanoparticles for degradation of chlorinated hydrocarbons in water. *Environ Sci Technol* **2005,** *39*, (9), 3314-3320.

10. Schrick, B.; Hydutsky, B. W.; Blough, J. L.; Mallouk, T. E., Delivery vehicles for zerovalent metal nanoparticles in soil and groundwater. *Chem Mater* **2004,** *16*, (11), 2187-2193.

11. Sun, Y. P.; Li, X. Q.; Zhang, W. X.; Wang, H. P., A method for the preparation of stable dispersion of zero-valent iron nanoparticles. *Colloid Surface A* **2007,** *308*, (1-3), 60-66.

12. Phenrat, T.; Saleh, N.; Sirk, K.; Kim, H. J.; Tilton, R. D.; Lowry, G. V., Stabilization of aqueous nanoscale zerovalent iron dispersions by anionic polyelectrolytes: adsorbed anionic polyelectrolyte layer properties and their effect on aggregation and sedimentation. *J Nanopart Res* **2008,** *10*, (5), 795-814.

13. Saleh, N.; Phenrat, T.; Sirk, K.; Dufour, B.; Ok, J.; Sarbu, T.; Matyiaszewski, K.; Tilton, R. D.; Lowry, G. V., Adsorbed triblock copolymers deliver reactive iron nanoparticles to the oil/water interface. *Nano Lett* **2005,** *5*, (12), 2489-2494.

14. Tiraferri, A.; Chen, K. L.; Sethi, R.; Elimelech, M., Reduced aggregation and sedimentation of zero-valent iron nanoparticles in the presence of guar gum. *J Colloid Interf Sci* **2008,** *324*, (1-2), 71-79.

15. Kocur, C. M.; O'Carroll, D. M.; Sleep, B. E., Impact of nZVI stability on mobility in porous media. *Journal of contaminant hydrology* **2013,** *145*, 17-25.

16. Nunez Garcia, A.; Boparai, H. K.; O'Carroll, D. M., Enhanced Dechlorination of 1,2-Dichloroethane by Coupled Nano Iron-Dithionite Treatment. *Environ Sci Technol* **2016,** *50*, (10), 5243-5251.

17. Rajajayavel, S. R. C.; Ghoshal, S., Enhanced reductive dechlorination of trichloroethylene by sulfidated nanoscale zerovalent iron. *Water research* **2015,** *78*, 144-153.

18. Kim, E. J.; Kim, J. H.; Azad, A. M.; Chang, Y. S., Facile Synthesis and Characterization of Fe/FeS Nanoparticles for Environmental Applications. *ACS Appl. Mater. Inter.* **2011,** *3*, (5), 1457-1462.

19. Kim, E.-J.; Le Thanh, T.; Kim, J.-H.; Chang, Y.-S., Synthesis of metal sulfide-coated iron nanoparticles with enhanced surface reactivity and biocompatibility. *RSC Advances* **2013,** *3*, (16), 5338-5340.

20. Kim, E.-J.; Murugesan, K.; Kim, J.-H.; Tratnyek, P. G.; Chang, Y.-S., Remediation of Trichloroethylene by FeS-Coated Iron Nanoparticles in Simulated and Real Groundwater: Effects of Water Chemistry. *Ind Eng Chem Res* **2013,** *52*, (27), 9343-9350.

21. Han, Y.; Yan, W., Reductive Dechlorination of Trichloroethene by Zero-valent Iron Nanoparticles: Reactivity Enhancement through Sulfidation Treatment. *Environ Sci Technol* **2016,** *50*, (23), 12992-13001.

22. Li, D.; Mao, Z.; Zhong, Y.; Huang, W.; Wu, Y.; Peng, P. a., Reductive transformation of tetrabromobisphenol A by sulfidated nano zerovalent iron. *Water research* **2016,** *103*, 1-9.

23. Tang, J.; Tang, L.; Feng, H.; Zeng, G.; Dong, H.; Zhang, C.; Huang, B.; Deng, Y.; Wang, J.; Zhou, Y., pH-dependent degradation of p-nitrophenol by sulfidated nanoscale zerovalent iron under aerobic or anoxic conditions. *Journal of hazardous materials* **2016,** *320*, 581-590.

24. Song, S.; Su, Y.; Adeleye, A. S.; Zhang, Y.; Zhou, X., Optimal design and characterization of sulfide-modified nanoscale zerovalent iron for diclofenac removal. *Applied Catalysis B: Environmental* **2017,** *201*, 211-220.

25. Fan, D. M.; Anitori, R. P.; Tebo, B. M.; Tratnyek, P. G.; Pacheco, J. S. L.; Kukkadapu, R. K.; Engelhard, M. H.; Bowden, M. E.; Kovarik, L.; Arey, B. W., Reductive Sequestration of Pertechnetate ((TcO4-)-Tc-99) by Nano Zerovalent Iron (nZVI) Transformed by Abiotic Sulfide. *Environ Sci Technol* **2013,** *47*, (10), 5302-5310.

26. Su, Y.; Adeleye, A. S.; Keller, A. A.; Huang, Y.; Dai, C.; Zhou, X.; Zhang, Y., Magnetic sulfide-modified nanoscale zerovalent iron (S-nZVI) for dissolved metal ion removal. *Water research* **2015,** *74*, 47-57.

27. Cumbal, L. H.; Debut, A.; Delgado, D. A.; Jurado, C. B.; Stael, C., Synthesis of Multicomponent Nanoparticles for Immobilization of Heavy Metals in Aqueous Phase. *NanoWorld J* **2015,** *1*, (4), 103-109.

28. Fan, D.; Lan, Y.; Tratnyek, P. G.; Johnson, R. L.; Filip, J.; O'Carroll, D. M.; Nunez Garcia, A.; Agrawal, A., Sulfidation of Iron-Based Materials: A Review of Processes and Implications for Water Treatment and Remediation. *Environ Sci Technol* **2017**.

29. Amonette, J. E.; Szecsody, J. E.; Schaef, H. T.; Gorby, Y. A.; Fruchter, J. S.; Templeton, J. C., Abiotic Reduction of Aquifer Materials by Dithionite: A Promising In-Situ Remediation Technology. In *In-Situ Remediation: Scientific Basis for Current and Future Technologies*, Gee, G. W.; Wing, N. R., Eds. Battelle Press: Columbus, OH, 1994; pp 851-881.

30. He, F.; Zhao, D.; Paul, C., Field assessment of carboxymethyl cellulose stabilized iron nanoparticles for in situ destruction of chlorinated solvents in source zones. *Water research* **2010,** *44*, (7), 2360-70.

31. Kocur, C. M.; Chowdhury, A. I.; Sakulchaicharoen, N.; Boparai, H. K.; Weber, K. P.; Sharma, P.; Krol, M. M.; Austrins, L.; Peace, C.; Sleep, B. E.; O'Carroll, D. M.,

Characterization of nZVI Mobility in a Field Scale Test. *Environ Sci Technol* **2014,** *48*, (5), 2862-2869.

32. Bennett, P.; He, F.; Zhao, D. Y.; Aiken, B.; Feldman, L., In situ testing of metallic iron nanoparticle mobility and reactivity in a shallow granular aquifer. *Journal of contaminant hydrology* **2010,** *116*, (1-4), 35-46.

33. Ahn, J.-Y.; Kim, C.; Kim, H.-S.; Hwang, K.-Y.; Hwang, I., Effects of oxidants on in situ treatment of a DNAPL source by nanoscale zero-valent iron: A field study. *Water research* **2016,** *107*, 57-65.

34. Chowdhury, A. I. A.; Krol, M. M.; Kocur, C. M.; Boparai, H. K.; Weber, K. P.; Sleep, B. E.; O'Carroll, D. M., nZVI injection into variably saturated soils: Field and modeling study. *Journal of contaminant hydrology* **2015,** *183*, 16-28.

35. Johnson, R. L.; Nurmi, J. T.; Johnson, G. S. O.; Fan, D. M.; Johnson, R. L. O.; Shi, Z. Q.; Salter-Blanc, A. J.; Tratnyek, P. G.; Lowry, G. V., Field-Scale Transport and Transformation of Carboxymethylcellulose-Stabilized Nano Zero-Valent Iron. *Environ Sci Technol* **2013,** *47*, (3), 1573-1580.

36. de Carvalho, L. M.; Schwedt, G., Polarographic determination of dithionite and its decomposition products: kinetic aspects, stabilizers, and analytical application. *Analytica Chimica Acta* **2001,** *436*, (2), 293-300.

37. Zhang, W.-x.; Elliott, D. W., Applications of iron nanoparticles for groundwater remediation. *Remediation Journal* **2006,** *16*, (2), 7-21.

38. Leenhouts, J. M.; Bassett, R. L.; Maddock, T., Utilization of intrinsic boron isotopes as co-migrating tracers for identifying potential nitrate contamination sources. *Ground Water* **1998,** *36*, (2), 240-250.

39. Hingston, F. J.; Quirk, J. P.; Posner, A. M., Anion Adsorption by Goethite and Gibbsite .1. Role of Proton in Determining Adsorption Envelopes. *J Soil Sci* **1972,** *23*, (2), 177-&.

40. Quast, K. W.; Lansey, K.; Arnold, R.; Bassett, R. L.; Rincon, M., Boron isotopes as an artificial tracer. *Ground Water* **2006,** *44*, (3), 453-466.

41. Nurmi, J. T.; Tratnyek, P. G.; Sarathy, V.; Baer, D. R.; Amonette, J. E.; Pecher, K.; Wang, C. M.; Linehan, J. C.; Matson, D. W.; Penn, R. L.; Driessen, M. D., Characterization and properties of metallic iron nanoparticles: Spectroscopy, electrochemistry, and kinetics. *Environ Sci Technol* **2005,** *39*, (5), 1221-1230.

42. Busch, J.; Meißner, T.; Potthoff, A.; Bleyl, S.; Georgi, A.; Mackenzie, K.; Trabitzsch, R.; Werban, U.; Oswald, S. E., A field investigation on transport of carbon-supported nanoscale zero-valent iron (nZVI) in groundwater. *Journal of contaminant hydrology* **2015,** *181*, 59-68.

43. Phenrat, T.; Cihan, A.; Kim, H. J.; Mital, M.; Illangasekare, T.; Lowry, G. V., Transport and Deposition of Polymer-Modified Fe-0 Nanoparticles in 2-D Heterogeneous Porous Media: Effects of Particle Concentration, Fe-0 Content, and Coatings. *Environ Sci Technol* **2010,** *44*, (23), 9086-9093.

44. Velimirovic, M.; Tosco, T.; Uyttebroek, M.; Luna, M.; Gastone, F.; De Boer, C.; Klaas, N.; Sapion, H.; Eisenmann, H.; Larsson, P. O.; Braun, J.; Sethi, R.; Bastiaens, L., Field assessment of guar gum stabilized microscale zerovalent iron particles for in-situ remediation of 1,1,1-trichloroethane. *Journal of contaminant hydrology* **2014,** *164*, 88-99.

45. Quinn, J.; Geiger, C.; Clausen, C.; Brooks, K.; Coon, C.; O'Hara, S.; Krug, T.; Major, D.; Yoon, W. S.; Gavaskar, A.; Holdsworth, T., Field demonstration of DNAPL dehalogenation using emulsified zero-valent iron. *Environ Sci Technol* **2005,** *39*, (5), 1309-1318.

46. Elliott, D. W.; Zhang, W.-x., Field Assessment of Nanoscale Bimetallic Particles for Groundwater Treatment. *Environ Sci Technol* **2001,** *35*, (24), 4922-4926.

47. Wei, Y.-T.; Wu, S.-C.; Chou, C.-M.; Che, C.-H.; Tsai, S.-M.; Lien, H.-L., Influence of nanoscale zero-valent iron on geochemical properties of groundwater and vinyl chloride degradation: A field case study. *Water research* **2010,** *44*, (1), 131-140.

48. Shi, Z. Q.; Fan, D.; Johnson, R. L.; Tratnyek, P. G.; Nurmi, J. T.; Wu, Y. X.; Williams, K. H., Methods for characterizing the fate and effects of nano zerovalent iron during groundwater remediation. *Journal of contaminant hydrology* **2015,** *181*, 17-35.

49. Shi, Z. Q.; Nurmi, J. T.; Tratnyek, P. G., Effects of Nano Zero-Valent Iron on Oxidation-Reduction Potential. *Environ Sci Technol* **2011,** *45*, (4), 1586-1592.

50. Qin, H.; Guan, X.; Bandstra, J. Z.; Johnson, R. L.; Tratnyek, P. G., Modeling the Kinetics of Hydrogen Formation by Zerovalent Iron: Effects of Sulfidation on Micro- and Nano-Scale Particles. *Environ Sci Technol* **2018**.

51. He, F.; Li, Z.; Shi, S.; Xu, W.; Sheng, H.; Gu, Y.; Jiang, Y.; Xi, B., Dechlorination of Excess Trichloroethene by Bimetallic and Sulfidated Nanoscale Zero-Valent Iron. *Environ Sci Technol* **2018,** *52*, (15), 8627–8637.

52. Fan, D.; Lan, Y.; Tratnyek, P. G.; Johnson, R. L.; Filip, J.; O'Carroll, D. M.; Nunez Garcia, A.; Agrawal, A., Sulfidation of Iron-Based Materials: A Review of Processes and Implications for Water Treatment and Remediation. *Environ Sci Technol* **2017,** *51*, (22), 13070-13085.

53. Duan, J.; Ji, H.; Liu, W.; Zhao, X.; Han, B.; Tian, S.; Zhao, D., Enhanced immobilization of U(VI) using a new type of FeS-modified Fe0 core-shell particles. *Chem Eng J* **2018**.

54. Su, Y.; Jassby, D.; Song, S.; Zhou, X.; Zhao, H.; Filip, J.; Petala, E.; Zhang, Y., Enhanced Oxidative and Adsorptive Removal of Diclofenac in Heterogeneous Fenton-like Reaction with Sulfide Modified Nanoscale Zerovalent Iron. *Environ Sci Technol* **2018,** *52*, (11), 6466-6475.

55. Dong, H.; Zhang, C.; Deng, J.; Jiang, Z.; Zhang, L.; Cheng, Y.; Hou, K.; Tang, L.; Zeng, G., Factors influencing degradation of trichloroethylene by sulfide-modified nanoscale zero-valent iron in aqueous solution. *Water research* **2018,** *135*, 1-10.

56. Bibi, I.; Singh, B.; Silvester, E., Akaganéite (β-FeOOH) precipitation in inland acid sulfate soils of south-western New South Wales (NSW), Australia. *Geochimica et Cosmochimica Acta* **2011,** *75*, (21), 6429-6438.

57. Morin, K. A. In *Rates of sulfide oxidation in submerged environments: Implications for subaqueous disposal.*, In: 17th Annual Mine Reclamation Symposium, Port Hardy, BC, Canada, May 4 - 7, 1993; Port Hardy, BC, Canada, 1993; pp 235 - 247.

58. An, X.-L.; Huang, F.-G.; Ren, H.-T.; Wang, Y.-F.; Chen, Y.; Liu, Z.-M.; Zhang, H.-W.; Han, X., Oxidative dissolution of amorphous FeS and speciation of secondary Fe minerals: Effects of pH and As(III) concentration. *Chem Geol* **2017,** *462*, 44-54.

59. Jeong, H. Y.; Han, Y.-S.; Hayes, K. F., X-ray Absorption and X-ray Photoelectron Spectroscopic Study of Arsenic Mobilization during Mackinawite (FeS) Oxidation. *Environ Sci Technol* **2010,** *44*, (3), 955-961.

60. Chowdhury, A. I. A.; O'Carroll, D. M.; Xu, Y.; Sleep, B. E., Electrophoresis enhanced transport of nano-scale zero valent iron. *Adv Water Resour* **2012,** *40*, 71-82.

61. He, F.; Zhang, M.; Qian, T. W.; Zhao, D. Y., Transport of carboxymethyl cellulose stabilized iron nanoparticles in porous media: Column experiments and modeling. *J Colloid Interf Sci* **2009,** *334*, (1), 96-102.

62. Bhattacharjee, S.; Ghoshal, S., Optimal design of sulfidated nanoscale zerovalent iron for enhanced trichloroethene degradation. *Environ Sci Technol* **2018**.

63. Su, Y.; Adeleye, A. S.; Huang, Y.; Zhou, X.; Keller, A. A.; Zhang, Y., Direct Synthesis of Novel and Reactive Sulfide-modified Nano Iron through Nanoparticle Seeding for Improved Cadmium-Contaminated Water Treatment. *Scientific Reports* **2016,** *6*, 24358.

64. Gong, Y.; Gai, L.; Tang, J.; Fu, J.; Wang, Q.; Zeng, E. Y., Reduction of Cr(VI) in simulated groundwater by FeS-coated iron magnetic nanoparticles. *Science of The Total Environment* **2017,** *595*, 743-751.

65. Phenrat, T.; Saleh, N.; Sirk, K.; Tilton, R. D.; Lowry, G. V., Aggregation and sedimentation of aqueous nanoscale zerovalent iron dispersions. *Environ Sci Technol* **2007,** *41*, (1), 284-290.

66. Saleh, N.; Sirk, K.; Liu, Y. Q.; Phenrat, T.; Dufour, B.; Matyjaszewski, K.; Tilton, R. D.; Lowry, G. V., Surface modifications enhance nanoiron transport and NAPL targeting in saturated porous media. *Environ Eng Sci* **2007,** *24*, (1), 45-57.

67. Phenrat, T.; Kim, H. J.; Fagerlund, F.; Illangasekare, T.; Tilton, R. D.; Lowry, G. V., Particle Size Distribution, Concentration, and Magnetic Attraction Affect Transport of Polymer-

Modified Fe-0 Nanoparticles in Sand Columns. *Environ Sci Technol* **2009,** *43*, (13), 5079-5085.

Chapter 4

4 Sulfidated Nano Zerovalent Iron (S-nZVI) for In-Situ Treatment of Chlorinated Solvents: A Field Study

4.1 Introduction

Sulfidation is a recent development related to the use of zerovalent iron (ZVI) based materials for groundwater remediation.[1, 2] Though most of the focus in recent years has been on engineered sulfidation of nano ZVI (nZVI), biogenic sulfidation of ZVI has been extensively investigated since the 1990s.[3-11] Earlier studies focused on the identification of authigenic mineral phases formed during the application of ZVI permeable reactive barriers (PRBs). Formation of mackinawite and ferrous sulfide was attributed to the concurrent oxidation of iron and generation of sulfide via biogeochemical processes (e.g., microbial reduction of SO_4^{2-} by sulfate reducing bacteria (SRB)). These mineral phases were studied in the context of the hydraulic performance of the PRBs, noting that the accumulated iron sulfide (FeS) precipitates as coating on ZVI filings could contribute to pore clogging, decreasing permeability, and reducing groundwater flow. However, parallel work on the dechlorination of chlorinated volatile organic compounds (cVOCs) by FeS[12-14] led to the recognition of these mineral phases as an additional remediant during the operation of PRBs.[15, 16] Similar field work utilized the *in situ* formation of iron sulfides to promote abiotic reduction of chlorinated solvents, in a technology referred to as Biogeochemical Reductive Dechlorination (BiRD).[17, 18] Investigations on reactive iron sulfides for remediation purposes is now a thriving field, as demonstrated by recent advances on its synthesis, stabilization and applicability for the removal of organic and inorganic contaminants.[19]

In contrast to the biogenic processes described above, abiotic sulfidation can be achieved by modifying the nZVI particles with sulfur compounds of various oxidation states, mainly sulfate,[20] dithionite,[21-33] thiosulfate,[34] and sulfide.[31, 35-37] The resultant sulfidated nZVI (S-nZVI) is more reactive than sulfur-free nZVI for dechlorination of cVOCs,[21, 23, 32, 34, 36, 38] adsorption of heavy metals,[20, 25, 35] and transformation of various organic contaminants.[26-28, 30, 33, 37] Increased longevity[32] and higher colloidal stability[30, 33, 39] in suspension has also been reported for S-nZVI.

Mechanistic understanding of S-nZVI reactivity is still evolving, with two major explanations proposed in the literature: inhibition of hydrogen recombination[34] and increase in electron transfer through the modified sulfidated shell.[36] To the best of our knowledge, published studies on S-nZVI have been performed solely at the laboratory scale. As such, the field-performance of S-nZVI for chlorinated solvents degradation as well as the scalability of its synthesis process have yet to be evaluated.

Multiple pilot-scale projects and field-scale studies have been conducted to evaluate the field efficacy of nZVI for *in situ* treatment of contaminated soil and groundwater.[40-48] However, application of nZVI has often faced limitations related to colloidal instability and side oxidation reactions with natural *in situ* oxidants, causing rapid passivation.[49, 50] While a significant amount of research has been directed to improve colloidal stability, fewer studies have been dedicated to the minimization of undesirable oxidation reactions. Controlled abiotic sulfidation of nZVI has shown potential to minimize such reactions and improve selectivity towards targeted pollutants.[31] Such functionality makes S-nZVI more advantageous than nZVI for large scale applications, as more electron equivalents would hypothetically be directed to the reduction of contaminants, resulting in a more cost-effective treatment.

With emerging types of nZVI being tested in pilot-scale studies,[47, 51, 52] field evaluation of the application of S-nZVI for *in situ* remediation becomes essential. Herein, we report results from a field synthesis and injection of S-nZVI into an aquifer contaminated with chlorinated ethanes, ethenes and methanes. To assess the effectiveness of S-nZVI for the *in situ* transformation of contaminants, Compound Specific Isotope Analysis (CSIA) was used to differentiate between physical mechanisms (dilution and/or mobilization) and abiotic and biotic transformations.[53] CSIA has previously been conducted on cVOCs in groundwater samples from an nZVI field trial[54] and serves as a powerful tool to elucidate the chemical processes taking place after emplacement of the colloidal suspension. The specific objectives of the current study were to (1) assess the spatial and temporal variability of cVOC concentrations in groundwater and soil after injection of S-nZVI, (2) evaluate the short- and long-term field performance of S-nZVI for the *in situ* transformation of chlorinated ethanes, ethenes and methanes, and (3) utilize CSIA as an advanced diagnostic tool to distinguish chemical dechlorination from physical processes such as mobilization or dilution.

4.2 Materials and Methods

4.2.1 Site History and Description

Located in Sarnia, Ontario, the site was home to cVOCs production facilities, resulting in the accumulation of a multicomponent dense non-aqueous phase liquid (DNAPL) source zone. Borehole logs, advanced with an AMS PowerProbe drill rig, revealed three major sections composed of a clayey fill at the top, sandy material in the middle and the native clay at the bottom of the geologic system. These sections are not continuous, containing in some instances traces of gravel, brick and wood fragments. Due to the differences in permeability between the backfill and the surrounding clay, DNAPL primarily migrated and accumulated between 4 and 5 m below ground surface (bgs). This was consistent with the appearance of the grey clay, as revealed by the borehole logs, and visual observations of DNAPL in the form of staining and/or sheening of soil cores. DNAPL was further confirmed by organic vapor monitoring (OVM) measurements using a photoionization detector (PID) (11.6 electron volt [eV]) (Figure B.1).

The wide range of cVOCs production processes on this site contributed to the formation of a complex source zone, with major compounds previously reported as tetrachloroethene (PCE), trichloroethene (TCE) and chloroform (CF).[45] The distribution and composition of the cVOCs in the source zone could have been impacted by past remedial activities as well as natural attenuation. The abundance of typical daughter products from parent compounds PCE (i.e., dichloroethenes and ethene) and carbon tetrachloride (CCl_4) (i.e., CF and dichloromethane - DCM), present in background samples (Figure B.2), supports the hypothesis that transformation of parent products has occurred over time. The present study was conducted at the fringes of a previous field test that took place 4 years prior to this study, when a total of 620 L of 1 g L^{-1} nZVI stabilized with carboxymethyl cellulose (CMC) was introduced into four wells.[45, 55, 56] A plan view of the study area with the sets of wells from both studies is presented in Figure B.3. Evidence of natural attenuation at the site has been previously reported and attributed to the abundant population of *Dehalococcoides spp.* (Dhc) in the background samples prior to the delivery of nZVI.[45] This is indicative of biotic reductive dechlorination of cVOCs.

4.2.2 Monitoring Network

Eight multilevel bundle piezometers were installed, six downstream (NA1, NB1, NC1, NA2, NB2 and NA4) and two upstream (NA3 and NB3) of the injection well (NIW) (Figures B.3 and B.4). The injection well consists of a conventional 5 cm (2 in) well, 0.61 m screen (2 ft), advanced using hollow stem augers. Bundled piezometers were made up of seven color coded ¼" teflon tubes mounted on a ¼" stainless steel rod for stability. The screen length of each teflon tube was 0.127 m and placed 0.305 m vertically apart in order to target different sampling depths (Figure B.5). Unless otherwise specified, each color denotes the following depths (m bgs) for all wells: Black - 2.9 m, Yellow - 3.2 m, Green - 3.51 m, Clear - 3.81 m, Blue - 4.12 m and White - 4.42 m. The Red level was emplaced within the source zone and therefore not sampled for cVOCs analysis. The bundles of tubing were inserted into open boreholes supported by the outer rod utilized during direct push drilling. After insertion, the outer rod was then withdrawn, relying on the collapsing nature of the sandy backfill to fill the annulus. Finally, a 15 cm (6 in) piece of PVC was placed at the surface to house the tubing (Figure B.5). Information on bundle piezometers for multilevel sampling can be found in Appendix B.

4.2.3 S-nZVI Synthesis Procedure

Details on the synthesis procedure were described previously.[39] Briefly, nZVI was synthesized on site by first mixing ferrous sulfate heptahydrate ($FeSO_4 \cdot 7H_2O$) with CMC (90K) (pre-synthesis stabilization) and then reducing the mixture using sodium borohydride ($NaBH_4$). Aqueous-solid sulfidation was carried out by treating the nZVI with sodium dithionite ($Na_2S_2O_4$) to produce a suspension of 1 g L^{-1} S-nZVI particles, stabilized in 0.8% w/v CMC and 22 mM dithionite (S/Fe = 2.45). A total of 620 L of the suspension was prepared in 4 distinct batches, 155 L each, and introduced under gravity-feed conditions via the injection well for 16 hours.

4.2.4 Sampling and Analytical Methods

Groundwater samples were collected using 40 mL VOA (volatile organic analysis) glass vials, leaving no headspace and preserved with 0.2 grams of sodium bisulfate ($NaHSO_4$). Unless otherwise specified, background samples were collected ~28.5 hours before the injection and are referred only as 'background' or '0 days' (0 d). Chlorinated compounds (PCE, CCl_4,

tetrachloroethanes - 1,1,1,2-TeCA & 1,1,2,2-TeCA, TCE, trichloroethanes - 1,1,1-TCA & 1,1,2-TCA, and 1,2-dichloroethane - 1,2-DCA) were extracted by transferring 250 µL aliquots to 1 mL hexane and analyzed with a modified version of EPA 8021 method utilizing an Agilent 7890 Gas Chromatograph (GC) equipped with an Electron Capture Detector (ECD), a DB-624 capillary column, and an autosampler, as previously described.[45] For hydrocarbons (i.e., ethane and ethene) and lower chlorinated compounds (i.e., dichloroethenes - DCEs, 1,1-DCA, vinyl chloride - VC, chloroethane – CE, and DCM), aliquots of 1 mL were transferred to 2 mL GC vials and allowed to equilibrate for a minimum of one hour, before manually sampling 250 µL of the headspace and injecting into the GC. Analysis was carried out using a Flame Ionization Detector (FID) and a GS-Gaspro column. External standards were used for preparing calibration curves for all the cVOCs and hydrocarbons.

For cVOCs in soil, background samples were taken during the installation of the wells (25 - 28 days before S-nZVI injection), followed by post-injection sampling at 94 and 554 days. The soil cores were logged and sub-sampled either at pre-determined depths or at targeted locations considered to be highly impacted by cVOCs. Post-injection boreholes were located between the locations of the monitoring wells, 0.3 - 0.6 meters apart (1 - 2 ft), to sample along the S-nZVI flow path. Bulk soil samples were collected and stored in 60-mL jars, filling the container to the brim and leaving no headspace to minimize losses in accordance with EPA Method 5035A. Jars were stored on ice to keep them below 4 °C, transported to the laboratory and kept in a cold room (4 °C). This procedure eliminates the need for a second sample for dry weight determination. In the laboratory, 5 to 10 g of soil sample was quickly transferred into pre-weighted vials containing 10 mL methanol or water and the vials were kept on shaker for ten minutes for the cVOCs extraction. The extractant solution was then diluted with water, if needed. Analysis of the cVOCs was performed with a GC-ECD and a GC-FID, as described above.

Chloride was analyzed using a high-performance liquid chromatograph (HPLC) equipped with a conductivity detector (Model 432, Waters, Milford, MA), a 4.6 × 50 cm IC-Pak Anion column (#Wat007355) using a 12% water-acetonitrile eluent as mobile phase. Total iron and boron were analyzed as reported previously.[39]

4.2.5 Compound Specific Isotope Analysis (CSIA)

Background samples were collected from NB1-White and NB2-White 28.5 hours before injection. Samples were preserved in 40 mL VOA vials using $NaHSO_4$, following the standard procedure for groundwater cVOCs described above. Post-injection samples were also collected from the same wells 17 days after S-nZVI injection, preserved in 1 mL concentrated hydrochloric acid in 40 mL VOA vials with 5 mL headspace after the method of Elsner et al. [57] Vials were then covered with aluminum foil and frozen upside down to allow for a gradual freezing process and minimize losses through the septum. Headspace sampling and analysis was carried out using Gas Chromatograph - Combustion - Isotope Ratio Mass Spectrometer (GC-C-IRMS, Finnigan 252 IRMS). Stable carbon isotope values are reported in the δ-notation (‰), relative to the international Vienna Pee Dee Belemnite (V-PDB) standard, as follows (Eq. 4.1):

$$\delta^{13}C[‰] = \left(\frac{\left({}^{13}C/_{12}C\right)_{sample}}{\left({}^{13}C/_{12}C\right)_{standard}} - 1 \right) \quad (4.1)$$

where $\left({}^{13}C/_{12}C\right)_{sample}$ and $\left({}^{13}C/_{12}C\right)_{standard}$ are the ratios of carbon-13 and carbon-12 in the sample and standard, respectively. All stable carbon isotope values are reported with a 0.5-‰ error encompassing both accuracy and reproducibility.[58] A minimum of a 1 to 2‰ difference between two $\delta^{13}C$ values is considered significant.[53] Background information on CSIA and details on the GC method can be found in the Appendix B.

4.3 Results and Discussion

A previous field study at this site showed that significant cVOC transformation occurred over a three week period after CMC-nZVI injection, indicating the occurrence of short-term abiotic transformation which was then followed by long-term enhanced biotic transformation.[45] Given these observations, changes in cVOC concentrations after S-nZVI injection in the current study is presented as short-term and long-term transformations.

4.3.1 Short-Term Changes in cVOCs in Groundwater

Significant S-nZVI transport was observed 0.86 m (NB1-White), 0.91 m (NC1-White), and 2.7 m (NA4-Blue), downgradient of the injection well as well as 1.7 m (NA3-White) upgradient of the injection well, whereas limited S-nZVI breakthrough was found 1.78 m downgradient of the injection well (NB2-White) (Figure 4.1h). Of note is that some of these wells retained high iron concentrations even 17 days after injection. Coincident with the transport of S-nZVI and associated geochemical changes, as reported earlier,[39] immediate and considerable changes were observed in concentrations and distribution of aqueous cVOCs in these wells (Figures 4.1 and Figure B.6). Total iron concentrations did not change much at NA2-Blue and NB3-White, i.e., 1.78 m downgradient and 1.66 m upgradient of the injection well, respectively. As such, the results for these wells are not discussed here.

NB1-White showed a significant decrease in all the cVOCs on day 3 coincident with the high concentration of total iron (763 μM) detected at this location. This decrease in cVOC concentrations continued, even when iron concentration decreased to 96.7 μM on day 17. PCE declined by 31% on day 3, followed by a final decrease up to 80% (from 392 to 73.6 μM) on day 17. TCE also decreased 69% on day 3 but then increased on day 17 (from 28.7 to 62.6 μM) (Figure 4.1j and Figure B.6h). This increase in TCE concentration could have resulted from its generation as a dechlorination product of PCE (see Section 3.2). An appreciable reduction in *cis*-1,2-DCE concentration from 252 to 99.8 μM on day 17 is also attributed partly to its dechlorination, as indicated by CSIA results (Section 3.2). Like TCE, VC also decreased and then increased to its initial concentration on day 17. A decrease in ethene concentration on day 3 (244 to 72.8 μM) can be attributed to dilution/mobilization, however, it increased to 173 μM on day 17. This further shows that dechlorination occurred in NB1-W. All chloromethanes concentrations also decreased noticeably on day 3 and further declined by >70% on day 17. For instance, CCl_4 concentration decreased from 281 to 66.9 μM on day 17. A similar trend was observed for the chloroethanes where 1,1,2-TCA concentration decreased from 109 to 12.6 μM on day 17.

S-nZVI migrated to NA3-White during injection, with iron concentrations remaining relatively high for longer period (e.g., 220 μM iron on day 17). Like NB1-White, NA3-White showed a noticeable decrease in almost all cVOCs concentrations on day 3 which continued until day 17.

Although this decrease can be partly attributed to dilution/mobilization, noticeable increase in ethene concentration on day 17 indicates that dechlorination also took place.

NA4-Blue was another well with good S-nZVI breakthrough. In this monitoring well, concentrations of PCE, *cis*-1,2-DCE, and chloroethanes did not change considerably on day 3. However, TCE concentration decreased from 87.8 to 37.7 μM (~50 μM), concurrent with a proportional increase in VC (~11 μM) and ethene (~36 μM) concentrations on day 3, suggesting TCE dechlorination. A significant decrease in chloromethane concentrations was also observed on day 3. In contrast to NB1-White, the concentrations of all cVOCs, except VC, rebound significantly on day 17. For instance, PCE concentrations increased from 63.0 μM on day 3 to 116 μM on day 17. Interestingly, the iron concentration also increased simultaneously in this well. Transport data shows that NA4-Blue is connected to the injection well via preferential flow paths[39] which might have contributed to cVOCs and iron mobilization to NA4-Blue on day 17. However, further increase in ethene concentration to 181 μM on day 17 shows that cVOCs were also simultaneously dechlorinated. Like NA4-Blue, cVOCs concentrations at NC1-White also decrease on day 3 but the concentrations rebounded on day 17 with a concurrent increase in iron concentration.

Although limited S-nZVI migrated to NB2-White during injection, total iron concentration increased to 219 μM on day 17. At this location, limited change (<10%) in concentrations of parent compounds PCE, CCl_4, and TCE was observed but concentrations of lower chlorinated ethenes, ethanes and methanes continued to decrease noticeably up to day 17. The decrease in ethene concentration on day 3 suggests dilution/mobilization, however, its increased concentration on day 17 indicates occurrence of dechlorination.

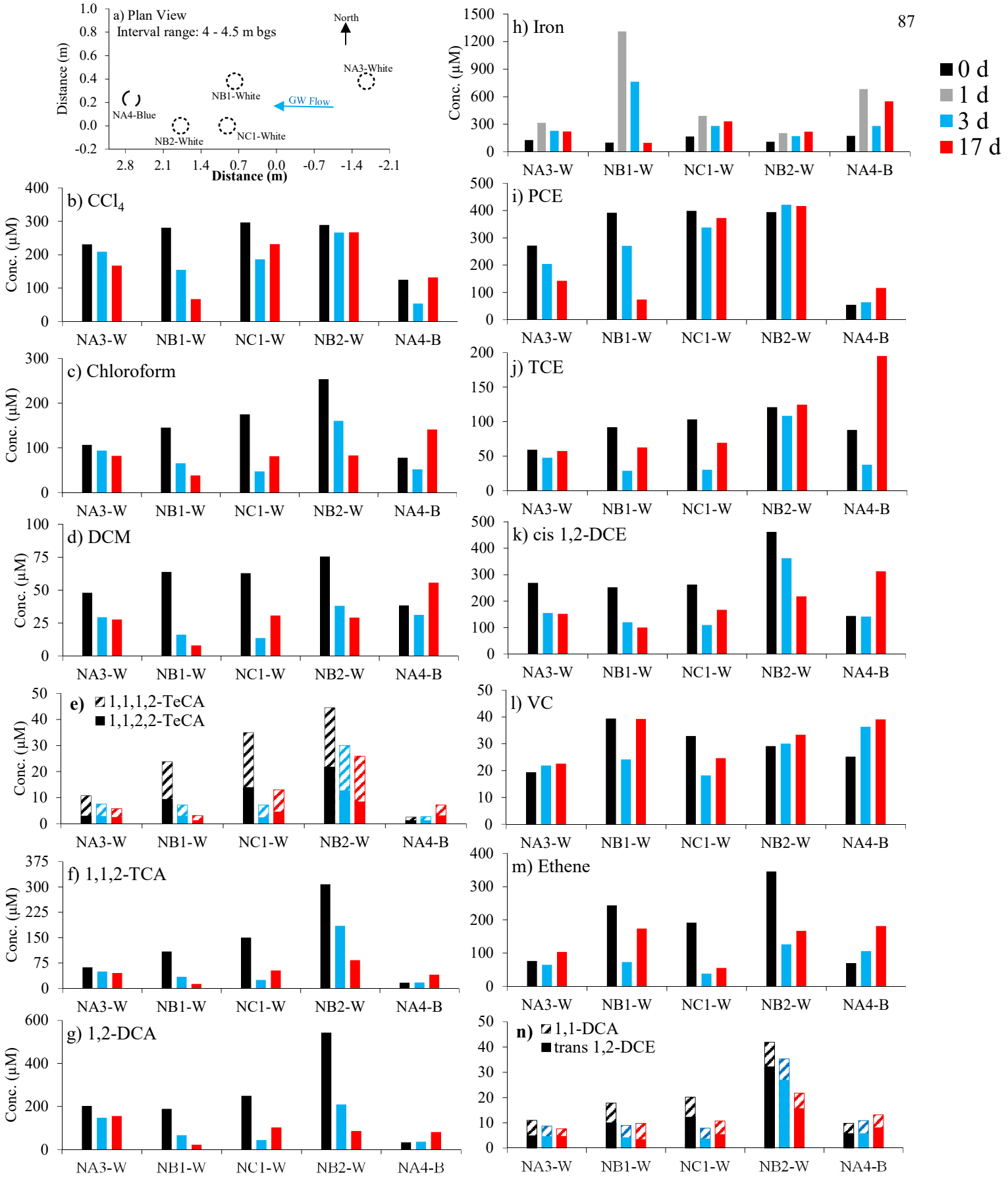

Figure 4.1 Short – term changes in cVOCs concentrations at five locations representing upstream and downstream conditions. h) Iron concentrations are shown for the same sampling times, including the peak concentrations measured during active injection (0 – 16 hours). a) Plan View is shown for reference and only relevant wells are presented.

Proximity of the Blue and White levels (4 - 4.5 m bgs) to the DNAPL pool and the dilution/mobilization interferences due to S-nZVI injection make it challenging to distinguish between the various processes that govern the changes in cVOCs concentrations. For example, despite these changes in cVOCs concentrations and generation of ethene, there was no proportional increase in chloride concentration from the background values (Figure B.7).

A clearer picture of potential dechlorination can be deduced from the changes in cVOC concentrations at the uppermost level of NB1 (2.9 m bgs - Black level), positioned approximately 1.5 m above the source zone. Vertical transport of the S-nZVI suspension to this location was observed by an increase in the total iron and total boron concentrations in the upper levels of NB1 at day 3 (Figure 4.2). At day 3, there was a 27% decrease in PCE (374 to 272 µM) which did not change much at day 17 (Figure 4.3). At the same time, the concentrations of *cis*-1,2-DCE and ethene increased from 70.6 to 169 µM and from 96.9 to 145 µM, respectively at day 3 but decreased to 110 and 101 µM at day 17. It is important to note that there was no appreciable accumulation of vinyl chloride, with *cis*-1,2-DCE and ethene observed as the main dechlorination products. Concomitantly, there was a reduction in the CCl_4 concentration, from 255 to 166 µM, followed by an increase in chloroform and dichloromethane (DCM). Unlike PCE, CCl_4 concentration decreased further to 124 µM at day 17. Decreases in concentration were also observed for other parent compounds (1,1,1,2-TeCA and 1,1,2,2-TeCA) matched by increases in daughter products (i.e., trans 1,2-DCE and 1,1-DCA) (Figure 4.3). The concurrent increased in chloride concentration at this level, from 7.3 mM at day 0 to 11.9 mM at day 3, exceeds what can be accounted from the changes in cVOC concentrations (Table B.1). This suggests that processes apart from the transformation of aqueous phase cVOCs are contributing to the changes in chloride concentrations. A detailed discussion on the changes in chloride concentrations for the NB1 well is presented in Section 4.3.2.

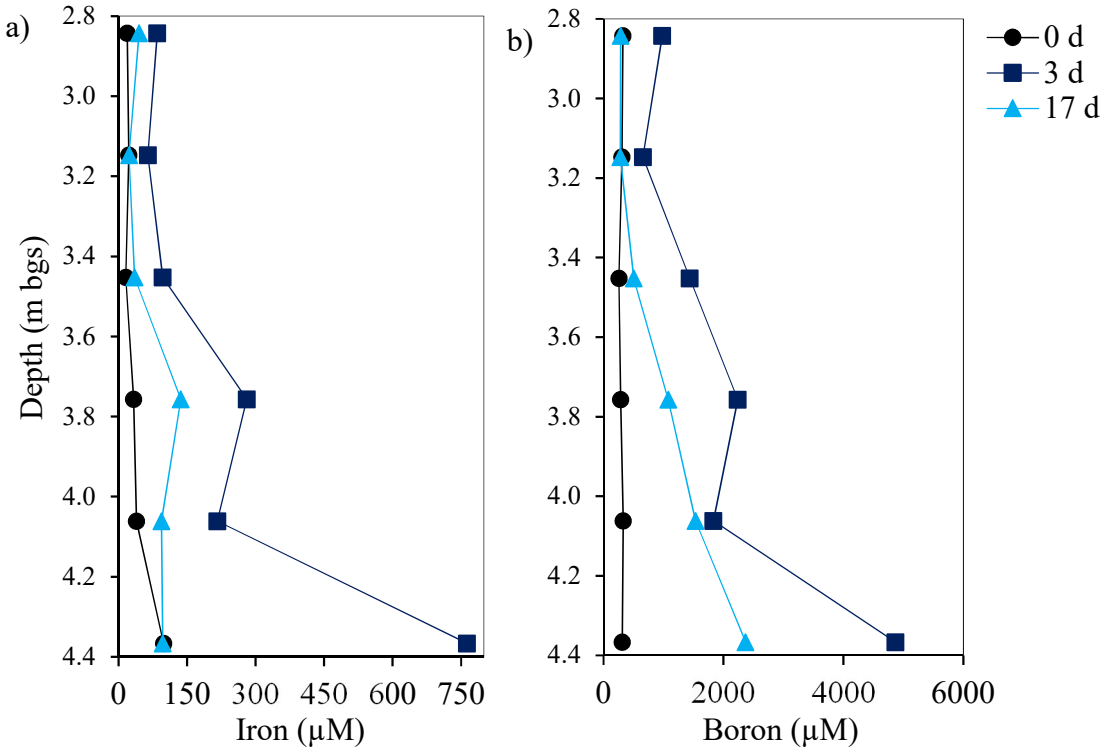

Figure 4.2 a) Total iron and b) total boron concentration of NB1 before and after injection.

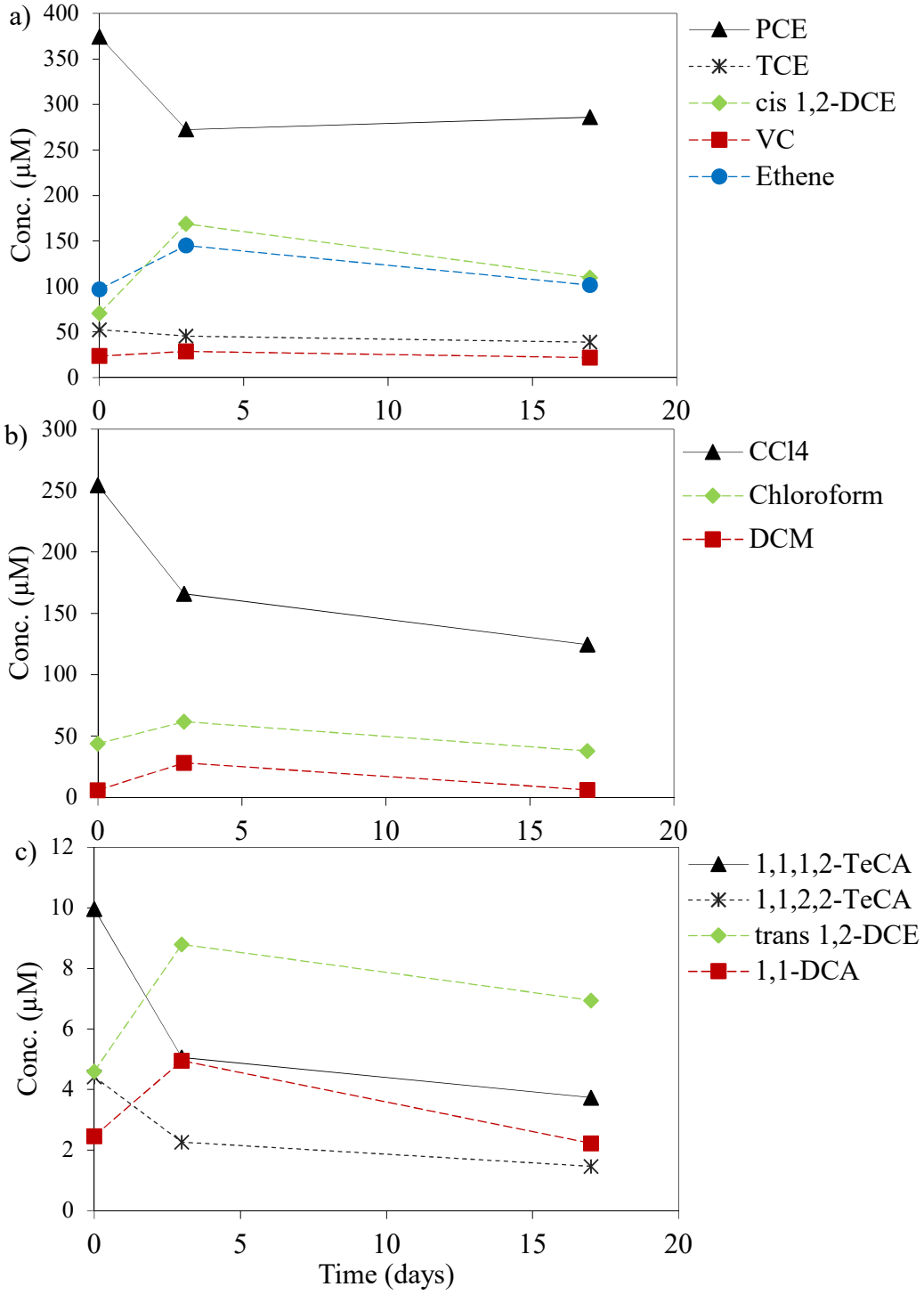

Figure 4.3 Short – term (0 – 17 days) changes in concentrations of a) PCE, TCE, cis-1,2-DCE, VC, Ethene; b) CCl_4, chloroform, DCM; c) 1,1,1,2-TeCA, 1,1,2,2-TeCA, trans 1,2-DCE and 1,1-DCA for the NB1-Black interval (~2.9 m bgs). This interval was chosen for detailed analysis due to its vertical distance from the source zone (~1.83 m).

4.3.2 Changes in cVOCs Concentrations Due to Physical versus Chemical Processes

The distribution and concentrations of cVOCs in groundwater samples could have changed due to a range of factors including dilution/mobilization, through injection of the cVOCs free S-nZVI suspension, and abiotic and biotic transformations. Contaminant transformation can be assessed by CSIA[54, 59] while dilution can be assessed by investigating changes in the concentrations of conservative species.[43]

Stable carbon isotope values were measured for PCE, TCE, *cis*-1,2-DCE, and VC for NB1-White and NB2-White groundwater samples before (day 0) and after (day 17) S-nZVI injection (Table 4.1). These sampling locations were chosen because of their significantly different S-nZVI breakthroughs though they were roughly on the same flow path, 0.86 (NB1-White) and 1.78 m (NB2-White) downgradient from the injection well (Figure B.3). Before injection, the concentrations of PCE, TCE, and VC were similar in the two wells; whereas those of *cis*-1,2-DCE were twice as large in NB2-White compared to NB1-White. The $\delta^{13}C$ values for PCE were the same, i.e., within ± 0.5 ‰ in NB1-White and NB2-White, suggesting that -26.0 ‰ was a relatively homogenous initial isotope signature for PCE at the site at the time of this study. Compared to NB1-White, TCE was significantly enriched in ^{13}C (with a remarkable positive isotopic signature of +1.2 ‰), whereas *cis*-1,2-DCE and VC were depleted in ^{13}C by -2.9 and -1.2 ‰, respectively, in NB2-White. These results indicate that transformation of TCE and *cis*-1,2-DCE already occurred prior to S-nZVI injection, as previously reported in an area directly adjacent to the site.[45, 55] This isotopic enrichment prior to the injection study does not impact the results of the study as the method involves determining absolute changes in isotopic composition before and after injection. After injection, the S-nZVI breakthrough was greater at NB1-White, with a maximum total iron concentration of 1300 µM, than at NB2-White where the maximum iron concentration was 219 µM.[39] After injection, PCE, TCE, and *cis*-1,2-DCE concentrations decreased significantly between days 0 and 17 in NB1-White, whereas VC remained constant. The decrease in PCE concentration was ~80%, from 392 to 73.6 µM, while its $\delta^{13}C$ value increased significantly from -26.0 to -24.6 ‰, consistent with *in situ* transformation of PCE at NB1-White between days 0 and 17. For TCE, the $\delta^{13}C$ value became more depleted in ^{13}C (-22.9 to -25.0 ‰) consistent with production from PCE degradation, even though its concentration decreased from 91.9 to 62.6 µM.

This suggests that TCE generation from PCE transformation was likely more significant than TCE transformation, consistent with the significant decrease in PCE concentration at NB1-White. In addition, the TCE $\delta^{13}C$ value was more negative than that of PCE in the day 17 sample indicating preferential incorporation of ^{12}C in TCE, further pointing to TCE as a transformation product of PCE. Past literature has reported that molecules containing exclusively light isotopes (^{12}C) are preferentially transformed leading to an accumulation of ^{12}C in product molecules.[54, 60-62] This Kinetic Isotope Effect can be characterized by an enrichment factor ε (‰), determined from the Rayleigh equation,[63] and whose amplitude depends on the rate-determining step of the reaction pathway. For PCE, TCE, *cis*-1,2-DCE and VC, the range of ε values overlaps for microbially-mediated reactions (-1.3 to -26.6 ‰)[60, 64-69] and abiotic degradation by ZVI (-5.7 to -26.5 ‰).[61, 70-73] The actual enrichment factor for the transformation of chlorinated ethenes by S-nZVI has not yet been determined, however, ε values similar to that of ZVI can be expected as both treatments have similar dechlorination pathways. In both NB1-White and NB2-White, *cis*-1,2-DCE concentrations decreased by approximately 50 to 60 % while becoming enriched in ^{13}C from -22.8 to -20.2 ‰ in NB1-White and -25.7 to -24.1 ‰ in NB2-White. Such enrichment trends are consistent with the breaking of bonds during transformation. The $\delta^{13}C$ value for *cis*-1,2-DCE in NB1-White was less negative than those for both PCE and TCE in the day 17 sample suggesting *cis*-1,2-DCE transformation may be occurring at a net rate that is greater than its generation as a PCE/TCE transformation product at NB1-White. Contrary to NB1-White, the concentrations and $\delta^{13}C$ values of PCE and TCE were relatively constant at NB2-White between days 0 and 17, indicating limited transformation likely due to the very limited S-nZVI breakthrough at this location. In both wells, VC concentrations remained constant and VC stable carbon isotope signatures did not change significantly. Overall, the CSIA results provided strong evidence for PCE, TCE and *cis*-1,2-DCE *in situ* transformation in the well with significant S-nZVI breakthrough (i.e., NB1-White) but limited transformation in the well with limited S-nZVI breakthrough (i.e., NB2-White).

Table 4.1 $\delta^{13}C$ values for selected compounds from NB1-White and NB2-White before (0 days) and after (17 days) the S-nZVI injection.

Location	Time (days)	PCE		TCE		cis 1,2-DCE		VC	
		[µM]	$\delta^{13}C$ (‰)	[µM]	$\delta^{13}C$ (‰)	[µM]	$\delta^{13}C$ (‰)	[µM]	$\delta^{13}C$ (‰)
NB1-White	0	391.8	-26.0	91.9	-22.9	251.8	-22.8	39.3	-23.0
	17	73.6	-24.6	62.6	-25.0	99.8	-20.2	39.2	-22.0
NB2-White	0	394.3	-26.3	120.7	-21.7	461.4	-25.7	29.1	-24.2
	17	416.2	-26.1	124.6	-22.6	217.3	-24.1	33.3	-25.0

The extent of cVOC transformation can be further explored through chloride ion analysis. Chloride ions are generated via reductive dechlorination of chlorinated hydrocarbons (Eq. 4.2). However, this analysis does not distinguish between possible distinct dechlorination pathways (e.g., biotic or abiotic).

$$Fe^0 + RCl + H^+ \rightarrow Fe^{2+} + RH + Cl^- \quad (4.2)$$

Some interesting changes in chloride concentrations were observed at select NB1 levels. For example, higher chloride concentrations were observed in the lower levels of NB1 (3.51 to 4.42 m bgs) before S-nZVI injection. However, the trend reversed after S-nZVI injection, with greater chloride concentrations detected at shallower depths (2.9 to 3.2 m bgs) (Figure 4.4a). Specifically, at day 3 the concentrations at the Black (2.9 m bgs) and Yellow (3.2 m bgs) levels increased by 4.5 mM (62%) and 7 mM (106%), respectively. On the other hand, concentrations decreased from 14.6 to 9.6 mM (34%) at the White (4.42 m bgs) level. Chloride concentrations also decreased significantly for Blue (4.12 m bgs), Clear (3.81 m bgs), and Green (3.51 m bgs) levels. The S-nZVI suspension reached the lower levels first, and at greater concentrations, which might have resulted in pushing the pre-existing well water vertically to the upper levels, resulting in upward mobilization of chloride in NB1. On day 17, chloride concentrations further decreased at White and Blue levels at NB1, increased for Green level but remained constant at the uppermost levels. Along with mobilization, dilution by the S-nZVI suspension might also have contributed to changes in chloride concentrations, especially at the lower levels. The chloride concentrations

calculated based on the generation of daughter products from the dechlorination of parent compounds account for only ~12% (0.5 mM) and ~15% (1.1 mM) of the total measured chloride in the Black and Yellow levels of NB1 on day 3, respectively (Table B.1). In this analysis, two key assumptions were made: 1) the generation of characteristic dechlorination products is solely due to the dechlorination of the highest chlorinated compounds (e.g., PCE and CCl_4) and 2) increases in chloride concentrations are only a consequence of aqueous cVOCs dechlorination and no other processes. The difference between the predicted and measured chloride could be due to mobilization and dilution as well as generation of unmonitored or unidentified dechlorination products. The changes in ultimate daughter product concentrations (e.g., ethene) also provide a means to quantify the extent of degradation. At day 3, the trend in ethene was similar to chloride with decreased concentrations at the lower levels and increased concentrations at the upper levels of NB1 (Figure 4.4b). Besides aqueous cVOCs dechlorination, the reason for this change could be partly attributed to upward mobilization of ethene when the S-nZVI suspension reached the lower levels, as explained for the chloride data. In contrast to chloride data, ethene concentrations increased significantly for all the levels, except Black, in NB1 from day 3 to day 17, indicating that dechlorination did occur in NB1 even if there were changes in cVOCs due to dilution and mobilization.

Although CSIA results and changes in ethene concentrations provide evidence of ongoing *in situ* dechlorination, changes in cVOC concentrations inevitably occurs due to dilution and mobilization caused by the S-nZVI suspension, as indicated by the changes in chloride concentrations. In order to evaluate the extent of dilution, the inorganic conservative constituent boron was analyzed. Boron at the White level in NB1, where chloride concentrations decreased, increased approximately seven-fold in comparison to boron at the Black level (Figure 4.2b). To make this observation more quantitative, the following relationship is used to determine the extent to which dilution contributes to the observed decrease in cVOCs (Eq. 4.3):[43]

$$D = 1 - \frac{C_{t(B)}}{C_{0(B)}} \tag{4.3}$$

where D is defined as a "dilution" factor, C_t is the boron concentration in the groundwater sample at t = 3 or 17 days and C_0 is the boron concentration in the injected suspension (37.7 mmol L^{-1}). Values approaching unity mean little to no dilution of the groundwater by the injected suspension. At day 3, dilution is most noticeable at NB1-White (D = 0.87, Figure B.8a), followed by NC1-White (0.92) and NA4-Blue (D = 0.93, Figure B.8b). All other wells, including NA3-White and upper levels of NB1, had D ≥0.95. At day 17, D values increased or remained constant for all the wells, except for NC1-White which decreased to 0.90 (Figure B.8b). The presence of boron above background concentrations indicates that the injected fluid could still be found in the targeted area at 3 days, and to a lesser extent, at 17 days after injection. This suggests that dilution might have contributed to changes in cVOCs concentrations.

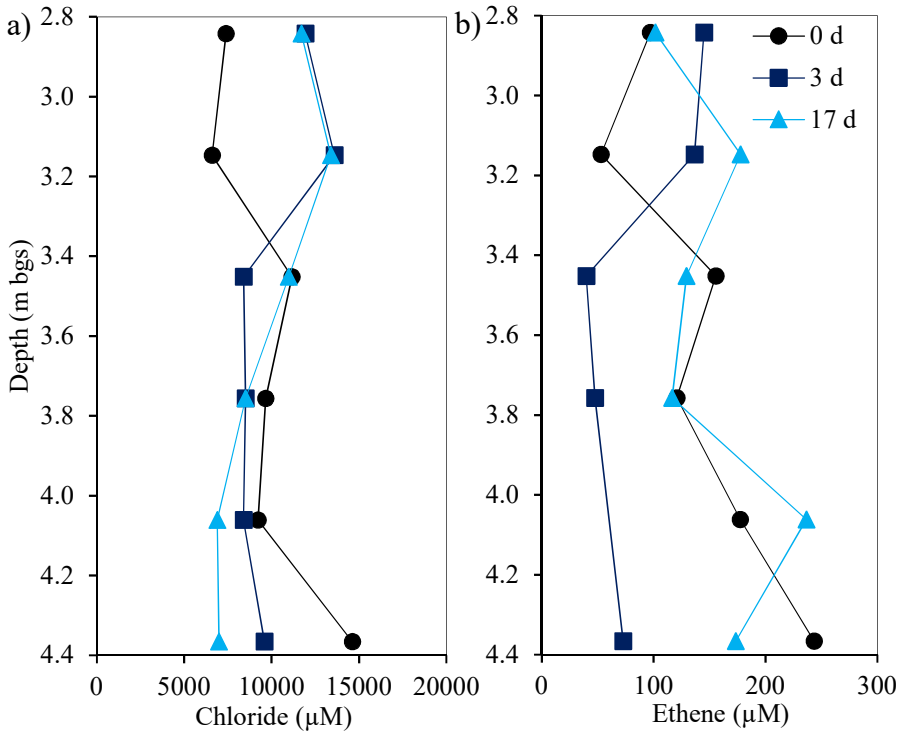

Figure 4.4 Vertical profile of a) chloride and b) ethene for the NB1 well.

4.3.3 Long - Term Site Response to S-nZVI: Changes in Aqueous cVOCs

NB1-White and NB1-Black were selected for further analysis of long-term dechlorination. NB1-White is just above the DNAPL pool whereas NB1-Black, the uppermost level located 1.5 m

above, is expected to be least affected by the source zone. Short-term monitoring indicated a significant decrease in parent compounds concentrations (i.e., PCE, $C0Cl_4$, and TeCAs) at both White and Black levels of NB1, which was partly due to dechlorination, as evidenced by CSIA results and changes in concentrations of daughter products (Figure 4.5). There was also a noticeable decrease in the concentrations of some of the daughter products on day 17 at both levels. Overall, the concentration of total cVOCs decreased from 922 μM to 692 μM at NB1-Black and from 1620 μM to 443 μM at NB1-White on day 17. However, the general trend in the long-term cVOC concentration was the opposite at these locations. For NB1-Black, the concentrations of parent compounds PCE, CCl_4, and TeCAs declined by ~70% on day 157, indicating transformation of these cVOCs (Figure 4.5a-d). Concurrently, the concentrations of daughter products (e.g., DCE isomers, chloroform, and 1,2-DCA) increased on day 157 but then decreased noticeably for the next sampling rounds. Production of ethene and increases in chloride concentrations at 157 days indicate the occurrence of dechlorination (Figure 4.5d and B.9a). Total cVOC concentrations decreased to as low as 245 μM at NB1-Black on day 561. In contrast, total cVOC concentration rebounded at NB1-White on day 157 and continuously increased to 2585 μM on day 561 (Figure 4.5e-h). There was a significant and continued increase in the concentrations of parent compounds as well as the daughter products at this level. The constant generation of ethene and chloride indicates that dechlorination was an operative process at NB1-White (Figure 4.5h and B.9b) although continued dissolution of the DNAPL pool below this sampling location appears to occur at a faster rate than dechlorination. Similar trends were observed for long-term cVOC data at NB2 where a continuous decrease in cVOC concentrations was observed at NB2-Black but cVOC concentrations at NB2-White increased with time, followed by increases in chloride concentrations (Figure B.9 and B.10).

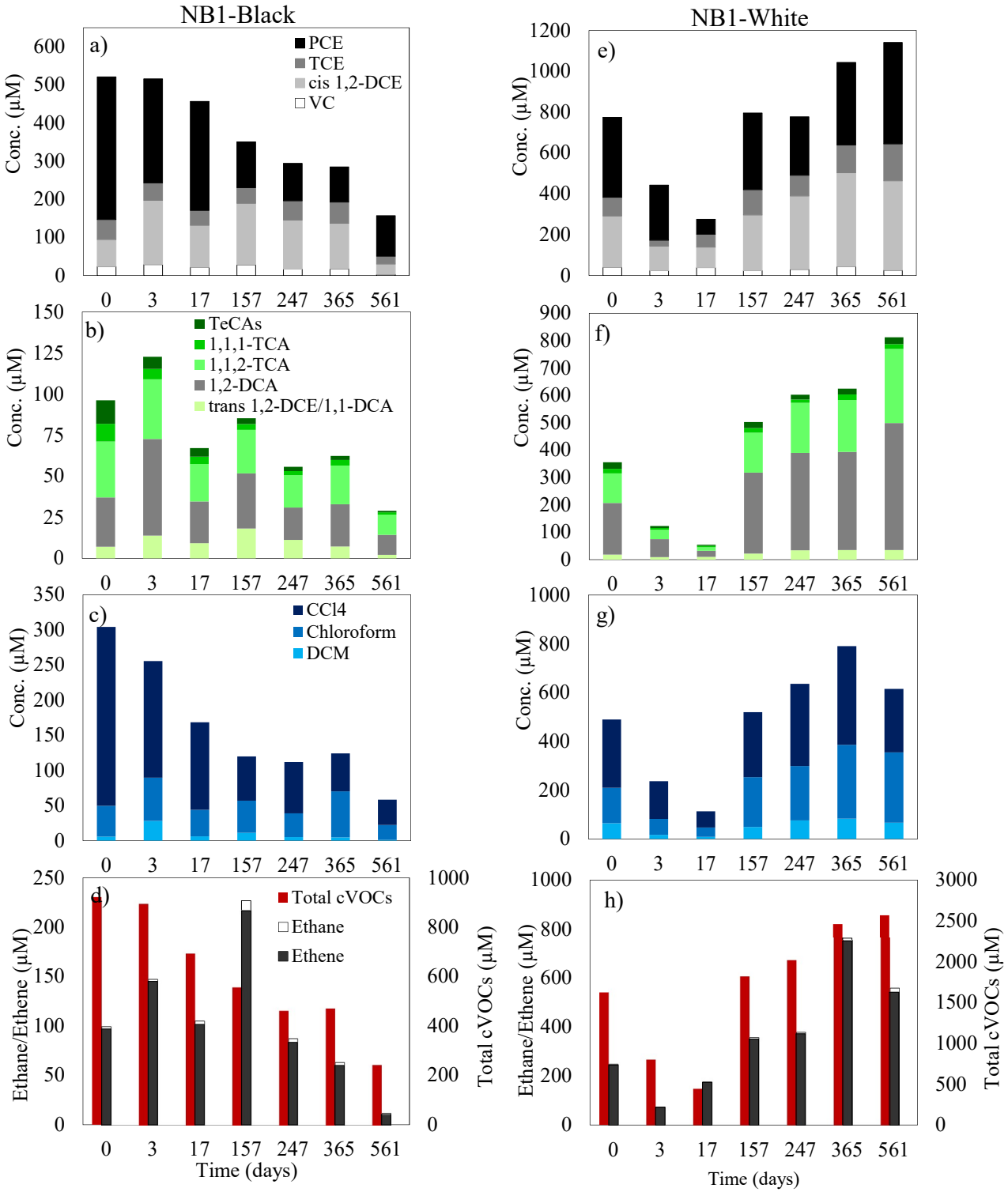

Figure 4.5 Background and Long – term post-injection concentrations for a – d) NB1-Black and e – h) NB1-White.

4.3.4 Possible Reaction Mechanisms

Detection of end products such as ethene and ethane in groundwater is a common metric used to determine if dechlorination is complete as these are common ultimate daughter products. The presence of ethene at almost all sampling locations throughout the monitoring period indicates the continuous occurrence of abiotic/biotic dechlorination even if changes in cVOCs concentrations could also be partially attributed to other physical/chemical processes such as dilution, mobilization, and/or dissolution from the DNAPL pool.

It is challenging to determine if changes in cVOCs concentrations were due to abiotic or biotic dechlorination. While the CSIA results for NB1-White confirmed the transformation of chlorinated ethenes, distinguishing between biotic and abiotic (via nZVI) processes for these cVOCs typically requires comparison of the isotope signatures of the dechlorination products *cis*-1,2-DCE, VC, acetylene, VC, and ethene. The 10‰ shift suggested by Elsner et al. [61] between products from abiotic dichloroelimination (e.g., ethene) and biotic hydrogenolysis via sequential reductive dechlorination (*cis*-1,2-DCE from TCE) was not observed in this field study, possibly due to the complexity of processes and remediation efforts that took place at this site over time. The presence of acetylene has been suggested as an indicator of abiotic reaction,[13, 74] given that biotransformation of chlorinated ethenes typically follows a sequential dichlorination pathway.[75] Even though acetylene was not detected, the rapid and efficient removal of cVOCs observed on day 17 suggests that dechlorination was mainly abiotic during this short-term monitoring period. A past field study in the adjoining area also showed significant cVOCs transformation within three weeks after CMC-nZVI injection, indicating the occurrence of short-term abiotic transformation followed by long-term biotransformation.[45] Injection of dithionite in the ISRM (*in situ* redox manipulation) technology successfully reduces native Fe(III) from aquifer sediments/soils to surface-bound and structural Fe(II) species, resulting in transformation of organic and inorganic contaminants.[76] As the injected S-nZVI suspension contained dithionite and the soil in the current study area is rich in iron (Figure B.11), reactive iron(II) species might also have contributed to the short-term abiotic dechlorination to a certain extent. It has been reported that ISRM maintains subsurface conditions conducive to effective abiotic dechlorination of contaminants for more than 3 years.[77] Moreover, the injected S-nZVI suspension retained in the injection well was still jet black in color after 197 days, indicating the presence of iron sulfides and iron(II) oxides.[39] This

suggests some possibility of long-term abiotic dechlorination. However, biotic dechlorination is also expected to contribute to the remediation taking place at longer time-scales. This has also been reported for an earlier nZVI field trial conducted in the adjacent area at this site.[55]

For short-term dechlorination, CSIA results confirm the generation of TCE as a product of PCE dechlorination in NB1-White, along with TCE removal. Other wells (e.g. NB1-Black) also showed a temporary increase in the concentrations of intermediates such as *cis*-1,2-DCE with concurrent dechlorination of PCE. This suggests hydrogenolysis as the dechlorination mechanism for chlorinated ethenes. However, PCE dechlorination generally exceeded the generation of intermediates and ethene, indicating the occurrence of reductive β-elimination in the current study as well. Similarly, dechlorination of *cis*-1,2-DCE (e.g. NB1-White and NB2-White) exceeded the formation of vinyl chloride and ethene. These results suggest that reductive β-elimination was also happening simultaneously. Past research has reported both reductive β-elimination and hydrogenolysis as the dechlorination mechanisms for TCE, treated by S-nZVI, where acetylene or ethene were reported as the major dechlorination products.[34, 36, 78] Experimental conditions, particularly the method of nZVI sulfidation, determine which mechanism would dominate. For example, Han and Yan [34] reported ethene as the major product, with ethane and acetylene as the minor products, while treating TCE with S-nZVI developed by post-synthesis addition of dithionite (method similar to the one used in this study). In the current field study, no acetylene was detected but this does not completely rule out its formation. The quantification of acetylene is challenging in the field as it quickly volatilizes in air. This may be the reason that reductive β-elimination products are rarely reported for the iron-treated field studies. In the case of chlorinated methanes, the formation of chloroform and DCM indicates the transformation of CT via sequential hydrogenolysis. Jin et al. [79] has also reported the production of chloroform during CT transformation by S-nZVI.

In the long-term dechlorination data the formation of intermediates (e.g., DCE isomers, chloroform, and DCM) at NB1-Black and NB2-Black indicate that hydrogenolysis was an operative process. Significant decrease in *cis*-1,2-DCE concentrations without equivalent production of VC suggest that reductive β-elimination was also an operative dechlorination mechanism. Microbial transformation of highly chlorinated ethanes and ethenes often results in partial dechlorination, leading to the accumulation of intermediates such as DCE isomers and

VC.[43, 55] The accumulation of vinyl chloride, a highly toxic and confirmed human carcinogen,[80] is usually of particular concern due to its poor biodegradability. The previous nZVI field trial in the adjacent area reported the generation and accumulation of vinyl chloride during long-term microbial transformation of PCE and TCE following a CMC-nZVI injection.[45, 55] However, one of the most positive outcome of this S-nZVI field treatment is the non-accumulation of lower chlorinated VOCs, particularly vinyl chloride. S-nZVI (dithionite sulfidated) injection would result in decreased H_2 evolution, higher concentrations of iron sulfides, and significant reduction of Fe(III) in sediments/soil to Fe(II) species whereas CMC-nZVI injection would generate higher amounts of H_2 and may not significantly impact the latter two conditions. Thus, there can be two possible reasons for the non-accumulation of VC in the S-nZVI field study as opposed to the nZVI field trial. First, differences in geochemical changes, along with the direct interactions between nZVI/S-nZVI and microbes, are expected to result in different inhibitory/stimulatory effects on the microbial communities for the two treatments. Certain classes of bacteria have the ability to intrinsically biodegrade VC in anaerobic aquifers.[81, 82] Although not yet investigated, the geochemical conditions in the subsurface created by S-nZVI injection might be conducive to the enrichment of these bacteria. Second, reactive Fe(II) species from dithionite-reduced sediments would result in reductive β-elimination for dechlorination of chlorinated ethenes as the preferential dechlorination pathway.[76] *Cis*-1,2-DCE dechlorinated by this mechanism does not generate vinyl chloride.

4.3.5 Changes in Soil cVOCs

Visual observations in the form of staining/sheening of soil cores as well as quantification of organic soil vapor measurements (Figure B.1) indicated that a large amount of cVOCs resided as DNAPL and/or sorbed mass and not in the aqueous phase. Soil cVOCs concentrations are considered as a better metric than aqueous phase concentrations for determining the mass reduction.[41] Thus, cVOC concentrations and distribution were examined for soil samples collected before and after S-nZVI injection to quantify changes in soil cVOCs. Since soil cores cannot be taken from the same spatial location multiple times, 'post-injection' soil samples were collected at locations adjacent to 'pre-injection' locations to obtain representative changes in soil cVOCs concentrations throughout the study area (Figure B.12). Table B.2 presents a summary of cVOCs concentrations in the soil samples collected between ~2.5 and 5 m bgs (8 – 16 ft bgs). The data

shows a significant decrease in concentrations of most of the chlorinated compounds in soil samples collected on day 94 after S-nZVI injection. There was an additional decrease in individual concentrations of all the cVOCs, including PCE, on day 554 where some cVOCs were not even detected at many locations. Figure B.13 shows a continuous decline in the total cVOCs concentrations where the background average of 1496 µmol/kg decreased to 653 and 125 µmol/kg, respectively on day 94 and 554 after S-nZVI injection. Table B.2 and Figure B.13 also show that soil cVOC concentrations are highly variable. For example, PCE concentrations varied between 35.5 and 1759 µmol/kg for the three zones on day 94. Thus, the results are also presented as 'box and whisker' plots for the cVOCs by grouping the data for each sampling event (Figure 4.6).

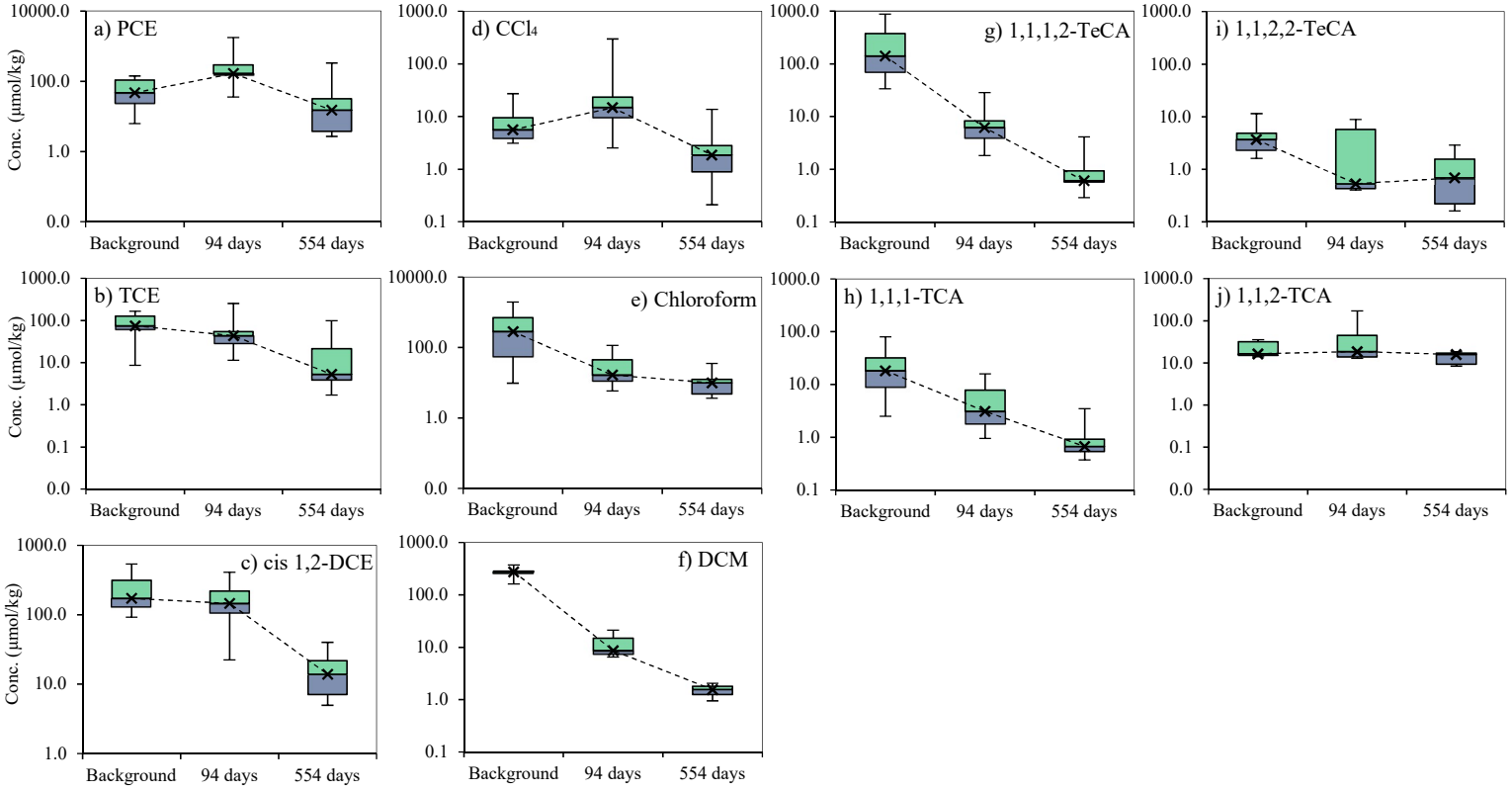

Figure 4.6 cVOCs concentrations in soil for background and post-injection (at 94 and 554 days) samples collected between 2.5 and 4.5 m bgs. The box-and-whisker plot shows the median (×), the interquartile range (box) and the extrema (whiskers). Dash lines are straight connectors between the medians.

Concentrations of PCE and CCl_4 showed some increase on day 94 but noticeably decreased on day 554. For all the other cVOCs (e.g., TCE, cis 1,2-DCE, chloroform, DCM, 1,1,1,2-TeCA and 1,1,1-

TCA), there was a downward trend in the median concentrations with time. Median concentrations for TCE decreased from 74.9 µmol/kg in background samples to 5.3 µmol/kg at 554 days. For chloroform and 1,1,1,2-TeCA changes were more noticeable, decreasing from 286 to 9.9 µmol/kg and from 141 to 0.6 µmol/kg, respectively. 1,1,1-TCA decreased from 18.1 µmol/kg to 0.67 µmol/kg. Similarly, DCM and *cis*-1,2-DCE median concentrations decreased considerably, from 278 to 1.5 µmol/kg and 172 to 13.9 µmol/kg, respectively. Trends between the ten compounds analyzed were not always consistent. For instance, median concentrations for 1,1,2-TCA remained relatively constant throughout the monitoring period, ranging between 16.3 and 18.5 µmol/kg. Quantification of the extent of remediation using soil cores is challenging, in part due to spatial variations and highly stratified distribution of contaminants within aquifers. This complexity is exacerbated by the different sampling depths between locations and time of sampling, not allowing for a systematic depth-by-depth comparison. A correlation analysis of the raw data, depicted in SI Table B.2, was carried out with the purpose of evaluating the overall effectiveness of the S-nZVI injection on altering the cVOCs concentrations in soil (Table B.3). The 'r' values indicate that the cVOCs concentrations correlate better with each other over time, suggesting the treatment was effective in causing a change in the concentrations and distribution of contaminants in the soil. This decrease in soil cVOCs might have occurred partly due to enhanced biological activity after S-nZVI injection. However, more work needs to be completed to investigate the effect of this S-nZVI formulation on the microbial communities in the treatment zone. Dithionite-reduced surface bound and structural Fe(II) in the aquifer sediments/soil might also have played a role in the transformation of soil cVOCs. These results suggest S-nZVI is an effective strategy for cVOCs dechlorination in soil.

4.4 Conclusions

Results reported herein demonstrate the suitability of S-nZVI as an effective remedial technique for soil and groundwater remediation at existing contaminated sites. A rapid decrease in cVOC concentrations was observed in groundwater samples immediately after injection, followed by sustained long-term dechlorination. Although S-nZVI injection resulted in some dilution and mobilization of cVOCs, the increase in ethene concentrations clearly indicate dechlorination. CSIA serves as another line of evidence, confirming the direct impact of abiotic/biotic transformation as shown by the changes in stable isotope values of key chlorinated compounds.

Proximity to the DNAPL pool resulted in mass transfer of non-aqueous constituents into the aqueous phase at the deeper Blue and White levels (4 - 4.5 m bgs), although, significant ethene generation indicated concurrent dechlorination. In contrast, the uppermost level (Black), which is expected to be least affected by the source zone, observed a continuous decline in cVOCs concentrations accompanied with generation of ethene, confirming the dechlorination of cVOCs. Transformation was not limited to the aqueous phase as concentrations of soil cVOCs also decreased significantly at 94 and 554 days after injection. Sulfidation of nZVI with dithionite may additionally result in reducing the native Fe(III) in aquifer sediments to the reactive Fe(II) species which can degrade contaminants.

Long-term success of *in situ* emplacement of nZVI often relies on the biotic dechlorination that follows,[55] and care must be taken not to inhibit the growth of healthy microbial communities. In this study it was shown that product distribution at multiple monitoring wells points to the contribution of microbially-mediated reactions, suggesting that growth of microbial communities was not inhibited. However, the extent to which biotic processes contributed to the transformation of cVOCs is unknown and further characterization of the microbial communities after emplacement of S-nZVI is needed.

As fundamental work continues into the synthesis, characterization, and overall mechanisms of reactivity, this project is the first pilot study to take abiotic sulfidation of CMC stabilized nZVI from bench – to field – scale applications. With the growing interest from all sectors of the remediation community, as evidenced by the introduction of new commercial products sulfidating (n)ZVI,[83] S-nZVI is likely to become an important *In Situ* Chemical Reduction (ISCR) technology.

4.5 References

1. Fan, D.; Lan, Y.; Tratnyek, P. G.; Johnson, R. L.; Filip, J.; O'Carroll, D. M.; Nunez Garcia, A.; Agrawal, A., Sulfidation of Iron-Based Materials: A Review of Processes and Implications for Water Treatment and Remediation. *Environ Sci Technol* **2017,** *51*, (22), 13070-13085.

2. Li, J.; Zhang, X.; Sun, Y.; Liang, L.; Pan, B.; Zhang, W.; Guan, X., Advances in Sulfidation of Zerovalent Iron for Water Decontamination. *Environ Sci Technol* **2017,** *51*, (23), 13533–13544.

3. Gu, B.; Phelps, T. J.; Liang, L.; Dickey, M. J.; Roh, Y.; Kinsall, B. L.; Palumbo, A. V.; Jacobs, G. K., Biogeochemical dynamics in zero-valent iron columns: Implications for permeable reactive barriers. *Environ Sci Technol* **1999,** *33*, (13), 2170-2177.

4. Herbert, R. B.; Benner, S. G.; Blowes, D. W., Solid phase iron-sulfur geochemistry of a reactive barrier for treatment of mine drainage. *Appl Geochem* **2000,** *15*, (9), 1331-1343.

5. Benner, S. G.; Blowes, D. W.; Gould, W. D.; Herbert, R. B.; Ptacek, C. J., Geochemistry of a permeable reactive barrier for metals and acid mine drainage. *Environ Sci Technol* **1999,** *33*, (16), 2793-2799.

6. Furukawa, Y.; Kim, J. W.; Watkins, J.; Wilkin, R. T., Formation of ferrihydrite and associated iron corrosion products in permeable reactive barriers of zero-valent iron. *Environ Sci Technol* **2002,** *36*, (24), 5469-5475.

7. Wilkin, R. T.; Puls, R. W.; Sewell, G. W., Long-term performance of permeable reactive barriers using zero-valent iron: Geochemical and microbiological effects. *Ground Water* **2003,** *41*, (4), 493-503.

8. Phillips, D. H.; Gu, B.; Watson, D. B.; Roh, Y.; Liang, L.; Lee, S. Y., Performance evaluation of a zerovalent iron reactive barrier: Mineralogical characteristics. *Environ Sci Technol* **2000,** *34*, (19), 4169-4176.

9. Puls, R. W.; Paul, C. J.; Powell, R. M., The application of in situ permeable reactive (zero-valent iron) barrier technology for the remediation of chromate-contaminated groundwater: a field test. *Appl Geochem* **1999,** *14*, (8), 989-1000.

10. Roh, Y.; Lee, S. Y.; Elless, M. P., Characterization of corrosion products in the permeable reactive barriers. *Environ Geol* **2000,** *40*, (1-2), 184-194.

11. Benner, S. G.; Blowes, D. W.; Ptacek, C. J.; Mayer, K. U., Rates of sulfate reduction and metal sulfide precipitation in a permeable reactive barrier. *Appl Geochem* **2002,** *17*, (3), 301-320.

12. Butler, E. C.; Hayes, K. F., Kinetics of the transformation of halogenated aliphatic compounds by iron sulfide. *Environ Sci Technol* **2000,** *34*, (3), 422-429.

13. Butler, E. C.; Hayes, K. F., Kinetics of the transformation of trichloroethylene and tetrachloroethylene by iron sulfide. *Environ Sci Technol* **1999,** *33*, (12), 2021-2027.

14. Butler, E. C.; Hayes, K. F., Effects of Solution Composition and pH on the Reductive Dechlorination of Hexachloroethane by Iron Sulfide. *Environ Sci Technol* **1998,** *32*, (9), 1276-1284.

15. He, Y. T.; Wilson, J. T.; Wilkin, R. T., Transformation of reactive iron minerals in a permeable reactive barrier (biowall) used to treat TCE in groundwater. *Environ Sci Technol* **2008,** *42*, (17), 6690-6696.

16. Shen, H.; Wilson, J. T., Trichloroethylene removal from groundwater in flow-through columns simulating a permeable reactive barrier constructed with plant mulch. *Environ Sci Technol* **2007,** *41*, (11), 4077-4083.

17. Kennedy, L. G.; Everett, J. W.; Becvar, E.; Defeo, D., Field-scale demonstration of induced biogeochemical reductive dechlorination at Dover Air Force Base, Dover, Delaware. *Journal of contaminant hydrology* **2006,** *88*, (1-2), 119-136.

18. Kennedy, L. G.; Everett, J. W.; Gonzales, J., Assessment of biogeochemical natural attenuation and treatment of chlorinated solvents, Altus Air Force Base, Altus, Oklahoma. *Journal of contaminant hydrology* **2006,** *83*, (3-4), 221-236.

19. Gong, Y.; Tang, J.; Zhao, D., Application of iron sulfide particles for groundwater and soil remediation: A review. *Water research* **2016,** *89*, 309-320.

20. Cumbal, L. H.; Debut, A.; Delgado, D. A.; Jurado, C. B.; Stael, C., Synthesis of Multicomponent Nanoparticles for Immobilization of Heavy Metals in Aqueous Phase. *NanoWorld J* **2015,** *1*, (4), 103-109.

21. Kim, E. J.; Kim, J. H.; Azad, A. M.; Chang, Y. S., Facile Synthesis and Characterization of Fe/FeS Nanoparticles for Environmental Applications. *ACS Appl. Mater. Inter.* **2011,** *3*, (5), 1457-1462.

22. Kim, E.-J.; Kim, J.-H.; Chang, Y.-S.; Turcio-Ortega, D.; Tratnyek, P. G., Effects of Metal Ions on the Reactivity and Corrosion Electrochemistry of Fe/FeS Nanoparticles. *Environ Sci Technol* **2014,** *48*, (7), 4002-4011.

23. Kim, E.-J.; Murugesan, K.; Kim, J.-H.; Tratnyek, P. G.; Chang, Y.-S., Remediation of Trichloroethylene by FeS-Coated Iron Nanoparticles in Simulated and Real Groundwater: Effects of Water Chemistry. *Ind Eng Chem Res* **2013,** *52*, (27), 9343-9350.

24. Su, Y.; Adeleye, A. S.; Huang, Y.; Zhou, X.; Keller, A. A.; Zhang, Y., Direct Synthesis of Novel and Reactive Sulfide-modified Nano Iron through Nanoparticle Seeding for Improved Cadmium-Contaminated Water Treatment. *Scientific Reports* **2016,** *6*, 24358.

25. Su, Y.; Adeleye, A. S.; Keller, A. A.; Huang, Y.; Dai, C.; Zhou, X.; Zhang, Y., Magnetic sulfide-modified nanoscale zerovalent iron (S-nZVI) for dissolved metal ion removal. *Water research* **2015,** *74*, 47-57.

26. Li, D.; Mao, Z.; Zhong, Y.; Huang, W.; Wu, Y.; Peng, P. a., Reductive transformation of tetrabromobisphenol A by sulfidated nano zerovalent iron. *Water research* **2016,** *103*, 1-9.

27. Li, D.; Zhu, X. F.; Zhong, Y.; Huang, W. L.; Peng, P., Abiotic transformation of hexabromocyclododecane by sulfidated nanoscale zerovalent iron: Kinetics, mechanism and influencing factors. *Water research* **2017,** *121*, 140-149.

28. Rayaroth, M. P.; Lee, C. S.; Aravind, U. K.; Aravindakumar, C. T.; Chang, Y. S., Oxidative degradation of benzoic acid using Fe-0 - and sulfidized Fe-0-activated persulfate: A comparative study. *Chem Eng J* **2017,** *315*, 426-436.

29. Gong, Y.; Gai, L.; Tang, J.; Fu, J.; Wang, Q.; Zeng, E. Y., Reduction of Cr(VI) in simulated groundwater by FeS-coated iron magnetic nanoparticles. *Science of The Total Environment* **2017,** *595*, 743-751.

30. Song, S.; Su, Y.; Adeleye, A. S.; Zhang, Y.; Zhou, X., Optimal design and characterization of sulfide-modified nanoscale zerovalent iron for diclofenac removal. *Applied Catalysis B: Environmental* **2017,** *201*, 211-220.

31. Fan, D.; O'Brien Johnson, G.; Tratnyek, P. G.; Johnson, R. L., Sulfidation of Nano Zerovalent Iron (nZVI) for Improved Selectivity During In-Situ Chemical Reduction (ISCR). *Environ Sci Technol* **2016,** *50*, (17), 9558-9565.

32. Nunez Garcia, A.; Boparai, H. K.; O'Carroll, D. M., Enhanced Dechlorination of 1,2-Dichloroethane by Coupled Nano Iron-Dithionite Treatment. *Environ Sci Technol* **2016,** *50*, (10), 5243-5251.

33. Cao, Z.; Liu, X.; Xu, J.; Zhang, J.; Yang, Y.; Zhou, J. L.; Xu, X. H.; Lowry, G. V., Removal of Antibiotic Florfenicol by Sulfide-Modified Nanoscale Zero-Valent Iron. *Environ Sci Technol* **2017,** *51*, (19), 11269-11277.

34. Han, Y.; Yan, W., Reductive Dechlorination of Trichloroethene by Zero-valent Iron Nanoparticles: Reactivity Enhancement through Sulfidation Treatment. *Environ Sci Technol* **2016,** *50*, (23), 12992-13001.

35. Fan, D. M.; Anitori, R. P.; Tebo, B. M.; Tratnyek, P. G.; Pacheco, J. S. L.; Kukkadapu, R. K.; Engelhard, M. H.; Bowden, M. E.; Kovarik, L.; Arey, B. W., Reductive Sequestration of Pertechnetate ((TcO4-)-Tc-99) by Nano Zerovalent Iron (nZVI) Transformed by Abiotic Sulfide. *Environ Sci Technol* **2013,** *47*, (10), 5302-5310.

36. Rajajayavel, S. R. C.; Ghoshal, S., Enhanced reductive dechlorination of trichloroethylene by sulfidated nanoscale zerovalent iron. *Water research* **2015,** *78*, 144-153.

37. Tang, J.; Tang, L.; Feng, H.; Zeng, G.; Dong, H.; Zhang, C.; Huang, B.; Deng, Y.; Wang, J.; Zhou, Y., pH-dependent degradation of p-nitrophenol by sulfidated nanoscale zerovalent iron under aerobic or anoxic conditions. *Journal of hazardous materials* **2016,** *320*, 581-590.

38. Kim, E.-J.; Le Thanh, T.; Kim, J.-H.; Chang, Y.-S., Synthesis of metal sulfide-coated iron nanoparticles with enhanced surface reactivity and biocompatibility. *RSC Advances* **2013,** *3*, (16), 5338-5340.

39. Nunez Garcia, A.; Boparai, H. K.; De Boer, C.; Chowdhury, A. I. A.; Kocur, C. M. D.; Austrins, L. M.; Sidebottom, A.; Herrera, J. E.; O'Carroll, D. M., Fate and Transport of Sulfidated Nano Zerovalent Iron (S-nZVI): A Field Study. In Preparation.

40. Elliott, D. W.; Zhang, W.-x., Field Assessment of Nanoscale Bimetallic Particles for Groundwater Treatment. *Environ Sci Technol* **2001,** *35*, (24), 4922-4926.

41. Henn, K. W.; Waddill, D. W., Utilization of nanoscale zero-valent iron for source remediation—A case study. *Remediation Journal* **2006,** *16*, (2), 57-77.

42. Bennett, P.; He, F.; Zhao, D. Y.; Aiken, B.; Feldman, L., In situ testing of metallic iron nanoparticle mobility and reactivity in a shallow granular aquifer. *Journal of contaminant hydrology* **2010,** *116*, (1-4), 35-46.

43. He, F.; Zhao, D.; Paul, C., Field assessment of carboxymethyl cellulose stabilized iron nanoparticles for in situ destruction of chlorinated solvents in source zones. *Water research* **2010,** *44*, (7), 2360-70.

44. Wei, Y.-T.; Wu, S.-C.; Chou, C.-M.; Che, C.-H.; Tsai, S.-M.; Lien, H.-L., Influence of nanoscale zero-valent iron on geochemical properties of groundwater and vinyl chloride degradation: A field case study. *Water research* **2010,** *44*, (1), 131-140.

45. Kocur, C. M. D.; Lomheim, L.; Boparai, H. K.; Chowdhury, A. I. A.; Weber, K. P.; Austrins, L. M.; Edwards, E. A.; Sleep, B. E.; O'Carroll, D. M., Contributions of Abiotic and Biotic Dechlorination Following Carboxymethyl Cellulose Stabilized Nanoscale Zero Valent Iron Injection. *Environ Sci Technol* **2015,** *49*, (14), 8648-8656.

46. Chowdhury, A. I. A.; Krol, M. M.; Kocur, C. M.; Boparai, H. K.; Weber, K. P.; Sleep, B. E.; O'Carroll, D. M., nZVI injection into variably saturated soils: Field and modeling study. *Journal of contaminant hydrology* **2015,** *183*, 16-28.

47. Sheu, Y. T.; Lien, P. J.; Chen, K. F.; Ou, J. H.; Kao, C. M., Application of NZVI-contained emulsified substrate to bioremediate PCE-contaminated groundwater – A pilot-scale study. *Chem Eng J* **2016,** *304*, 714-727.

48. Ahn, J.-Y.; Kim, C.; Kim, H.-S.; Hwang, K.-Y.; Hwang, I., Effects of oxidants on in situ treatment of a DNAPL source by nanoscale zero-valent iron: A field study. *Water research* **2016,** *107*, 57-65.

49. Fang, Y.; Wen, J.; Zeng, G.; Shen, M.; Cao, W.; Gong, J.; Zhang, Y., From nZVI to SNCs: development of a better material for pollutant removal in water. *Environ Sci Pollut R* **2018**.

50. Stefaniuk, M.; Oleszczuk, P.; Ok, Y. S., Review on nano zerovalent iron (nZVI): From synthesis to environmental applications. *Chem Eng J* **2016,** *287*, 618-632.

51. Busch, J.; Meißner, T.; Potthoff, A.; Bleyl, S.; Georgi, A.; Mackenzie, K.; Trabitzsch, R.; Werban, U.; Oswald, S. E., A field investigation on transport of carbon-supported nanoscale zero-valent iron (nZVI) in groundwater. *Journal of contaminant hydrology* **2015,** *181*, 59-68.

52. Vogel, M.; Nijenhuis, I.; Lloyd, J.; Boothman, C.; Pöritz, M.; Mackenzie, K., Combined chemical and microbiological degradation of tetrachloroethene during the application of

Carbo-Iron at a contaminated field site. *Science of The Total Environment* **2018,** *628–629*, 1027-1036.

53. Hunkeler, D.; Meckenstock, R. U.; Sherwood Lollar, B.; Schmidt, T. C.; Wilson, J. T. *A Guide for Assessing Biodegradation and Source Identification of Organic Ground Water Contaminants Using Compound Specific Isotope Analysis (CSIA)*; U.S. EPA: 2009; pp 1 - 82.

54. Elsner, M.; Couloume, G. L.; Mancini, S.; Burns, L.; Sherwood Lollar, B., Carbon Isotope Analysis to Evaluate Nanoscale Fe(O) Treatment at a Chlorohydrocarbon Contaminated Site. *Ground Water Monit R* **2010,** *30*, (3), 79-95.

55. Kocur, C. M. D.; Lomheim, L.; Molenda, O.; Weber, K. P.; Austrins, L. M.; Sleep, B. E.; Boparai, H. K.; Edwards, E. A.; O'Carroll, D. M., Long-Term Field Study of Microbial Community and Dechlorinating Activity Following Carboxymethyl Cellulose-Stabilized Nanoscale Zero-Valent Iron Injection. *Environ Sci Technol* **2016,** *50*, (14), 7658-7670.

56. Kocur, C. M.; Chowdhury, A. I.; Sakulchaicharoen, N.; Boparai, H. K.; Weber, K. P.; Sharma, P.; Krol, M. M.; Austrins, L.; Peace, C.; Sleep, B. E.; O'Carroll, D. M., Characterization of nZVI Mobility in a Field Scale Test. *Environ Sci Technol* **2014,** *48*, (5), 2862-2869.

57. Elsner, M.; Couloume, G. L.; Sherwood Lollar, B., Freezing to preserve groundwater samples and improve headspace quantification limits of water-soluble organic contaminants for carbon isotope analysis. *Anal Chem* **2006,** *78*, (21), 7528-7534.

58. Sherwood Lollar, B.; Hirschorn, S. K.; Chartrand, M. M. G.; Lacrampe-Couloume, G., An Approach for Assessing Total Instrumental Uncertainty in Compound-Specific Carbon Isotope Analysis: Implications for Environmental Remediation Studies. *Anal Chem* **2007,** *79*, (9), 3469-3475.

59. Elsner, M.; McKelvie, J.; Lacrampe Couloume, G.; Sherwood Lollar, B., Insight into Methyl tert-Butyl Ether (MTBE) Stable Isotope Fractionation from Abiotic Reference Experiments. *Environ Sci Technol* **2007,** *41*, (16), 5693-5700.

60. Liang, X.; Dong, Y.; Kuder, T.; Krumholz, L. R.; Philp, R. P.; Butler, E. C., Distinguishing abiotic and biotic transformation of tetrachloroethylene and trichloroethylene by stable carbon isotope fractionation. *Environ Sci Technol* **2007,** *41*, (20), 7094-7100.

61. Elsner, M.; Chartrand, M.; VanStone, N.; Lacrampe Couloume, G.; Sherwood Lollar, B., Identifying Abiotic Chlorinated Ethene Degradation: Characteristic Isotope Patterns in Reaction Products with Nanoscale Zero-Valent Iron. *Environ Sci Technol* **2008,** *42*, (16), 5963-5970.

62. Vanstone, N.; Elsner, M.; Lacrampe-Couloume, G.; Mabury, S.; Sherwood Lollar, B., Potential for identifyng abiotic chloroalkane degradation mechanisms using carbon isotopic fractionation. *Environ Sci Technol* **2008,** *42*, (1), 126-132.

63. Mariotti, A.; Germon, J. C.; Hubert, P.; Kaiser, P.; Letolle, R.; Tardieux, A.; Tardieux, P., Experimental determination of nitrogen kinetic isotope fractionation: Some principles; illustration for the denitrification and nitrification processes. *Plant and Soil* **1981,** *62*, (3), 413-430.

64. Abe, Y.; Aravena, R.; Zopfi, J.; Shouakar-Stash, O.; Cox, E.; Roberts, J. D.; Hunkeler, D., Carbon and Chlorine Isotope Fractionation during Aerobic Oxidation and Reductive Dechlorination of Vinyl Chloride and cis-1,2-Dichloroethene. *Environ Sci Technol* **2009,** *43*, (1), 101-107.

65. Bloom, Y.; Aravena, R.; Hunkeler, D.; Edwards, E.; Frape, S. K., Carbon isotope fractionation during microbial dechlorination of trichloroethene, cis-1,2-dichloroethene, and vinyl chloride: Implications for assessment of natural attenuation. *Environ Sci Technol* **2000,** *34*, (13), 2768-2772.

66. Hunkeler, D.; Aravena, R.; Cox, E., Carbon isotopes as a tool to evaluate the origin and fate of vinyl chloride: Laboratory experiments and modeling of isotope evolution. *Environ Sci Technol* **2002,** *36*, (15), 3378-3384.

67. Lee, P. K. H.; Conrad, M. E.; Alvarez-Cohen, L., Stable carbon isotope fractionation of chloroethenes by dehalorespiring isolates. *Environ Sci Technol* **2007,** *41*, (12), 4277-4285.

68. Slater, G. F.; Sherwood Lollar, B.; Sleep, B. E.; Edwards, E. A., Variability in carbon isotopic fractionation during biodegradation of chlorinated ethenes: Implications for field applications. *Environ Sci Technol* **2001,** *35*, (5), 901-907.

69. Wiegert, C.; Mandalakis, M.; Knowles, T.; Polymenakou, P. N.; Aeppli, C.; Macháčková, J.; Holmstrand, H.; Evershed, R. P.; Pancost, R. D.; Gustafsson, Ö., Carbon and Chlorine Isotope Fractionation During Microbial Degradation of Tetra- and Trichloroethene. *Environ Sci Technol* **2013,** *47*, (12), 6449-6456.

70. Audí-Miró, C.; Cretnik, S.; Otero, N.; Palau, J.; Shouakar-Stash, O.; Soler, A.; Elsner, M., Cl and C isotope analysis to assess the effectiveness of chlorinated ethene degradation by zero-valent iron: Evidence from dual element and product isotope values. *Appl Geochem* **2013,** *32*, (Supplement C), 175-183.

71. Lojkasek-Lima, P.; Aravena, R.; Shouakar-Stash, O.; Frape, S. K.; Marchesi, M.; Fiorenza, S.; Vogan, J., Evaluating TCE Abiotic and Biotic Degradation Pathways in a Permeable Reactive Barrier Using Compound Specific Isotope Analysis. *Ground Water Monit R* **2012,** *32*, (4), 53-62.

72. Slater, G. F.; Sherwood Lollar, B.; King, R. A.; O'Hannesin, S., Isotopic fractionation during reductive dechlorination of trichloroethene by zero-valent iron: influence of surface treatment. *Chemosphere* **2002,** *49*, (6), 587-596.

73. VanStone, N. A.; Focht, R. M.; Mabury, S. A.; Sherwood Lollar, B., Effect of Iron Type on Kinetics and Carbon Isotopic Enrichment of Chlorinated Ethylenes During Abiotic Reduction on Fe(0). *Groundwater* **2004,** *42*, (2), 268-276.

74. Arnold, W. A.; Roberts, A. L., Pathways and kinetics of chlorinated ethylene and chlorinated acetylene reaction with Fe(O) particles. *Environ Sci Technol* **2000,** *34*, (9), 1794-1805.

75. Lacinova, L.; Kvapil, P.; Cernik, M., A field comparison of two reductive dechlorination (zero-valent iron and lactate) methods. *Environmental technology* **2012,** *33*, (7), 741-749.

76. Fruchter, J. S.; Spane, F. A.; Amonette, J. E.; Fredrickson, J. K.; Cole, C. R.; Templeton, J. C.; Stevens, T. O.; Holford, D. J.; Eary, L. E.; Zachara, J. M.; Bjornstad, B. N.; Black, G. D.; Vermeul, V. R.; Simmons, C. S. *Interim report: Manipulation of natural subsurface processes: Field research and validation*; PNL-10123; Battelle Press: Richland, WA, 1994; pp 88-106.

77. Fruchter, J. S.; Cole, C. R.; Williams, M. D.; Vermeul, V. R.; Amonette, J. E.; Szecsody, J. E.; Istok, J. D.; Humphrey, M. D., Creation of a subsurface permeable treatment zone for aqueous chromate contamination using in situ redox manipulation. *Ground Water Monit R* **2000,** *20*, (2), 66-77.

78. He, F.; Li, Z.; Shi, S.; Xu, W.; Sheng, H.; Gu, Y.; Jiang, Y.; Xi, B., Dechlorination of Excess Trichloroethene by Bimetallic and Sulfidated Nanoscale Zero-Valent Iron. *Environ Sci Technol* **2018,** *52*, (15), 8627–8637.

79. Jin, X.; Chen, H.; Yang, Q.; Hu, Y. A.; Yang, Z. L., Dechlorination of Carbon Tetrachloride by Sulfide-Modified Nanoscale Zerovalent Iron. *Environ Eng Sci* **2018,** *35*, (6), 560-567.

80. Agency for Toxic Substances and Disease Registry (ATSDR). *Toxicological profile for Vinyl Chloride*; U.S. Department of Health and Human Services, Public Health Service: Atlanta, GA, 2006.

81. Bradley, P. M.; Chapelle, F. H.; Wilson, J. T., Field and laboratory evidence for intrinsic biodegradation of vinyl chloride contamination in a Fe(III)-reducing aquifer. *Journal of contaminant hydrology* **1998,** *31*, (1-2), 111-127.

82. Lorah, M. M.; Voytek, M. A., Degradation of 1,1,2,2-tetrachloroethane and accumulation of vinyl chloride in wetland sediment microcosms and in situ porewater: biogeochemical controls and associations with microbial communities. *Journal of contaminant hydrology* **2004,** *70*, (1), 117-145.

83. REGENESIS AquaZVI Specification Sheet. https://regenesis.com/wp-content/uploads/2018/04/AquaZVI_SpecSheet-8-1.pdf (November 19, 2018).

Chapter 5

5 Aging of Nano Zerovalent Iron Under Sulfidic Conditions: Characterization and Reactivity

5.1 Introduction

Passivation is one of the major drawbacks limiting widespread implementation of nano zerovalent iron (nZVI), leading to a loss in reactivity and subsequent inactivation for the degradation of pollutants.[1, 2] During passivation, formation and precipitation of iron oxides and iron (oxy)hydroxides on the Fe^0 surface results in a reduction of the electron transfer rate to the contaminant.[3] Though contaminant degradation can be sustained when a mixture of Fe^{2+}/Fe^{3+} species is prevalent on the Fe^0 surface, increases of Fe^{3+} species with continued aging time would ultimately limit reactivity.[4] The literature on the characterization of these oxidation products is extensive and sometimes difficult to synthesize due to different iron types, synthesis methods and experimental conditions under which particles are studied.[5-10] For commercial nZVI (Nanofer 25) aged for 90 days in static water exposed to air, the dominant oxidation products of bare-nZVI are magnetite and/or maghemite while for carboxymethyl cellulose stabilized nZVI (CMC-nZVI) is lepidocrocite.[9] In the CMC-nZVI bulk aggregates with some flaky-shaped structures have been observed.[8] The formation of flaky, acicular structures has been explained by a two-step process: first, outward diffusion of iron ions towards the shell forming hollowed out iron oxide shells, resulting in its collapse, and formation of flaky, acicular structures.[3] Besides influencing the transformation of iron oxides, CMC could also slow down aging rate.[9] For nZVI synthesized by chemical precipitation with sodium borohydride ($NaBH_4$), the composition of the corrosion product was found to be time dependent, transforming from magnetite and maghemite (Fe^{2+}/Fe^{3+}) after 5 days to lepidocrocite (Fe^{3+}) after 90 days.[3] In oxygenated water oxidation to (oxy)hydroxides, however, occur in a matter of hours.[10, 11] Several methods have been developed for the depassivation of ZVI particles, including surface complexation of divalent cations,[12] dosing with ferrous iron (Fe^{2+})[4] and inorganic salts,[13] implementation of magnetic fields,[14-16] acid washing,[17] and application of strong reductants.[17, 18] Besides depassivation procedures, efforts

have also been made to prevent oxidation by controlling air exposure, resulting in an iron oxide shell capable of minimizing further oxidation while maintaining reactivity.[5, 19] This shows that proper shell modification can also be used to preserve Fe^0 content and prolong the reactive life-span of ZVI particles.

A promising emerging modification method is the treatment of ZVI particles with sulfur compounds to develop a sulfur based-coating (i.e., sulfidation). Sulfidation was first developed as a synthesis method to produce biphasic FeS/Fe^0 (S-nZVI) particles,[20] but it has now grown to include micro-ZVI (mZVI).[21-25] S-nZVI studies have naturally expanded from the reduction of organohalides[26-32] to the sequestration of heavy metals,[33-38] removal of pharmaceuticals,[39-42] radionuclides,[43] nitrobenzene[44] as well as applications in advance oxidation processes (AOPs) for persulfate activation.[45] There has been evidence suggesting that sulfidation alleviates the negative effects of aging, resulting in greater re-usability, extended reactive life-span and improved conservation of the Fe^0 content in suspension.

Li et al. [32] found that after 11 weeks of aging, S-nZVI was still able to transform up to 56% of the initial tetrabromobisphenol A (TBBPA) within 24 hours, whereas nZVI only retained 5% of its original capacity after two weeks. Greater reusability of S-nZVI was also observed, maintaining 80% of its initial TBBPA transformation after 7 reuse cycles, compared to complete deactivation by the fourth cycle of nZVI. Dong et al. [46] reported sustained trichloroethene (TCE) dechlorination of S-nZVI aged for 20 – 30 days and efficient reactivation of aged nZVI by dithionite. Preservation of Fe^0 content with time is highly dependent on the sulfidating agent, with aqueous sulfide being a better inhibitor to nZVI corrosion than dithionite, but both able to prolong degradation rates over longer time periods than pristine nZVI.[47] Su et al. [33] found no negative effects of aging S-nZVI for 3 weeks for the removal of cadmium (Cd). Despite the remarkable improvements associated with sulfidation, it appears there are still some aging factors which influence S-nZVI reactivity, particularly changes in surface morphology and chemistry. Electrochemical characterization has shown that aging would also cause passivation of S-nZVI by growth of FeO and new FeS phases.[48] These oxidation processes, and the nature of the S-nZVI surface, are key drivers in particle reactivity and of significant importance for pollutant removal.[41]

Even though the understanding of aging characteristics of nZVI has been extensively studied, similar studies on S-nZVI are limited. The objective of this study was to investigate the evolution in surface composition during aging and the resultant pollutant removal performance of S-nZVI. To assess how modification to the synthesis process (and hence type of particles) can alter such interactions, S-nZVI was compared to carboxymethyl cellulose modified S-nZVI (CMC S-nZVI) prepared at low doses. Particles were stored without washing to mimic typical on-site post-synthesis conditions. TCE and chloroform (CF) were used as model pollutants in a co-contaminated system, characteristic of field sites. CF is a lesser studied pollutant and was chosen with TCE because it is the predominant product in the dechlorination of carbon tetrachloride (CT).[49, 50] Degradation of CT by S-nZVI resulted in the accumulation of CF and no other detectable chlorinated daughter compounds.[29] Reactivity data was combined with particle characterisation to track morphological and elemental changes. Concurrent monitoring of changes in particles' surface composition and degradation rates over short-time intervals would provide greater insights into S-nZVI transformation and efficiency for field applications.

5.2 Materials and Methods

5.2.1 Chemicals

Trichloroethene (TCE, >99.5%), chloroform (CF, 0.5-1% ethanol, >99.8%), sodium hydrosulfite ($Na_2S_2O_4$, technical grade 85%), sodium borohydride ($NaBH_4$, >98%), carboxymethyl cellulose (CMC, MW = 90k) and iron (II) sulfate heptahydrate ($FeSO_4 \cdot 7H_2O$, 99%) were purchased from Sigma-Aldrich Pty Ltd (Australia). Ultra-high purity helium, hydrogen, argon and nitrogen were from BOC gases (Australia).

5.2.2 Particles Preparation

nZVI was prepared by titrating sodium borohydride (0.16M) to $FeSO_4 \cdot 7H_2O$ (0.08M) at a rate of 10 ml min^{-1} and a 1:1 volume ratio.[51] After the formation of zerovalent iron particles, aqueous-solid sulfidation was carried out using sodium dithionite (S/Fe = 0.56) and left to react for 20 minutes while mixing constantly. For CMC S-nZVI, an appropriate amount of CMC was added to yield a concentration of 1.63×10^{-3} % wt/vol. Both bare S-nZVI and CMC S-nZVI were synthesized

under anaerobic conditions (<0.1 ppm O_2) and with 18MΩ·cm Milli-Q water purged with nitrogen for at least two hours. Particles were aged in a sulfidic environment immediately after synthesis.

5.2.3 Batch Experiments

S-nZVI and CMC S-nZVI particles were tested with TCE and CF at 1 hour (0 d), 7 d, 14 d and 21 d intervals following synthesis. Test experiments were conducted in triplicate with one control vial containing only Milli-Q water. Initial pH was measured by preparing two sacrificial vials, one with nZVI and one with water to serve as a control. All six empty test vials (120 mL nominal volume) were purged with nitrogen for approximately five minutes, crimped shut and wrapped in tinfoil to prevent degradation of cVOCs by photolysis. 1 ml of TCE (~99 mg L^{-1}) and 1 ml of CF (~99 mg L^{-1}) stock solution (prepared in Milli-Q water) was added to the test vials and allowed to equilibrate for 24 hours before the start of the experiment. At the corresponding aging time, 20 ml of nZVI was extracted from the synthesis stock and injected into the sealed vessel (total volume 22 mL, 1 g L^{-1} iron, ~4.5 mg L^{-1} TCE and CF). In the case of the controls, 20 mL of water was added to make up the volume. Vials were immediately placed on a platform shaker and mixed at 110 rpm (OM7 Orbital platform shaker, Ratek) throughout the test run.

50 µL headspace sample was withdrawn at selected times and analysed for TCE and CF by gas chromatography using an Agilent 7890B equipped with a flame ionization detector (GC-FID) and a DB-1 column (30 m x 0.32 mm diameter, 1 µm film thickness). Dechlorination products were identified by mass spectrometry (MS) in a 7000A Triple Quad GC with a HP-5MS column (30 m, 0.25 mm diameter, 0.25 µm film). Reactions between iron and model contaminants were fitted with pseudo first order kinetics. Information on the GC method and details on the calculation of kinetic rate constants for TCE and CF can be found in the Appendix C.

5.2.4 Characterization of S-nZVI particles

Solid phase analysis was performed for all samples and preparations made inside a glove box unless otherwise stated. Details of analytical procedures are provided in Appendix C. The size, morphology and composition of the particles were characterized using Transmission Electron Microscopy (TEM, FEI Tecnai G2 20 TEM, 200kV) and Scanning Electron Microscopy (SEM, FEI Nova NanoSEM 230, 5kV). Elemental analysis of the nanoparticles was performed by energy-

dispersive-x-ray spectroscopy (EDS) (Bruker EDS detector) and elemental mapping done on one sample only. Identification of the chemical state of surface atoms was accomplished by x-ray photoelectron spectroscopy (XPS) using a Kα mono-chromated aluminium (Al) radiation source, 13kV, and calibrated with adventitious hydrocarbon (Thermo-Fischer Scientific, ESCALAB250Xi). The crystal phase of the particles was identified by x-ray diffraction (XRD) using a Kα cobalt (Co) radiation source, scan 5.0°-135.0°, 45kV (PANalytical, Empyrean X-ray diffractometer). Dynamic light scattering analysis (DLS) and zeta-potential were measured in folded capillary cells using a Malvern Zetasizer Nano ZS. Colloidal stability was determined using a UV-Vis spectrophotometer (Cary Series, Agilent). Measurements were taken at 508 nm for 30 min at 5 min intervals.

The Fe^0 content was determined by quantifying H_2 evolution following acid digestion with hydrochloric acid (10 mL of 32% HCl). Headspace was sampled and analysed using a GC with a pulse discharge ionisation detector (PDD).

5.3 Results and Discussion

5.3.1 Characterization

5.3.1.1 Size and sedimentation

Size distributions (Figure C.1) were calculated from TEM images by manually examining 1096 particles. S-nZVI had a median size of 86.6 nm, with an average of 102 ± 62.3 nm (n = 585). For CMC S-nZVI, the median size is 96.4 nm, with an average of 107.9 ± 51.7 nm (n = 511). There wasn't a statistically significant difference between the sizes of the two particle types at a 95% confidence interval (unequal variances 2-tail *t*-test, $t = 1.713$, $p = 0.087$). There was a weak trend in the aggregate size with aging time (Table C.1), which was also reflected in the increasing rates of sedimentation with time (Figure C.2). Previous studies have reported the opposite for nZVI, with faster agglomeration and sedimentation for fresh nZVI relative to aged samples, most likely due to the higher Fe^0 content.[52] This difference was attributed to the sulfidation step. It is well documented that sulfidation inhibits aggregation and sedimentation of nZVI.[53] Some have attributed this to improved steric stability offered by iron sulphides,[40] as well as their lower magnetic attractions.[33, 35]

There was no improvement in colloidal stability by CMC, leading to similar sedimentation rates between the two particle types (Figure C.2). These results indicate the inclusion of CMC at the selected low concentration did not provide significant electrosteric repulsion. However, as discussed in the following sections, its presence had a major impact on the physicochemical transformations of the particles with aging.

5.3.1.2 TEM - EDS

Immediately after synthesis TEM showed S-nZVI particles were spherical and formed chain like structures (Figure 5.1), consistent with SEM images (Figure C.3). Other cubic and laminar phases were also visible, identified as iron sulfides (FeS), most likely mackinawite. As aging continued there was an apparent transformation in S-nZVI from cubic/laminar (Figure 5.1 A – B) to needle-like structures (Figure 5.1 D). These secondary structures were not uniformly distributed, with some spherical particles maintaining their structural integrity at day 21. For CMC S-nZVI these changes were not present, and the particles appeared unaffected during the aging period (Figure 5.1 E – H). CMC is known to suppress the formation of FeS crystals[54] and thus could be functioning as an inhibitory agent for the crystallization of FeS particles in the present study. CMC S-nZVI also lacked cubic-like structures at day zero, only containing the laminar structures.

EDS data revealed distinct iron and sulfur proportions in the various morphological structures visible by TEM (Figure 5.1a-d and Figure 5.1e-h). The spherical particles consistently showed higher abundance of iron ($S/Fe_{S\text{-}nZVI} = 0.39 \pm 0.21$ and $S/Fe_{CMC\ S\text{-}nZVI} = 0.12 \pm 0.09$), whereas in the cubic/laminar sulfur was predominant ($S/Fe_{S\text{-}nZVI} = 1.16 \pm 0.08$ and $S/Fe_{CMC\ S\text{-}nZVI} = 1.05 \pm 0.07$) (Table C.2). In the case of the needle-like structures the S/Fe ratio was 1. Elemental mapping for the 21 d S-nZVI shows a clear overlap between the iron and sulfur (Figure C.4). Iron is present mostly around the amorphous spherical components and sulfur is more abundant in areas dominated by the laminar phases.

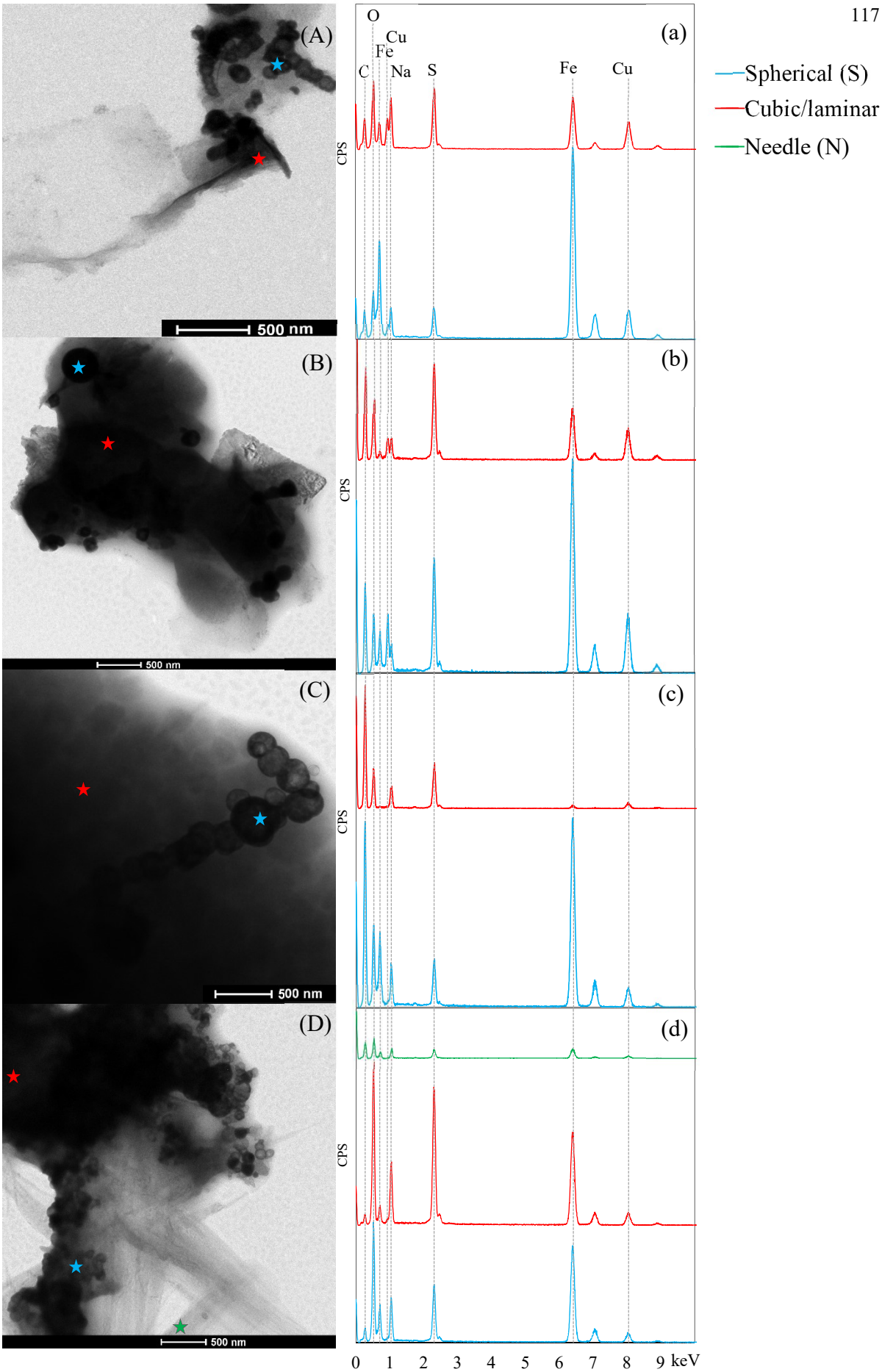

Figure 5.1 TEM images with EDS spectra of S-nZVI at (A) 0 d, (B) 7 d, (C) 14 d and (D) 21 d.

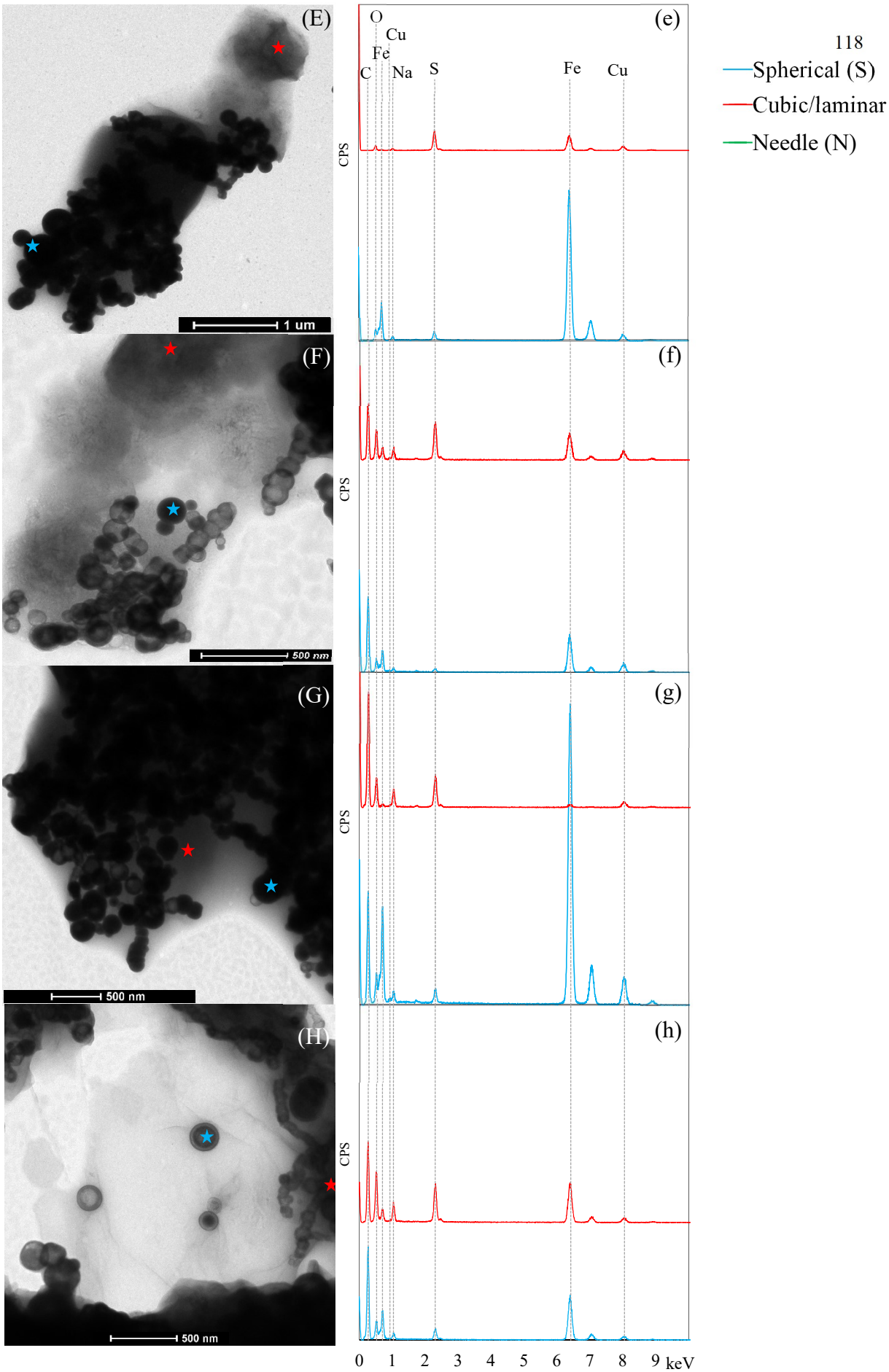

Figure 5.1 Continuation: TEM images with EDS spectra of CMC S-nZVI at (E) 0 d, (F) 7 d, (G) 14 d and (H) 21 d.

5.3.1.3 XPS and XRD analysis

The chemical composition and oxidation state of surface-bound elements was assessed using XPS (Table C.3). The high-resolution spectra for the Fe $2p_{3/2}$ (Figure 5.2) region shows the characteristic peaks of Fe(III) and Fe^0 at 710.7 eV and 706.7 eV, respectively.[2] Unlike unmodified nZVI, where the Fe^0 intensity gradually decreases with aging time,[3] the peak at ~706.7 eV showed minimal attenuation due to the influence of Fe(II)-S, whose binding energy overlapped with that of Fe^0.[28, 43] The intensity of the Fe(II)-S peak has been associated with the sulfidation process employed, with the aqueous-solid method yielding larger peaks and greater coverage.[55]

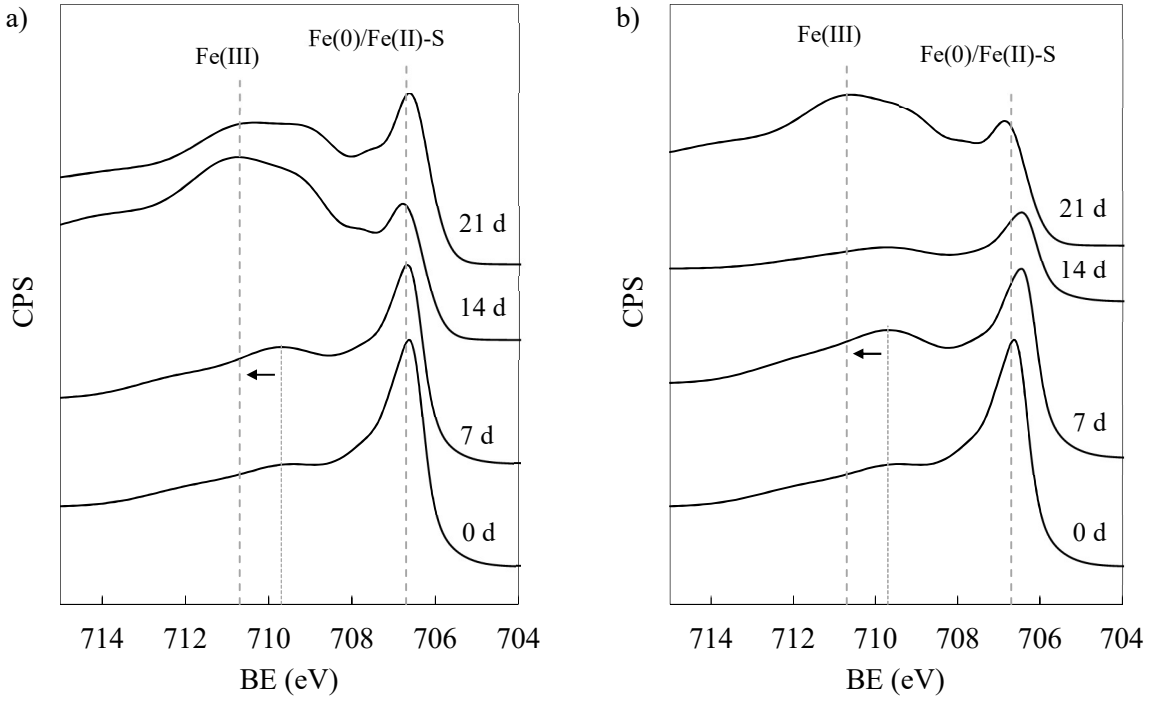

Figure 5.2 High-resolution scan in the Fe $2p_{2/3}$ region for a) S-nZVI and b) CMC S-nZVI.

The abundance of FeS at the surface of nZVI is supported by the survey scans, where sulfur accounts for 10% to 17% of the surface composition, closely resembling that of iron (i.e., 13% to 18%) (Table C.3). The contribution of iron sulfides was further confirmed by fitting the S 2p spectra with doublets characteristic of the spin-orbit splitting of S $2p_{1/2}$ and S $2p_{3/2}$ (Figure C.5). Sulfur species were identified based on reported binding energies as monosulfide (S^{2-}), polysulfide (S_n^2), elemental sulfur (S^0), sulfite (SO_3^2) and sulfate (SO_4^{2-}).[28, 33, 56] The relative atomic abundance of S^{2-} shows low variability throughout the aging period and is the predominant species for both

types of nZVI particles (Figure C.6 and Table C.4). Signs of oxidation are also visible by the presence other sulfur compounds (e.g., S^0, SO_3^{2-}, SO_4^{2-}), accounting on average 42.6 % and 46% of sulfur in S-nZVI and CMC S-nZVI, respectively. Some level of oxidation could have taken place during the storage or transport of the particles for analysis. S_n^{2-} is found in similar amounts in both particles, revealing the possibility of Fe(III) phases from surface oxidation of FeS. The formation and nature of the iron sulfides formed during sulfidation has been well documented.[55] The amorphous phase of mackinawite (FeS_m) is first formed, which further transform to crystalline mackinawite and/or sulfide phases like greigite (Fe_3S_4) or pyrite (FeS_2). Oxidation to Fe_3S_4 or FeS_2 can occur through multiple mechanisms, including 1) solid state reaction of mackinawite to greigite through the oxidation of two thirds of Fe(II) to Fe(III), with the S^{2-} remaining unoxidized (Eq. 5.1), 2) a polysulfide pathway where FeS react with S^0, S_n^{2-} or other S intermediates to form pyrite (Eq. 5.2 and Eq. 5.3), 3) greigite to pyrite formation (Eq. 5.4) and 4) a H_2S oxidation pathway observed under anoxic conditions (Eq. 5.5).[57] Besides S intermediates, sulfides could also mediate the oxidation of mackinawite when found in excess in anoxic systems. Similar observations have been made during long sulfidation periods or extended exposure to sulfidic environments with the appearance of secondary FeS phases with distinct structures.[55] In addition to greigite and pyrite, it is widely accepted that both iron and sulfur in FeS could undergo independent oxidation by oxygen, making the conversion to iron oxides and iron hydroxides possible.[58] Direct oxidation of Fe is evident in changes of the main Fe(III) peak. There is a chemical shift from lower binding energies (~709.7 eV) at 0 d and 7 d to higher energies at 14 d and 21 d (Figure 5.2). For these later times the peak around the 710.7 eV region broadens and increases, pointing to the possible presence of different iron oxides with a mixture of Fe(II)/ Fe(III) or iron (oxy)hydroxides containing Fe(III) (e.g., Fe_2O_3, Fe_3O_4, $Fe(OH)_3$ and/or FeOOH), typical of the autoxidation of Fe^0 after exposure to water.[5, 10] Since these oxide species have similar XPS features and close peak positions, the O 1s is used as a surrogate to elucidate which are the favorable corrosion products. The spectrum for oxygen was deconvoluted into three peaks (Figure C.7), corresponding to lattice O^{2-} (529.9 eV), lattice OH^- (531.7 eV) and chemically or physically absorbed water (533 eV).[10] The presence of OH^- and O^{2-} confirm the existence of iron oxides/(oxy)hydroxides[5] and provide insights into their formation and changes with time. Liu et al. [3] reported an increase in the OH^-:O^{2-} ratio with time, from 0.68 at 5 d to 1.09 at 90 d, indicating the formation of lepidocrocite (γ-FeOOH) and/or goethite (α-FeOOH) over γ-Fe_2O_3 and/or Fe_3O_4.

In the present study, the initial value for the OH^-:O^{2-} ratio in S-nZVI and CMC S-nZVI is higher than unity (Figure C.8), suggesting iron hydroxides ($Fe(OH)_x$) to be a more prominent component of the oxide shell than iron oxides.[59] The higher ratio at 0 d of S-nZVI (8.14) might indicate a higher degree of corrosion at the beginning of the aging period as compared to CMC S-nZVI (4.14). $FeOH_x$ will undergo subsequent dehydration to generate FeOOH.[60] The low contribution of O^{2-} is due to the anoxic conditions under which particles were synthesized.

$$3FeS + S^0 \rightarrow Fe_3S_4 \quad (5.1)$$

$$FeS + S^0 \rightarrow FeS_2 \quad (5.2)$$

$$FeS + S_n^{2-} \rightarrow FeS_2 + S_{n-1}^{2-} \quad (5.3)$$

$$Fe_3S_4 + 2S^0 \rightarrow 3FeS_2 \quad (5.4)$$

$$FeS + H_2S \rightarrow FeS_2 + H_2 \quad (5.5)$$

These results are corroborated by the indistinct XRD patterns (Figure 5.3). The lack of the characteristic iron sulfides peaks and the broad Fe^0 band at 52.4° observed mainly for S-nZVI reveals the poorly ordered nature and/or low concentration of such particles. Acid digestion further confirmed the presence of Fe^0 in fresh and 12 d aged samples (data not shown). For the 21 d old S-nZVI, the Fe^0 band disappeared and other weak peaks for iron sulfides and iron oxides became noticeable. Most of these features were not found in the 21 d old CMC S-nZVI, in agreement with observations from TEM images. As aging continued more ordered structures develop in S-nZVI but poorly-ordered formations (e.g., amorphous iron sulfides) remain in CMC S-nZVI, akin to the freshly synthesized particles. This data suggests the presence of even low amounts of CMC can influence the transformation products of iron. A common feature to both types of particles is the appearance of a large peak at ~19° for the 21 d samples (not shown). The latter could be the sulfate form of green rust (GRII), which occur as intermediate phases during the oxidation of Fe(II) to iron oxides in neutral or alkaline solutions.[61] Table C.5 summarizes some of the possible solid

phases that can be formed in sulfidated nZVI systems, with their reflection angle and corresponding interplanar spacings.

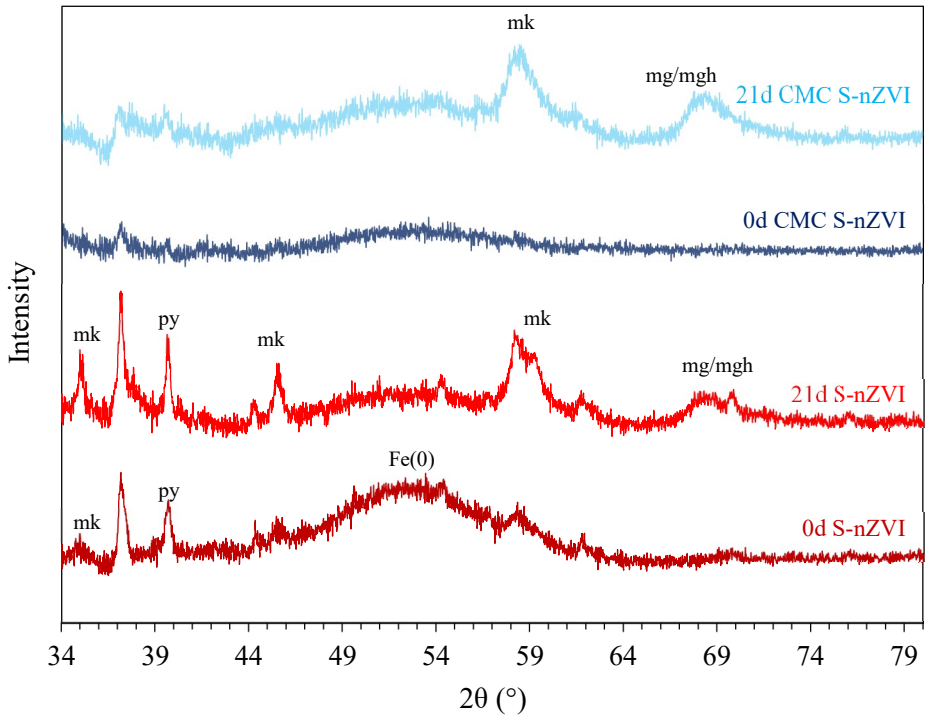

Figure 5.3. XRD diffractogram at 0 d and 21 d. Identifiable peaks are shown as mk (mackinawite), py (pyrite), magnetite/maghemite (mg/mgh) and zerovalent iron (Fe(0)).

A literature study found that when S-nZVI was aged in DI water, clearer signs of structural transformation were observed, with sharper and more distinct peaks after 20 d for lepidocrocite, magnetite/maghemite, mackinawite and greigite.[46] Under sulfidic conditions, phase transition from FeS_m to greigite would be preferred over its iron oxides counterpart due to the excess sulfur in the form of polysulfides in solution.[62] This transition is favoured under more acidic and oxidizing conditions, indicating that such reactions would be slow at the pH range of the current study (Table C.1). Although oxidation and crystallization appear to be occurring, as also shown in the TEM images, further transformation of Mackinawite would require longer reaction times.[55] Taken together, these results indicate that: 1) nanoparticles are chemically stable when stored under sulfidic conditions, 2) nZVI is surrounded by a mixture of iron oxides and more abundant

iron sulfides which crystallize with time, 3) CMC appears to slow the oxidation and crystallization of the S-nZVI.

5.3.2 TCE and CF degradation by sulfidated nZVI

Mass normalized TCE degradation rates (k_m) increased ~2.3 times for S-nZVI during the first 7 days, from 7.03×10^{-3} L g^{-1} h^{-1} to 1.59×10^{-2} L g^{-1} h^{-1}, with no significant increase thereafter (Figure 5.4). On the other hand, increases of similar magnitude were not observed in CMC S-nZVI, ranging from 4.92×10^{-3} L g^{-1} h^{-1} (0 d) to 7.01×10^{-3} L g^{-1} h^{-1} (21 d). The kinetic results shown in Figure 5.4 suggest that S-nZVI is more effective than CMC S-nZVI and that aging did not negatively impact reactivity. Unlike TCE, where complete degradation was achieved, removal of CF for S-nZVI and CMC S-nZVI was only 26.8% and 27.9% of its initial concentration after 20 – 21 days, respectively (Figure C.9). The reason for the differences in reactivity between TCE and CF could be due to differences in the rate limiting step for both compounds. Degradation of these compounds involves diffusion to the reactive site, adsorption to the iron surface, reaction, desorption and diffusion of the products away from the reactive site. It is noted that the reaction pathway could differ for TCE and CF (e.g., β-elimination or hydrogenolysis) as will be discussed.

TCE degradation products were identified by mass spectrometry as cis-1,2-dichloroethene (cis 1,2-DCE), vinyl chloride (VC), acetylene and ethene. Their appearance is presented as the sum of all products, with the concurrent disappearance of TCE (Figure C.10). Recent research proposed the dechlorination of TCE on S-nZVI to occur mainly by β-elimination to acetylene, followed by its hydrogenation to ethene.[63] Though β-elimination is considered to be the dominant pathway for chlorinated ethenes,[55] detection of other chlorinated intermediates point to hydrogenolysis. The relative abundance of each compound was not determined, hence the contribution of the two pathways could not be assessed. In the case of CF, dichloromethane (DCM) and methane degradation products were the main products identifiable via mass spectrometry.

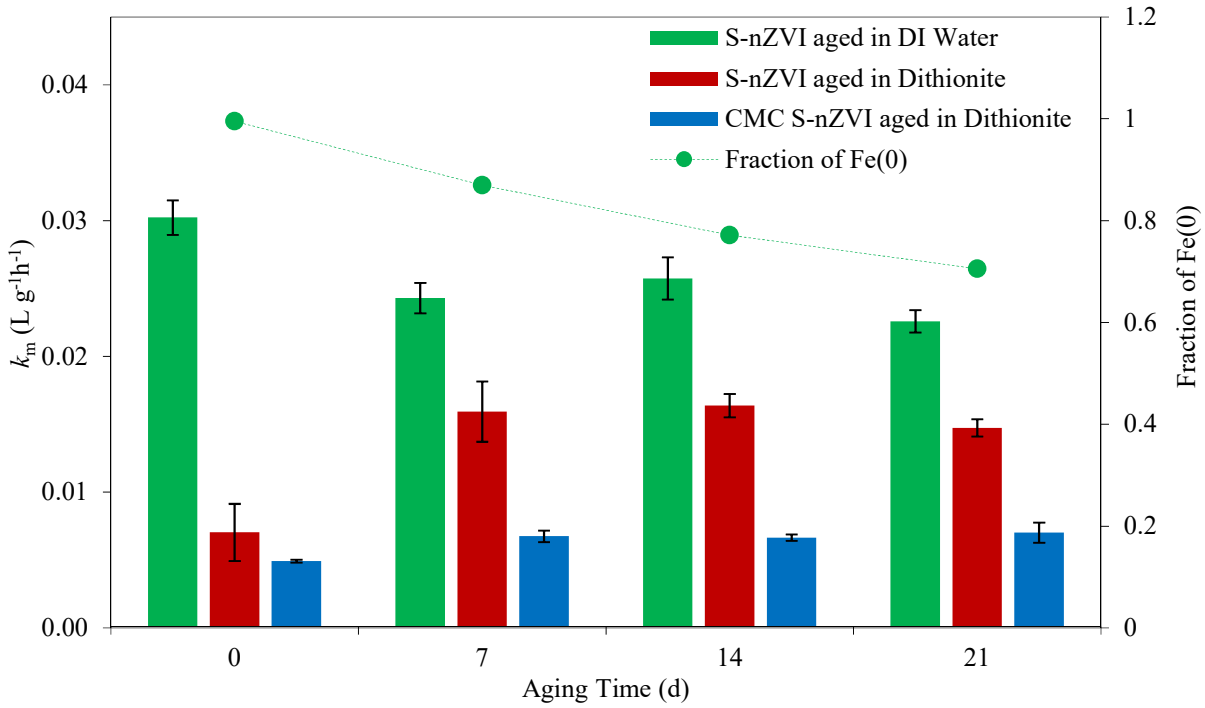

Figure 5.4 Mass normalized TCE degradation rate constant (k_m). Concentrations of S-nZVI and CMC S-nZVI aged in dithionite = 1 g L^{-1} at S/Fe 0.56. Concentration of S-nZVI aged in DI water = 1.9 g L^{-1} at S/Fe = 0.6. In the latter case particles were sulfidated for 24 hours, washed and rinsed three times. Fraction of zerovalent iron shown only for S-nZVI aged in DI water. Error bars represent standard deviations of triplicates.

Thus far aging studies on S-nZVI has been conducted by storing the particles in a sulfide free environment (e.g., DI water). Dong et al. [46] found that for the first 20 days particles retained a high capacity for TCE dechlorination (27.5% reduction), though lower than fresh S-nZVI (31.2% reduction). The decrease in reactivity was attributed to passivation, due to accumulation of iron oxides. Li et al. [32] observed a decrease with time in the capacity to transform tetrabromobisphenol A (TBBPA), but even after 11 weeks of aging S-nZVI still maintain reactivity comparable with freshly prepared nZVI. The long-lasting capacity of S-nZVI was attributed to a reducing environment and a reduction in agglomeration. On the other hand, Su et al. [33] reported an increase in Cd removal after aging S-nZVI for 3 weeks. Rate enhancement was explained by an increase in binding sites caused by breaking of the S – S dumbbell (releasing -SH groups) and sustained by the slow aggregation of S-nZVI. These results are somewhat conflicting. However, the prevailing

factors for sustained reactivity of aged S-nZVI seem to be a decrease in agglomeration and increase (or sustained) availability of substrate binding sites.

Rate increases in S-nZVI cannot be merely attributed to a lack in aggregation and/or changes in solution chemistry (e.g., pH), as the same would have been observed in CMC S-nZVI. From the characterization results it was concluded that at the selected concentration, CMC did not provide significant electrosteric repulsion to alter the agglomeration and deposition of particles. Thus, its inclusion offered no advantage to this effect. Unlike S-nZVI, CMC S-nZVI did not undergo major structural changes during the aging period, hence its consistent reaction rates. Moreover, polyelectrolytes (e.g., CMC) applied in a post-synthesis fashion are known to decrease the reactivity of nZVI towards TCE.[64] Such processes depend on the polyelectrolyte of choice and its concentration. At low surface excess, relevant to this study, the primary mechanism is the blocking of reactive surface sites. Therefore, we hypothesized that both the increased reaction rates associated with S-nZVI, and its increase with time, are due to shell transformations and higher availability of reactive sites.

In the current system, competition for reactive sites can occur between contaminants (TCE and CF) and/or other species, such as CMC (if applicable) or sulfur. At high S/Fe ratios and prolonged sulfidation duration, formation of secondary (less conductive) FeS precipitates due to excess sulfur in solution can lead to a decrease in reactivity by blocking reactive sites, and inhibiting corrosion of Fe^0.[55] Based on these conditions a decrease in reactivity would be expected while aging in sulfidic environments but the opposite was observed in the present study. Similar observations were made in the degradation of CCl_4 by aging metallic iron in a sulfidic solution.[65] Higher degradation rates at late aging times were attributed to increased surface area made available by pitting and stress-induced cracking of the FeS layer. Pit formations and other surface modifications, such as increases in roughness by sulfidation, are known to contribute to removal enhancements by S-(n)ZVI.[20, 21, 23, 37, 38] Hence the coarser and rougher particles with higher fraction of edges developed in S-nZVI may have contributed to its superior reaction rate. This would imply that, besides blocking reactive sites, lower rates in CMC S-nZVI could be partly caused by the inhibitory role of CMC in the development of such particles, as attested by the TEM-EDS data. However, at longer aging times under sulfidic conditions (and/or high S/Fe ratios), the accumulation of less reactive iron sulfides (e.g., FeS_2) could then cause a decrease in reactivity. A

slight decrease in the rates of TCE was observed at later aging times for S-nZVI, from 1.64×10^{-2} g L^{-1} h^{-1} (14 d) to 1.47×10^{-2} g L^{-1} h^{-1} (21 d). This data suggests that reactivity of S-nZVI aged in a sulfur rich environment is dominated by at least two time-dependent mechanisms: increase in reactivity at early times due to cracking and pit formations, followed by a decrease at latter times due to transformation of the FeS layer and accumulation of secondary FeS phases. Longer aging times would be necessary to further test this hypothesis.

Even with the sustained reactions rates observed during aging, it should be noted that rate constants presented in Figure 5.4 are significantly lower than published values on TCE dechlorination by S-nZVI (e.g., refs [20] & [27]). The lower reaction rates could be associated with the excess dithionite in solution. Performance enhancements have been made after washing the S-nZVI and removing excess aqueous sulfide from solution.[27, 43] To test if the remaining dithionite was responsible for the lower rates, additional experiments were conducted comparing the reactivity with TCE of 'Washed' and 'Unwashed' particles, sulfidated for 30 minutes at a S/Fe of 0.6. Similarly, two separate 'washed' particles were re-suspended in dithionite solutions yielding a S/Fe of 0.1 and 0.6, categorized as 'Washed-low dose' and 'Washed-high dose', respectively (Figure C.11). After 24 hours, 'Washed' S-nZVI had the highest percent removal with 74.2%, followed by 'Washed-low dose (0.1 S/Fe)' with 35.7%. Both 'Unwashed (0.6 S/Fe)' and 'Washed-high dose (0.6 S/Fe)' experienced similar removal at 11.3% and 8.2%, respectively. To further test the influence of residual dithionite on the reactivity, S-nZVI particles were washed and aged for 21 days in DI water. In this experiment, 1.9 g L^{-1} nZVI was sulfidated at 0.6 S/Fe ratio for 24 hours before the start of the experiment (Figure 5.4). There is a downward trend in the k_m values, decreasing 1.34 times from 3.02×10^{-2} L g^{-1} h^{-1} at 0 days to 2.26×10^{-2} L g^{-1} h^{-1} at 21 days. This trend closely resembles the consumption of Fe^0 content. However, capacity for contaminant removal remained higher throughout than in the S-nZVI aged under dithionite. This data suggest that excess dithionite could be slowing down reduction of contaminants, possibly by generating excessive FeS and blocking reactive sites.

5.4 Environmental Significance

The experiments described in this study indicate sulfidation will preserve the reactive lifespan of nZVI under conditions representative of field application, that being storage of S-nZVI particles

on site for finite periods prior to subsurface injection or the possibility of continued in-situ sulfidation due to residual sulfur in the injection solution. However, the performance of S-nZVI was found to be dependent on other surface modifiers (e.g., CMC affected the transformation products during aging, inhibiting the development of distinct needle-like FeS phases at 21 days of aging as well as inhibiting the reactivity of S-nZVI). This data shows that when S-nZVI is to be used in conjunction with polyelectrolytes, attention should be given not only to the key operational variables of sulfidation (e.g., S/Fe ratio and sulfidation duration) but also to how the polyelectrolyte is applied. Operational parameters in this study (e.g., S/Fe ratio, other sulfidating agents such as thiosulfate and sulfide) were not optimized therefore other sulfidation conditions would likely further improve performance metrics such as the impact of aging on reactivity. When assessing the right formulation for field implementation, the use of dithionite or any other sulfur-based compound to sulfidate and subsequently store S-nZVI should be weighed against the potential detrimental effects of storing the nZVI particles in DI water. This study suggests that sulfidation has significant potential to not only improve initial nZVI reaction rates, as has been documented in the literature, but will lead to prolonged improvement in reaction rates.

5.5 References

1. Wang, Q.; Lee, S.; Choi, H., Aging Study on the Structure of Fe-0-Nanoparticles: Stabilization, Characterization, and Reactivity. *J Phys Chem C* **2010,** *114*, (5), 2027-2033.

2. Sarathy, V.; Tratnyek, P. G.; Nurmi, J. T.; Baer, D. R.; Amonette, J. E.; Chun, C. L.; Penn, R. L.; Reardon, E. J., Aging of iron nanoparticles in aqueous solution: Effects on structure and reactivity. *J Phys Chem C* **2008,** *112*, (7), 2286-2293.

3. Liu, A. R.; Liu, J.; Zhang, W. X., Transformation and composition evolution of nanoscale zero valent iron (nZVI) synthesized by borohydride reduction in static water. *Chemosphere* **2015,** *119*, 1068-1074.

4. Liu, T. X.; Li, X. M.; Waite, T. D., Depassivation of Aged Fe-0 by Ferrous Ions: Implications to Contaminant Degradation. *Environ Sci Technol* **2013,** *47*, (23), 13712-13720.

5. Kim, H. S.; Ahn, J. Y.; Hwang, K. Y.; Kim, I. K.; Hwang, I., Atmospherically Stable Nanoscale Zero-Valent Iron Particles Formed under Controlled Air Contact: Characteristics and Reactivity. *Environ Sci Technol* **2010,** *44*, (5), 1760-1766.

6. Kim, H. S.; Kim, T.; Ahn, J. Y.; Hwang, K. Y.; Park, J. Y.; Lim, T. T.; Hwang, I., Aging characteristics and reactivity of two types of nanoscale zero-valent iron particles (Fe-BH and Fe-H2) in nitrate reduction. *Chem Eng J* **2012,** *197*, 16-23.

7. Xie, Y.; Fang, Z.; Qiu, X.; Tsang, E. P.; Liang, B., Comparisons of the reactivity, reusability and stability of four different zero-valent iron-based nanoparticles. *Chemosphere* **2014,** *108*, 433-436.

8. Dong, H.; Zhao, F.; He, Q.; Xie, Y.; Zeng, Y.; Zhang, L.; Tang, L.; Zeng, G., Physicochemical transformation of carboxymethyl cellulose-coated zero-valent iron nanoparticles (nZVI) in simulated groundwater under anaerobic conditions. *Separation and Purification Technology* **2017,** *175*, 376-383.

9. Dong, H.; Zhao, F.; Zeng, G.; Tang, L.; Fan, C.; Zhang, L.; Zeng, Y.; He, Q.; Xie, Y.; Wu, Y., Aging study on carboxymethyl cellulose-coated zero-valent iron nanoparticles in water: Chemical transformation and structural evolution. *Journal of hazardous materials* **2016,** *312*, 234-242.

10. Liu, A. R.; Liu, J.; Pan, B. C.; Zhang, W. X., Formation of lepidocrocite (gamma-FeOOH) from oxidation of nanoscale zero-valent iron (nZVI) in oxygenated water. *Rsc Advances* **2014,** *4*, (101), 57377-57382.

11. Greenlee, L. F.; Torrey, J. D.; Amaro, R. L.; Shaw, J. M., Kinetics of Zero Valent Iron Nanoparticle Oxidation in Oxygenated Water. *Environ Sci Technol* **2012,** *46*, (23), 12913-12920.

12. Liu, T. X.; Li, X. M.; Waite, T. D., Depassivation of Aged Fe-0 by Divalent Cations: Correlation between Contaminant Degradation and Surface Complexation Constants. *Environ Sci Technol* **2014,** *48*, (24), 14564-14571.

13. Liu, T. X.; Li, X. M.; Waite, T. D., Depassivation of Aged Fe-0 by Inorganic Salts: Implications to Contaminant Degradation in Seawater. *Environ Sci Technol* **2013,** *47*, (13), 7350-7356.

14. Xu, C. H.; Zhang, B. L.; Zhu, L. J.; Lin, S.; Sun, X. P.; Jiang, Z.; Tratnyek, P. G., Sequestration of Antimonite by Zerovalent Iron: Using Weak Magnetic Field Effects to Enhance Performance and Characterize Reaction Mechanisms. *Environ Sci Technol* **2016,** *50*, (3), 1483-1491.

15. Liang, L. P.; Guan, X. H.; Shi, Z.; Li, J. L.; Wu, Y. N.; Tratnyek, P. G., Coupled Effects of Aging and Weak Magnetic Fields on Sequestration of Selenite by Zero-Valent Iron. *Environ Sci Technol* **2014,** *48*, (11), 6326-6334.

16. Xu, H.; Sun, Y.; Li, J.; Li, F.; Guan, X., Aging of Zerovalent Iron in Synthetic Groundwater: X-ray Photoelectron Spectroscopy Depth Profiling Characterization and Depassivation with Uniform Magnetic Field. *Environ Sci Technol* **2016,** *50*, (15), 8214-8222.

17. Zhu, B. W.; Lim, T. T., Catalytic reduction of Chlorobenzenes with Pd/Fe nanoparticles: reactive sites, catalyst stability, particle aging, and regeneration. *Environ Sci Technol* **2007,** *41*, (21), 7523-7529.

18. Xie, Y.; Cwiertny, D. M., Use of Dithionite to Extend the Reactive Lifetime of Nanoscale Zero-Valent Iron Treatment Systems. *Environ Sci Technol* **2010,** *44*, (22), 8649-8655.

19. Sohn, K.; Kang, S. W.; Ahn, S.; Woo, M.; Yang, S. K., Fe(0) nanoparticles for nitrate reduction: Stability, reactivity, and transformation. *Environ Sci Technol* **2006,** *40*, (17), 5514-5519.

20. Kim, E. J.; Kim, J. H.; Azad, A. M.; Chang, Y. S., Facile Synthesis and Characterization of Fe/FeS Nanoparticles for Environmental Applications. *ACS Appl. Mater. Inter.* **2011,** *3*, (5), 1457-1462.

21. Shao, Q.; Xu, C.; Wang, Y.; Huang, S.; Zhang, B.; Huang, L.; Fan, D.; Tratnyek, P. G., Dynamic interactions between sulfidated zerovalent iron and dissolved oxygen: Mechanistic insights for enhanced chromate removal. *Water research* **2018,** *135*, 322-330.

22. Gu, Y.; Wang, B.; He, F.; Bradley, M. J.; Tratnyek, P. G., Mechanochemically Sulfidated Microscale Zero Valent Iron: Pathways, Kinetics, Mechanism, and Efficiency of Trichloroethylene Dechlorination. *Environ Sci Technol* **2017,** *51*, (21), 12653-12662.

23. Huang, S.; Xu, C.; Shao, Q.; Wang, Y.; Zhang, B.; Gao, B.; Zhou, W.; Tratnyek, P. G., Sulfide-modified zerovalent iron for enhanced antimonite sequestration: Characterization, performance, and reaction mechanisms. *Chem Eng J* **2018,** *338*, 539-547.

24. Wang, Y.; Shao, Q.; Huang, S.; Zhang, B.; Xu, C., High performance and simultaneous sequestration of Cr(VI) and Sb(III) by sulfidated zerovalent iron. *J Clean Prod* **2018,** *191*, 436-444.

25. Xu, C. H.; Zhang, B. L.; Wang, Y. H.; Shao, Q. Q.; Zhou, W. Z.; Fan, D. M.; Bandstra, J. Z.; Shi, Z. Q.; Tratnyek, P. G., Effects of Sulfidation, Magnetization, and Oxygenation on Azo Dye Reduction by Zerovalent Iron. *Environ Sci Technol* **2016,** *50*, (21), 11879-11887.

26. Kim, E.-J.; Murugesan, K.; Kim, J.-H.; Tratnyek, P. G.; Chang, Y.-S., Remediation of Trichloroethylene by FeS-Coated Iron Nanoparticles in Simulated and Real Groundwater: Effects of Water Chemistry. *Ind Eng Chem Res* **2013,** *52*, (27), 9343-9350.

27. Rajajayavel, S. R. C.; Ghoshal, S., Enhanced reductive dechlorination of trichloroethylene by sulfidated nanoscale zerovalent iron. *Water research* **2015,** *78*, 144-153.

28. Nunez Garcia, A.; Boparai, H. K.; O'Carroll, D. M., Enhanced Dechlorination of 1,2-Dichloroethane by Coupled Nano Iron-Dithionite Treatment. *Environ Sci Technol* **2016,** *50*, (10), 5243-5251.

29. Jin, X.; Chen, H.; Yang, Q.; Hu, Y. A.; Yang, Z. L., Dechlorination of Carbon Tetrachloride by Sulfide-Modified Nanoscale Zerovalent Iron. *Environ Eng Sci* **2018,** *35*, (6), 560-567.

30. Han, Y.; Yan, W., Reductive Dechlorination of Trichloroethene by Zero-valent Iron Nanoparticles: Reactivity Enhancement through Sulfidation Treatment. *Environ Sci Technol* **2016,** *50*, (23), 12992-13001.

31. Li, D.; Zhu, X. F.; Zhong, Y.; Huang, W. L.; Peng, P., Abiotic transformation of hexabromocyclododecane by sulfidated nanoscale zerovalent iron: Kinetics, mechanism and influencing factors. *Water research* **2017,** *121*, 140-149.

32. Li, D.; Mao, Z.; Zhong, Y.; Huang, W.; Wu, Y.; Peng, P. a., Reductive transformation of tetrabromobisphenol A by sulfidated nano zerovalent iron. *Water research* **2016,** *103*, 1-9.

33. Su, Y.; Adeleye, A. S.; Keller, A. A.; Huang, Y.; Dai, C.; Zhou, X.; Zhang, Y., Magnetic sulfide-modified nanoscale zerovalent iron (S-nZVI) for dissolved metal ion removal. *Water research* **2015,** *74*, 47-57.

34. Du, J. K.; Bao, J. G.; Lu, C. H.; Werner, D., Reductive sequestration of chromate by hierarchical FeS@Fe-0 particles. *Water research* **2016,** *102*, 73-81.

35. Su, Y.; Adeleye, A. S.; Huang, Y.; Zhou, X.; Keller, A. A.; Zhang, Y., Direct Synthesis of Novel and Reactive Sulfide-modified Nano Iron through Nanoparticle Seeding for Improved Cadmium-Contaminated Water Treatment. *Scientific Reports* **2016,** *6*, 24358.

36. Gong, Y.; Gai, L.; Tang, J.; Fu, J.; Wang, Q.; Zeng, E. Y., Reduction of Cr(VI) in simulated groundwater by FeS-coated iron magnetic nanoparticles. *Science of The Total Environment* **2017,** *595*, 743-751.

37. Lv, D.; Zhou, X.; Zhou, J.; Liu, Y.; Li, Y.; Yang, K.; Lou, Z.; Baig, S. A.; Wu, D.; Xu, X., Design and characterization of sulfide-modified nanoscale zerovalent iron for cadmium(II) removal from aqueous solutions. *Applied Surface Science* **2018,** *442*, 114-123.

38. Wu, D.; Peng, S.; Yan, K.; Shao, B.; Feng, Y.; Zhang, Y., Enhanced As(III) sequestration using sulfide-modified nanoscale zerovalent iron with a characteristic core-shell structure: Sulfidation and As distribution. *ACS Sustainable Chemistry & Engineering* **2018,** *6*, 3039-3048.

39. Cao, Z.; Liu, X.; Xu, J.; Zhang, J.; Yang, Y.; Zhou, J. L.; Xu, X. H.; Lowry, G. V., Removal of Antibiotic Florfenicol by Sulfide-Modified Nanoscale Zero-Valent Iron. *Environ Sci Technol* **2017,** *51*, (19), 11269-11277.

40. Song, S.; Su, Y.; Adeleye, A. S.; Zhang, Y.; Zhou, X., Optimal design and characterization of sulfide-modified nanoscale zerovalent iron for diclofenac removal. *Applied Catalysis B: Environmental* **2017,** *201*, 211-220.

41. Su, Y.; Jassby, D.; Song, S.; Zhou, X.; Zhao, H.; Filip, J.; Petala, E.; Zhang, Y., Enhanced Oxidative and Adsorptive Removal of Diclofenac in Heterogeneous Fenton-like Reaction with Sulfide Modified Nanoscale Zerovalent Iron. *Environ Sci Technol* **2018,** *52*, (11), 6466-6475.

42. Tang, J.; Tang, L.; Feng, H.; Zeng, G.; Dong, H.; Zhang, C.; Huang, B.; Deng, Y.; Wang, J.; Zhou, Y., pH-dependent degradation of p-nitrophenol by sulfidated nanoscale zerovalent iron under aerobic or anoxic conditions. *Journal of hazardous materials* **2016,** *320*, 581-590.

43. Fan, D. M.; Anitori, R. P.; Tebo, B. M.; Tratnyek, P. G.; Pacheco, J. S. L.; Kukkadapu, R. K.; Engelhard, M. H.; Bowden, M. E.; Kovarik, L.; Arey, B. W., Reductive Sequestration of Pertechnetate ((TcO4-)-Tc-99) by Nano Zerovalent Iron (nZVI) Transformed by Abiotic Sulfide. *Environ Sci Technol* **2013,** *47*, (10), 5302-5310.

44. Zhang, D.; Li, Y.; Tong, S.; Jiang, X.; Wang, L.; Sun, X.; Li, J.; Liu, X.; Shen, J., Biochar supported sulfide-modified nanoscale zero-valent iron for the reduction of nitrobenzene. *RSC Advances* **2018,** *8*, (39), 22161-22168.

45. Rayaroth, M. P.; Lee, C. S.; Aravind, U. K.; Aravindakumar, C. T.; Chang, Y. S., Oxidative degradation of benzoic acid using Fe-0 - and sulfidized Fe-0-activated persulfate: A comparative study. *Chem Eng J* **2017,** *315*, 426-436.

46. Dong, H.; Zhang, C.; Deng, J.; Jiang, Z.; Zhang, L.; Cheng, Y.; Hou, K.; Tang, L.; Zeng, G., Factors influencing degradation of trichloroethylene by sulfide-modified nanoscale zero-valent iron in aqueous solution. *Water research* **2018,** *135*, 1-10.

47. Fan, D.; O'Brien Johnson, G.; Tratnyek, P. G.; Johnson, R. L., Sulfidation of Nano Zerovalent Iron (nZVI) for Improved Selectivity During In-Situ Chemical Reduction (ISCR). *Environ Sci Technol* **2016,** *50*, (17), 9558-9565.

48. Kim, E.-J.; Kim, J.-H.; Chang, Y.-S.; Turcio-Ortega, D.; Tratnyek, P. G., Effects of Metal Ions on the Reactivity and Corrosion Electrochemistry of Fe/FeS Nanoparticles. *Environ Sci Technol* **2014,** *48*, (7), 4002-4011.

49. Lee, M.; Wells, E.; Wong, Y. K.; Koenig, J.; Adrian, L.; Richnow, H. H.; Manefield, M., Relative Contributions of Dehalobacter and Zerovalent Iron in the Degradation of Chlorinated Methanes. *Environ Sci Technol* **2015,** *49*, (7), 4481-4489.

50. Koenig, J. C.; Lee, M. J.; Manefield, M., Successful microcosm demonstration of a strategy for biodegradation of a mixture of carbon tetrachloride and perchloroethene harnessing sulfate reducing and dehalorespiring bacteria. *Journal of hazardous materials* **2012,** *219-220*, 169-175.

51. Hwang, Y.-H.; Kim, D.-G.; Shin, H.-S., Effects of synthesis conditions on the characteristics and reactivity of nano scale zero valent iron. *Applied Catalysis B: Environmental* **2011,** *105*, (1), 144-150.

52. Phenrat, T.; Long, T. C.; Lowry, G. V.; Veronesi, B., Partial Oxidation ("Aging") and Surface Modification Decrease the Toxicity of Nanosized Zerovalent Iron. *Environ Sci Technol* **2009,** *43*, (1), 195-200.

53. Li, J.; Zhang, X.; Sun, Y.; Liang, L.; Pan, B.; Zhang, W.; Guan, X., Advances in Sulfidation of Zerovalent Iron for Water Decontamination. *Environ Sci Technol* **2017,** *51*, (23), 13533–13544.

54. Gong, Y. Y.; Liu, Y. Y.; Xiong, Z.; Kaback, D.; Zhao, D. Y., Immobilization of mercury in field soil and sediment using carboxymethyl cellulose stabilized iron sulfide nanoparticles. *Nanotechnology* **2012,** *23*, (29).

55. Fan, D.; Lan, Y.; Tratnyek, P. G.; Johnson, R. L.; Filip, J.; O'Carroll, D. M.; Nunez Garcia, A.; Agrawal, A., Sulfidation of Iron-Based Materials: A Review of Processes and Implications for Water Treatment and Remediation. *Environ Sci Technol* **2017,** *51*, (22), 13070-13085.

56. Mullet, M.; Boursiquot, S.; Abdelmoula, M.; Genin, J. M.; Ehrhardt, J. J., Surface chemistry and structural properties of mackinawite prepared by reaction of sulfide ions with metallic iron. *Geochimica Et Cosmochimica Acta* **2002,** *66*, (5), 829-836.

57. He, Y. T.; Wilson, J. T.; Wilkin, R. T., Impact of iron sulfide transformation on trichloroethylene degradation. *Geochimica et Cosmochimica Acta* **2010,** *74*, (7), 2025-2039.

58. Fan, D.; Anitori, R. P.; Tebo, B. M.; Tratnyek, P. G.; Lezama Pacheco, J. S.; Kukkadapu, R. K.; Kovarik, L.; Engelhard, M. H.; Bowden, M. E., Oxidative Remobilization of Technetium Sequestered by Sulfide-Transformed Nano Zerovalent Iron. *Environ Sci Technol* **2014,** *48*, (13), 7409-7417.

59. Boparai, H. K.; Joseph, M.; O'Carroll, D. M., Cadmium (Cd2+) removal by nano zerovalent iron: surface analysis, effects of solution chemistry and surface complexation modeling. *Environ Sci Pollut R* **2013,** *20*, (9), 6210-6221.

60. Li, X.-q.; Zhang, W.-x., Sequestration of Metal Cations with Zerovalent Iron NanoparticlesA Study with High Resolution X-ray Photoelectron Spectroscopy (HR-XPS). *The Journal of Physical Chemistry C* **2007,** *111*, (19), 6939-6946.

61. Boparai, H. K.; Comfort, S. D.; Satapanajaru, T.; Szecsody, J. E.; Grossl, P. R.; Shea, P. J., Abiotic transformation of high explosives by freshly precipitated iron minerals in aqueous Fe-II solutions. *Chemosphere* **2010,** *79*, (8), 865-872.

62. Csakberenyi-Malasics, D.; Rodriguez-Blanco, J. D.; Kis, V. K.; Recnik, A.; Benning, L. G.; Posfai, M., Structural properties and transformations of precipitated FeS. *Chem Geol* **2012,** *294*, 249-258.

63. He, F.; Li, Z.; Shi, S.; Xu, W.; Sheng, H.; Gu, Y.; Jiang, Y.; Xi, B., Dechlorination of Excess Trichloroethene by Bimetallic and Sulfidated Nanoscale Zero-Valent Iron. *Environ Sci Technol* **2018,** *52*, (15), 8627–8637.

64. Phenrat, T.; Liu, Y. Q.; Tilton, R. D.; Lowry, G. V., Adsorbed Polyelectrolyte Coatings Decrease Fe-0 Nanoparticle Reactivity with TCE in Water: Conceptual Model and Mechanisms. *Environ Sci Technol* **2009,** *43*, (5), 1507-1514.

65. Hansson, E. B.; Odziemkowski, M. S.; Gillham, R. W., Influence of Na2S on the degradation kinetics of CCl4 in the presence of very pure iron. *Journal of contaminant hydrology* **2008,** *98*, (3-4), 128-134.

Chapter 6

6 Conclusions

6.1 Summary

Sulfidation has the potential to increase the selectivity and reactivity of nZVI with halogenated hydrocarbon contaminants as well as decrease interparticle aggregation, improving remediant mobility. These developments help in addressing some of the long-standing challenges associated with nZVI-based remediation formulations and are of great interest for in-situ applications. Despite positive results from bench – scale treatability studies, no field evaluation of S-nZVI had been performed. This thesis reports results from the first field – scale injection of S-nZVI conducted at a site contaminated with a broad range of cVOCs. Synthesis of CMC stabilized nZVI was performed on – site, followed by sulfidation with sodium dithionite ($Na_2S_2O_4$) *via* the aqueous – solid method. Further characterization of a similar S-nZVI formulation was performed in a subsequent study focusing on the aging characteristics of the nanoparticles. This subsequent study is important as field application often requires storage of the nanoparticles prior injection.

TEM – EDS of field synthesized S-nZVI, from synthesis barrels, confirm the presence of both discrete, spherical nZVI-like particles (~ 90 nm) as well as larger irregular structures (~ 500 nm) comprising of iron sulfides. These particles were gravity fed into an injection well for approximately 16 hours and delivery tracked through multiple multi-level monitoring wells located upstream and downstream of the injection well. The non-native sandy backfill of the study area was highly heterogenous, resulting in complicated flow paths. Nevertheless, samples collected from the monitoring wells indicate good radial and vertical iron distribution. TEM-EDS analysis of well samples showed both nZVI-like particles as well as larger flake-like structures, similar to those found in the injected S-nZVI suspension. The increase in total iron at monitoring wells was accompanied by decrease in aqueous phase concentrations of cVOCs. Though background sampling showed transformations of parent compounds occurred prior to injection (indicative of natural attenuation or a result of previous remedial activities), daughter products from tetrachloroethene (PCE) and carbon tetrachloride (CCl_4) dechlorination, present at elevated

concentrations after treatment, suggest both abiotic and biotic degradation took place. Post-treatment soil cores also revealed significant decreases in cVOC concentrations throughout the targeted treatment zones. *In situ* degradation was confirmed by Compound Specific Isotope Analysis (CSIA), as shown by the enrichment in ^{13}C for PCE (from -26.0 ‰ to -24.6 ‰) and the concurrent depletion in TCE (from -22.9 ‰ to -25.0 ‰) at select sampling points. Rebound of cVOC concentrations, though expected, complicates assessment of the long-term effects of the treatment. Despite increases in cVOC concentrations during long-term monitoring at deeper locations (4 to 4.5 m bgs), concurrent increases in ethene and chloride showed that dechlorination was also an active operative process. Overall, results from this field study show sulfidation is a suitable amendment for the development of efficient nZVI-based treatments for *in situ* remediation. It demonstrates that S-nZVI stabilized with CMC can be safely synthesized on-site and is highly reactive, mobile, and stable in the subsurface.

The second bench – scale study investigated the effects of aging on S-nZVI together with S-nZVI stabilized with low concentrations of CMC. Aging was completed under a sulfidic environment over short-time intervals (0 – 21 days). Nanoparticles retained their spherical morphology throughout the aging period of 21 days, with acid digestion confirming the presence of Fe^0. Transformation of iron sulfides in the form of cubic/laminar to needle-like structures were apparent for S-nZVI, but not for CMC S-nZVI. Reactivity was tested against trichloroethene (TCE) and chloroform (CF) in a co-contaminated system. During the 21 day aging period S-nZVI particles retained rate constants for TCE that were on par or higher to the initial values. CMC S-nZVI yielded lower rate constants for TCE than as compared to S-nZVI, possibly due to blocking of reactive sites by CMC. Complete dechlorination could not be achieved for chloroform, obtaining on average 27% removal for S-nZVI and CMC S-nZVI. In both cases, however, reactivity against the model pollutant was not negatively affected by aging. This study provides greater insights into transformations taking place during aging of S-nZVI and furthers its relevance for *in situ* treatment of organohalide pollutants.

6.2 Future Outlook and Research Needs

Success pilot trials of new remediation technologies at active contaminated sites represent a major step for their wider acceptance by consultants and regulators. Results reported herein directly

address this challenge. Nevertheless, multiple recommendations can be made to improve the efficiency and feasibility of the treatment as well as to increase the understanding of the biogeochemical processes occurring in the subsurface after S-nZVI injection. The first set of recommendations are on particle design and synthesis protocol. Such changes can first be addressed by optimizing the S-nZVI formulation for site specific conditions. Second, additional analytical techniques can be implemented to elucidate corollary subsurface processes. Recommendations in these two general aspects are discussed below.

6.2.1 Synthesis Protocol and Particle Design

S/Fe ratio and the sulfidation duration has been identified as two of the major operational variables influencing the structure and morphology of sulfidated particles. In terms of the S/Fe ratio, it is now common practice to test for a range of ratios in studies evaluating the removal of contaminants by S-(n)ZVI. The selection criteria for the optimal ratio is typically based on the formulation yielding the highest Fe^0 content or reaction rates against target pollutants. This is achievable by varying either the sulfur source or concentration of sulfur and iron. However, other aspects pertaining to the synthesis scale – up process would also play a role and should be addressed in the design process. For example, rationale for the selection of the source of sulfur and its concentration should also consider practical aspects such as ease of handling and onsite storage. Other factors related to how sulfur is utilized during the synthesis procedure should be considered, as this has potential health and safety considerations. Generation of toxic fumes (e.g., hydrogen sulfide) can take place if not controlled properly (or planned for) during synthesis. Based on the preliminary observations of this study, off – gassing of H_2S from synthesis barrels would depend on the concentrations of both borohydride and sulfur. Further studies could evaluate the S/BH_4^- ratio with various sulfidating agents to determine optimal conditions for preventing H_2S formation without compromising the chemical and structural integrity of the particles. Careful consideration must be taken to not compromise the latter, since borohydride is normally applied in excess to ensure complete reduction of the iron salt. Nonetheless, optimizing the concentration of borohydride could also decrease the overall cost of the treatment since it is usually the most expensive reagent of the synthesis protocol.

To aid in the final design of the formulation, the reactivity and longevity of S-nZVI under various S/Fe ratios could be tested using groundwater samples. This would provide a more realistic scenario of nanoparticles performance. Though studies on the interactions of common groundwater constituents with S-nZVI had been conducted, these are limited in number and scope. Studies of this nature are normally conducted in well controlled environments aimed at preserving as much of the Fe^0 content as possible, for example, by resuspending the particles in deoxygenated water. The effect of groundwater anions and natural organic matter (NOM) on the aging of S-nZVI, its reactivity and stability, need to be further evaluated. Similarly, to date a sound systematic comparison of the reactivities and structural evolution with aging of S-nZVI obtained using the most common sulfidating agents have not been reported in the open literature yet. As shown in Table 2.3, these sulfur sources would consist mainly of dithionite, elemental sulfur and sulfide. In addition, thiosulfate should also be included as it is a lesser studied compound for S-nZVI research, despite yielding suflidated nanoparticles with reactivity that are on par with the other sources. With respect to particle design, other sulfidated iron – based materials can be evaluated at the field scale and their performance compared to nZVI. Sulfidation of iron oxides has also led to improvement in their reactivity but these treatments have not been tested in the field. Due to the limited research conducted in the area, future field work should be preceded by more extensive treatability studies to better confirm their efficiency for contaminant degradation.

6.2.2 Complementary Analysis

Based on the distribution of the dechlorination products it is suspected biotic degradation took place. Previous field work has demonstrated that enhanced biotic degradation follows the injection of CMC stabilized nZVI. However, it is not yet known how the sulfidation step would influence the native populations of organohalide-respiring microorganisms at a contaminated field site treated with nZVI. The inhibition of hydrogen evolution reactions (HER) by nZVI, a significant positive attribute following sulfidation, can affect the key microbial processes. Future work should evaluate phylum level microbial community composition after injection of S-nZVI. Additionally, to further evaluate the impact of sulfidation on the microbial community, results can be compared to treatment zones where only nZVI has been injected. Unique to this site is the proximity to monitoring wells used in a past nZVI injection trial. Wells from this project are still functioning, but most importantly, microbial communities have already been extensively characterized. This

would facilitate comparison between both treatments since in the absence of nZVI *in-situ* injections microbial communities are expected to be similar. In the same way, the relative importance of differences in microbial growth (if any) on the long – term degradation of cVOCs caused by sulfidation remains to be further investigated.

Appendices

Appendix A

Synthesis Conditions

Table A.1 Reagent mass and volume per batch.

Reagent	Mass (kg)	Volume (L)
Ferrous Sulfate-Heptahydrate ($FeSO_47H_2O$)	0.78	15
Carboxymethyl Cellulose (CMC)	1.2	96
Sodium Borohydride ($NaBH_4$)	0.21	9
Sodium Dithionite ($Na_2S_2O_4$)	0.7	35

The final molar concentration of iron was 14.9 mmol/L and boron 37.7 mmol/L, as compared to the theoretical concentration of 17.91 mmol/L and 35.81 mmol/L, respectively.

Results

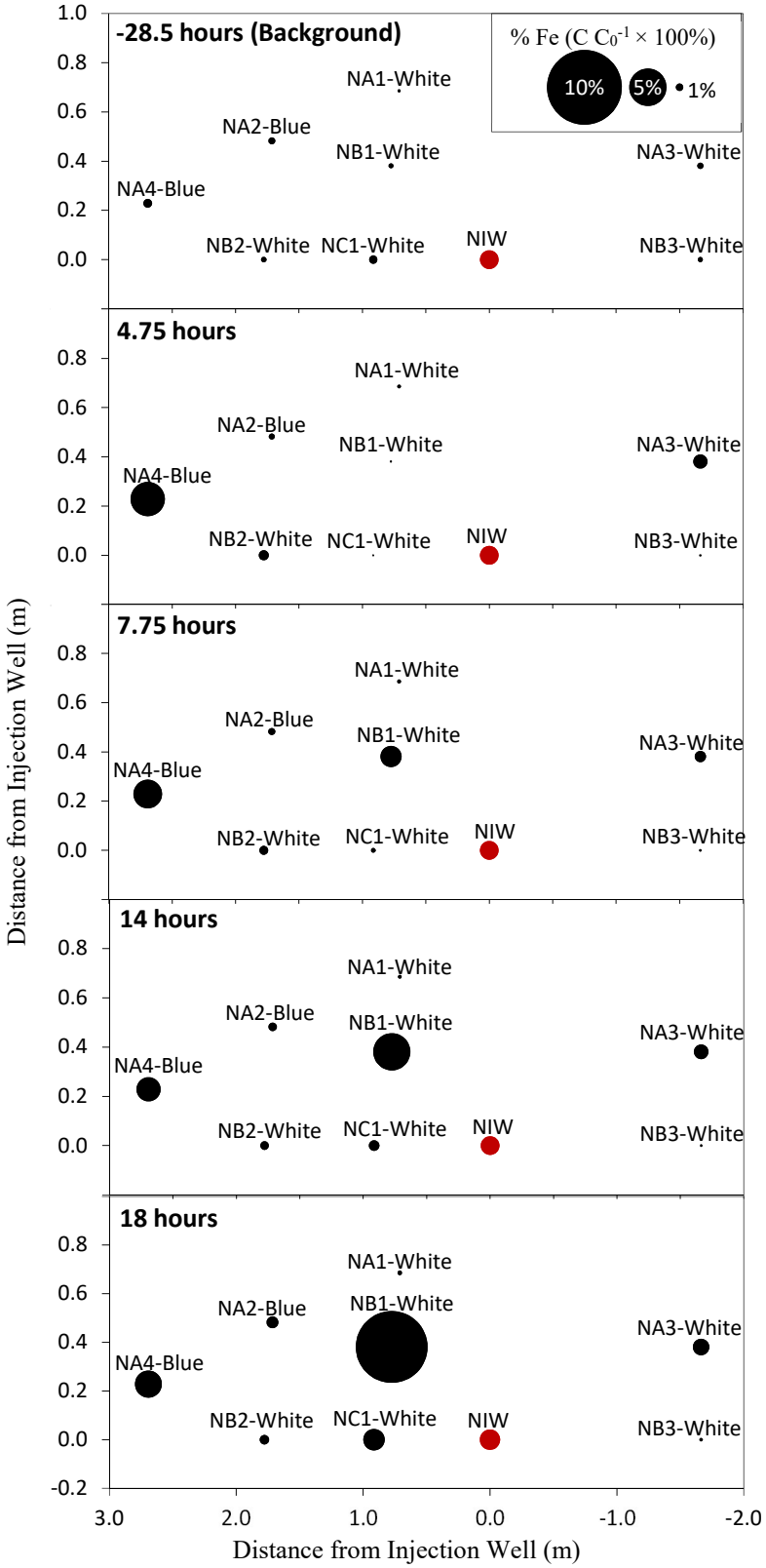

Figure A.1 Plan view of monitoring wells with iron expressed as percentage of injected concentration (14.89 mmol L^{-1}) before and after injection. Injection well (NIW) presented as reference only.

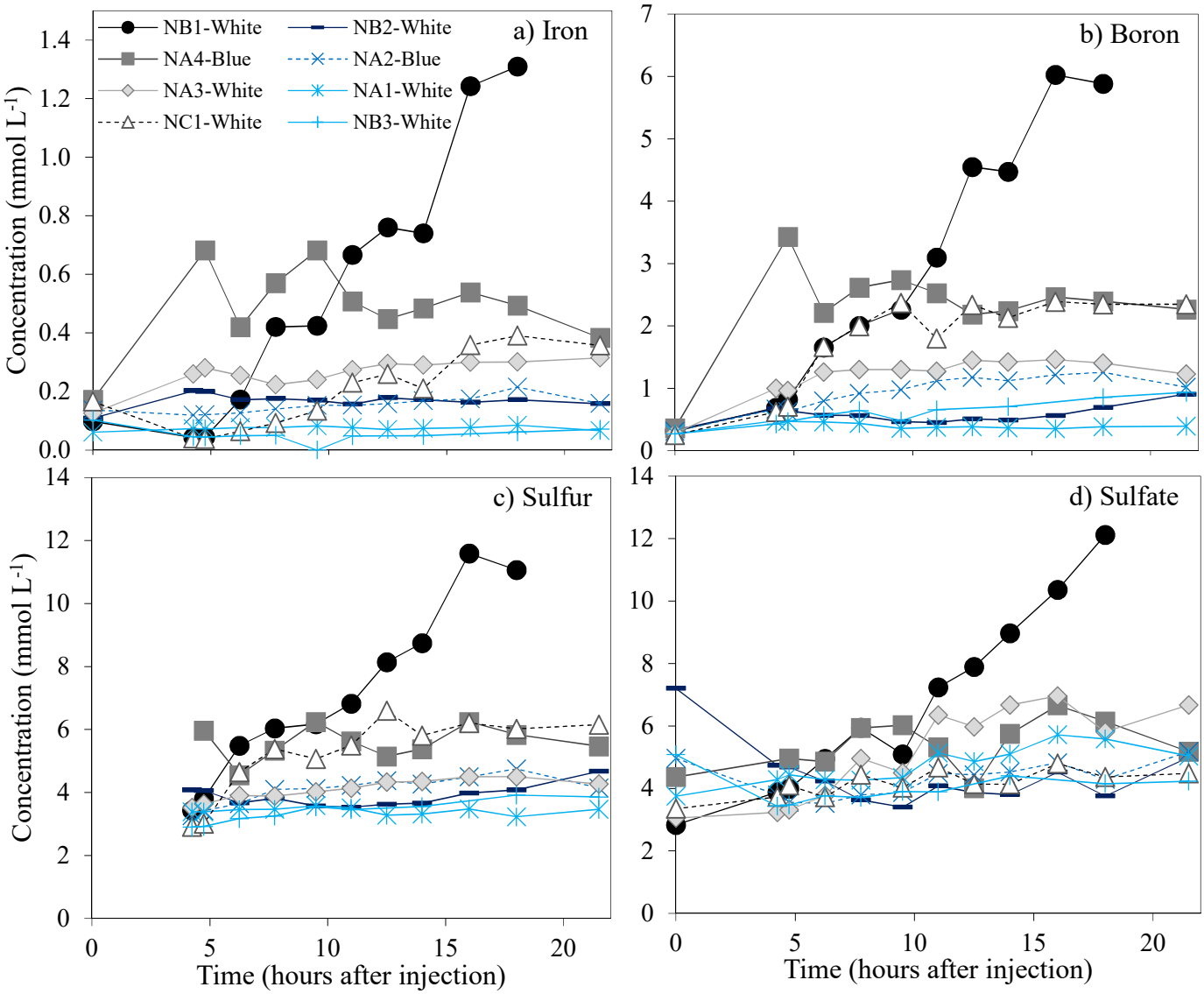

Figure A.2 Changes in a) iron, b) boron, c) sulfur, and d) sulfate molar concentrations during S-nZVI injection. Initial time refers to background samples collected 28.5 hours prior.

Boron comes from the synthesis process and can be considered as a conservative tracer. Sulfur comes from both ferrous sulfate (iron precursor) as well as dithionite and was found predominantly as sulfate. Breakthrough of easily detected total iron and tracers in this study shows a marked improvement in mobility over previous nZVI injections.

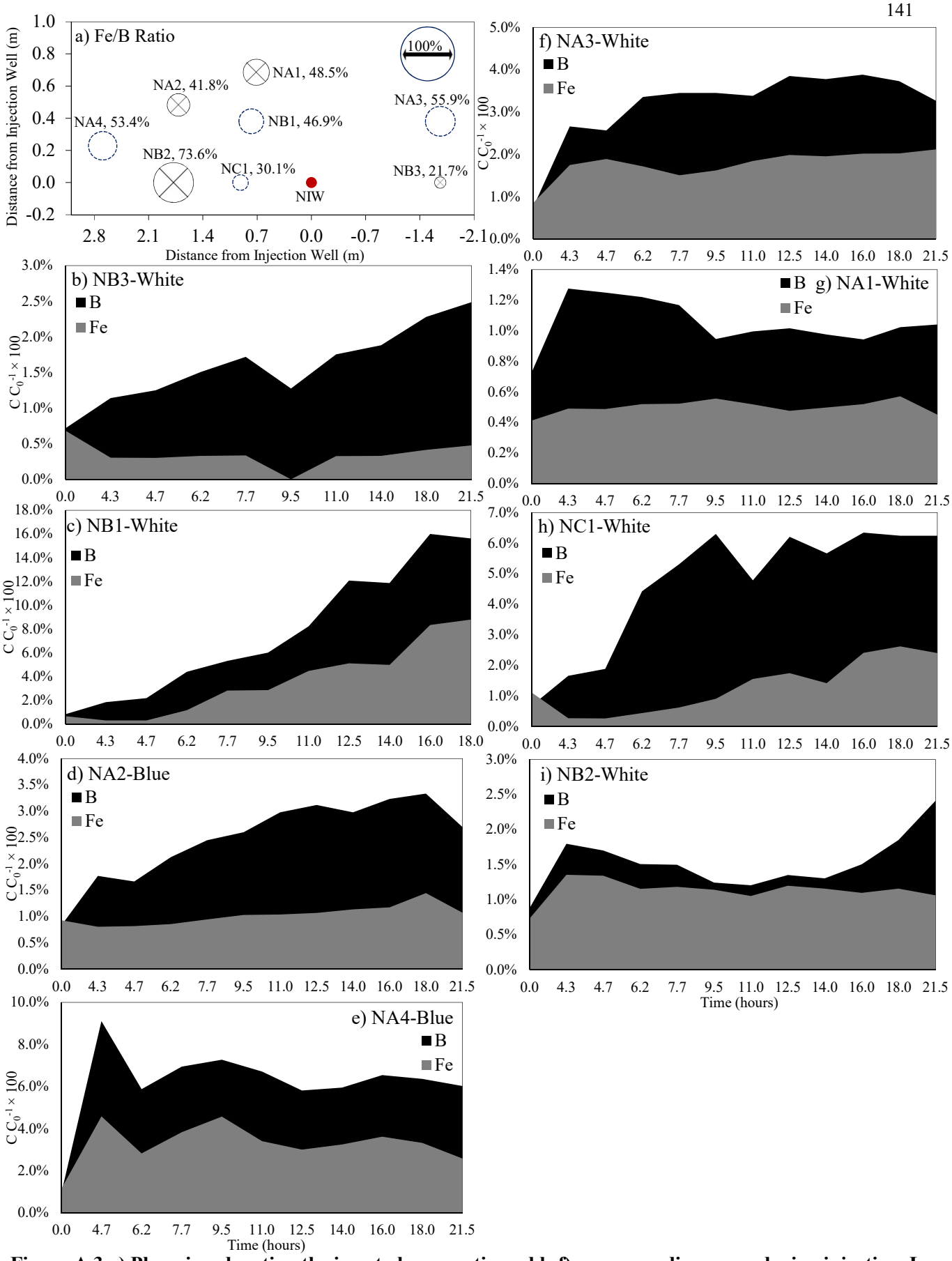

Figure A.3 a) Plan view denoting the iron to boron ratio and b-f) corresponding areas during injection. Locations identified with an (×) are excluded due to their low concentrations (see discussion in main text). Injection well (NIW) is shown for reference. Initial time refers to background samples collected 28.5 hours before injection.

Table A.2 Iron concentration (µM) for all wells up to 17 days after injection. Initial time (t = 0) represent background samples.

	Iron (µM)					
Time (days)	**NB1-White**	**NB1-Blue**	**NB1-Clear**	**NB1-Green**	**NB1-Yellow**	**NB1-Black**
0	98	39	33	16	22	19
1	1309	307	286	363	183	371
3	763	216	281	97	64	84
17	97	94	136	35	23	45
Time (days)	**NB2-White**	**NB2-Blue**	**NB2-Clear**	**NB2-Green**	**NB2-Yellow**	**NB2-Black**
0	109	210	61	148	133	103
1	158	637	142	235	100	87
3	171	292	142	218	N/A	N/A
17	219	278	261	308	N/A	N/A
Time (days)	**NA1-White**	**NA1-Blue**	**NC1-White**	**NC1-Blue**	**NA4-Blue**	**NA2-Blue**
0	61	61	166	24	172	138
1	67	77	357	394	383	159
3	N/A	N/A	280	N/A	280	147
17	N/A	N/A	330	N/A	549	168
Time (days)	**NA3-White**	**NA3-Blue**	**NB3-White**	**NB3-Blue**		
0	126	358	102	161		
1	315	383	71	1007		
3	226	108	134	108		
17	220	69	124	69		

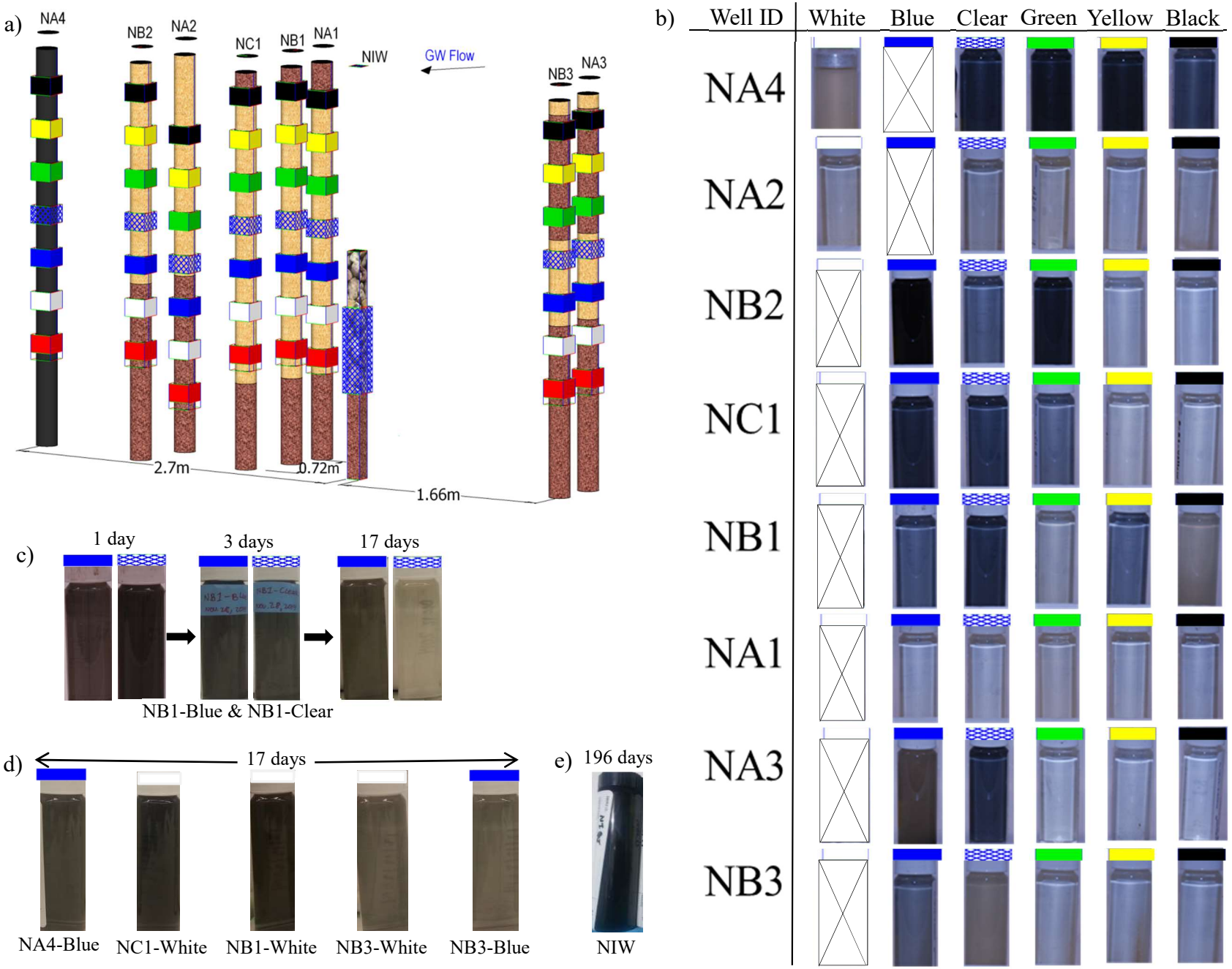

Figure A.4 Groundwater samples containing S-nZVI. a) Isometric view of study area is shown to aid in the identification of the locations relative to the injection well. Nanoparticles in monitoring wells are shown b) immediately after injection, c-d) after a short-term (1 - 17 days), and e) long-term period (196 days).

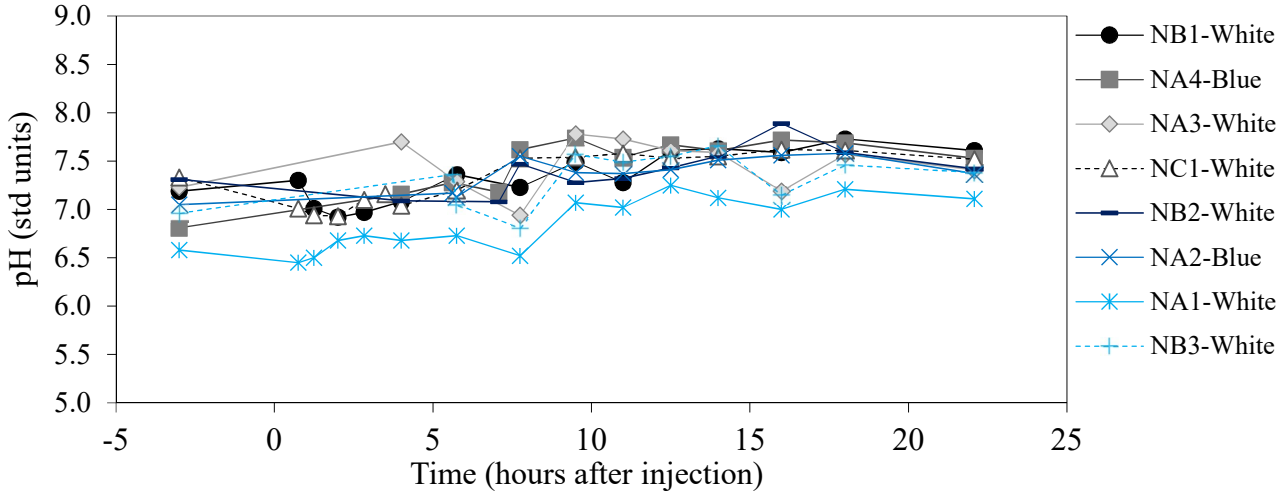

Figure A.5 Changes in pH during injection of S-nZVI.

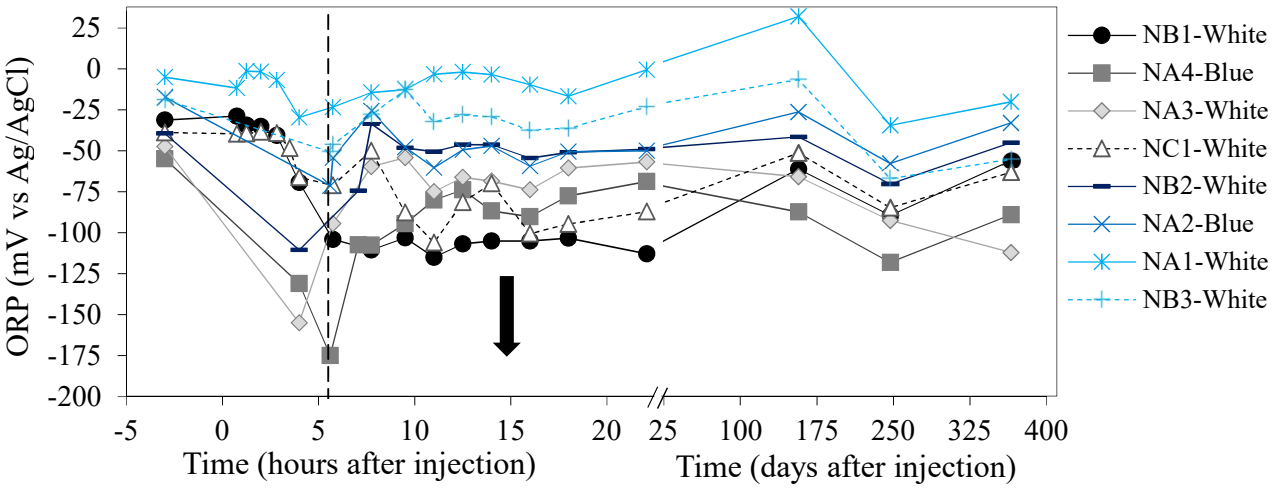

Figure A.6 Changes in oxidation-reduction potential (ORP). Due to time constraints during injection (0 – 22 hours) not enough time was allocated to allow for enough equilibration time of the ORP. An arrow is used to indicate that actual values might had been lower for sampling times right to the dashed line.

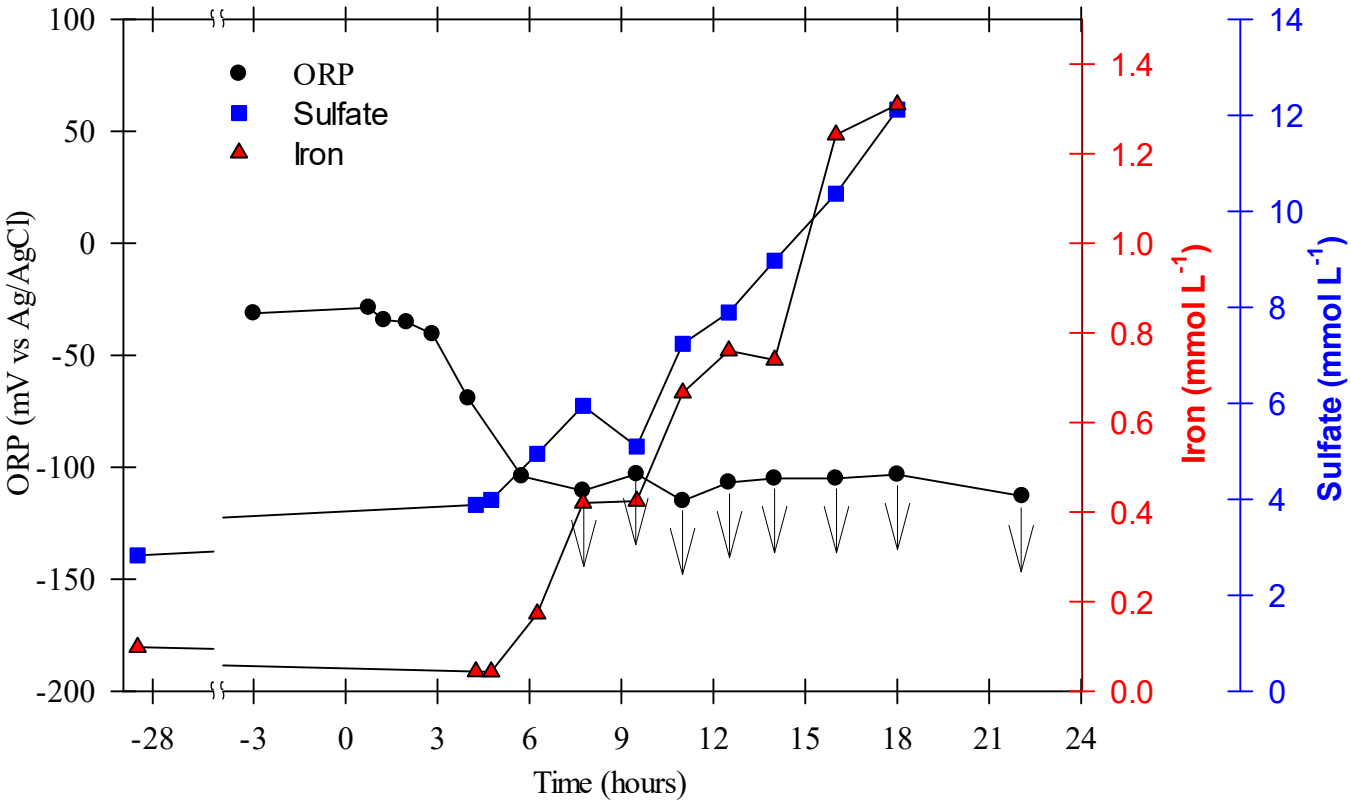

Figure A.7 ORP versus iron and sulfate breakthrough for NB1-White. Arrows indicate actual ORP values might had been lower.

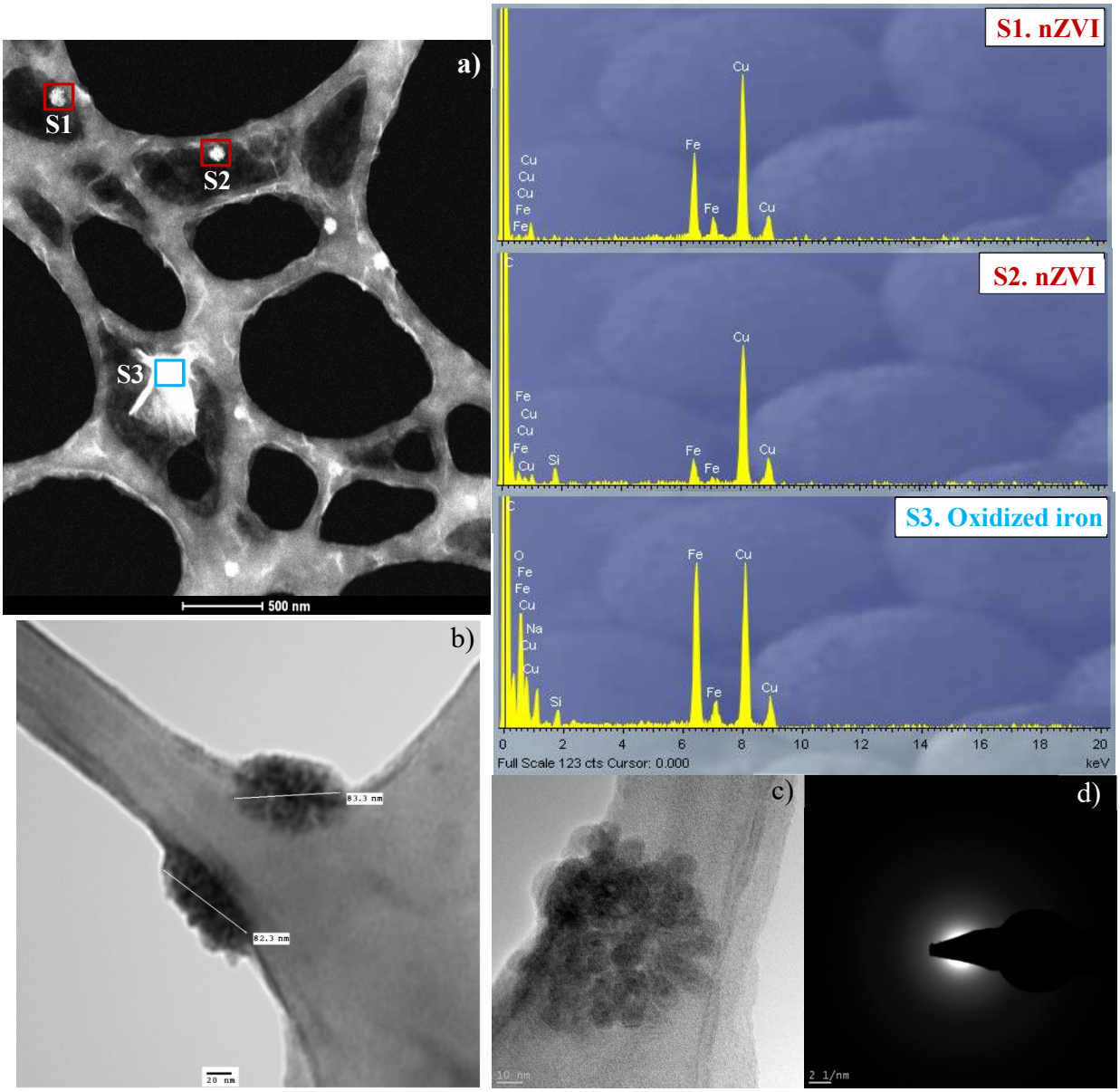

Figure A.8 TEM images, SAED pattern, and EDS spectra for the nZVI particles from the synthesis batch before dithionite addition.

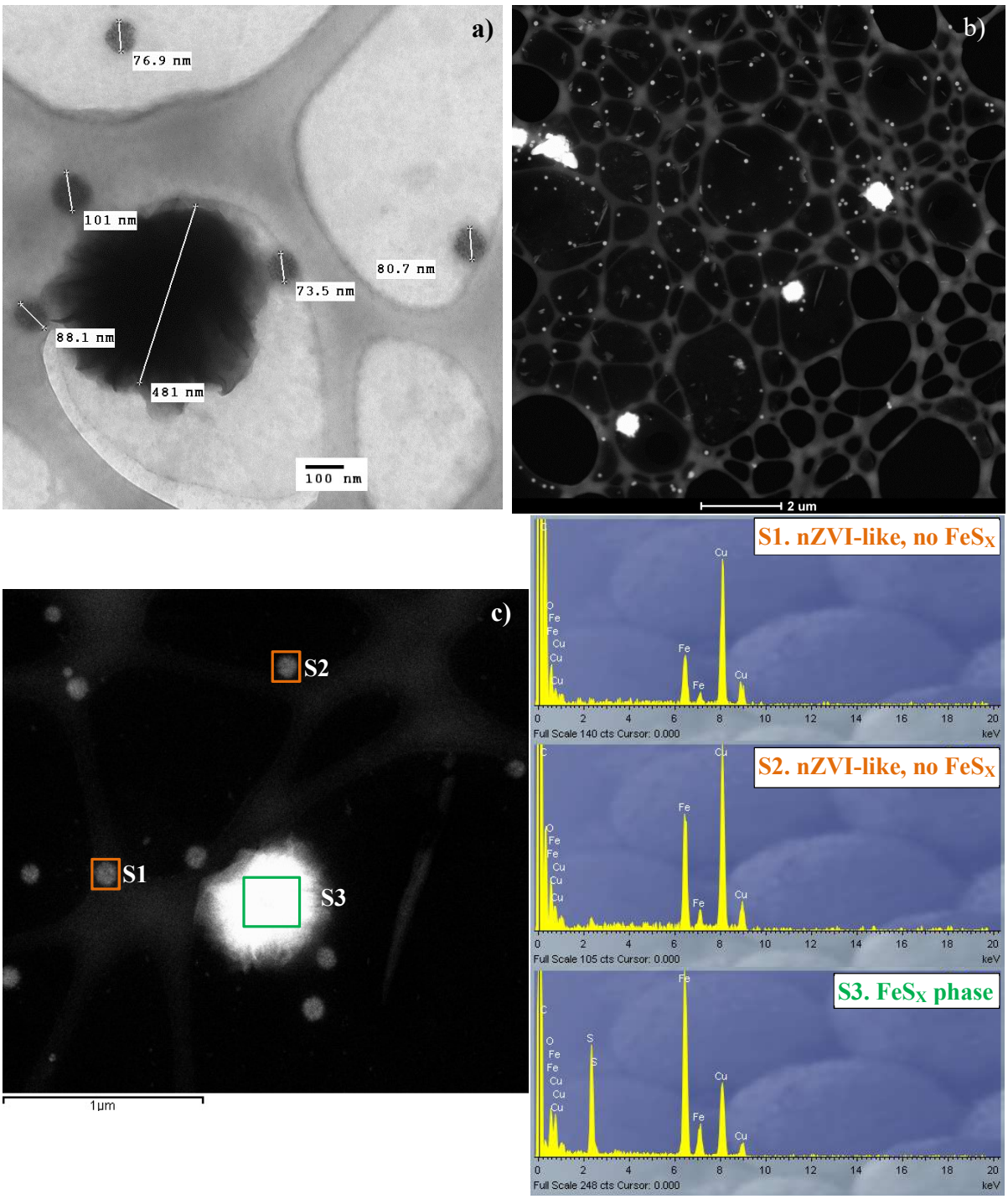

Figure A.9 TEM images and EDS spectra for the S-nZVI particles from the synthesis batch after dithionite addition.

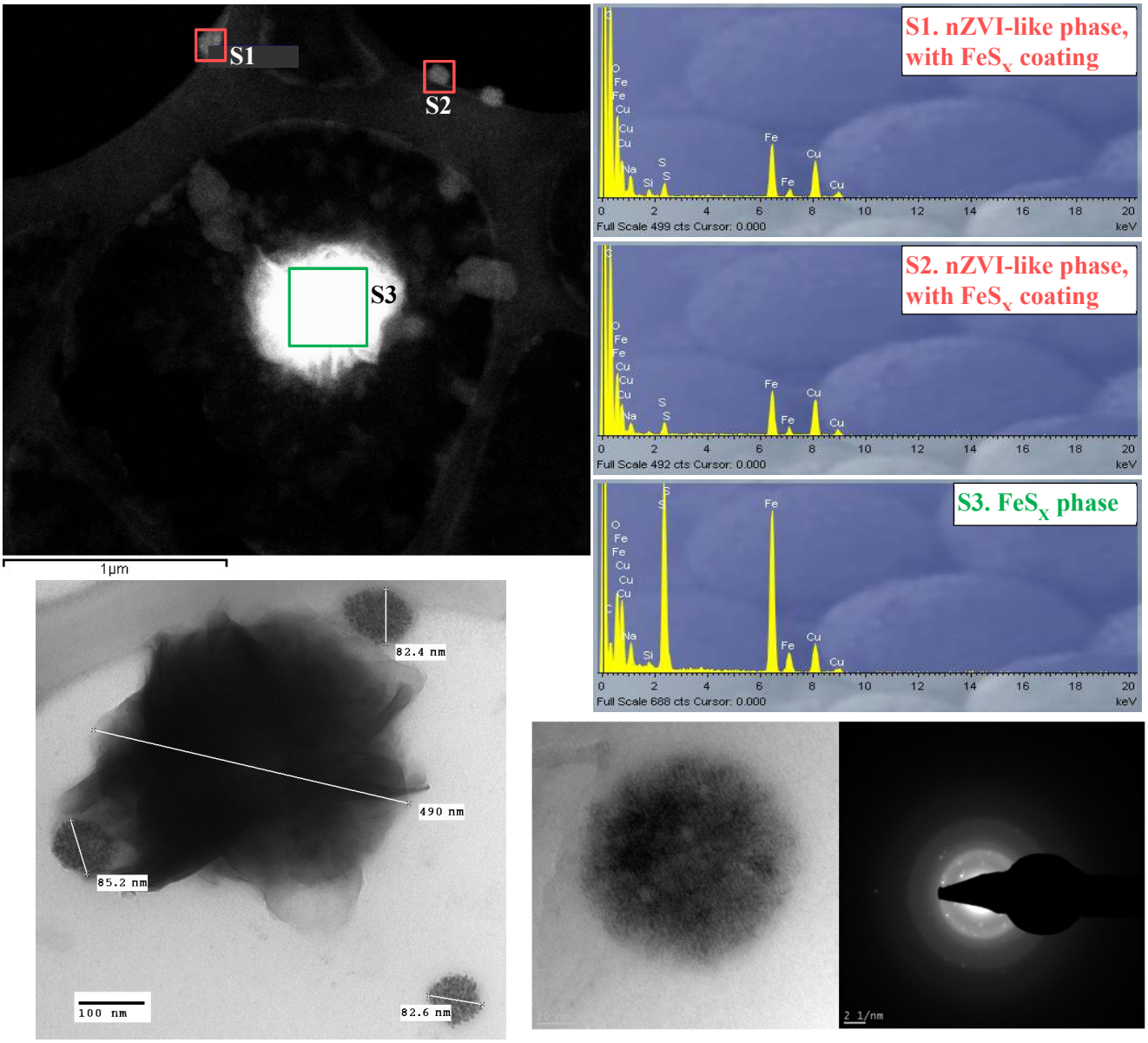

Figure A.10 TEM images, SAED pattern, and EDS spectra for the S-nZVI particles from the synthesis batch after dithionite addition.

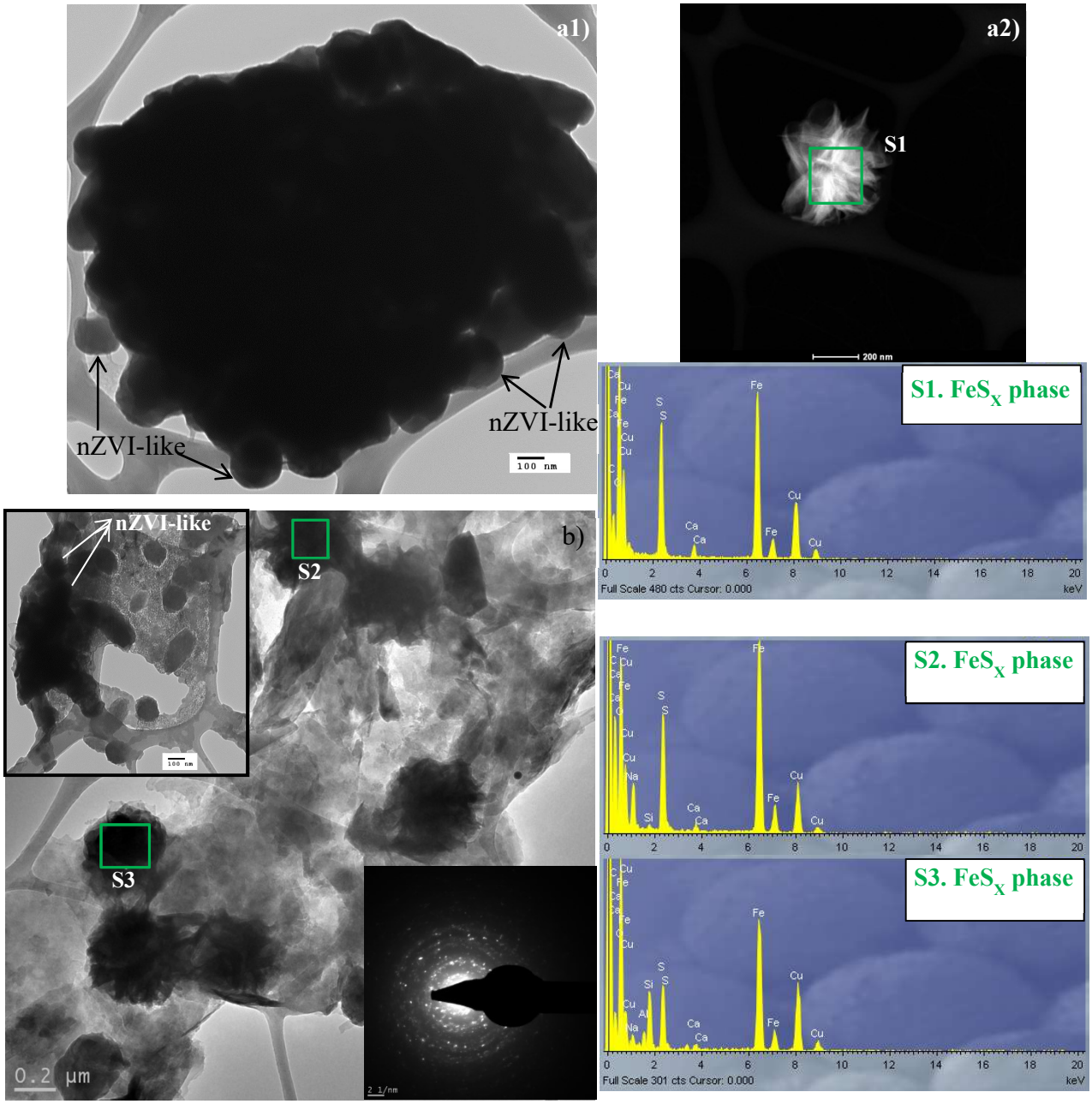

Figure A.11 TEM images, SAED pattern, and EDS of a) NB1-Blue, and b) NB1-Clear at t = 72 hours after injection.

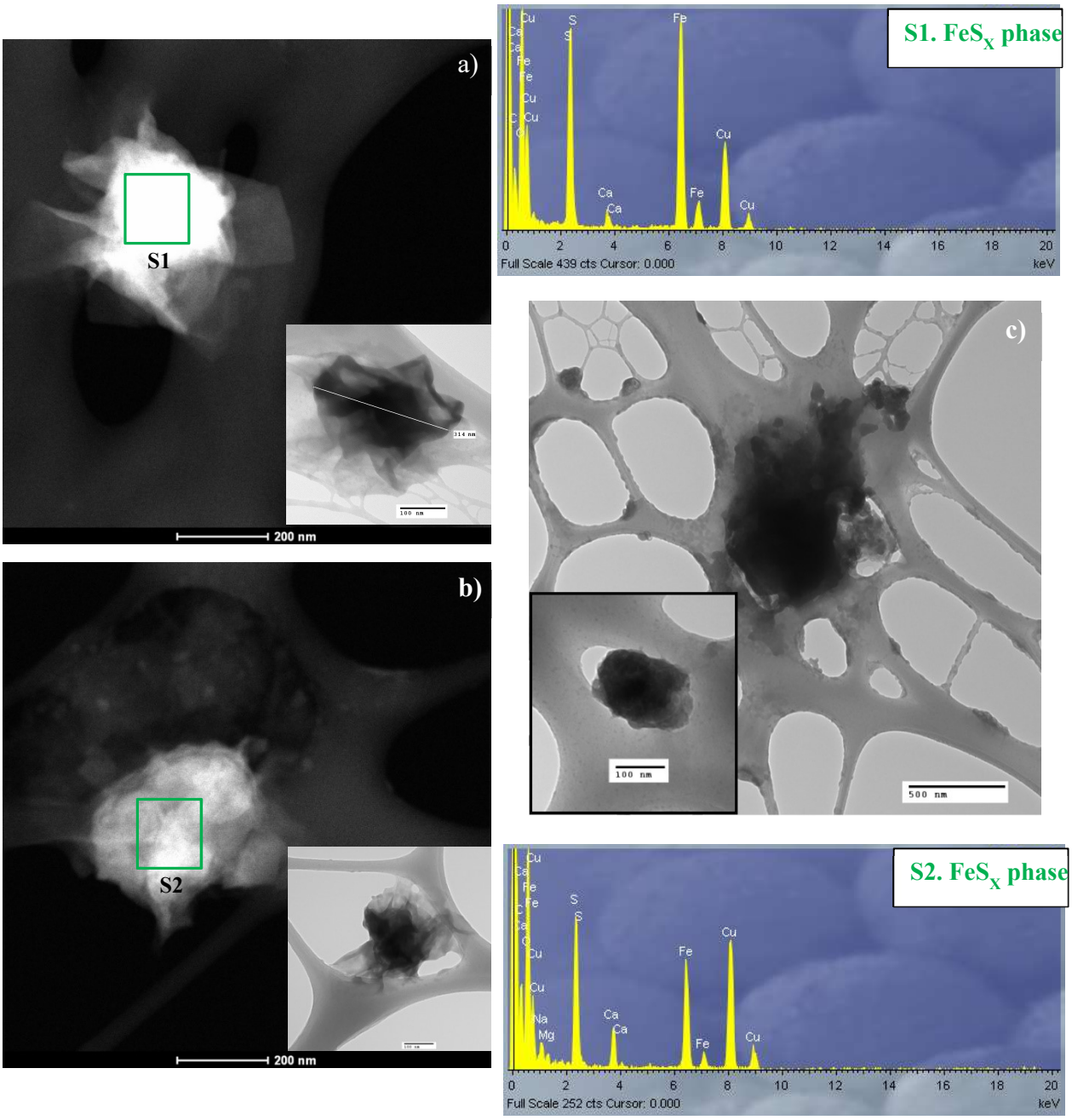

Figure A.12 TEM images and EDS of a) NB2-Clear, b) NB2-Green, and c) NB2-Blue at t = 72 hours after injection.

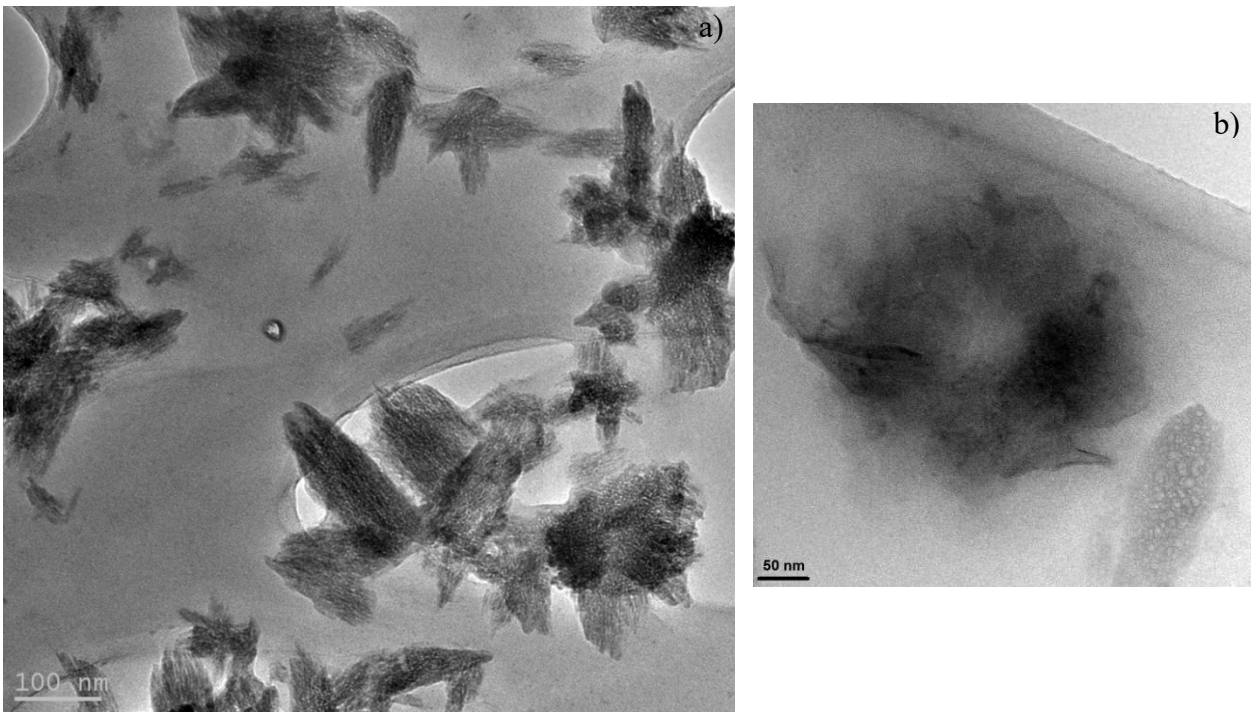

Figure A.13 TEM images of NIW at t = 196 days after injection.

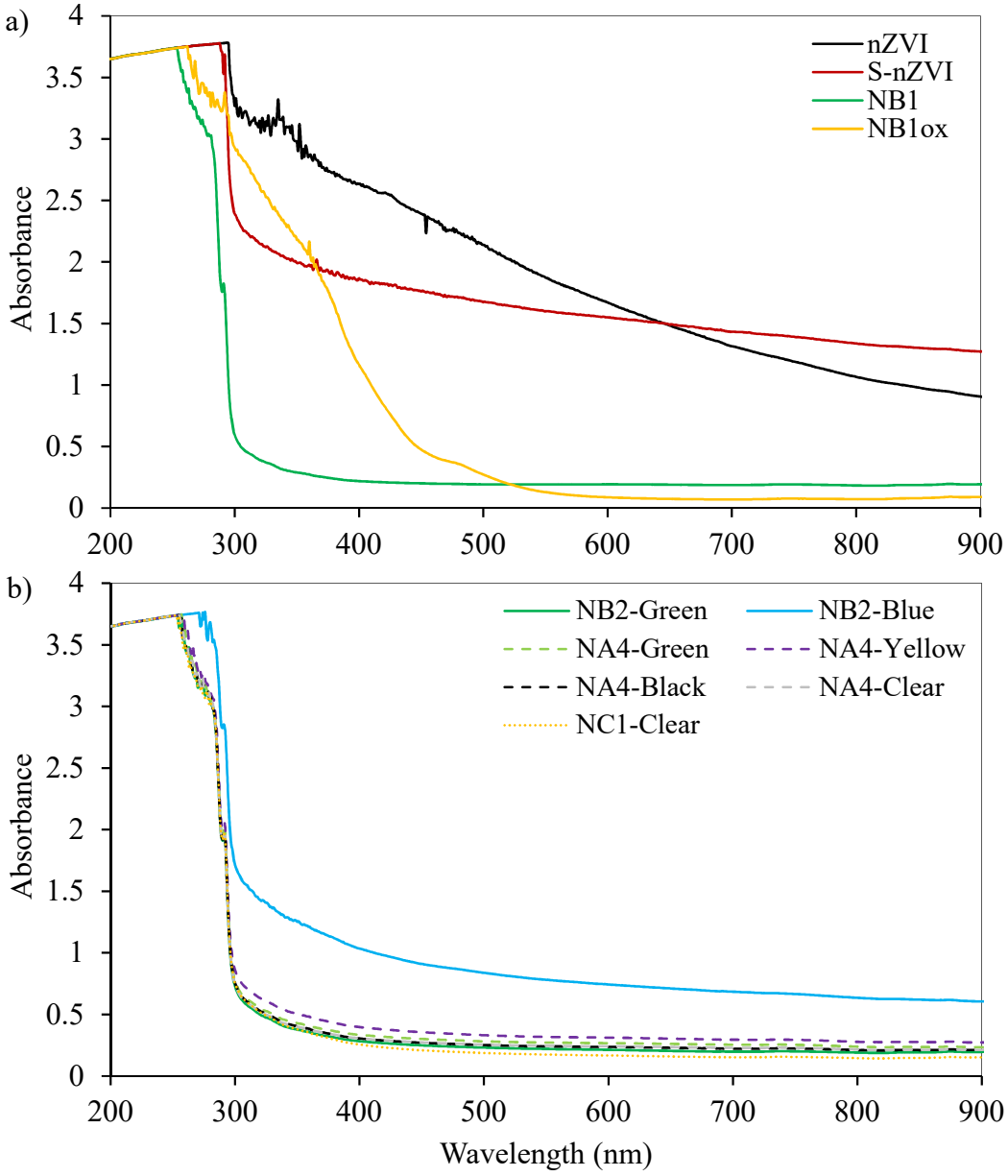

Figure A.14 Absorbance spectra of nZVI and S-nZVI from synthesis batches. $NB1_{ox}$ is a groundwater sample from the NB1 well intentionally oxidized in the laboratory by exposing it to air.

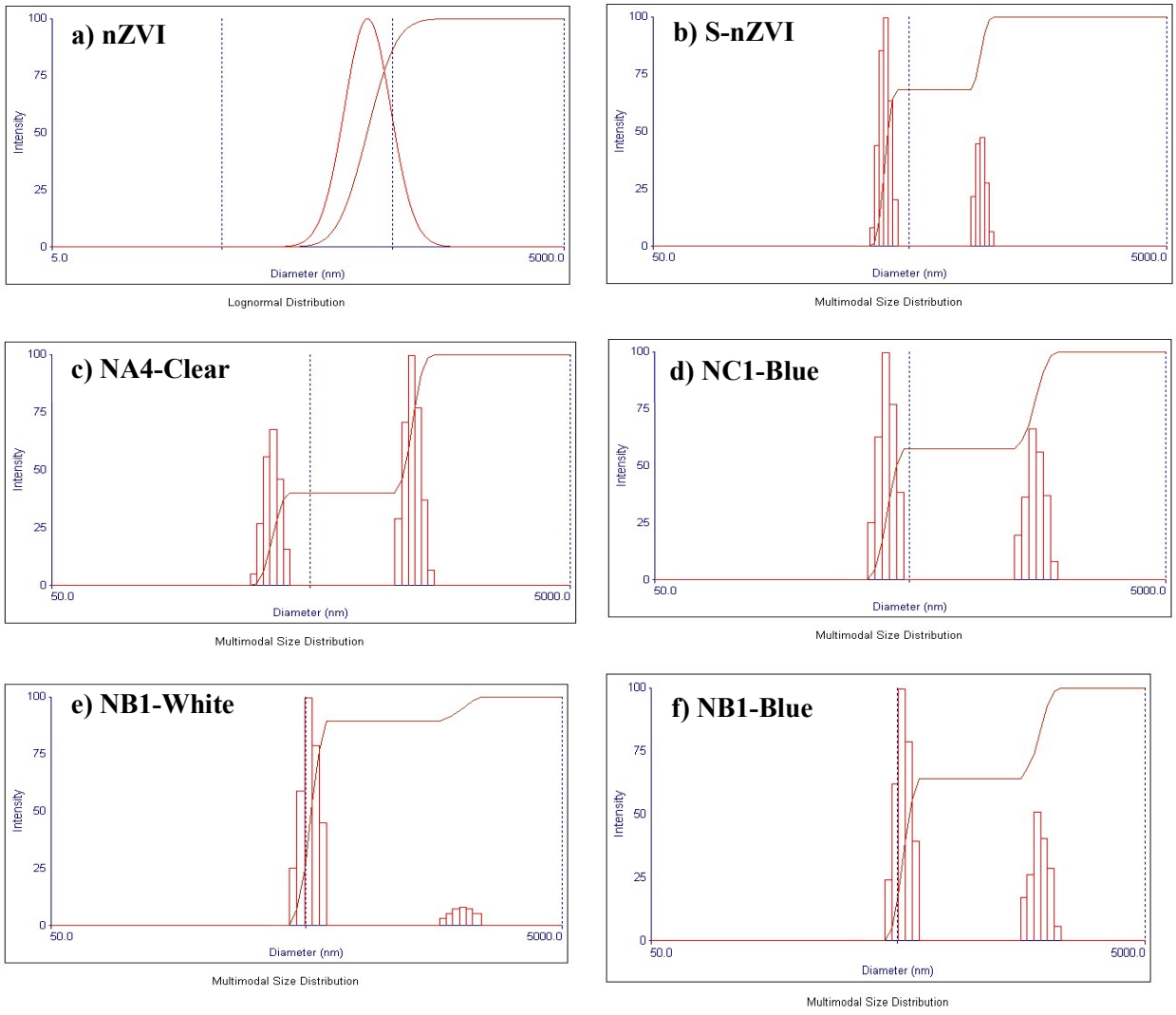

Figure A.15 Particle Size Distribution (PSD) for a) nZVI, b) S-nZVI, and c – f) particles in groundwater samples. Samples were analyzed by Dynamic Light Scattering (DLS) in a Zeta Plus particle analyzer.

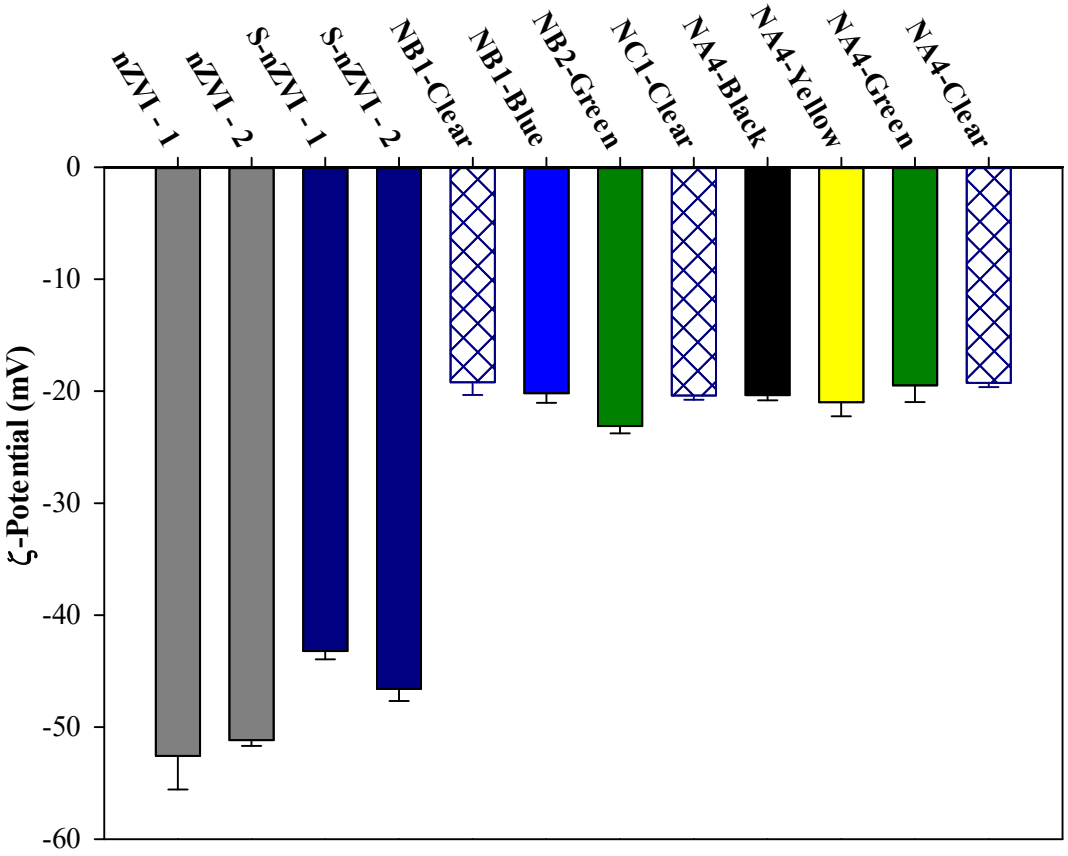

Figure A.16 ζ-Potential of S-nZVI, nZVI and groundwater samples.

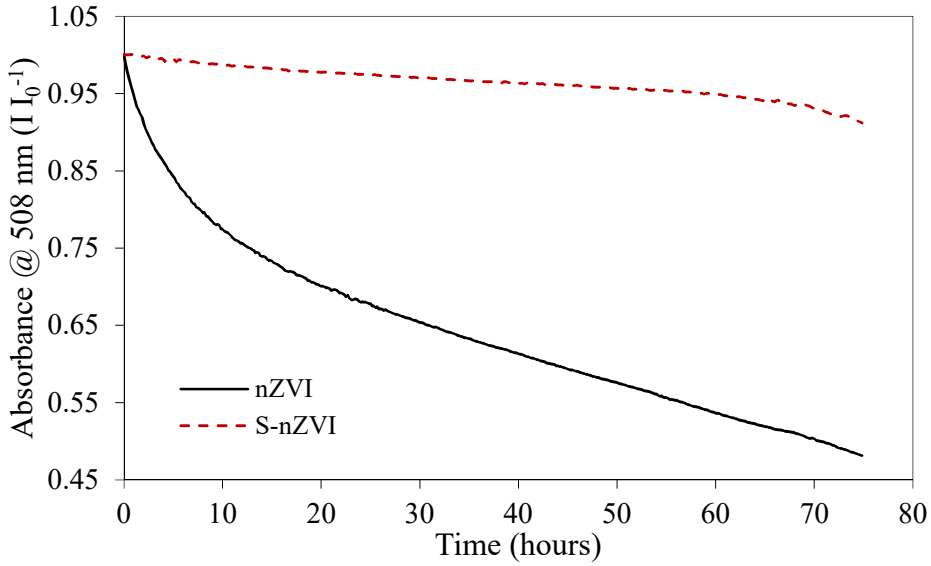

Figure A.17 Sedimentation curves for field synthesized (S –) nZVI, stabilized with ~0.77% wt/vol CMC.

Appendix B

Monitoring Wells

Bundle piezometers have been implemented for over 30 years in unconsolidated materials to collect depth-discrete groundwater samples.[1] This type of device offers numerous advantages for profiling contaminated sites, including: a) high versatility, b) rapid construction, c) applicability to both shallow and deep water table, and d) cost effectiveness, necessitating only a single borehole and therefore minimum drill-rig time. Bundle piezometers are mainly suited for cohesionless aquifers, with high content of sand and gravel. They are not suited, however, for aquifers with appreciable content of silt or clay, or for retrieving large sample volumes from a single sampling point. Extensive experience of practitioners has demonstrated that, given low vertical hydraulic gradients, vertical migration of contaminants is negligible. Yet uncertainty still remains as to the possibility of vertical movement along the zone of borehole disturbance.[2] To address this, mesh sleeves with bentonite were wrapped around in between sampling point during installation.

Compound Specific Isotope Analysis (CSIA)

Introduction:

Compound Specific Isotope Analysis (CSIA) uses Kinetic Isotope Effects (KIEs) during isotopic fractionation.[3] The presence of additional neutrons in chemical species will result in mass-dependent fractionation. In the case of carbon, the lower activation energy required for light isotopes (^{12}C) yields faster reaction rates (^{12}k) in comparison to the heavier isotopes (^{13}C). Molecules with ^{13}C in the reacting position are degraded more slowly, resulting in lower rate constants (^{13}k). As a result, heavy isotopologues will be enriched in the reactants during normal isotope fractionation ($KIE_c > 1$, where $KIE_c = {}^{12}k/{}^{13}k$). It is often assumed that KIEs associated with physical processes such as dilution, diffusion, sorption or volatilization are significantly smaller and therefore neglected.[4]

Method

Temperature Program #1 – Column #1

For PCE, TCE, and cis-DCE, a 60 m × 0.32 mm × 3 μm VOCOL column was used. The temperature program started at 35 °C for 3 min, then increased up to 160 °C at a rate of 5 °C/min, the temperature was held at 160 °C for 1 min, then increased to 200 °C at 5 °C/min, and stayed at 200 °C for 5 min. Under these conditions, the approximate retention times were 960 seconds for cDCE, 1220 seconds for TCE, and 1560 seconds for PCE.

Temperature Program #2 – Column #2

For VC and cDCE, a 60 m × 0.32 mm GSQ column was used. The temperature program started at 35 °C for 3 min, then increased up to 160 °C at a rate of 5 °C/min, then immediately ramped up to 210 °C at 10 °C/min, and stayed at 210 °C for 10 min. Under these conditions, the approximate retention times were 1458 seconds for VC and 2260 seconds for cis-DCE.

Results:

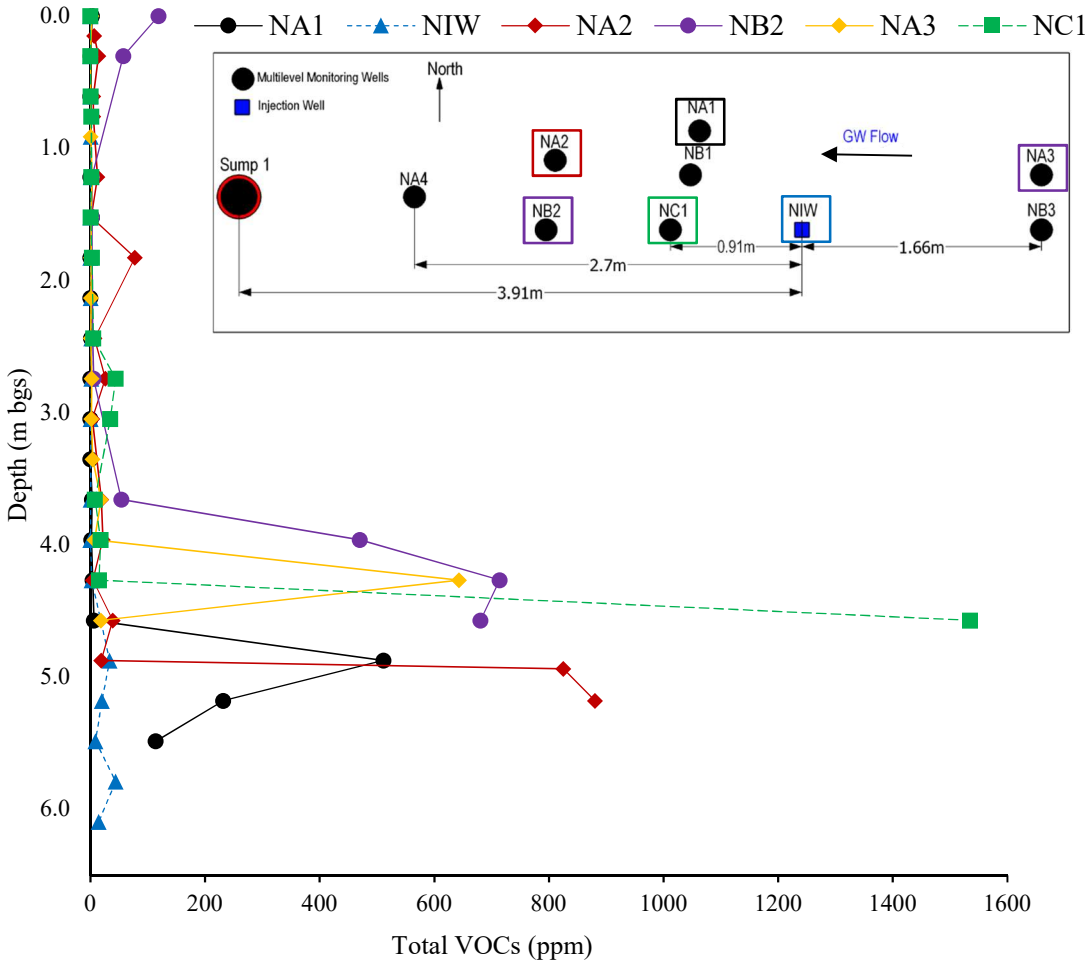

Figure B.1 Volatile Organic Compounds (VOCs) in soil cores during well installation. Measurements were taken using a Photoionization Detector (PID).

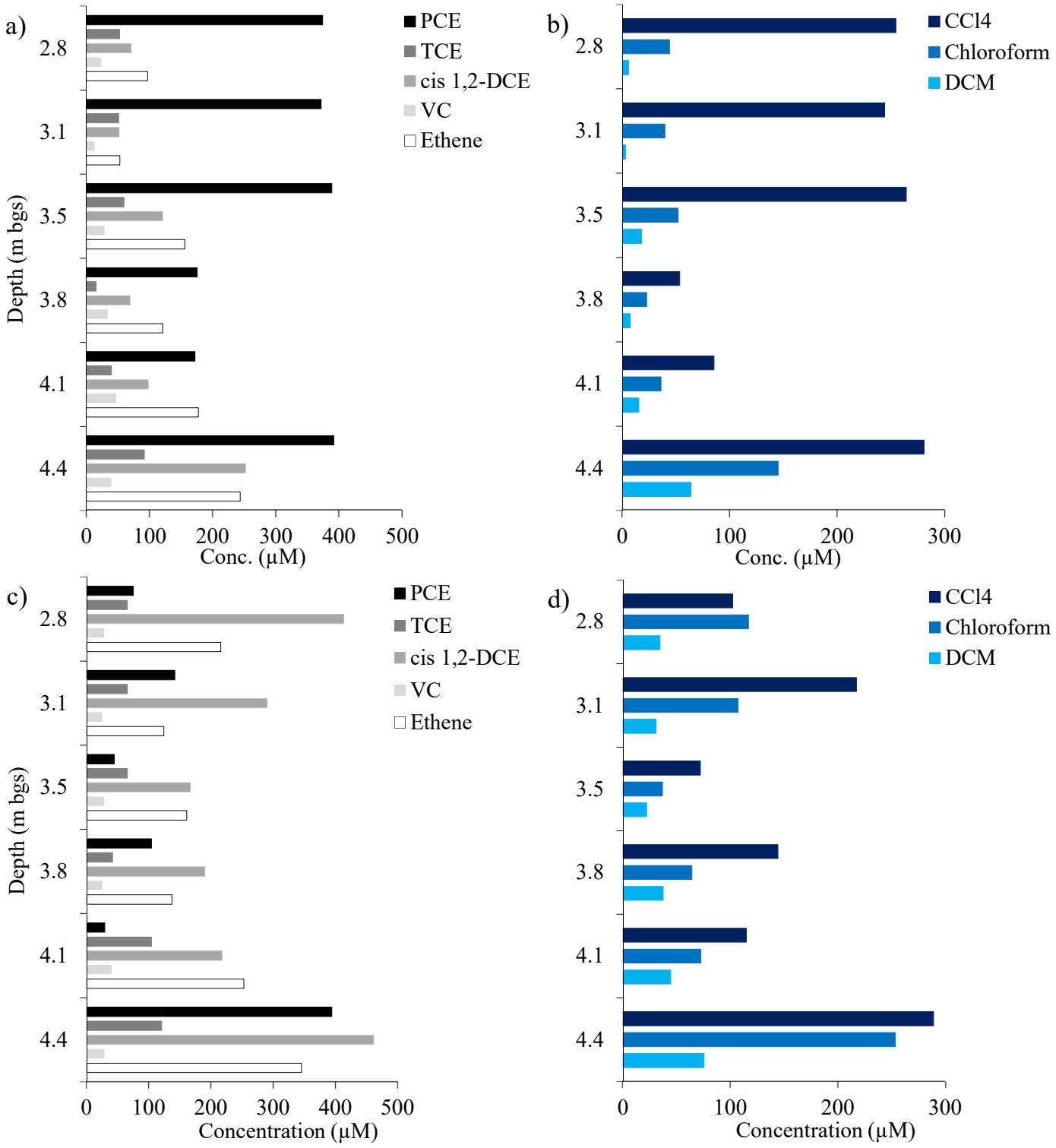

Figure B.2 Background concentrations of PCE, TCE, cis 1,2-DCE, Ethene, CCl_4, Chloroform and DCM for the (a – b) NB1 and (c – d) NB2 well.

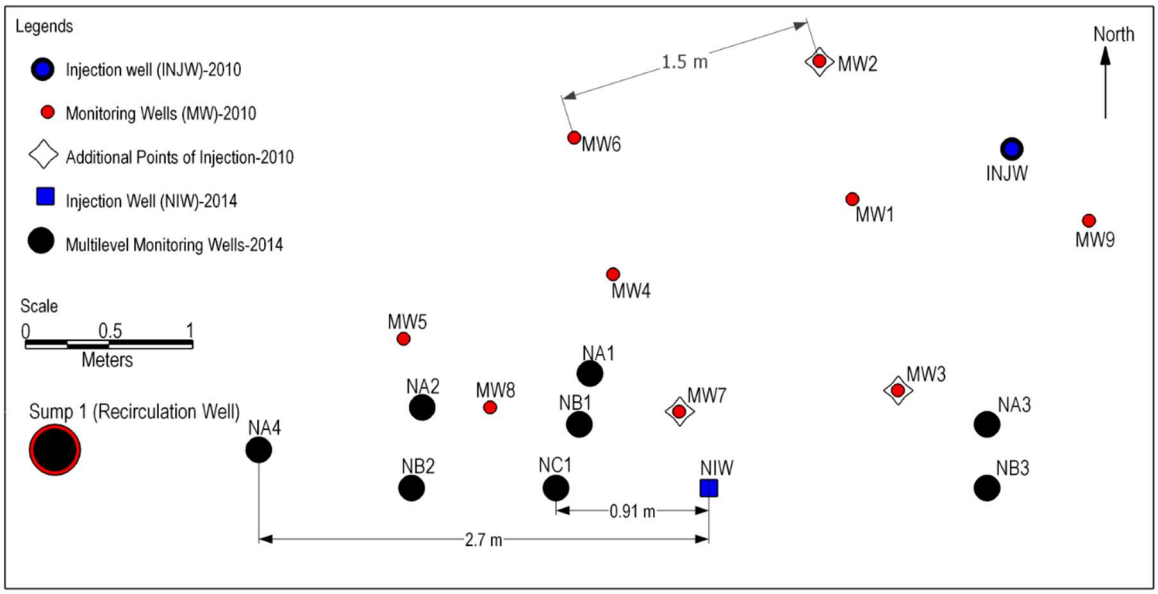

Figure B.3 Plan view of field site.

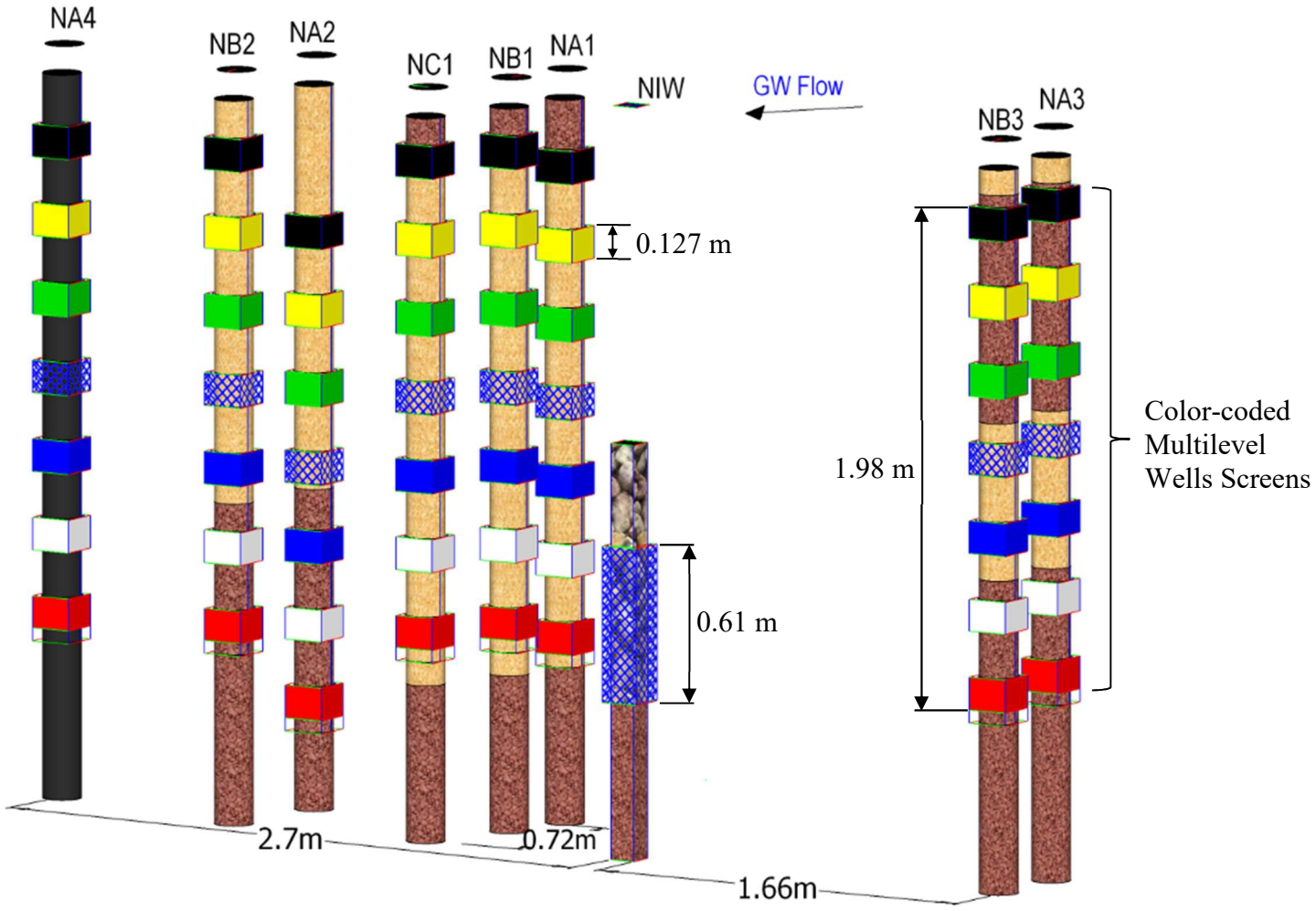

Figure B.4 Isometric view of field site.

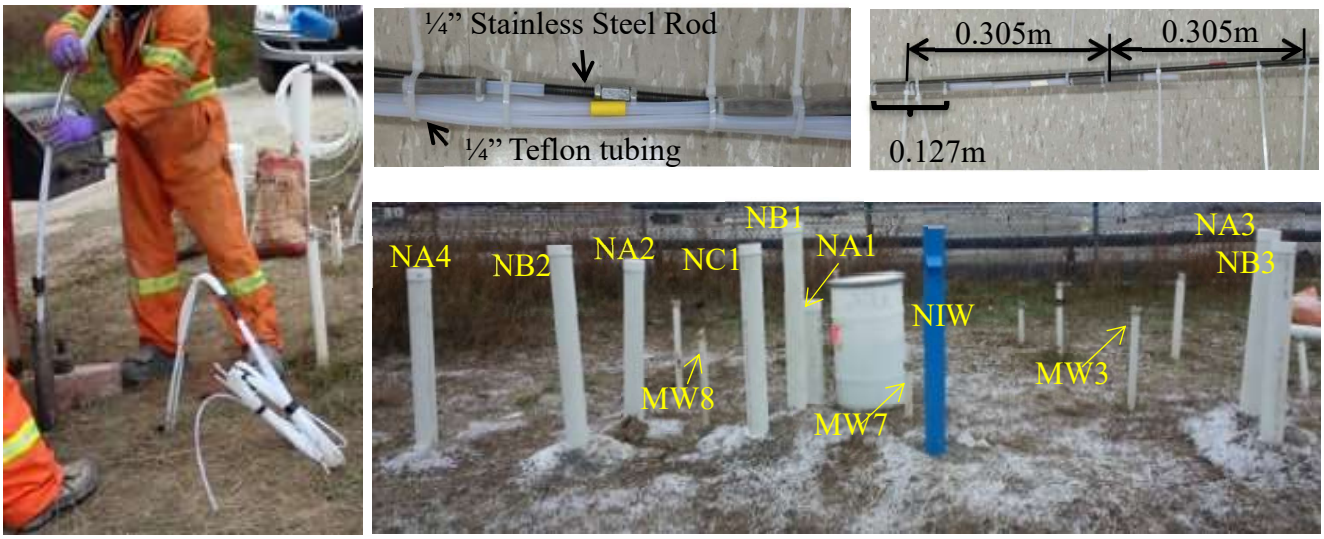

Figure B.5 Description and installation of Bundle Piezometers

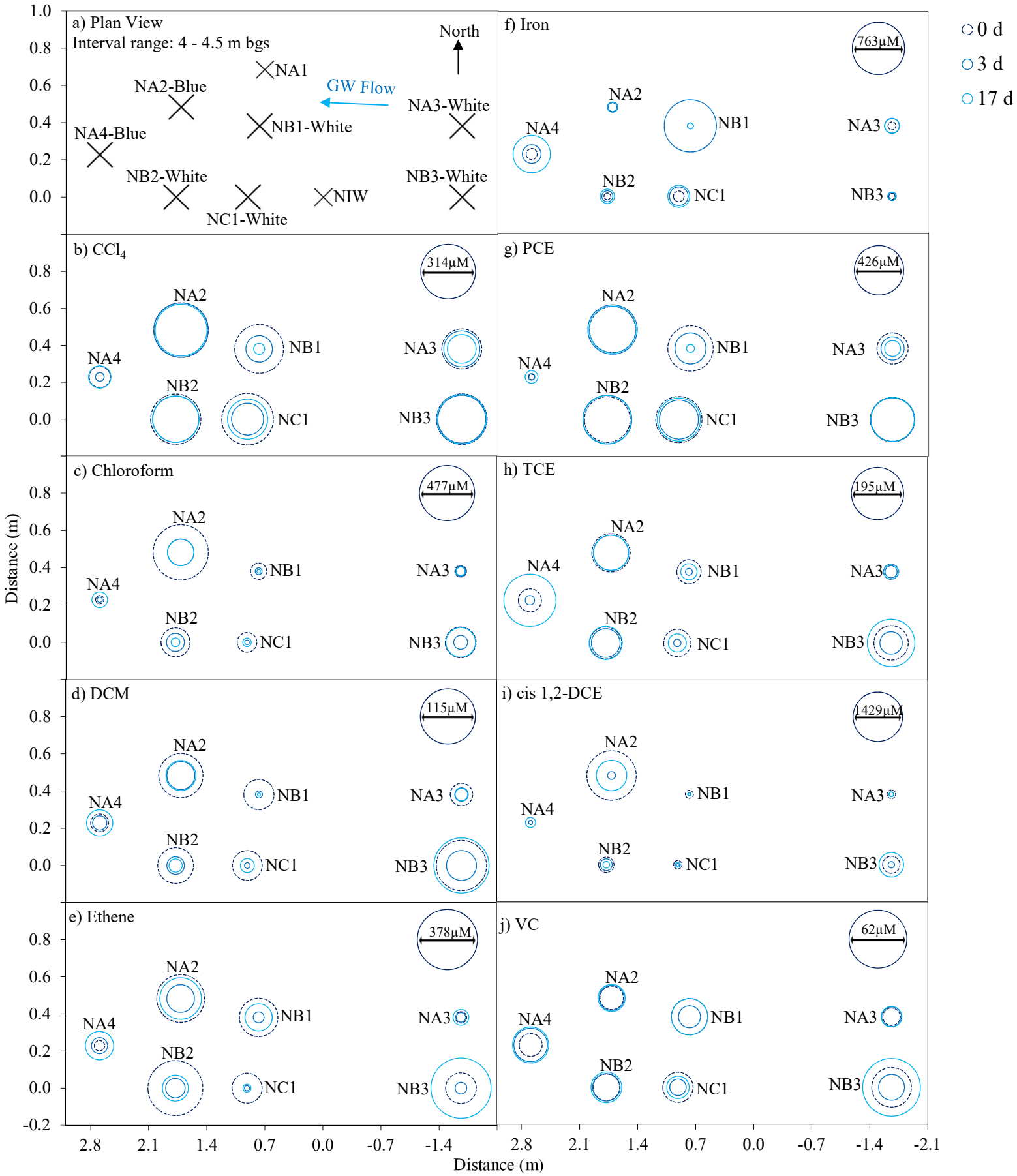

Figure B.6 f) Total iron and b – e & g – j) cVOCs concentrations for background (○) and post-injection samples at 3 days (○) and 17 days (○) after injection. (a) Plan view is shown as reference. No data available for NA1 and NIW. Upper right circle represents the maximum concentration between all three sampling times for the selected compound. Changes in concentration are illustrated by the changes in diameter in each location.

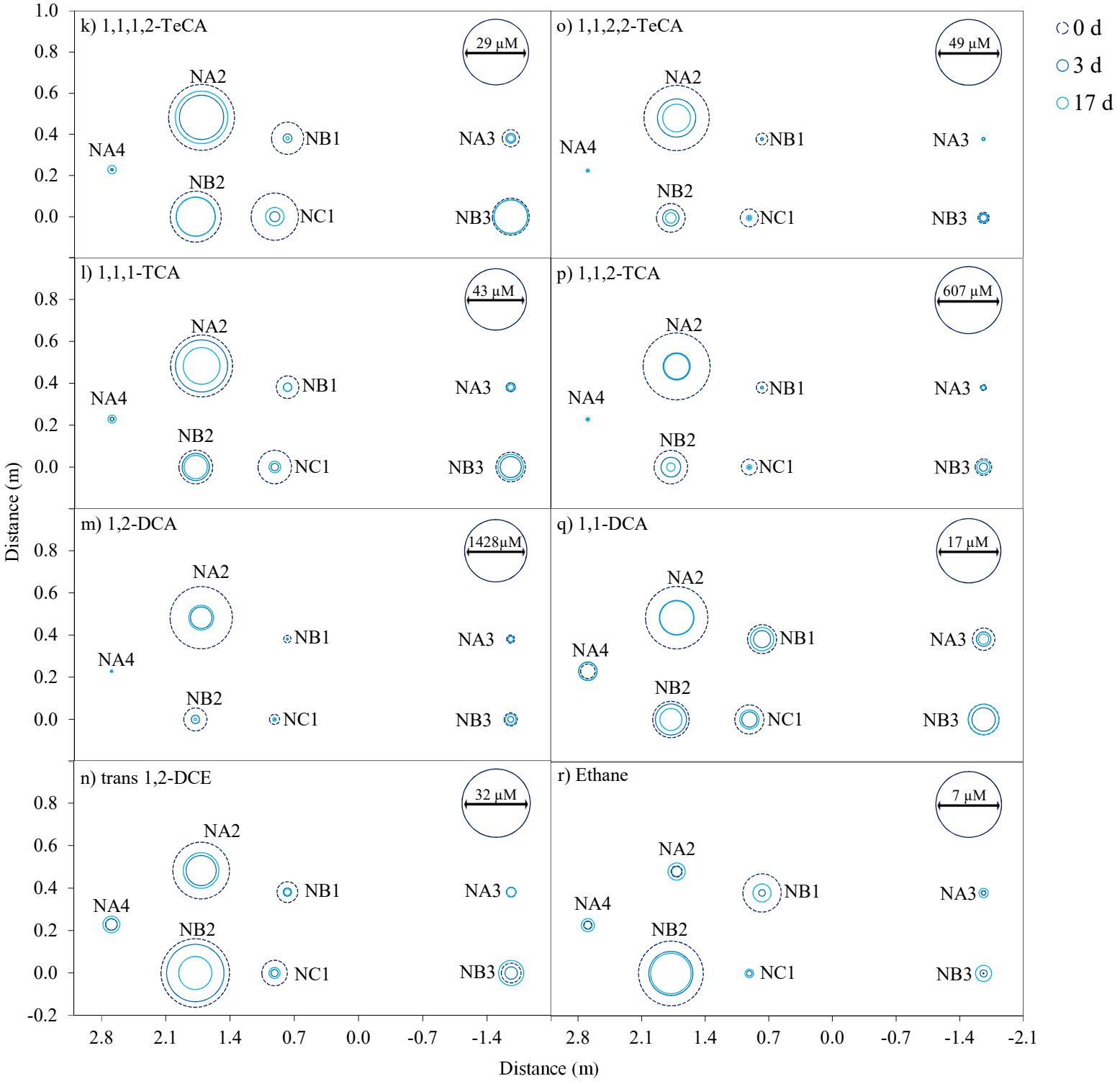

Figure B.6. Continuation: k – r) cVOCs concentrations for background (○) and post-injection samples at 3 days (○) and 17 days (○) after injection. Upper right circle represents the maximum concentration between all three sampling times for the selected compound. Changes in concentration are illustrated by the changes in diameter in each location.

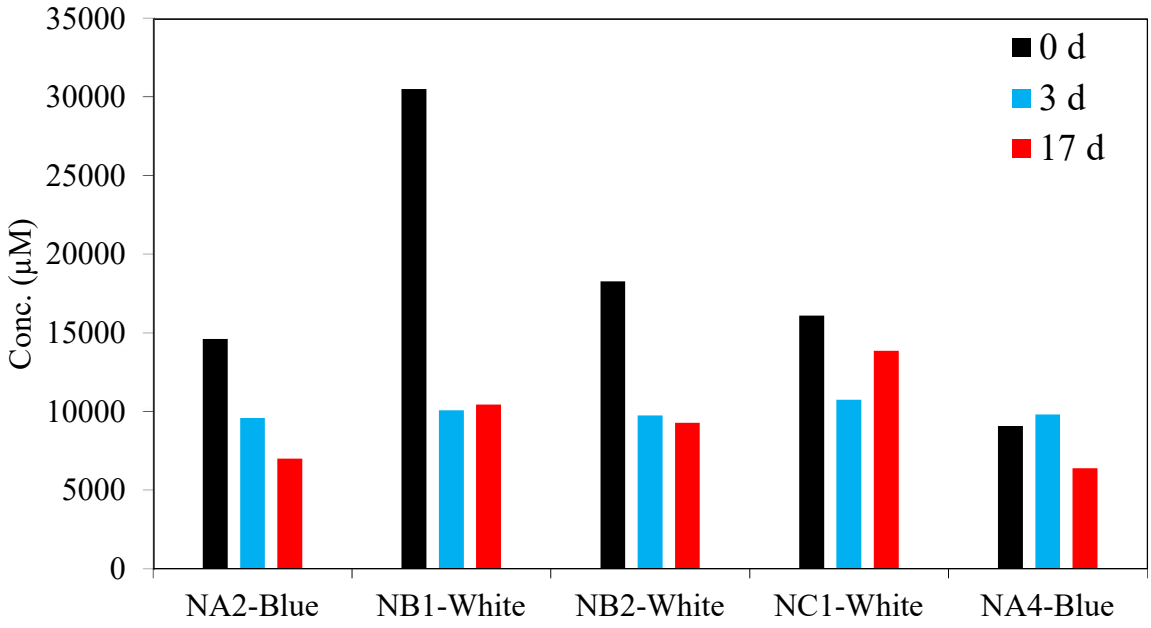

Figure B.7 Chloride concentrations at 3 and 17 days after injection.

Table B.1 Chloride mass balance.

		NB1-Black				NB1-Yellow			
Compound (µM)	**# Chloride***	**Conc. at day 0 (µM) (C_0)**	**Conc. at day 3 (µM) (C_3)**	**Change (C_3 - C_0)**	**Moles of Chloride**	**Conc. at day 0 (µM) (C_0)**	**Conc. at day 3 (µM) (C_3)**	**Change (C_3 - C_0)**	**Moles of Chloride**
PCE	0	374.2	272.5	-101.8	N/A	371.6	363.5	-8.1	N/A
1,1,1,2-TeCA	0	10.0	5.1	-4.9	N/A	8.2	7.9	-0.3	N/A
1,1,2,2-TeCA	0	4.4	2.3	-2.2	N/A	3.4	3.3	-0.1	N/A
TCE	1	52.5	45.5	-7.0	N/A	51.0	55.5	4.4	4.4
1,1,2-TCA	1	33.9	36.2	2.3	2.3	26.0	50.7	24.7	24.7
1,1,1-TCA	1	10.8	6.4	-4.4	N/A	8.3	8.5	0.3	0.3
cis 1,2-DCE	2	70.6	168.8	98.2	196.3	51.6	298.1	246.4	492.9
trans 1,2-DCE	2	4.6	8.8	4.2	8.4	3.1	13.9	10.8	21.6
1,1-DCE	2	0.4	0.4	0.04	0.1	0.2	0.5	0.3	0.5
1,1-DCA	2	2.5	5.0	2.5	5.0	1.9	4.4	2.5	5.1
1,2-DCA	2	30.0	58.9	28.9	57.8	22.4	55.4	33.0	66.0
VC	3	23.6	28.7	5.0	15.1	13.0	27.3	14.3	42.8
Chloroethane	3	0.0	0.2	0.2	0.7	0.0	0.2	0.2	0.7
Ethene	4	97.0	145.1	48.1	192.5	53.0	136.4	83.4	333.7
Ethane	4	2.6	2.2	-0.4	N/A	1.6	4.7	3.0	12.2
CCl_4	0	254.5	165.9	-88.6	N/A	244.1	226.1	-18.0	N/A
Chloroform	1	43.7	61.6	17.9	17.9	39.4	72.2	32.8	32.8
DCM	2	5.9	28.0	22.2	44.4	3.1	18.6	15.5	30.9
Chloride (Cl^-)	N/A	7384.5	11930.3	**4545.8**	↓	6596.5	13592.0	**6995.5**	↓
Sum Cl^- released	N/A	N/A	N/A	N/A	**540.4**	N/A	N/A	N/A	**1068.6**
% Cl^- accounted	N/A				**11.9%**				**15.3%**

*Assuming Cl^- release based on the generation of daughter products from the dechlorination of parent compounds

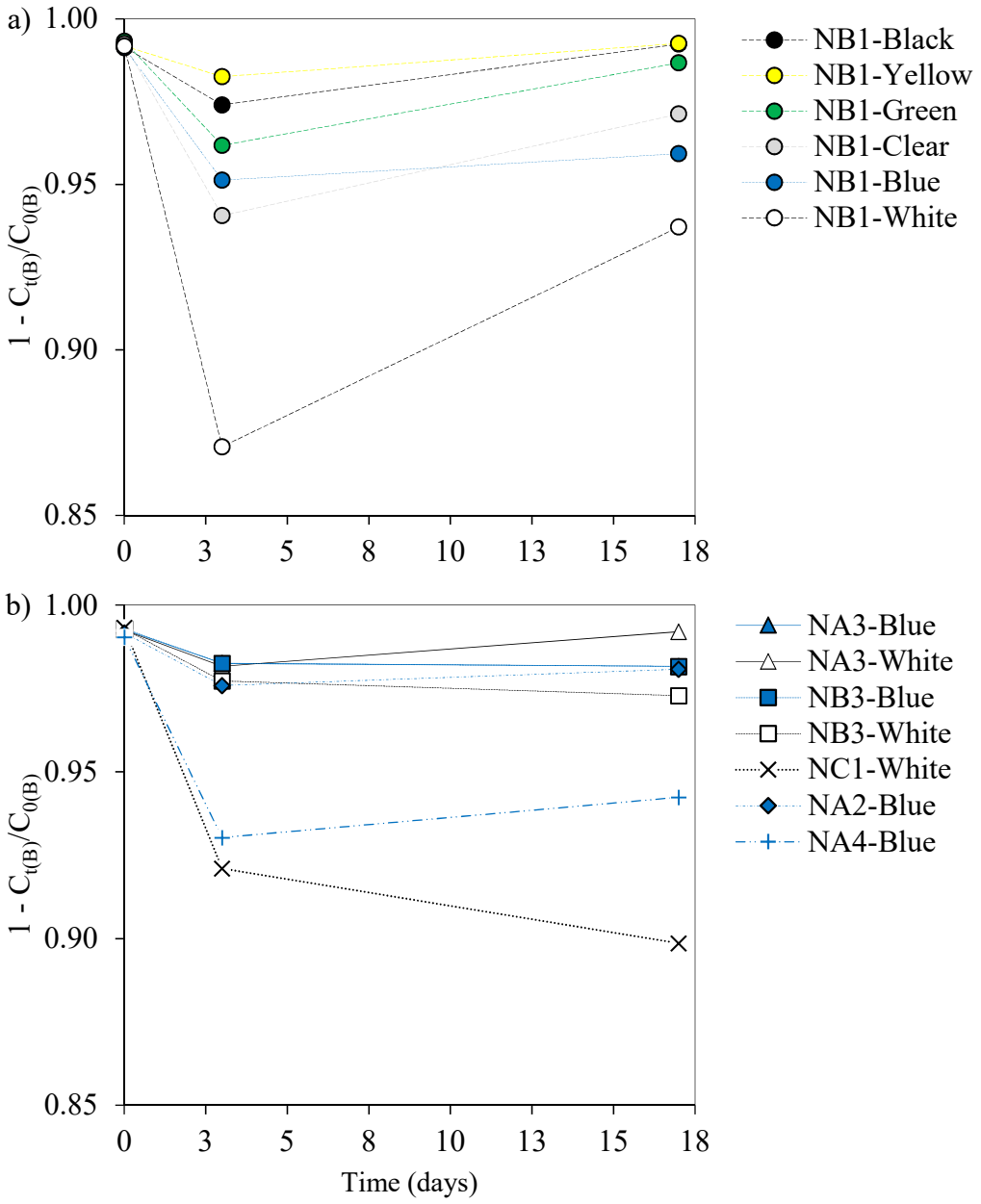

Figure B.8 Estimation of the dilution effect following injection of S-nZVI in a) NB1 and b) NA3-Blue, NA3-White, NB3-Blue, NB3-White, NC1-White, NA2-Blue, and NA4-Blue. Background boron concentrations were on average 300 ± 34 µM, yielding an initial value of 0.99.

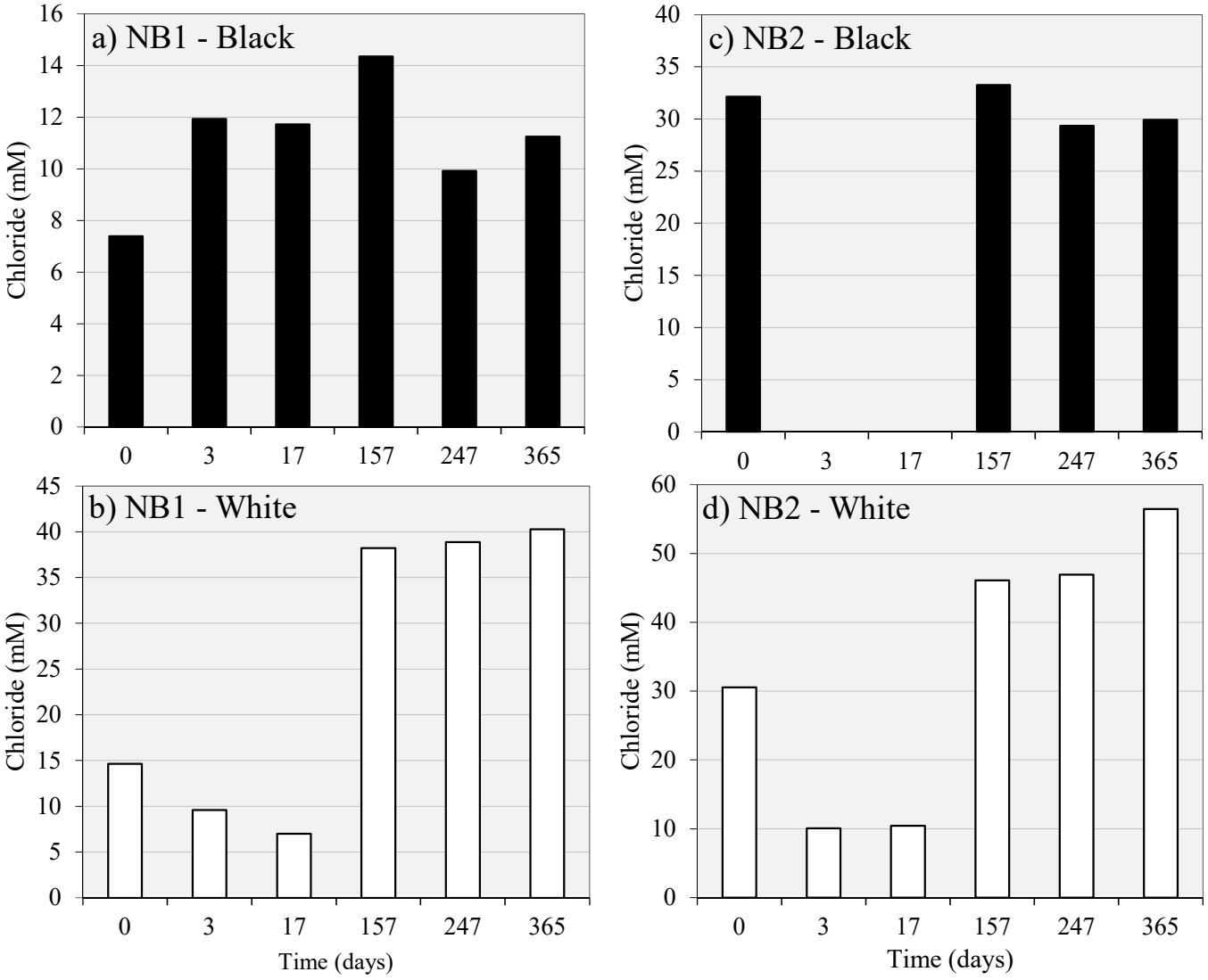

Figure B.9 Long-term chloride concentration for a) NB1-Black, b) NB1-White, c) NB2-Black and d) NB2-White.

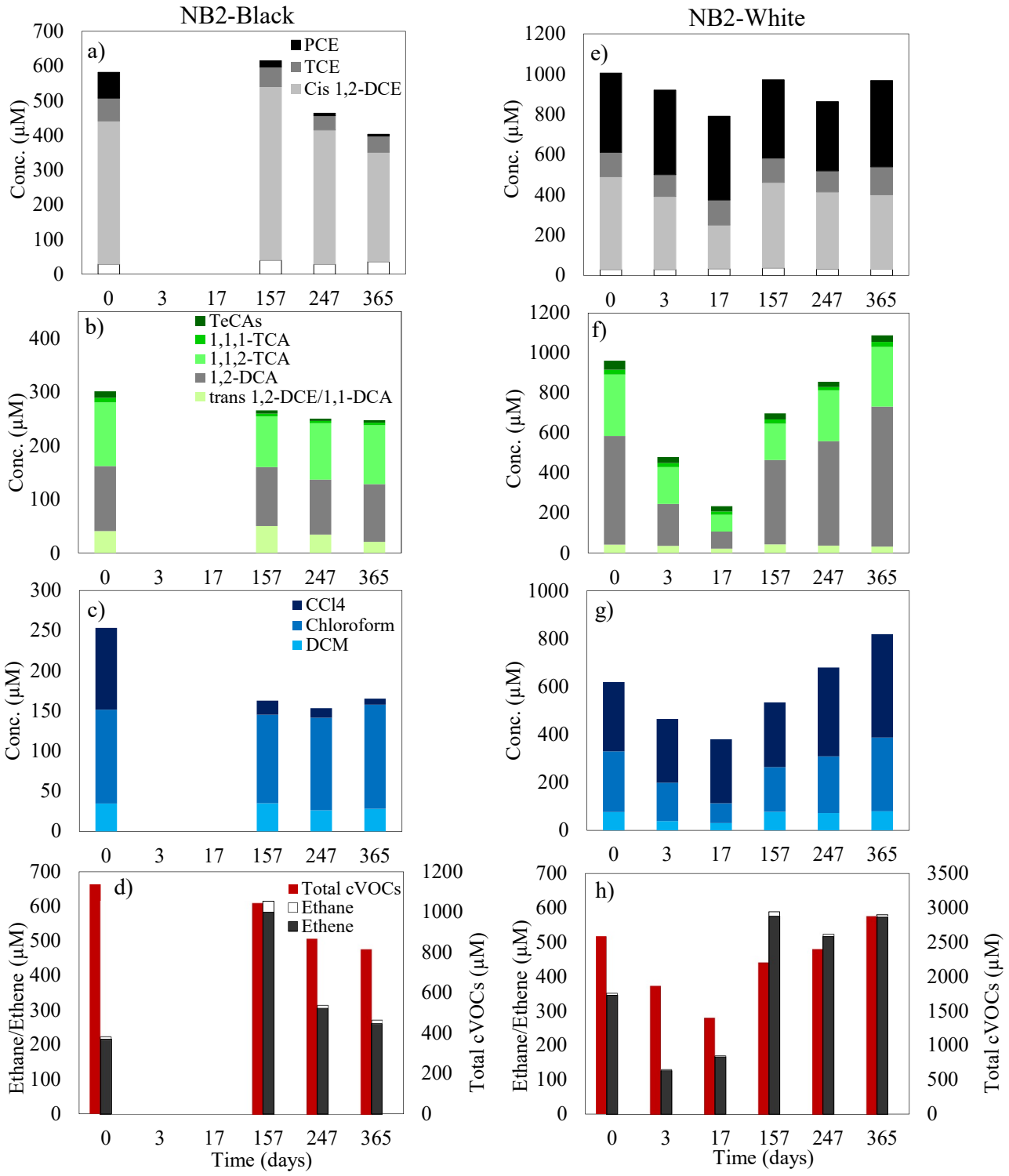

Figure B.10 Background and Long – term post-injection concentrations for a – d) NB2-Black and e – h) NB2-White. No data available for NB2-White at 3 and 17 days.

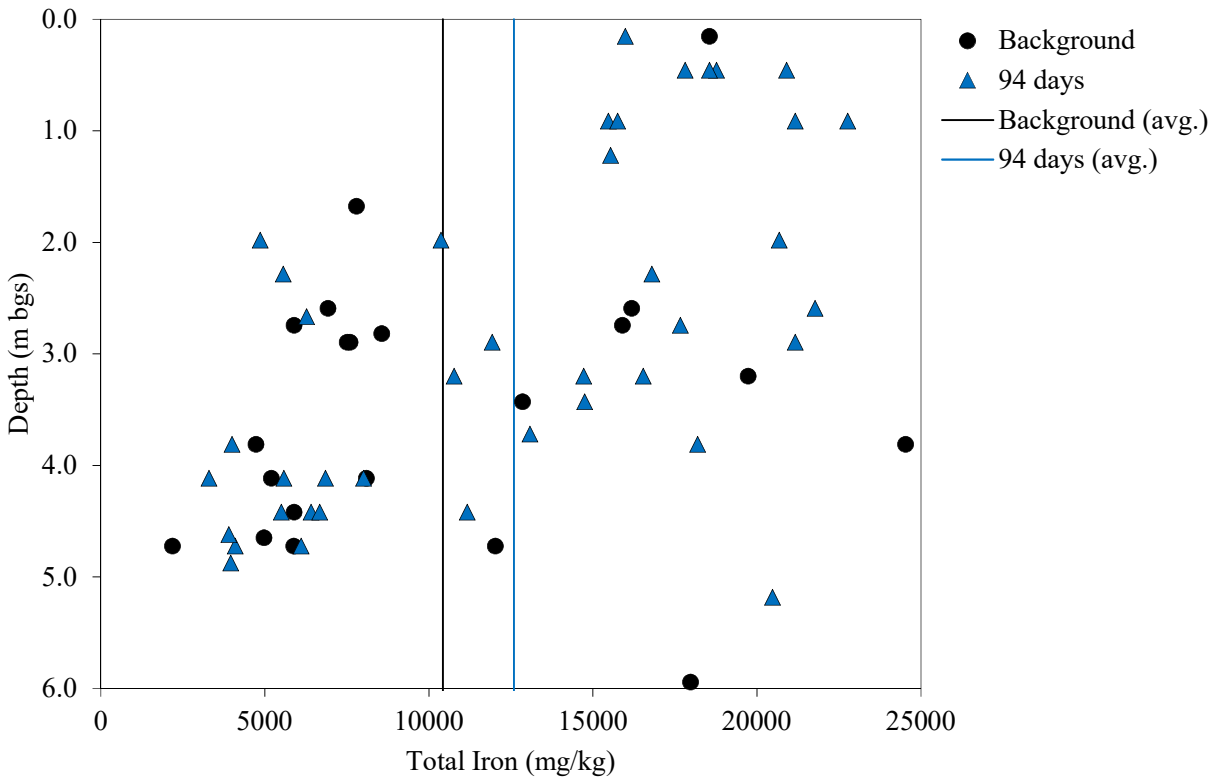

Figure B.11 Changes in concentration of total iron in soil.

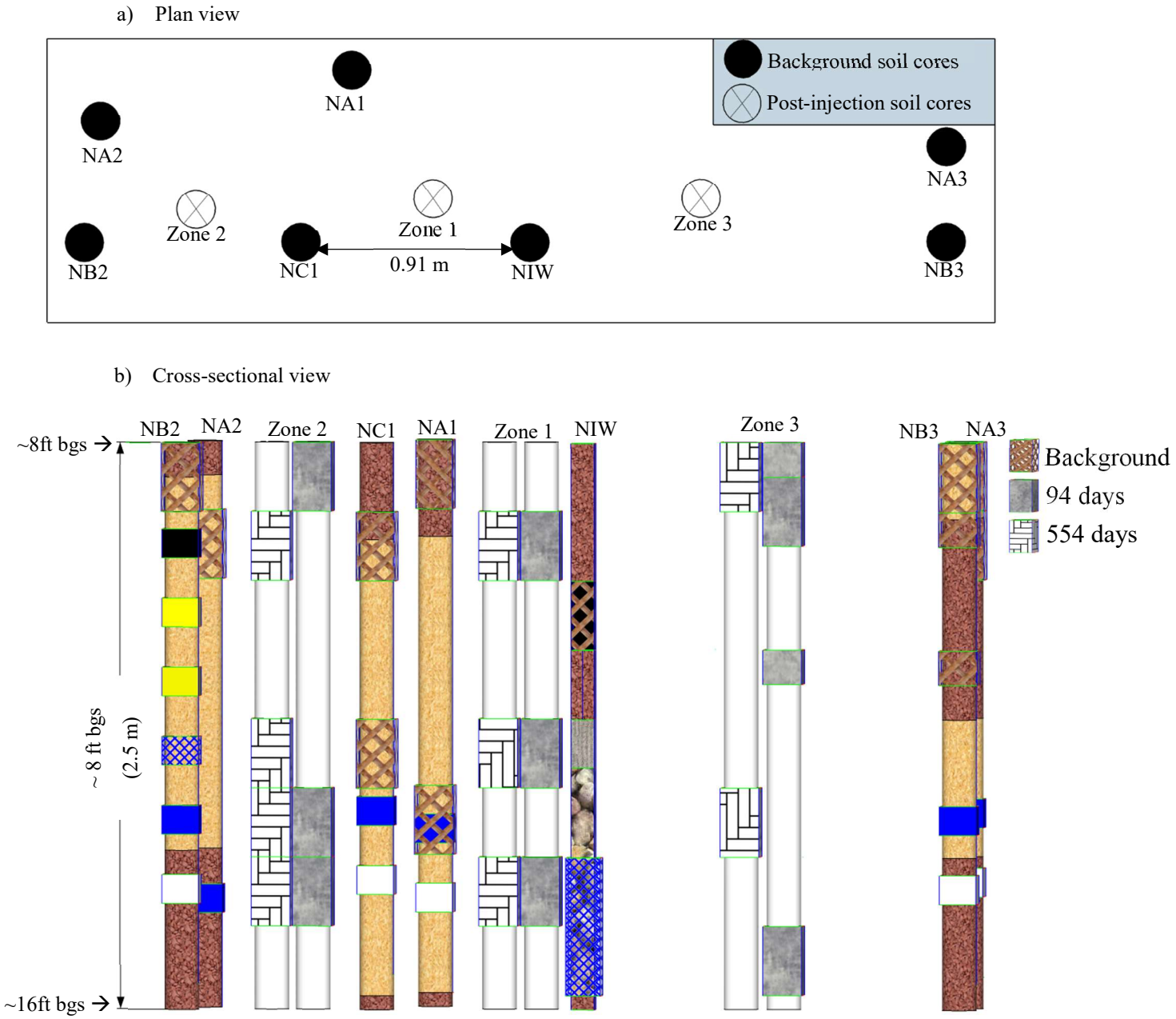

Figure B.12 Locations of a) boreholes and b) depths of soil samples for cVOCs analysis.

Table B.2. Summary of cVOCs concentrations in soil samples presented as µmol/kg of dry soil.

Time	Location	Interval (ft bgs) Top Depth	Interval (ft bgs) Bottom Depth	Approximate Depth (m bgs)	Concentrations (µmol/kg) PCE	TCE	cis 1,2-DCE	CCl_4	Chloroform	DCM	1,1,1,2-TeCA	1,1,2,2-TeCA	1,1,2-TCA	1,1,1-TCA
Background	NIW	10	11	3.2	18.8	62.1	111.7	3.7	286.3	265.0	419.6	6.5	30.1	18.6
	NA1	8	9	2.6	47.2	144.1	92.3	5.0	1312.4	371.6	876.9	11.5	15.0	61.7
	NA1	13	14	4.0	118.4	117.4	281.6	18.8	859.2	292.6	326.6	4.5	34.1	39.5
	NC1	9	10	3.0	51.2	65.8	537.9	11.9	555.9	187.1	269.5	4.9	14.9	24.7
	NC1	12	13	4.0	6.3	8.7	108.9	4.1	27.1	280.5	54.5	1.6	16.3	2.5
	NA2	10	11	3.1	23.5	41.5	171.8	6.2	1980.1	280.2	523.7	4.7	13.7	79.6
	NB2	8	9	2.7	24.6	61.8	347.1	7.0	9.8	302.5	39.5	2.6	33.2	5.8
	NA3	9	10	2.9	142.0	128.5	265.6	27.2	38.4	278.0	136.1	3.7	24.9	8.9
	NB3	8	9	2.7	98.3	74.9	341.4	3.1	377.7	161.1	141.0	2.3	10.8	18.1
	NB3	9	10	3.0	124.8	124.8	149.6	5.7	171.4	250.7	33.7	2.3	15.2	8.8
	NB3	11	12	3.6	29.2	165.3	171.1	3.6	73.4	263.3	85.2	1.9	35.4	9.1
94 days	Zone 1	9	10	3.0	153.4	55.0	ND	8.8	11.6	ND	6.9	ND	23.4	3.1
	Zone 1	12	13	4.0	166.9	43.5	410.4	23.3	32.8	ND	3.5	0.4	18.6	3.2
	Zone 1	14	15	4.6	274.8	29.0	135.8	20.9	16.7	ND	4.3	0.5	13.8	1.8
	Zone 2	8	9	2.7	292.7	254.3	154.6	42.7	116.1	21.3	28.4	7.4	171.0	15.9
	Zone 2	13	14	4.2	35.5	11.3	ND	2.5	6.3	ND	3.9	0.6	13.3	0.9
	Zone 2	14	15	4.5	1759.4	43.9	ND	298.6	76.4	6.5	18.7	8.8	52.8	10.3
	Zone 3	9	10	2.8	152.3	37.3	ND	13.1	5.9	ND	8.3	ND	7.2	2.5
	Zone 3	11	12	3.6	332.1	142.4	22.4	9.6	45.3	ND	1.8	ND	44.9	7.8
	Zone 3	15	16	4.9	43.3	19.8	ND	14.7	16.2	8.6	6.2	0.4	17.2	1.7
554 days	Zone 1	9	10	3.0	332.2	99.1	40.0	13.7	35.6	ND	4.1	2.9	18.2	3.5
	Zone 1	12	13	4.0	19.1	5.8	7.3	2.0	5.0	ND	0.3	ND	2.4	0.4
	Zone 1	14	15	4.6	19.0	4.8	6.5	2.1	4.1	ND	ND	ND	ND	0.4
	Zone 2	9	10	3.0	3.2	1.7	17.1	1.7	9.3	ND	0.6	ND	13.4	0.6
	Zone 2	13	14	4.2	4.0	4.0	28.4	0.9	11.9	2.1	0.6	0.2	17.1	0.6
	Zone 2	14	15	4.5	2.7	3.7	19.5	0.8	10.6	0.9	0.6	ND	15.8	0.7
	Zone 3	8	9	2.7	68.9	18.8	5.0	0.2	3.6	ND	0.9	0.2	5.4	1.2
	Zone 3	13	14	4.3	11.2	29.4	10.8	4.8	13.7	1.6	1.0	1.1	16.7	0.8

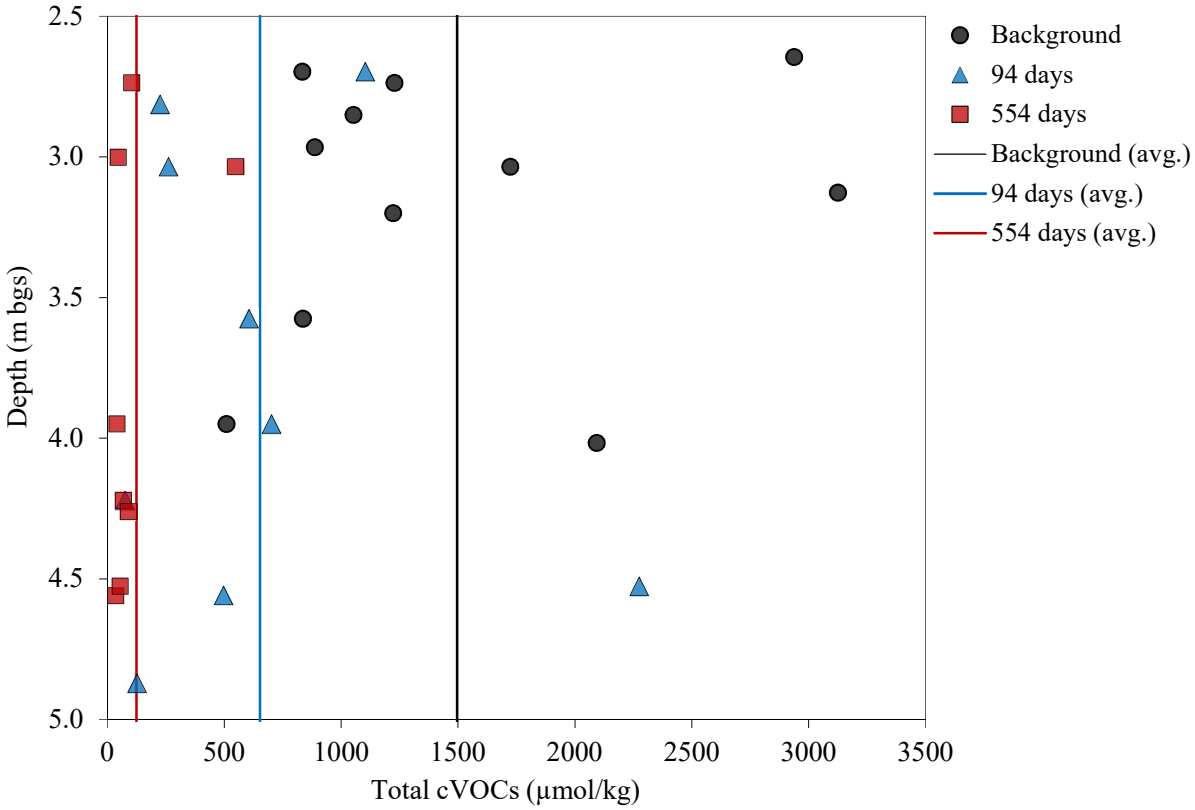

Figure B.13 Changes in concentrations of total cVOCs in soil.

Table B.3 Pearson Correlations (r) among soil cVOCs.

		Chloroform	1,1,1-TCA	CCl4	TCE	1,1,2-TCA	PCE	1,1,1,2-TeCA	1,1,2,2-TeCA
Background (n = 11)	**Chloroform**	***1.000***	0.994	-0.071	-0.068	-0.367	-0.140	0.791	0.577
	1,1,1-TCA	0.994	***1.000***	-0.044	0.001	-0.312	-0.131	0.842	0.648
	CCl4	-0.071	-0.044	***1.000***	0.266	0.249	0.656	-0.086	-0.005
	TCE	-0.068	0.001	0.266	***1.000***	0.327	0.502	0.132	0.230
	1,1,2-TCA	-0.367	-0.312	0.249	0.327	***1.000***	-0.067	-0.226	-0.144
	PCE	-0.140	-0.131	0.656	0.502	-0.067	***1.000***	-0.199	-0.120
	1,1,1,2-TeCA	0.791	0.842	-0.086	0.132	-0.226	-0.199	***1.000***	0.944
	1,1,2,2-TeCA	0.577	0.648	-0.005	0.230	-0.144	-0.120	0.944	***1.000***
94 days (n = 9)	**Chloroform**	***1.000***	0.978	0.491	0.818	0.925	0.499	0.862	0.895
	1,1,1-TCA	0.978	***1.000***	0.454	0.870	0.929	0.481	0.855	0.908
	CCl4	0.491	0.454	***1.000***	-0.042	0.188	0.986	0.499	0.776
	TCE	0.818	0.870	-0.042	***1.000***	0.924	0.007	0.659	0.601
	1,1,2-TCA	0.925	0.929	0.188	0.924	***1.000***	0.188	0.870	0.726
	PCE	0.499	0.481	0.986	0.007	0.188	***1.000***	0.455	0.773
	1,1,1,2-TeCA	0.862	0.855	0.499	0.659	0.870	0.455	***1.000***	0.912
	1,1,2,2-TeCA	0.895	0.908	0.776	0.601	0.726	0.773	0.912	***1.000***
554 days (n = 8)	**Chloroform**	***1.000***	0.901	0.934	0.915	0.657	0.868	0.943	0.965
	1,1,1-TCA	0.901	***1.000***	0.899	0.971	0.370	0.982	0.991	0.904
	CCl4	0.934	0.899	***1.000***	0.961	0.447	0.911	0.950	1.000
	TCE	0.915	0.971	0.961	***1.000***	0.377	0.962	0.983	0.975
	1,1,2-TCA	0.657	0.370	0.447	0.377	***1.000***	0.264	0.435	0.570
	PCE	0.868	0.982	0.911	0.962	0.264	***1.000***	0.981	0.891
	1,1,1,2-TeCA	0.943	0.991	0.950	0.983	0.435	0.981	***1.000***	0.953
	1,1,2,2-TeCA	0.965	0.904	1.000	0.975	0.570	0.891	0.953	***1.000***

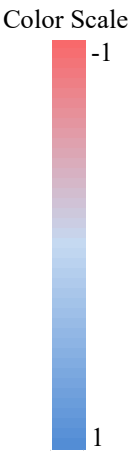

References

1. Einarson, M. D., Multilevel ground-water monitoring. In Practical Handbook of Environmental Site Characterization and Ground-Water Monitoring, Nielsen, D. M., Ed. CRC Press: Boca Raton, FL, 2006; pp 808-848.

2. Cherry, J. A.; Gillham, R. W.; Anderson, E. G.; Johnson, P. E., Migration of contaminants in groundwater at a landfill: A case study: 2. Groundwater monitoring devices. Journal of Hydrology 1983, 63, (1), 31-49.

3. Elsner, M., Stable isotope fractionation to investigate natural transformation mechanisms of organic contaminants: principles, prospects and limitations. J Environ Monitor 2010, 12, (11), 2005-2031.

4. Elsner, M.; McKelvie, J.; Lacrampe Couloume, G.; Sherwood Lollar, B., Insight into Methyl tert-Butyl Ether (MTBE) Stable Isotope Fractionation from Abiotic Reference Experiments. Environ Sci Technol 2007, 41, (16), 5693-5700.

Appendix C

Analysis of Model Pollutants

GC Method Details

For TCE and CF analysis the GC is an Agilent 7890B. The inlet was set at 250 °C and 14.4 psi. The flow was 24 mL min^{-1}, with a septum purge flow of 3 mL min^{-1} and a split ratio of 5:1. The column is an Agilent DB-1 (30 m, 0.32 mm diameter, 1 μm film), set at a flow of 3.5 mL min^{-1}, 14.361 psi and an average velocity of 50 cm s^{-1}. The temperature ramp is as follow: initial temperature 40°C (0.2 min hold), increase at 5°C min^{-1} until 60°C and hold for 0.1 min. Total time is 4.3 min. The FID detector temperature was 200°C, air flow 200 mL min^{-1}, H_2 flow (for flame) 15 mL min^{-1}, make-up/N_2 flow 16 mL min^{-1}. A six-point calibration developed with this method was used for the kinetic analysis.

Calculation of kinetic constants

Results were fitted using a pseudo first order kinetic model (Eq. C.1).

$$C = C_0 e^{-k_{obs}\, t} \tag{C.1}$$

where C and C_0 are the concentrations (mg L^{-1}) at time t_x and time t_0, respectively, k_{obs} is the observed rate constant (h^{-1}), and t is the time (h). The concentrations of the test vessels measured during the first 5 hours were discarded for the analysis because headspace/water equilibrium was not considered to be reached. For this reason, the initial concentration of the controls at t = 5 hours was chosen as the C_0 for all four vessels during each experiment (except for the CMC S-nZVI aged for two weeks, where the C_0 was taken from the control at 48 hours due to lack of data in the early hours of the experiment).

TCE losses ranging between 14% and 17% were observed in the controls of some experiments. To account for possible losses in the TCE concentration due to adsorption to the reactor walls or volatilization through the septa, Eq. C.2 was employed when calculating the reaction rates.

$$\frac{C}{C_0} = \frac{C_{t-x}}{C_{0-x}} + \left(1 - \frac{C_{t-c}}{C_{0-x}}\right) \quad \text{(C.2)}$$

where $C_{0\text{-}x}$ is the initial concentration of test vessels, $C_{t\text{-}x}$ is the concentration at time t_x, $C_{0\text{-}c}$ is the initial concentration of the controls and $C_{t\text{-}c}$ the concentration at time t_x of the controls. k_{obs} values were calculated from the normalized concentrations (C/C_0) obtained from equation 2 with the aim to avoid overestimation of kinetic constants.

Characterization Methodology

Transmission Electron Microscopy (TEM) with Energy-dispersive X-ray Spectroscopy (EDS):

Add a droplet of an aqueous nZVI sample to a 200-mesh copper grid coated with formvar and carbon and leave to dry for 24hrs. To minimized exposure to air, samples were taken to the lab for analysis in a desiccator. 24 TEM images were taken of various locations within the grid, together with 21 EDS images. Elemental mapping was done for 1 sample.

Scanning Electron Microscopy (SEM):

Add a droplet of an aqueous sample of nZVI to a silicon wafer mount and leave to dry for 24hrs. Transport samples in a desiccator to minimized exposure to air.

X-ray Photoelectron Spectroscopy (XPS)

Extract a 10-20 ml sample of nZVI and add to polypropylene weighing pans. The pans are placed on a magnetic stirrer to aid in nZVI settlement. Excess water is removed, and sample is left to dry for 24 hours. After drying time has elapsed, crush the dried samples using a spatula in the weighing pans to create a powder. Mount the powder onto Indium foil mount. Remove the mounted sample from the glovebox and take to the lab for analysis in a desiccator for minimal air exposure.

X-ray Diffraction (XRD)

Extract a 10-20 ml sample of nZVI and add to polypropylene weighing pans. The pans are placed on a magnetic stirrer to aid in nZVI settlement. Excess water is removed and left to dry for ~24hrs.

After drying time has elapsed, crush the dried samples using a spatula in the weighing pans to create a powder. Mount the powder onto Kapton foils held in a metal ring. Remove the mounted sample from the glovebox and take to the lab for analysis in a desiccator for minimal air exposure.

Fe^0 content

A H_2 calibration curve was developed using pure H_2 and a GC-PDD equipped with a HP-MOLESIEVE column (inlet temperature 250 °C, detector 250 °C, oven 50 °C, 1.2 min hold, and column flow with He at 3 mL min^{-1}). Zerovalent iron (Fe^0) content was calculated from the number of moles of H_2 produced after acid digestion with HCl (Eq. C.3).

$$Fe^0 + 2H^+ \rightarrow Fe^{2+} + H_2 \uparrow \quad \text{(C.3)}$$

For the purposes of this study initial measurements (referred to as 'fresh') are those taken at 1 day and 4-days for CMC S-nZVI and S-nZVI, respectively. Aged samples were 12-days old. Fresh particles were rinsed with ethanol, dried and ~0.1g added to purged vessels while for aged samples particles were analyzed as wet slurries (50 ml). Upon acid digestion each of the 4 vessels were placed on a platform shaker and mix for 5 hours at 110 rpm.

Results

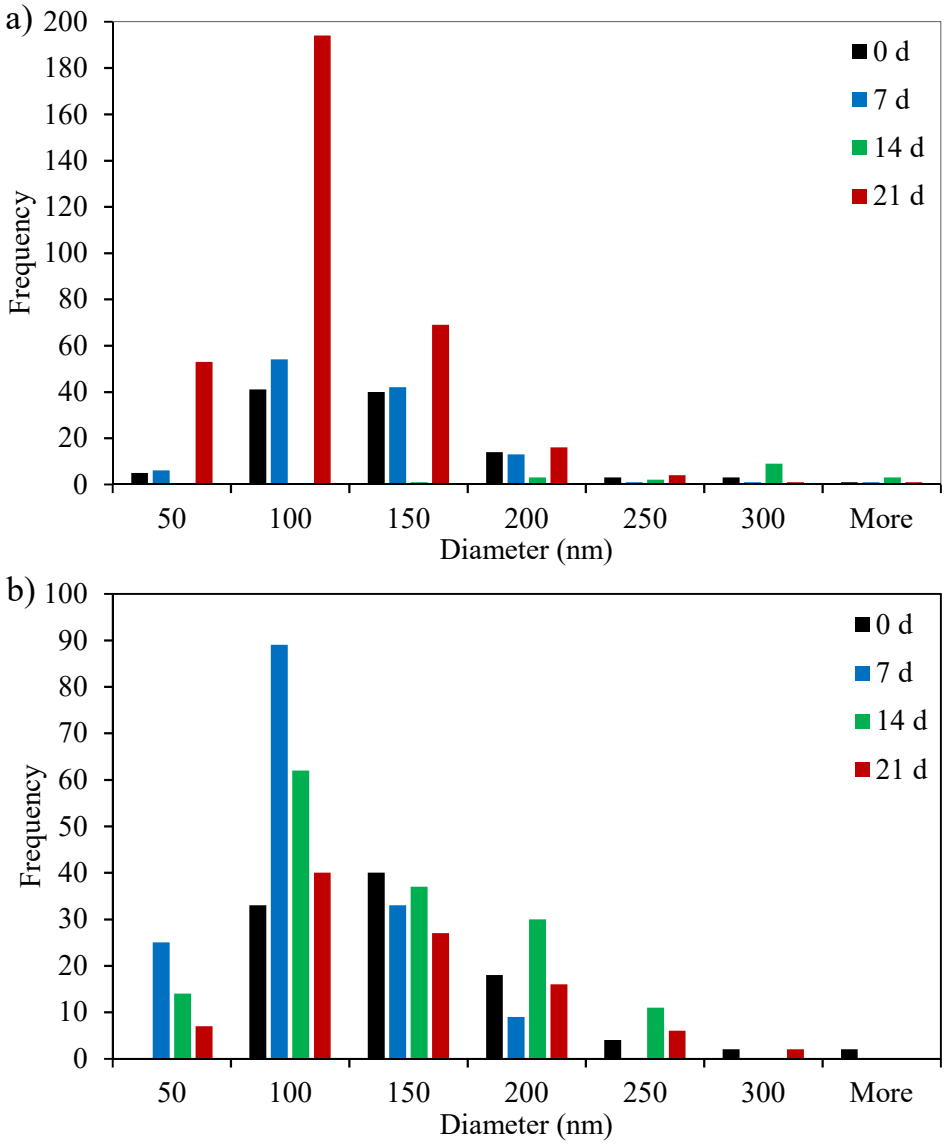

Figure C.1 Size distribution of a) S-nZVI and b) CMC S-nZVI during aging.

Table C.1 Properties of sulfidated nZVI.

ID	Time	Primary Particle Size	Hydrodynamic Diameter (nm)	$pH_{initial}$
S-nZVI	0 d	118.6 ± 50.6 (n = 108)	3816	7.37
	7 d	107.5 ± 49.9 (n = 119)	1430	8.34
	14 d	283.8 ± 135 (n = 19)	2259	8.28
	21 d	84.7 ± 41.5 (n = 339)	5059	8.54
CMC S-nZVI	0 d	130.4 ± 55.6 (n = 100)	2515	6.94
	7 d	83.7 ± 33.4 (n = 157)	N/A	7.91
	14 d	113.4 ± 54.5 (n = 106)	2859.33	8.26
	21 d	114.6 ± 52.7 (n = 148)	3310	8.40

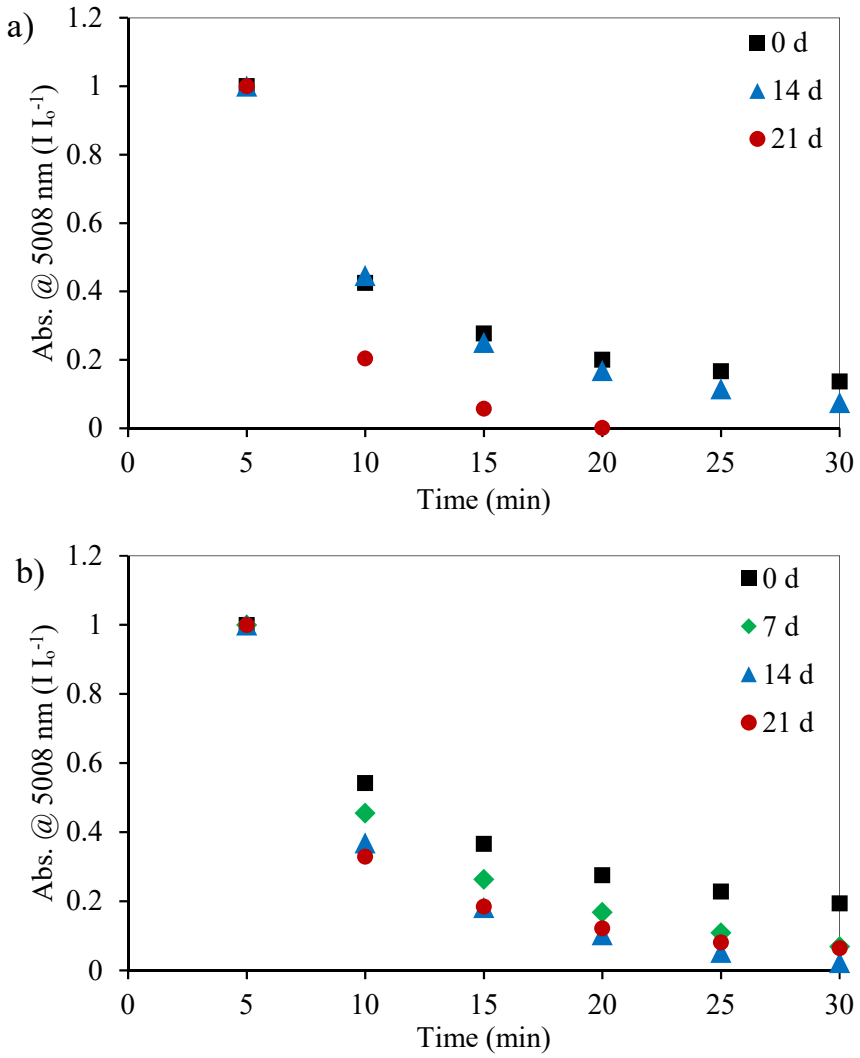

Figure C.2 Sedimentation curves for a) S-nZVI and b) CMC S-nZVI. Data not available for 7 d S-nZVI.

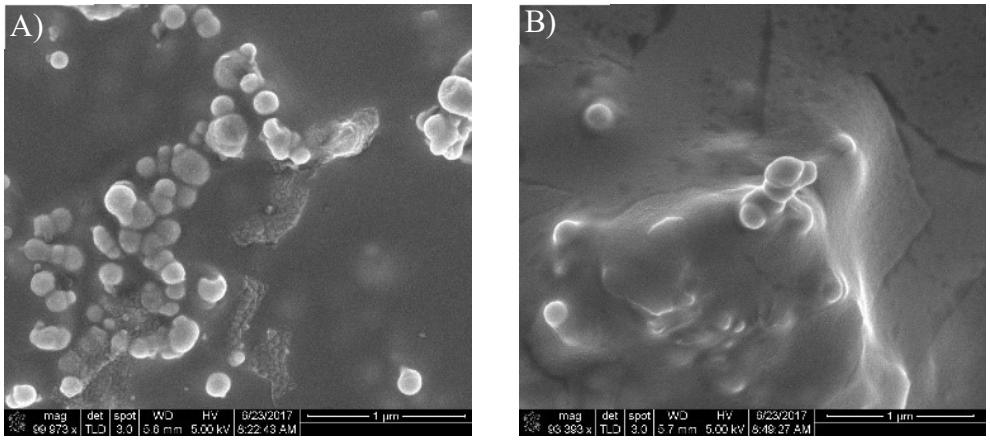

Figure C.3 SEM images of S-nZVI (A) and CMC S-nZVI (B) at 0 d.

Table C.2 S/Fe of spherical, cubic/laminar, and needle particles based on EDS spectra.

ID	Time	Spherical	Cubic/Laminar	Needle
S-nZVI	0 d	0.17	1.04	-
	7 d	0.54	1.17	-
	14 d	0.26	1.21	-
	21 d	0.60	1.21	1.00
CMC S-nZVI	0 d	0.07	1.02	-
	7 d	0.10	1.05	-
	14 d	0.06	1.15	-
	21 d	0.26	1.00	-

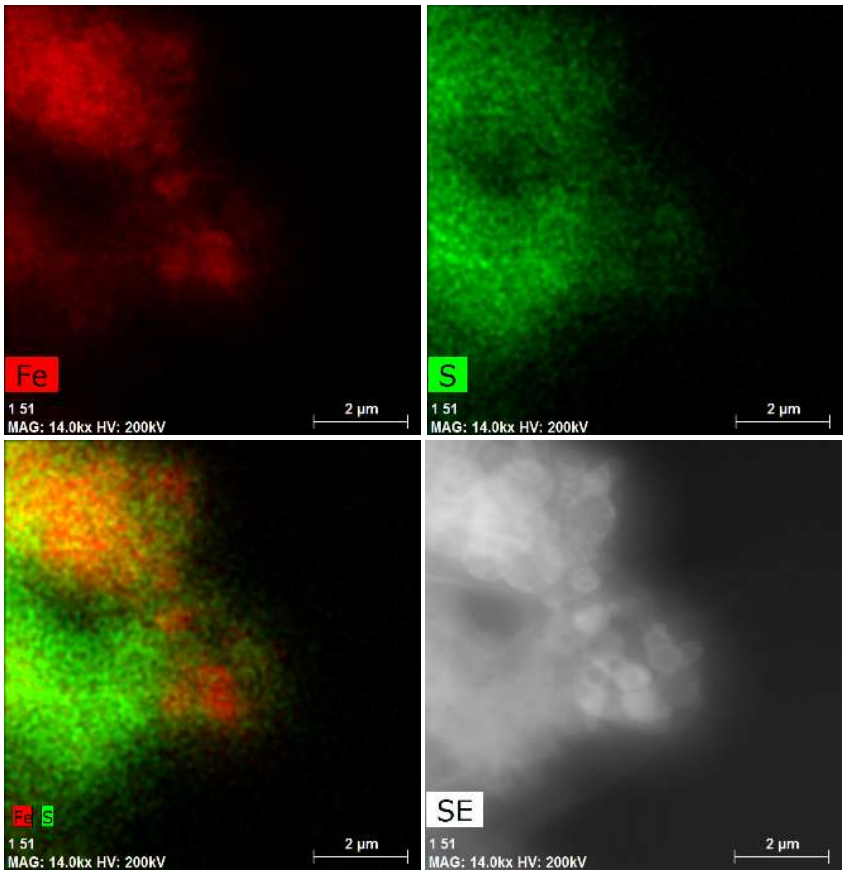

Figure C.4 Elemental mapping of S-nZVI at 21 d.

Table C.3 Chemical composition (in atomic %) of surface-bound elements from XPS analysis.

ID	Time	Fe 2p	S 2p	O 1s	B 1s	C 1s	F 1s	Na 1s
S-nZVI	0 d	15.19	17.1	31.4	15.7	11.6	0.33	8.57
	7 d	20.13	18.08	31.3	13.4	10.8	0.38	5.87
	14 d	18.63	14.92	47	6.81	7.76	0.43	4.45
	21 d	17.5	15.48	41	9.87	8.76	0.43	6.97
CMC S-nZVI	0 d	16.66	11.97	36.5	13.3	14.3	0.46	6.81
	7 d	15.05	12.12	37	12.2	14.3	0.38	8.94
	14 d	7.23	6.79	42.5	19	15.5	0.32	8.69
	21 d	12.12	11.78	44.2	10.5	11.9	0.38	9.14

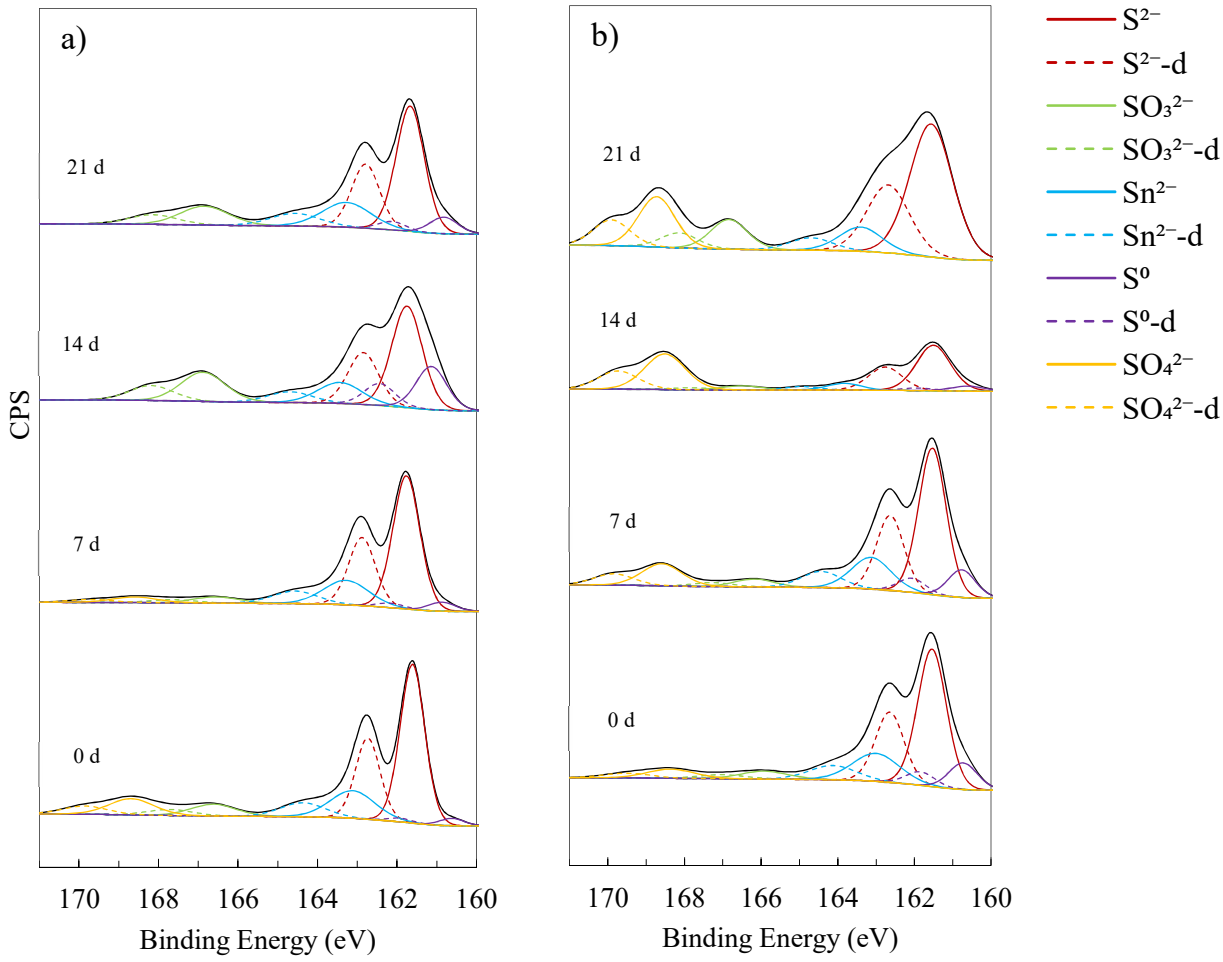

Figure C.5 High-resolution scan in the S 2p region for a) S-nZVI and b) CMC S-nZVI.

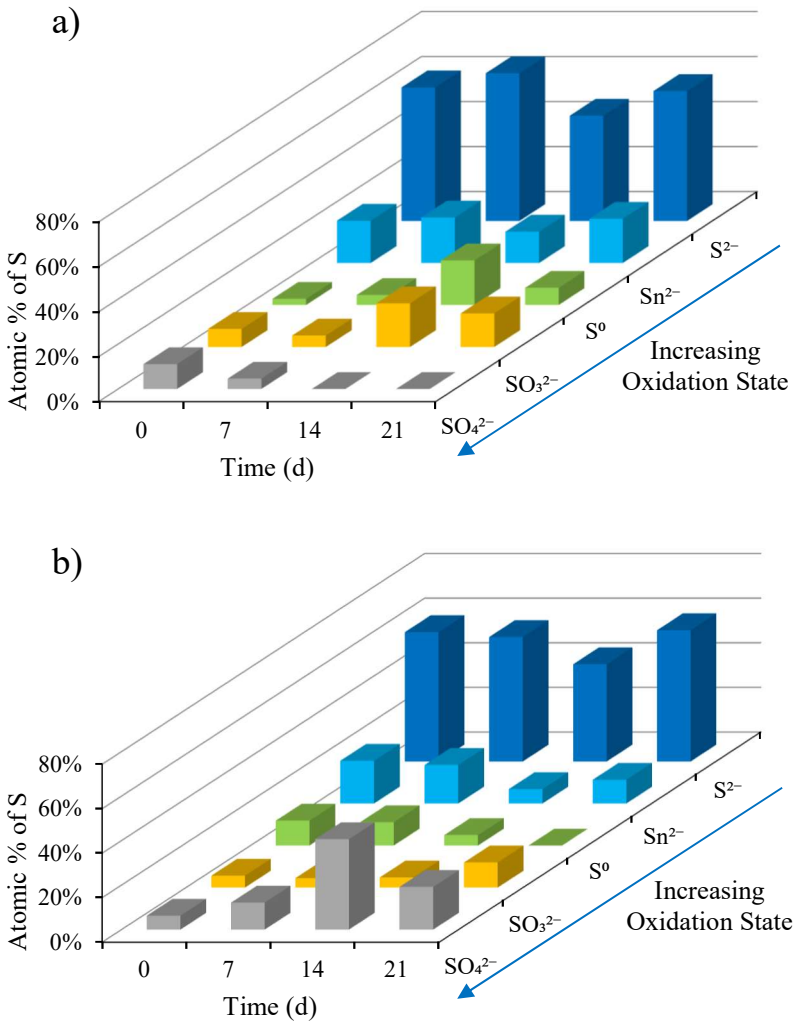

Figure C.6 Relative atomic abundance of sulfur species in a) S-nZVI and b) CMC S-nZVI (values are summarized in Table C.4).

Table C.4 Relative atomic abundance of sulfur.

ID	Element	0 d	7 d	14 d	21 d
S-nZVI	S^{2-}	59.4%	65.7%	46.8%	57.8%
	Sn^{2-}	18.8%	20.2%	13.9%	19.7%
	S^0	2.7%	4.4%	19.8%	7.6%
	SO_3^{2-}	8.0%	5.1%	19.4%	14.9%
	SO_4^{2-}	11.1%	4.6%	0.0%	0.0%
CMC S-nZVI	S^{2-}	58.0%	55.8%	43.6%	58.8%
	Sn^{2-}	19.2%	17.3%	6.5%	10.7%
	S^0	11.2%	10.5%	4.7%	0.0%
	SO_3^{2-}	5.3%	4.3%	4.6%	11.3%
	SO_4^{2-}	6.3%	12.1%	40.6%	19.2%

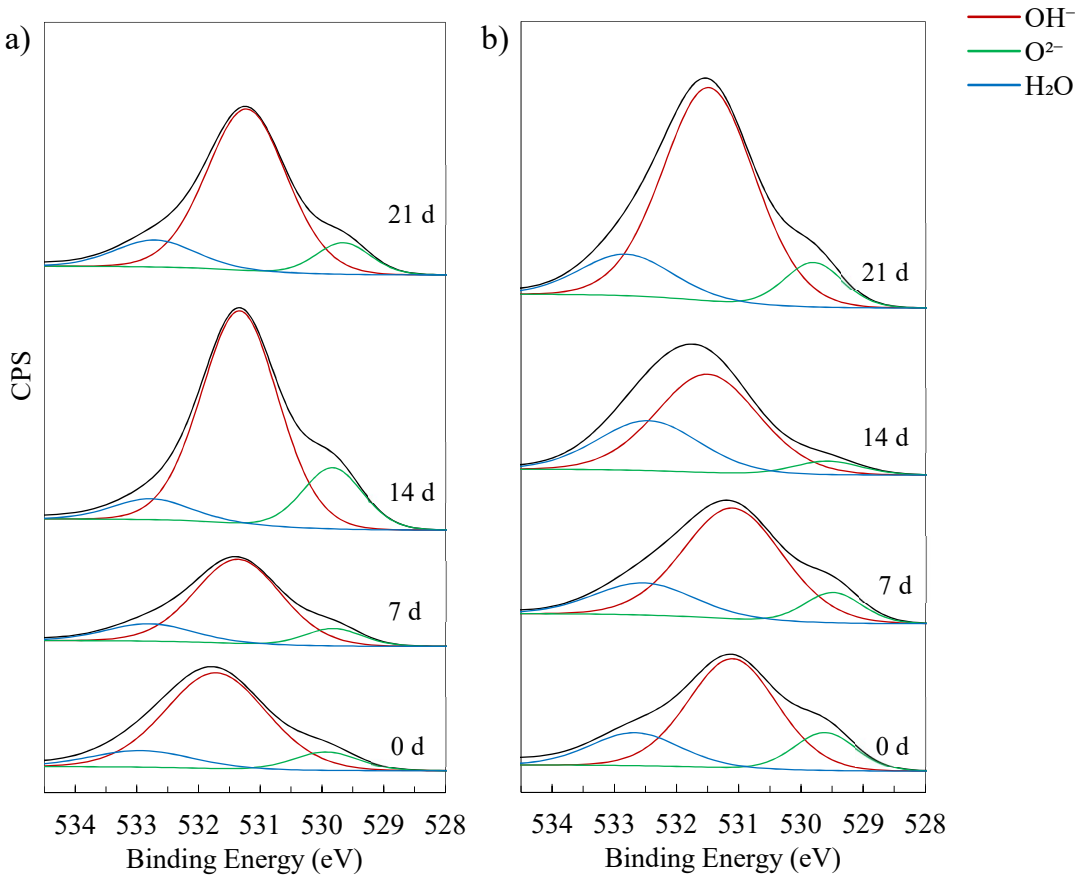

Figure C.7 O 1s region for a) S-nZVI and b) CMC S-nZVI.

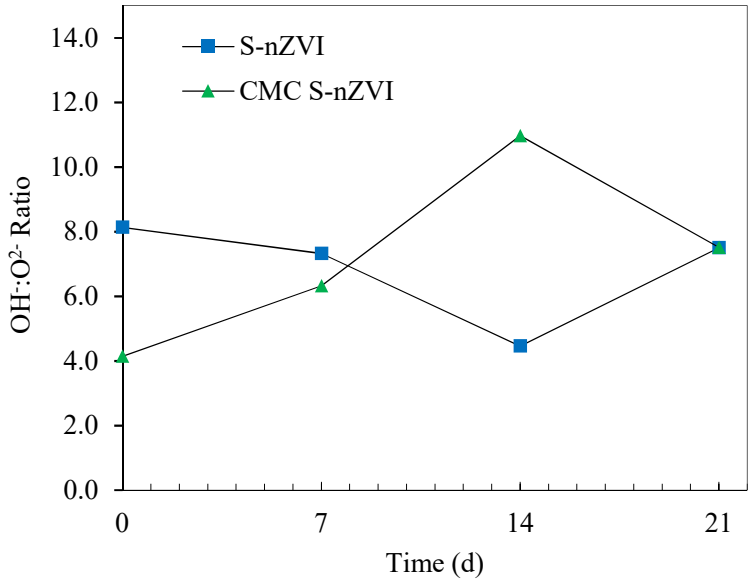

Figure C.8 Variations in the OH^-:O^{2-} ratio throughout the aging period.

Table C.5 Possible solid phases in the sulfidated nZVI system. Values in parenthesis represent corresponding interplanar spacings (D-spacings) in angstroms (Å).

Material	Composition	2θ Co Kα (D-spacing in Å)		
Iron	α-Fe^0	52.37 (2.027)	99.73 (1.17)	77.25 (1.433)
Magnetite	Fe_3O_4	41.41 (2.53)	74.19 (1.483)	67.31 (1.614)
Maghemite	γ-Fe_2O_3	41.58 (2.52)	67.5 (1.61)	35.3 (2.95)
Hematite	α-Fe_2O_3	38.84 (2.69)	63.91 (1.69)	41.75 (2.51)
Lepidocrocite	γ-FeOOH	16.43 (6.26)	31.55 (3.29)	42.46 (2.47)
Goethite	α-FeOOH	24.71 (4.18)	38.84 (2.69)	42.79 (2.452)
Mackinawite	FeS_m	20.49 (5.03)	35.06 (2.97)	45.56 (2.31)
Greigite	Fe_3S_4	34.93 (2.98)	61.63 (1.746)	42.48 (2.469)
Pyrite	FeS_2	66.43 (1.633)	38.56 (2.709)	43.33 (2.423)
Pyrrhotite	$Fe_{1-x}S$	51.55 (2.057)	39.69 (2.635)	35.1 (2.966)

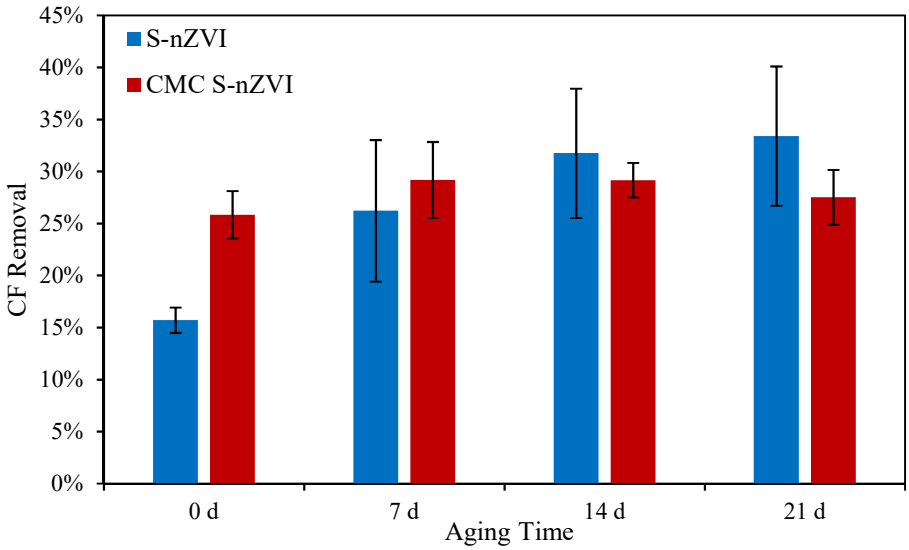

Figure C.9 Percent Removal of Chloroform after 21 days reactivity (20 days for 0 d and 7d CMC S-nZVI). Error bars represent standard deviations of triplicates.

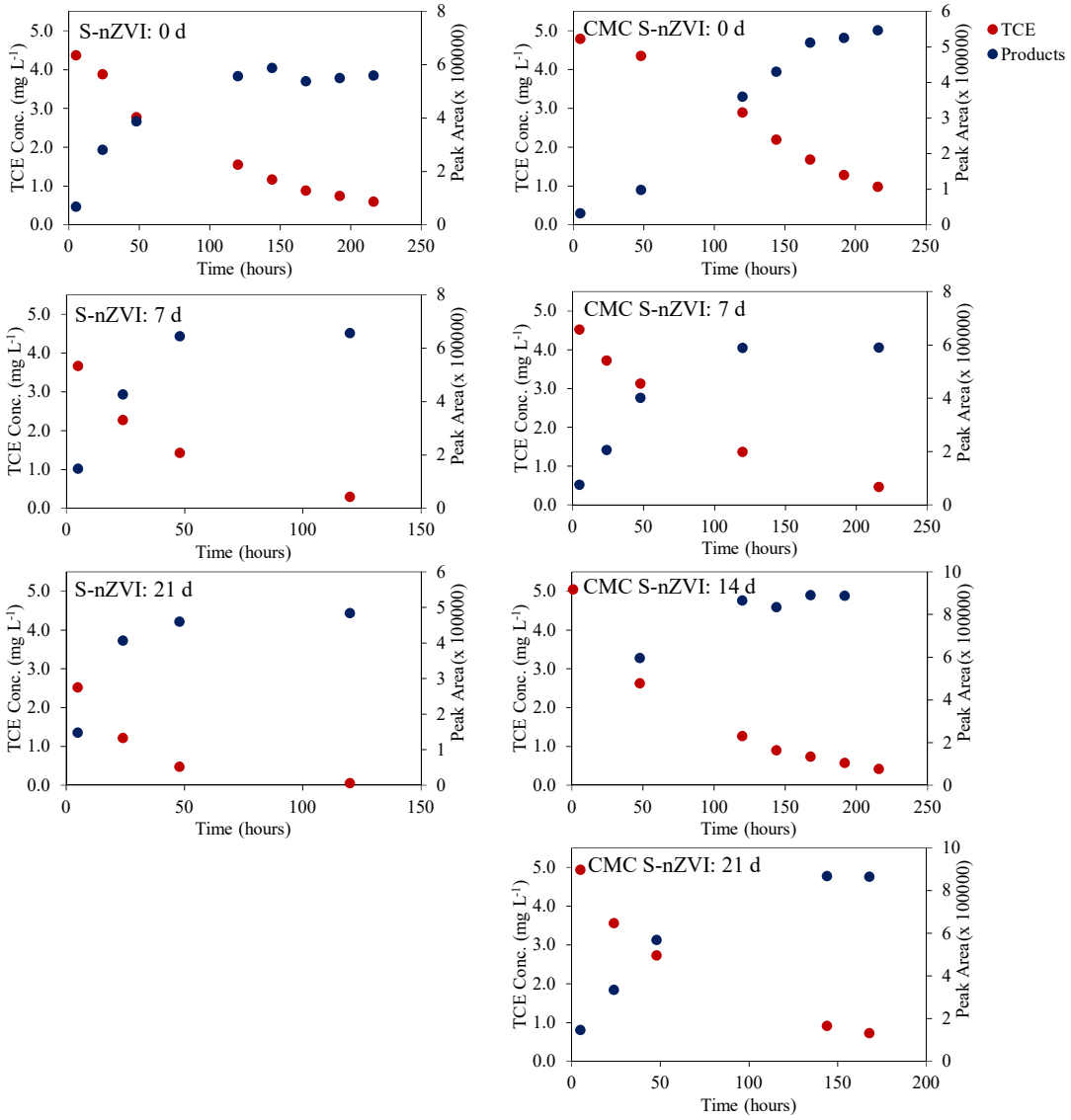

Figure C.10 TCE removal and product generation S-nZVI and CMC S-nZVI. Data for 14 d S-nZVI not available.

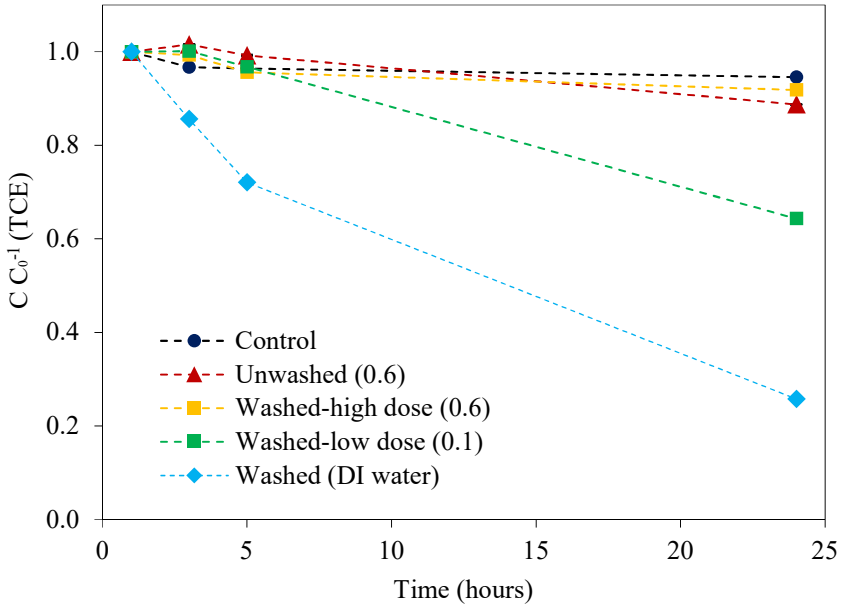

Figure C.11 Effect of residual dithionite on TCE degradation. $[TCE]_0$ = 5 mg/L, S-nZVI = 1 g L^{-1} at S/Fe = 0.6. Particles were sulfidated for 30 minutes, washed and then resuspended either in DI water or a solution yielding a S/Fe ratio of 0.1 or 0.6.

Curriculum Vitae

Name: Ariel Nunez Garcia

Post-secondary Education and Degrees:

Utah State University
Logan, Utah, United States
2007 – 2012 B.E.Sc.

Western University
London, Ontario, Canada
2012 – 2014 M.E.Sc.

Western University
London, Ontario, Canada
2015 – 2019 Ph.D.

Honours and Awards:

Industrial Post-Graduate Scholarship (IPS)
Natural Sciences and Engineering Research Council (NSERC)
2015 – 2017

R.M. Quigley Award
Western University
2013

Presidential Scholarship
Dominican Republic
2007 – 2012

Related Work Experience

Teaching Assistant
Western Ontario
2012 – 2018

Research Assistant
Western University
2012 – 2019

Publications:

Nunez Garcia, A.; Boparai, H. K.; O'Carroll, D. M., Enhanced Dechlorination of 1,2-Dichloroethane by Coupled Nano Iron-Dithionite Treatment. Environ Sci Technol 2016, 50, (10), 5243-5251.